A Ph.D. Dissertation on

URBAN FLOOD MODELING AND EVALUATION OF MITIGATION MEASURES CONSIDERING LAND USE AND CLIMATE CHANGES

Submitted by

Amrutha Suresh

(Roll No. 166104025)

Under the guidance of

Dr. Sreeja Pekkat

CIVIL ENGINEERING DEPARTMENT
INDIAN INSTITUTE OF TECHNOLOGY GUWAHATI
GUWAHATI, ASSAM, INDIA- 781039

February, 2024

Declaration

I hereby certify that the contents of this doctoral dissertation are the result of my research at the Department of Civil Engineering, Indian Institute of Technology Guwahati, Assam, India. In accordance with the standard practice for reporting scientific observations, appropriate citations have been included whenever the work described relies on the findings of other researchers. To the best of my knowledge, the work presented here is free of plagiarism, and I accept responsibility for any problems. I also affirm that my thesis supervisor is not responsible for any instances of probable plagiarism in the work submitted.

Amrutha Suresh
166104025

Date: Monday 5th February, 2024

Certificate

This is to certify that the work presented in the thesis entitled "**Urban Flood Modeling and Evaluation of Mitigation Measures Considering Land Use and Climate Changes**" is carried out by **Mrs. Amrutha Suresh** for the award of **Doctor of Philosophy** in the Department of Civil Engineering from the Indian Institute of Technology Guwahati, Assam. The thesis embodies the result of original work and studies carried out by the student herself under my supervision and has not been submitted elsewhere for the degree.

Sreeja Pekkat

Associate Professor
Department of Civil Engineering
Indian Institute of Technology Guwahati

Date: Monday 5th February, 2024

Acknowledgements

After a long and challenging journey, I find myself at the pivotal moment of crafting the opening page of this dissertation. Completing my doctoral studies at the renowned Indian Institute of Technology Guwahati fills me with a deep sense of privilege and accomplishment. The realization of this dissertation owes its existence to the invaluable contributions of several individuals who have played a significant role in the pursuit of this study. It has been a long, challenging and exhausting journey, but also been incredibly insightful and educational.

First, I would like to extend my heartfelt gratitude to my supervisor, Dr. Sreeja Pekkat, for her invaluable guidance and unwavering support throughout this journey. It is difficult to adequately express the depth of my appreciation for her constant inspiration and encouragement. Without her guidance, this thesis would not have reached its completion. There were numerous occasions when I contemplated giving up, but her motivation, recommendations, remarks, and, above all, her patience with a novice like myself greatly enhanced and streamlined my journey. She has been an exceptional mentor, a true friend, and, above all, a remarkable human being. I am immensely grateful for her genuine concern for my well-being and for consistently encouraging me to engage in critical thinking within the realm of research.

I sincerely thank my doctoral committee chairman, Prof. Rajib Kumar Bhattacharjya, for his invaluable contributions and timely assistance throughout this research. I sincerely appreciate his constructive suggestions, which have significantly enhanced the quality of this work. Additionally, I express my heartfelt appreciation to the doctoral committee members, Prof. Suresh A. Kartha and Dr. Rishikesh Bharti, for their fruitful discussions and invaluable suggestions that have greatly enriched the research process.

I would like to extend my heartfelt appreciation to Prof. Sreedeep S. for his helpful advice and inspiring support throughout my study period. The Civil Engineering Department provided me with countless memorable experiences to cherish, and I am immensely grateful for the positive environment fostered by all the faculty members and staff. I thank Prof. Sentilmurugan S. for his support during this journey.

I would like to express my heartfelt appreciation to the dear acquaintances, seniors, and juniors at IIT Guwahati who have played a significant role in my academic journey: Priya, Abdul, Sachin, Piyush, Akhil, Subrasekhar, Vijendra, Shabeeb, Gangadhar, Biplab, Aakarsh, Yaswanth, Vinay, Ashutosh, Ketan, Somesh, Avinash, Bazal, Suman, Satish, Aswanth, Anjani, Geetanjali, Vishnu,

Dileep, Sajeer, Reshma, Jomi, and Wafa. I am incredibly grateful to my little brother, Kashinath, for his unwavering love and support.

At this pivotal moment, I would like to take a moment to acknowledge and express deep gratitude to all of my teachers and well-wishers who have guided and directed me towards the realization of my goals.

I would like to extend my heartfelt appreciation to three remarkable individuals who have been my unwavering pillars of support throughout my entire Ph.D. journey: Anjaneyulu, Chandan, and Aparimita. The moments we shared together hold a special place in my heart, especially our evening tea time, which brought us closer. The guidance, motivation, and invaluable advice provided by Anjaneyulu have always been of immense value to me. Words fail to express the depth of my gratitude towards Aparimita and Chandan. They have been by my side throughout this transformative journey, witnessing both my ups and downs and embracing me for who I am. Their unwavering support and endless motivation have been instrumental in my success.

I want to express my heartfelt appreciation to Meenaskhi for her unwavering love and constant support, which has been instrumental in helping me reach this significant milestone. I want to thank Anita, Shreshta, Digvijay, Meenu, Shruti, Rogers, Rohan, Shruthi, Kuldeep, Uma, Aiyyapan, Karki, Sathish, Rajashri, Pratyush, Yukti, Gnanaprakash, Vedhapriya, Ritvika, Ranajit, Rajesh, Veena, Adwait, Roshan, Shabnam, Reju for their support.

I am deeply indebted to my beloved parents and in-laws for providing unwavering support and encouragement, despite the physical distance that separates us by hundreds of miles. My mother, whose persistent encouragement has always propelled me towards higher education. I want to express my heartfelt gratitude to my sister, Sumitha, my niece Aditi, and my brothers: Shinoj, Vinay, and Priyesh, as well as my aunt, Kanakalatha and uncle Padmanabhan, for their unwavering support during the challenging phases of my life. Furthermore, I thank Suveesh, Swapna, Shravan, Suvina, Prabeesh, and Parthiv for their support throughout my journey.

Last but certainly not least, I want to extend my heartfelt appreciation to my better half, Suvin. Throughout my life and my Ph.D. journey, he has been an unwavering pillar of support. Words fail to capture the depth of my gratitude, as it knows no bounds. He has not only been my most ardent cheerleader but also my best friend and an incredible husband. During times of hardship, he provided constant inspiration and unwavering encouragement. Together, we have embarked on this incredible journey.

Finally, I would like to express my gratitude to the Almighty. In awe of the wonders of the universe and the mysteries of life, I acknowledge the divine presence that transcends our understanding. Through the grace and blessings of the Almighty, I have been granted the opportunity to embark on this profound journey of knowledge and growth. I offer my humble thanks for the guidance, strength, and inspiration that have accompanied me throughout this endeavour.

I dedicate this thesis to my

Supervisor

&

Husband

who have always believed in me and supported me throughout this voyage

Abstract

Urban flooding and its associated fury have become very common in this century. Unplanned and indiscriminate urbanization and climate change are considered as the major causes of urban flood. Urbanization has increased the impervious areas, resulting in less infiltration of rainwater, thereby increasing the surface runoff. Climate change has affected the intensities and frequencies of rainfall, increasing flooding vulnerability in urban areas. Many studies have been done to quantify the impact of land use and climate change on various hydrological processes like streamflow, snow melt, soil moisture, droughts, etc. However, not many studies have been reported on the impact of land use and climate change on urban flooding (especially for Indian catchments). Therefore, the present study aims to quantify the impacts of climate change and land use on urban flooding for an urban catchment in northeast India.

The last few decades have witnessed drastic changes in rainfall patterns and changes in their extremes, primarily associated with the climate change, thereby making cities and major infrastructure more vulnerable to flooding. Extreme rainfall is incorporated in the design of hydraulic infrastructure through the intensity duration frequency (IDF) curve. Therefore, studying the possible drift in the IDF curves associated with the changing trends in historical rainfall data and future climatic conditions is important. Based on the understanding of the negative correlation between rainfall intensity and duration, this study employed a bivariate copula-based approach for IDF curve development. The study identified Frank copula (from 24 candidate copulas) with its parameters estimated by Bayesian inference and a hybrid-evolution Monte Carlo Markov Chain. In addition, the IDF curve was developed for four future climate scenarios corresponding to three different time periods (2021-2047 (P1), 2048-2074 (P2), and 2075-2100 (P3)). The observed disparity between the future IDF curve and the historical IDF curve provides clear evidence that climate change will bring about changes in rainfall extremes. This study enlist recommendations for incorporating the influence of climate change while designing hydraulic infrastructure. For near-future climate change and infrastructure with a design life of $\leq$ 50 years , the RCP 6.0 scenario would yield the critical IDF curve. For long-term planning with a design life of > 50 years, it is desirable to consider the IDF curve based on the RCP 8.5 scenario. For the intermittent period, both RCP 6.0 and RCP 8.5 exhibited a similar trend in terms of rainfall intensity for higher return periods and for shorter return periods (2-10 years) RCP 4.5 can be considered.

Quantification of imperviousness is essential for urban hydrological analysis and urban flood management. Effective impervious area (EIA) gives a fair estimate of the imperviousness required

for urban hydrological analysis. A semi-automated direct method was used to estimate EIA from fine-resolution satellite images. An increase in built-up area was observed from 1980 to 2022 (2.85% to 50.56%). It was observed that this increase in the built-up area was occurring at the expense of converting the agricultural area, swampy land and forest area. Watershed 3 showed the highest percentage of imperviousness of 12.06%, 13.22%, 13.74%, 15.10%, and 22.37% for the years 2011, 2013, 2017, 2020, and 2022, respectively.

The stormwater management model (SWMM) was used to simulate the runoff associated with changing LULC and climate change. The impact of various observed rainfall events on the runoff patterns for different EIA conditions was studied. The impact of LULC changes on urban flood was studied by varying the LULC from 2011 to 2022 and keeping the rainfall intensity constant. The analysis indicates that EIA-related changes from 2011 to 2022 have resulted in 1.3 times increase in peak runoff. Similarly, the impact of climate change on urban flood has been studied by considering the LULC of the year 2022 and varying the rainfall intensity across the three different climate periods. The far-end future period (P3) and the near-future period (P1) exhibit higher runoff values compared to the mid-future period (P2). The future runoff projections under different RCPs reveal that RCP 6.0 results in 4.9 times greater runoff compared to historical levels, RCP 4.5 will have 3.6 times more runoff, and RCP 8.5 will encounter 6.1 times more runoff compared to the historical runoff.

Low impact developments (LIDs) have gained wide acceptance as a sustainable and effective technique for mitigating urban flooding. Assessing the efficacy of LIDs on a watershed scale is difficult due to the non-availability of high-resolution data for the entire watershed. Hence, to implement LIDs in any watershed, there is a need to identify the best-performing LIDs on a micro-watershed scale, which are small-scale drainage areas. By studying these small-scale drainage areas, researchers can better understand the best-suited LIDs for a particular watershed and develop effective flood management strategies. The hydrological impact of LIDs on mitigating runoff depth and peak runoff in the context of climate change for four micro-watersheds (A, B, C and D) in northeast India was studied. Based on the analysis, best-performing LID was chosen. It was found that LIDs were effective in managing the stormwater in all four micro-watersheds, and among the four LIDs considered (green roof, permeable pavements, infiltration trenches, and rain barrels), the green roof showed the highest percentage reduction in runoff characteristics. For watersheds A, B, C, and D, the green roof effectively reduced runoff by 30-38%, 83%, 50%, and 34%, respectively. This knowledge of best-performing LID (i.e., green roof) was used, and it was implemented in the most urbanized watershed in Guwahati city (watershed 3) at 5%, 10%, 15%, 20%, and 25% of the built-up area. Implementing green roofs has reduced peak runoff for both historical and future. However, it was observed that climate change will increase the intensity of rainfall, and hence hybrid methods of flood mitigation may be needed and the same needs to be explored in detail.

Keywords: *climate change, copula, effective impervious area, imperviousness, intensity duration frequency curve, land use land cover change, low impact developments, urban flood*

Contents

List of Figures

List of Tables

List of Abbreviations

AET	Actual evapotranspiration
AIC	Akaike information criteria
AM	Adaptive metropolis
AMR	Annual maximum rainfall
AMS	Annual maximum rainfall series
AR	Assesment report
BIC	Bayesian information criteria
BIDF	Bivariate intenisty duration frequency curve
BMPs	Best management practices
BS	Birnbaum saunders
CDF	Cumulative distribution function
CMIP	Coupled Model Intercomparison Project
COE	Centre of excellence
CTs	Compensatory techniques
DCIA	Directly connected impervious area
DEM	Digital elevation model
DN	Digital number
EIA	Effective impervious area
EM	Empirical method
ENVI	Environment for visualising images
EPA	Environmental protection agency
ET	Evapotranspiration
FCC	False colour composite
GCMs	Global Climate Models

GEV	Generalised extreme value
GHGs	Greenhouse gases
GMC	Guwahati municipal Corporation
GMDA	Guwahati metropolitan development authority
GP	Generalized pareto
GR	Green roof
HE-MCMC	Hybrid-evolution monte carlo markov chain
HR	Heavy rain
IDF	Intensity duration frequency
IPCC	Intergovernmental panel on climate change
IT	Infiltration trench
LHS	Latin hypercube sampling
LIDs	Low impact developments
LIUDD	Low impact urban design and development
LULC	Land use and land cover
MCMC	Monte carlo markov chain
MLC	Maximum likelihood classifier
MSL	Mean sea level
NBS	Nature-based solutions
NCMs	Non-central moments
NEIA	Non-effective impervious area
NRSC	National Remote Sensing Centre
OA	Overall accuracy
PA	Producer accuracy
PET	Potential evapotranspiration
PP	Permeable pavements
QGIS	Quantum geographic information system
RB	Rain barrel
RCP	Representative Concentration Pathway
RE	Rainfall event
REA	Reliability ensemble averaging

RWH	Rain water harvesting
SC	Sponge city
SCMs	Stormwater control measures
SUDS	Sustainable urban drainage system
SWMM	Storm water management model
TCC	True colour composite
TIA	Total impervious area
UA	User's accuracy
UIDF	Univariate intensity duration frequency curve
VHR	Very heavy rain
WSUD	Water sensitive urban design

List of Symbols

A	Cross-sectional area of the channel
a	Constant
$A_i(t_k)$	Gaussian membership function
α	Scale parameter of the generalized extreme value distribution
α_s	Significance level
b	Constant
$\beta_i(t_k)$	Crisp membership
$C_{I\|D=d}$	Conditional Frank copula
$\mathcal{C}$	Constant
C	Copula
c	Constant
C_n	Covariance matrix
C_i	Captured component
C_R	Runoff coefficient
$Cost_{crisp}(t)$	Crisp segmentation cost
$\mathcal{D}$	Number of parameters of the statistical model
d	Depth of water in catchment
D	Storm duration
$d_n(\mathbf{v})$	Discriminant function
d_1	Depth of water on the surface layer
D_1	First-order Debye function
d_2	Depth of water on the storage layer
D_2	Thickness of the soil layer
D_4	Thickness of the pavement layer
d_s	Maximum depression storage depth
$D^2(x_k, v_i^x)$	Distance between the centre of cluster and data point
e	Rate of evaporation
e_1	Evapotranspiration rate of surface layer

e_2	Evapotranspiration rate of soil layer
e_3	Evapotranspiration rate of storage layer
e_4	Evapotranspiration rate of pavement layer
ϵ	Location parameter of the generalized extreme value distribution
$F(x)$	Cumulative distribution function
f	Infiltration rate
f_1	Infiltration rate of surface water into soil layer
f_2	Percolation rate into the storage layer from the soil layer
f_3	Exfiltration rate into the native soil from the storage layer
f_4	Draining rate of water out of the pavement layer
F_4	Fraction of the surface area taken by the impermeable paver blocks
$F_X(x)$	Marginal distribution function of X
$F_Y(y)$	Marginal distribution functions of Y
g	Acceleration due to gravity
Γ	Gamma function
GCM_b	Mean values of rainfall from GCM baseline scenarios
GCM_f	Mean values of rainfall from GCM future scenarios
H	Joint probability distribution
i	Number of GCMs
I	Rainfall intensity
$\bar{J}$	Modified objective function
J	Objective function
K	Constant
$\mathcal{K}$	Kappa coefficient
κ	Shape parameter of the generalized extreme value distribution
l	Log-likelihood value
$L(\Theta\|\tilde{x})$	Likelihood function
$l(\Theta\|\tilde{x})$	Log-likelihood function
λ^{beta}	Scale factor
M	Number of bands
m	Number of tied groups
$\mu_{(i,k)}$	Degree of membership
μ_n	Mean vector
n	Manning's roughness coefficient
N	Total number of points in the confusion matrix

$P(\mathbf{v})$	Probability that **v** is observed
$P(\mathbf{v}\|n)$	Class specific probability density function
$P(\Theta\|\tilde{x})$	Posterior distribution
$P(\Theta)$	Prior distribution
$P(n)$	Prior probability of feature vector
$P(n\|\mathbf{v})$	Posterior distribution of feature vector
P_f	Projected future daily rainfall
P_{obs}	Observed daily rainfall
P_{total}	Total rainfall depth
$\phi(t)$	Generator of Frank copula
ϕ_1	Void fraction of surface layer
ϕ_3	Void fraction of storage layer
q	Number of rows in the confusion matrix
q_s	Runoff rate
q_0	Inflow to the surface layer
q_1	Overflow rate in the surface layer
q_3	Outflow rate of storage layer underdrain
Q_s	Surface runoff
Q_i	Sen's estimator
Q_{med}	Median of these Sen's estimator
R	Hydraulic radius
R^2_{24}	24-hour two-years rainfall
$R_{c,i}$	Model convergence criterion
R_i	Reliability ensemble averaging weights
R_{LID}	Indicator with LID
$R_{m,i}$	Model performance criterion
R_{noLID}	Indicator without LID
R_{total}	Total runoff depth
S	Slope of catchment
$\mathcal{S}$	Mann-Kendall test statistics
S_0	Channel bottom slope
S_f	Friction slope
t	Time
T	Return period
T_n	Time series

$T(I\|D = d)$	Conditional return period
τ	Kendall Tau coefficient
θ	Copula parameter
θ_2	Moisture content of soil pavement
θ_4	Moisture content of permeable pavement
t_i	Number of ties for time-extend
U	Uniformly distributed random variable
$\mathbf{v}$	Feature vector
V	Uniformly distributed random variable
$V(\mathcal{S})$	Variance of Mann-Kendall test statistics
w	Width of the sub-catchment
x	Distance in the direction of flow
$\mathbf{x}$	Rainfall quantiles
X	Random variables
x_i	Data values in the series
x_j	Data values in the series
y	Flow depth in channel
Y	Random variables
z	Number of data points in the time series
Z	Standardized test statistic
z_k	Probability of the data points

Chapter 1

Introduction

1.1 General

Flooding is the common and expensive natural disaster worldwide, causing extensive damage to both human life and the economy. Frequent urban flooding is becoming common globally and presents a considerable challenge for urban planners and city administrators. The impacts of urban floods can range from isolated incidents to more widespread and prolonged flooding, causing significant damage to cities and their inhabitants. The twentieth century has witnessed several urban flooding and the associated furies due to unplanned urbanization and alterations in the precipitation patterns caused by climate change.

The world's population is growing at an alarming rate, leading to a surge in migration of people from rural to urban areas in search of better living standards, employment, business, education, and other commercial activities. The global urban population currently comprises around 55% of the total population, which is expected to rise to 68% by 2050 (Andimuthu et al., 2019; UN, 2019). Figure 1.1 shows the 2050 urban population projection for the world. To cater to the needs of the expanding urban population, there has been a rapid and extensive modification of land use and land cover (LULC) patterns leading to rapid and unplanned urbanization. However, this rapid and unplanned urbanization has led to frequent urban flooding, which is a significant issue faced by urban areas. The increase in impervious surfaces due to urbanization hinders the natural water pathways and the infiltration of rainwater, resulting in an increase in surface runoff. As a result, urban areas are more susceptible to flooding, as excess water cannot infiltrate the ground and instead accumulates on the surface. This can cause extensive damage to infrastructure and property, as well as threaten the lives and safety of residents.

The climate of the earth is changing day by day. As per the IPCC AR6 report, the energy balance of the earth is disturbed as a result of changes in the concentration of greenhouse gases (GHGs), land cover, aerosols, and solar radiation (IPCC, 2021). Anthropogenic activity is considered as one of the leading causes of the increase in GHGs concentration . Evidence of climate change can be noted from changing patterns of rainfall, rise in temperature, sea level rise, melting of ice, increase

in extreme events etc. Climate change is a major issue worldwide as natural calamities, global warming, and extreme events appear to increase in frequency day by day (Singh et al., 2016). The climate projections over India indicate that temperature rise is likely to be around $3°C$ and rainfall increase is expected by 10–20% by the end of this century (IPCC, 2014, 2021). Figure 1.1 shows the increase in the percentage of precipitation for the world.

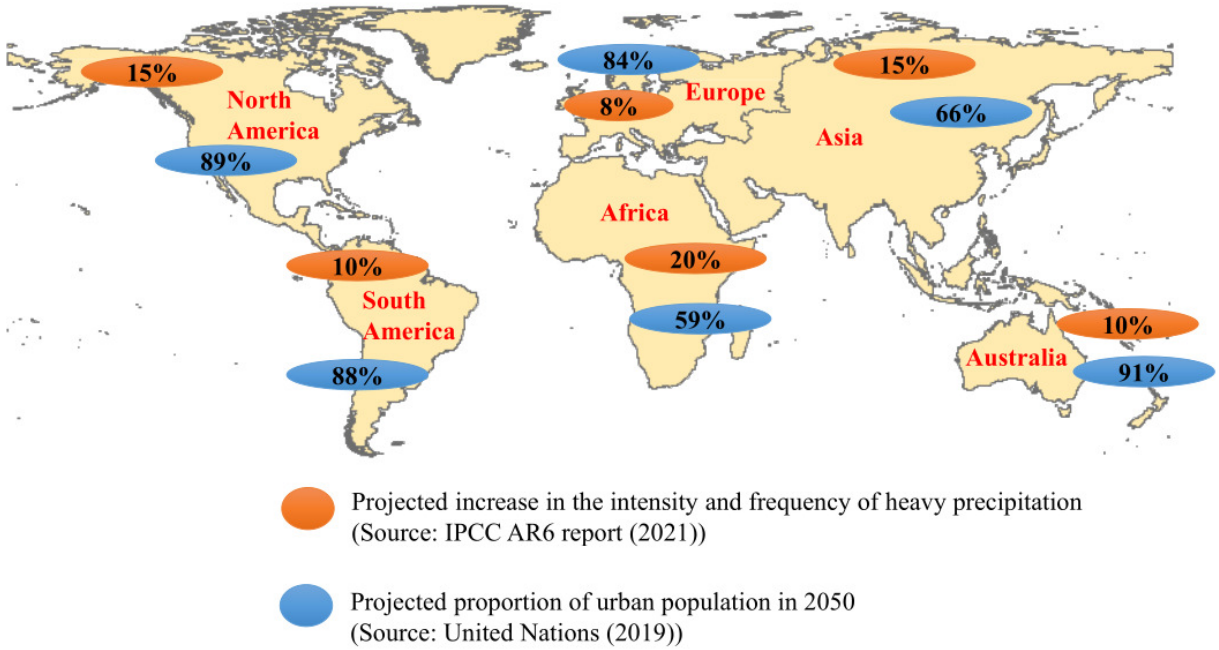

Figure 1.1: Projected increase in percentage of precipitation and urban population

Climate change has altered the daily and short-duration extreme rainfall events (IPCC, 2021; Zahmatkesh et al., 2015a). The unexpected rise in extreme rainfall can cause the stormwater infrastructure systems to malfunction, making cities and major infrastructure more vulnerable to flooding (Cheng et al., 2014; Mailhot et al., 2007; Sarhadi et al., 2016). The failure of stormwater infrastructure can be mainly attributed to the non-consideration of changing climate and inappropriate anticipation of future rainfall scenarios (Agilan and Umamahesh, 2016; Willems et al., 2012; Zahmatkesh et al., 2015b).

The poor drainage standards followed in the design of the urban stormwater system, insignificant drainage capacity, aged drainage facilities, and complex drainage pipe networks has also caused an increased risk of urban flooding (Bai et al., 2018). Studies (Alfieri et al., 2016; Arnone et al., 2018; Zhou et al., 2018) have shown that urbanization and climate change may increase the drainage overflow in cities. Preventing urban floods is challenging; however, their impact can be minimized by adopting proper flood management strategies. Modifying the existing drainage system to accommodate excess runoff is costly and not sustainable in many situations. Moreover, the limited space availability in the urban environment limits the possibility of expansion of the existing drainage system. Therefore, an appropriate stormwater management strategy through an effective alternative measure needs to be implemented. However, such a measure should be cost-effective, sustainable, and consume no or minimal space. Understanding the underlying factors

contributing to the changes in flood characteristics is crucial in developing effective strategies for mitigating and adapting to future flood events.

1.2 Motivation of the Research

Urban floods are not an unknown event in India. Urban flooding and its accompanying devastation have become increasingly frequent in the 21st century and it is visible from various flood events like Ahmedabad (2001), Chennai (2004 and 2015), Delhi (1924, 1947, 1976, 1978, 1988, 1995, 2000, 2003, and 2009), Guwahati (2010), Hyderabad (2000 and 2008), Kolkata (2007), Kerala (2018), Mumbai (2005), Noida (2010), and Surat (2006). Urban flooding is primarily attributed to three significant factors: rapid urbanization, high-intensity rainfall events of short duration, and the influence of climate change. Studies have shown that climate change has increased the occurrence of flash floods both in urban and rural areas (Perumal and Sahoo, 2010).

The leading cause of increase in urban floods in recent years is unplanned urbanization and climate change. In this decade, changing climate has become an important issue to the entire world. Climate change is an important global issue as natural calamities, global warming, and extreme events appear to increase in frequency day by day (Singh et al., 2016). Many studies have been done to quantify the impact of land use and climate change on various hydrological processes like streamflow (Chawla and Mujumdar, 2015; Choto and Fetene, 2019; Getachew et al., 2021), evapotranspiration (Berihun et al., 2019; Kumar et al., 2022a; Odongo et al., 2019), water quality (Santy et al., 2020), snow melt (Woltemade et al., 2020), soil erosion (Belay and Mengistu, 2021), droughts (Kandakji et al., 2021; Li et al., 2020a), etc. Not many studies have been reported on the impact of land use and climate change on urban flooding (especially for Indian catchments).

The motivation for researching the impact of land use and climate change on urban flood characteristics arises from the growing concerns over the increasing frequency and severity of urban floods. Urbanization and climate change alter the natural hydrological cycle, resulting in more frequent and intense floods, which can cause devastating consequences for urban communities. Understanding the complex interactions between land use land cover, climate change, and urban flood characteristics makes it possible to develop effective flood management strategies and urban planning policies. Therefore, this research is crucial in identifying the key factors influencing urban floods and determining the most effective approaches for mitigating their impacts. Also, floods cannot be prevented, but their impact can be reduced by adopting proper flood management strategies. The success of flood management measures depends on the hydrological and meteorological factors. Such need has motivated to study the effect of land use and climate change on urban flooding.

Ultimately, this research aims to contribute to the development of sustainable and resilient urban environments that can withstand the challenges posed by land use land cover changes and climate change, thereby ensuring that all communities have the information required to make good choices in the rehabilitation and protection of infrastructure and population.

1.3 Research Objectives

The main objective of the study is to carry out urban flood modeling and evaluate the mitigation measures considering land use and climate changes. This is achieved through the following scopes:

(i) To develop the rainfall intensity duration frequency (IDF) curves incorporating climate change

(ii) To quantify the land use land cover (LULC) changes and imperviousness of the study area

(iii) To carry out the flow modeling for different rainfall scenarios and to assess the impact of land use and climate change on urban flooding

(iv) To assess the efficacy of best management practices in mitigating the flood

The overview of the current research work is presented in Fig. 1.2.

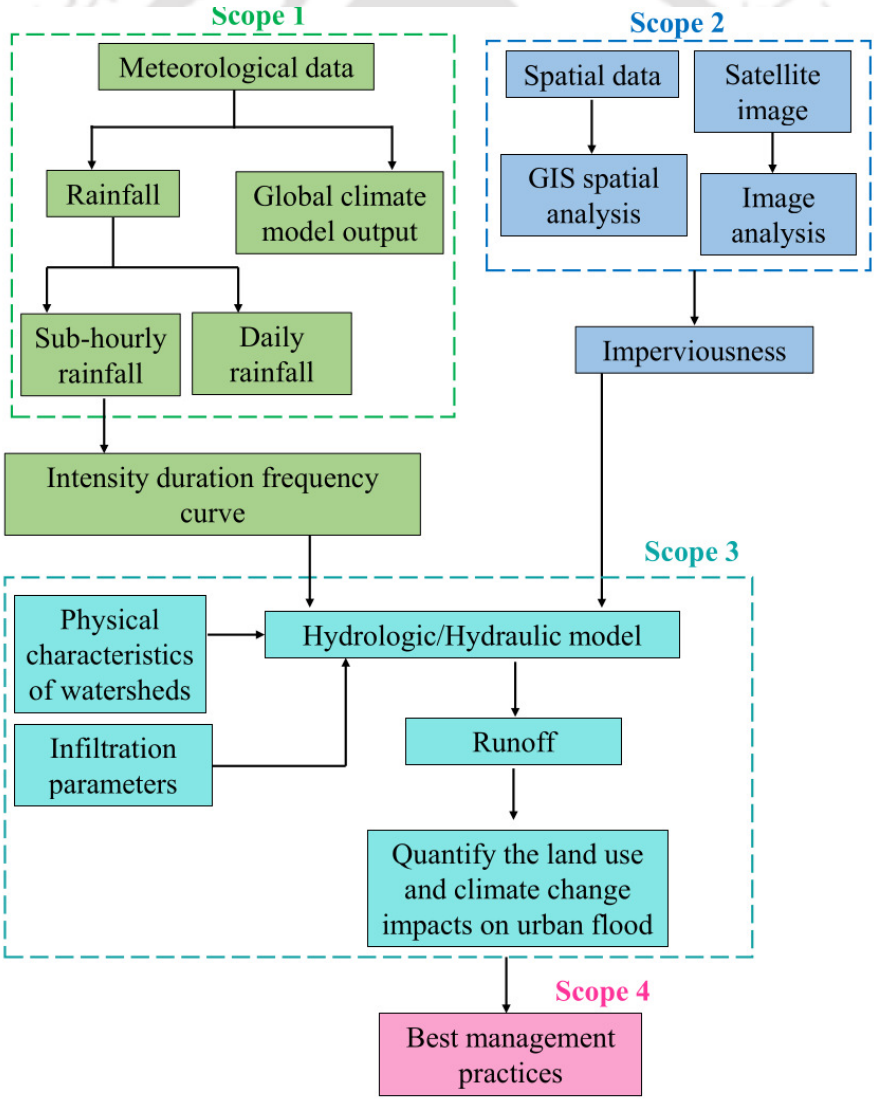

Figure 1.2: General synopsis of the thesis

1.4 Organization of the Thesis

Figure 1.3 graphically depicts the organization of this thesis. Each box represents a chapter, and the arrow between the boxes indicates the relationship between the chapters. A detailed description of the thesis organization is as follows.

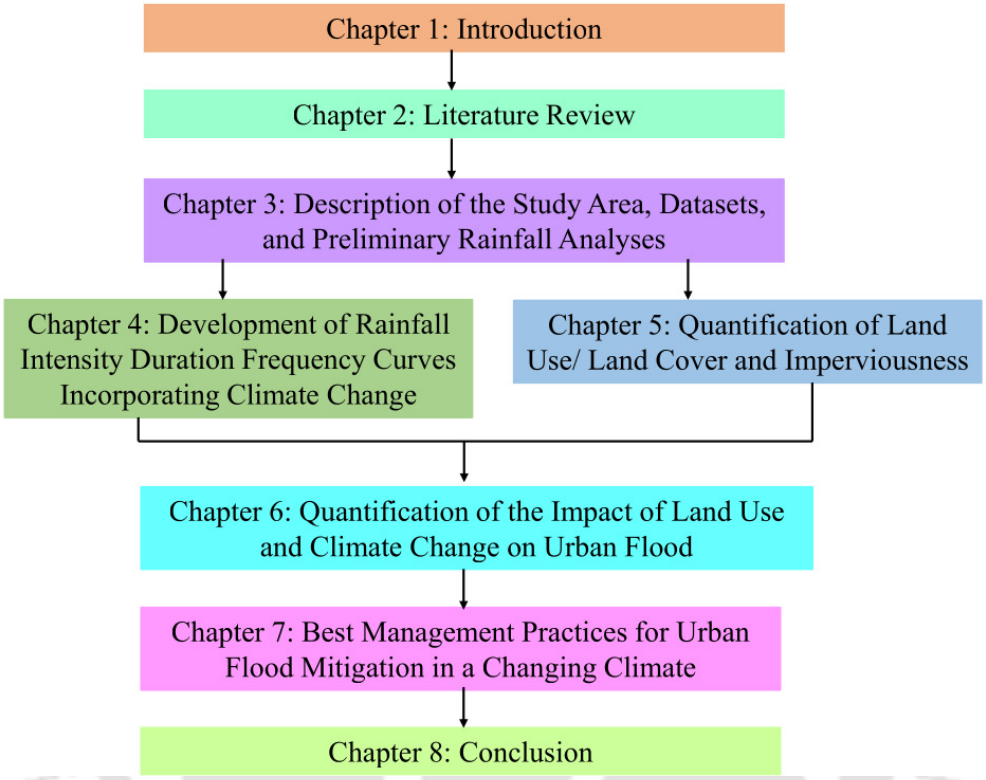

Figure 1.3: Thesis structure and relations between chapters

- **Chapter 1** provides an overview of the research topic and its motivation and research significance. Additionally, the chapter will outline the structure and organization of the thesis, which will help to understand the flow and sequence of the subsequent chapters and how they are interrelated.
- **Chapter 2** is centred around a comprehensive evaluation of the literature, with the primary objective of identifying the limitations and shortcomings in the current state-of-the-art and finally summarizes the literature and highlights the research gaps.
- **Chapter 3** presents an overview and detailed information on the study area and the data used for the research. The last section of this chapter briefly describes the trends in the historical rainfall data of the study area.
- **Chapter 4** is dedicated to assessing the impact of climate change on Guwahati city by analysing the intensity duration frequency curve (IDF). This chapter discusses the downscaling and disaggregation methodologies used in the research, followed by the different techniques used in developing IDF curves.

- **Chapter 5** explores the quantification of land use land cover (LULC) and imperviousness of the study area. The chapter provides an overview of the quantification of LULC changes through remote sensing techniques and geographic information system (GIS) analysis, and the methodology used for determining imperviousness is discussed.
- **Chapter 6** investigates the influence of LULC and climate change on urban floods. The main emphasis of this chapter lies in examining the behavior of urban floods during various rainfall events, analyzing the impact of LULC on the urban flood, and projecting how future climate changes will further affect urban flood dynamics.
- **Chapter 7** examines the effectiveness of various flood management practices in mitigating the urban flood. Specifically, this chapter primarily evaluates the efficacy of low impact developments (LIDs) in reducing urban runoff and its associated consequences.
- **Chapter 8** summarizes the main findings and contributions of the research. This chapter also discusses the potential avenues for further research.

Chapter 2

Literature Review

2.1 General

This chapter overviews numerous studies on the effects of climate change, land use, and land cover changes on various hydrological processes. Additionally, it explores the research undertaken in urban flooding and flood management. Figure 2.1 shows the overview of the literature review. The final section of the chapter offers a critical evaluation of the literature that has been reviewed.

Figure 2.1: Components of the literature review

2.2 Climate Change

Climate is the statistics of weather and atmospheric conditions over long periods. Climate change caused by external factors like human activities are challenging to predict, particularly over a large scale (IPCC, 2007). Earth's climate is shaped through the interplay of different processes occurring within the atmosphere, hydrosphere, cryosphere, land surface, and biosphere (IPCC, 2021). These interactions among various spheres are very complex and hence the impact of increase in green house gases (GHG) on climate is difficult to explain. It is a known fact that the human activities are unpredictable in future leading to human-induced climate change, which is supported by scientific evidence and proper understanding. This includes the relationship between GHG concentrations and the earth's energy balance, historical climate changes, and the attribution of recent warming to human activities. Even though, the overall trend of global warming and its consequences are well-established, the regional scale climate change impacts are difficult to predict.

2.2.1 Impact of Climate Change on Hydrology

Global warming has led to an acceleration of climate change on a global scale, which has severely impacted the hydrological cycle by altering the precipitation pattern, temperature, sea level, snow-melt, droughts, floods and so on. Due to the intricate nature of the climate system, accurately predicting the impacts of climate change is a formidable task. However, climate models incorporating the hydrological cycle serve as a valuable tool to conceptualize future scenarios, enabling effective decision-making processes. These models provide a framework for understanding potential changes in precipitation, evaporation, and other hydrological processes, facilitating informed actions to mitigate and adapt to the challenges posed by climate change. In recent years, there has been a global surge of interest in understanding and assessing the potential impacts of climate change on water resources. Several research studies have investigated the impact of climate change on the hydrological variables of various regions around the world, and table 2.1 shows the synopsis of such studies.

Table 2.1: Summary of the studies on impact of climate change on different hydrologic variables

Author (Year)	Study area	Hydrologic variable	Remarks
Arnell (1999)	Global scale	Impact on the global hydrological regimes and water resources	• Increase in annual runoff in high latitudes regions like Africa and Asia and decrease in the mid-latitudes and most subtropical regions • Increase in the number of people living in water-stressed countries by 2025

Nicholls et al. (1999)	Global scale	Impact of sea level rise on floods	• Western Africa, Eastern Africa, the southern Mediterranean, south Asia, south-east Asia, the Caribbean, and the small islands in the Indian Ocean and Pacific Ocean are particularly susceptible to heightened flood risks due to the projected rise in sea levels
Dankers et al. (2007)	Upper Danube basin, Central Europe	Flood hazards	• Increase in the discharge characteristics of the river and flood hazard
Akhtar et al. (2008)	Hunza, Gilgit, and Astore river basin, Pakistan	Water resources	• Increase in temperature and precipitation in 21^{st} century • Increase in flood magnitude for all return periods under climate change
Abbaspour et al. (2009)	Iran	Water resources	• Wet regions might have frequent and larger-intensity floods and dry regions might experience prolonged droughts • Increase in soil moisture in future • 50–100% decrease in groundwater recharge
Chang and Jung (2010)	Willamette River basin, Oregon	Water balance	• Substantial decrease in summer runoff and modestly increases in winter runoff • High and low flow events are likely to increase
Dobler et al. (2011)	Upper Danube and Upper Brahmaputra River basin	Runoff	• A 25% increase in dry days was observed in Assam regions during monsoon • Tibetan Plateau was sensitive to climate changes
Wang et al. (2011b)	Shiyang river basin, China	Streamflow	• Increase in the streamflow by 0.7–6.1% for the years 2020s, 2050s and 2080s
Ruelland et al. (2012)	Sudano-Sahelian catchment, West Africa	Water resources	• Decrease in the future rainfall by 15-17% • Future potential evapotranspiration (PET) shows an increase by 16-18% • Rainfall deficit together with increasing future PET suggests a decrease in runoff from the basin leading to drought conditions in future

Ficklin et al. (2012)	Mono Lake Basin, California	Hydrology	• Increase in temperature by $2.5^{\circ}C$ and $4.1^{\circ}C$ for the B1 and A2 emission scenarios respectively. • Increase in annual total evapotranspiration by 10 mm for both the emission scenarios • 3% decrease in precipitation • Decrease in streamflow along with a shift in the streamflow timing was observed due to earlier spring snowmelt due to higher spring temperatures
Zhang et al. (2013)	Huaihe river basin, China	Runoff	• Runoff was more sensitive to changes in precipitation than temperature changes • Rise in temperature and decrease in rainfall resulted in decrease in runoff
Faramarzi et al. (2013)	Africa	Fresh water availability	• Increase in temperature by $10 - 20^{\circ}C$ • Mean total quantity of water resources was likely to increase. • Decrease in the water yield, deep aquifer recharge and soil moisture in future due to climate change
Islam and Gan (2014)	South Saskatchewan River basin, Alberta	Surface water management	• Mean annual average streamflow will decrease by 14, 12 and 18% in 2010-2039, 2040-2069 and 2070-2099 respectively
Camici et al. (2014)	Tiber River basin, Central Italy	Flood frequency	• 30% decrease in mean annual rainfall and an approximate 40% increase in mean annual temperature under A2 emission scenario • Decrease in flood magnitude is projected
Yan et al. (2015)	Pearl River, China	Seasonal discharge and extreme flows	• Decrease in the flow during dry season leading to increase of salt water intrusion in the delta • Increase in flow leading to increased flood risks
Pandey et al. (2016)	Armur watershed, Godavari river, India	Hydrology	• Increase in average temperature by $3.25^{\circ}C$ • 28% increase in average annual rainfall • Increase in evapotranspiration by 28% • 49% increase in the water yield
Khare et al. (2016)	Mandakini River Basin, Uttarakhand , India	Soil erosion	• Increase in the future rainfall has caused an increase in the soil erosion

Teklesadik et al. (2017) Teklesadik et al. (2017)	Upper Blue Nile	Discharge and evapotranspiration (ET)	• Projected changes in actual evapotranspiration (AET) were 2.3 and 3.6% for the mid and far future periods, respectively • Mean annual discharge was observed to be insignificant
Reshmidevi et al. (2018)	Malaprabha River basin, North Karnataka, India	Water balance	• 4.1% increase in ET • Irrigation demand is projected to increase by 7.7% • Decline in groundwater recharge by 7.3% • Streamflow projection showed a reduction in the average annual and monsoon flows • Possibility of water stress in the catchment in future
Nilawar and Waikar (2019)	Purna river basin, India	Streamflow and sediment concentration	• Increase in the average monthly streamflow 24.47 to 115.94 m^3/s whereas average monthly sediment concentration by 32.58 to 162.96 mg/l under Representative Concentration Pathway (RCP) 4.5 and 8.5 scenario
Chanapathi and Thatikonda (2020)	Krishna river basin, India	Water balance	• Increase in surface runoff, water yield, and streamflow by 50% under RCP 4.5 • These parameters may double under the RCP 8.5 scenario by the end of the century
Yamamoto et al. (2021)	Sumatra Island, Indonesia	Flood	• Increase in flooding • 3.3 times increase in flood inundation volume for 20-year return period
Yılmaz et al. (2022)	Coruh River, northeastern Turkey	Drought	• Decrease in annual precipitation by 15.46% to 8.74% • Frequency of hydrological drought durations will be higher under RCP 4.5 and RCP 8.5
Hao et al. (2022)	Kaidu River basin, North-west China	Snow melt runoff	• Decrease in runoff by 15% to 30% in 2085s
Shi et al. (2023)	Bahe River, Shaanxi Province, China	Streamflow and baseflow	• Streamflow was susceptible to precipitation • Baseflow was susceptible to PET • Climate change can increase the streamflow by 37–75% and baseflow by 90–147%

A comprehensive examination of various studies indicates that climate change has affected the hydrological cycle. However, it is essential to understand that the impacts of climate change are not uniform globally. Different regions are expected to experience diverse outcomes, leading to an uneven distribution of changes in the hydrological cycle. Certain regions may experience substantial reductions in precipitation, leading to drier conditions, while others may encounter significant alterations in the timing and intensity of wet and dry seasons (Camici et al., 2014; Khare et al., 2016; Pandey et al., 2016; Yılmaz et al., 2022). Arnell and Gosling (2014) tried to assess the implications of climate change for global river flood risk and found that there was a consistent increase in flood magnitude across Africa, Asia, South America, and North America and consistent decreases in flood magnitude was observed around the Mediterranean, in south-west Africa, Central America, central Europe and some parts of Russia. There was less consistency in change in other parts of the world, including Western Europe and much of North America.

Overall, the literature demonstrates that climate change has the potential to significantly alter the hydrological cycle, with implications for precipitation patterns, flood risk, and water availability. The uneven distribution of these changes emphasizes the importance of region-specific analysis and adaptation strategies to effectively manage the impacts of climate change on water resources and associated hazards.

2.2.2 Impact of Climate Change on Intensity Duration Frequency Curves

Climate change profoundly impacts urban catchments, leading to significant alterations in hydrological processes and posing challenges for water management in cities. The previous section has examined literature which focuses on the impact of climate change on a larger scale, like river basin, regional scale or global scale. However, these may not apply to urban areas. Research on the impact of climate change on urban catchments is still relatively scarce due to its requirement for a specific focus on small-scale urban catchments (typically less than 500 km^2) and short-duration rainfall (usually less than 1-h) (Willems et al., 2012). Acquiring short-duration rainfall data remains challenging, particularly in developing countries, where the process can be time-consuming and labour-intensive.

Drastic changes in climate during the last decades have resulted in frequent occurrences of extreme events/ disasters, including floods, drought, heat waves and landslides. The factors contributing to climate change have caused a sharp variation in the atmospheric variables, especially the temperature, causing an increase in the intensity and frequency of short-duration extreme rainfall (Cheng and AghaKouchak, 2014; Douglas and Fairbank, 2011; Kuo et al., 2015; Westra et al., 2014). Past studies have reported that the frequency and magnitude of extreme rainfall are increasing faster than the mean rainfall in Europe, Africa, and Asia (Vinnarasi and Dhanya, 2016; Vittal et al., 2013). Such an unanticipated increase in extreme rainfall results in the malfunctioning of stormwater infrastructure systems and thereby makes the cities and major infrastructures more vulnerable than in the past (Cheng et al., 2014; Mailhot et al., 2007; Sarhadi et al., 2016). The failure of stormwater infrastructure can be mainly attributed to the non-consideration of changing climate

and inappropriate anticipation of future rainfall scenarios (Agilan and Umamahesh, 2016; Willems et al., 2012; Zahmatkesh et al., 2015b). The consideration of extreme events in the infrastructure design is fulfilled using the intensity duration frequency (IDF) curves. Therefore, it is essential to design the hydraulic infrastructure taking into consideration of IDF curves, capturing extreme rainfall characteristics and, presumably, how these extreme rainfall characteristics will change over time. IDF curves were traditionally developed by fitting a suitable probability distribution to the annual maximum rainfall series (AMS) or partial duration series (Agilan and Umamahesh, 2017). It is developed based on the assumption that historical rainfall series are stationary. This means that the parameters of the probability distribution that describes rainfall data are time-invariant (Salas and Obeysekera, 2014; Simonovic et al., 2017; Willems et al., 2012). However, under changing climatic conditions, the hypothesis of stationarity of extreme hydrological events is no longer tenable (Cancelliere, 2017; Cheng et al., 2014; Cook et al., 2020; IPCC, 2007; Mohebbi et al., 2021; Salas and Obeysekera, 2014). Therefore, the credibility of the stationary methods are no longer valid. This has necessitated the need for integrating the dynamic behaviour of changing climate into the existing methodologies of IDF curve development.

Previous studies have shown a significant change in the IDF curves due to climate change, especially in urbanized areas. Lee et al. (2020) have observed an approximately 10% rise in the extreme rainfall intensities in Namyangju, South Korea. Studies have reported that the extreme precipitation would become more common by the 2050s in southern Ontario, Canada (Deng et al., 2015; Ganguli and Coulibaly, 2019; Mailhot et al., 2011). Mirhosseini et al. (2014) observed a 33-74% decrease in the rainfall intensity with duration less than 2-h for Alabama, United States. Kourtis et al. (2022) predicted an increase in the 1-h rainfall intensity by the year 2100 for Athens, Greece. According to several studies across the world, the climate change resulted in an increase in the rainfall intensities (Noor et al., 2018; Shrestha et al., 2017; Singh et al., 2016; de Souza Costa et al., 2019; Srivastav et al., 2014; Vu et al., 2018), whereas in other areas, the researchers have observed a decrease in the rainfall intensities (Herath et al., 2016; Paola et al., 2014). This non-uniformity in the rainfall intensities might be due to the variablity in the locations, climate scenarios and climate models used.

These discussions show that it is important to update the IDF curves by incorporating the changes in rainfall patterns associated with climate change (Dourte et al., 2013; Khazaei, 2021; Mohebbi et al., 2021; Switzman et al., 2017; Westra et al., 2014). The updated IDF curve will be helpful for policymakers and designers for constructing hydraulic infrastructures with adequate capacity (Gebru, 2020; Hosseinzadehtalaei et al., 2020; Requena et al., 2019).

Conventional IDF curve development methods are either based on univariate frequency analysis of rainfall or by empirical models developed for different regions. Sherman (1931) has proposed an empirical relation between average rainfall intensity I (inches/h) and duration D (min) that can be expressed as Eq. 2.1

$$I = \frac{a}{(D+b)^c} \tag{2.1}$$

where, a, b, and c are constants that vary with return periods and geographical regions. Bernard (1932) derived one of the earliest empirical IDF relationships, from which Kothyari and Garde (1992) developed a generalised empirical model for India. The authors analysed rainfall data from 78 rain gauge stations between 1950-1980 and generated IDF curves for the Indian subcontinent. Babu et al. (1979) analysed the rainfall characteristics of 42 rain gauge stations all over India and proposed an equation for obtaining the rainfall intensity for any duration and return period. One of the limitations of these models is that their parameters cannot be generalized and may be inconsistent for different locations (Singh and Zhang, 2007). It is also not valid for specific urban catchments where the extreme events are magnified due to complex topographical settings.

The IDF curve development is also possible through the univariate frequency analysis by considering only the rainfall intensity. Koutsoyiannis et al. (1998) had provided a statistical model for developing IDF curves using a probability distribution. Many studies carried out across the globe have utilized different probability distributions such as Generalised extreme value (GEV) distribution (Hassanzadeh et al., 2014; Lee et al., 2020; Mirhosseini et al., 2014), Gumbel distribution (Pereira et al., 2015; Simonovic et al., 2017), Weibull distribution (Dourte et al., 2013), and Normal distribution (Mamo, 2015). The univariate rainfall frequency analysis was widely used because the traditional statistical methods have difficulty in deriving the joint distributions of rainfall characteristics (intensity and duration) (Singh and Zhang, 2007). However, rainfall characteristics are correlated with each other, and hence univariate analysis may lead to over/under estimation of risk associated with the events (Yue et al., 2001).

The limitations of the univariate frequency analysis can be overcome by using multivariate analysis. The copula is a versatile approach for multivariate frequency analysis that avoids the assumption that the rainfall variables are independent or normally distributed, or have the same marginal distributions. Copulas have been widely used in hydrology for drought analysis (Zhao et al., 2021), risk assessment of compound floods (Bevacqua et al., 2017; Jane et al., 2020; Moftakhari et al., 2019), analysis of rainfall characteristics (Kao and Govindaraju, 2007; Wang et al., 2010), and dependence modeling of hydroclimatic variables (Uttarwar et al., 2020; Xu et al., 2014). Apart from this Vinnarasi and Dhanya (2019), Bezak et al. (2016), Ariff et al. (2012), and Singh and Zhang (2007) have used copula for developing historical IDF curves.

2.3 Land Use and Land Cover Changes (LULC)

LULC changes occur predominantly intending to maximize the economic benefits for human activities. According to estimates, approximately 17% of the Earth's land surface has undergone at least one land cover change between the years 1960 and 2019 (Winkler et al., 2021). These changes have resulted in significant global transformations, including a loss of approximately 0.8 million square kilometres of forested areas and increased agricultural and urban lands (Arif et al., 2023; Winkler et al., 2021). These alterations are just some examples of the various changes that have occurred during this period (Kayitesi et al., 2022; Winkler et al., 2021). The drivers behind these

changes are influenced and amplified by various factors, including population growth, migration of people from rural to urban areas in search of employment and better living standards, education, deforestation, agriculture intensification, and so on (Roy et al., 2022).

Assessing the impact of LULC changes on hydrology is of utmost importance for effectively managing and developing watersheds. It is crucial to evaluate and understand how alterations in LULC patterns impact the hydrological processes within a watershed (Akpoti et al., 2016). Changes in LULC has found to alter the streamflow (Hurkmans et al., 2009), evapotranspiration (Kiptala et al., 2013), infiltration (Barron et al., 2012), surface runoff (Sajikumar and Remya, 2015; Shi et al., 2007), rainfall (Paul et al., 2016) and thereby the flood frequency (Du et al., 2012; Hamzah et al., 2021; Sahoo and Sreeja, 2013). Urbanization has been found to reduce the groundwater quality and quantity (Han et al., 2017; Salem et al., 2023; Siddik et al., 2022).

By 2050, the global urban population is expected to rise to 68% of the total population (Andimuthu et al., 2019; UN, 2019). Urbanization has increased the built-up area in cities, thereby increasing the impervious surface, reducing the infiltration and increasing the surface runoff (Arnone et al., 2018; Ramezani et al., 2023). Natural ground cover facilitates a 50% infiltration of stormwater and 40% evapotranspiration, whereas highly urbanized areas experience a significant increase in runoff, reaching up to 45% (Sohn et al., 2020). An increase in the built-up area has increased the temperature of the cities, thereby resulting in the urban heat island phenomenon (Bottyán et al., 2005; Jamei et al., 2019). This increase in temperature also changes the precipitation pattern of the cities. These, along with improper drainage system, has increased the frequency of flooding in urban areas. Urbanization has increased flooding in cities even for very small rainfall events (Chen et al., 2017; Fletcher et al., 2013; Guan et al., 2015). Due to this reason, the drainage capacity needs to be increased to accommodate this runoff, which may not be economical (Sohn et al., 2020). Studies have shown that urbanization has reduced the efficiency of stormwater drainage systems (Bibi et al., 2023; Hussain et al., 2021; Neupane et al., 2021). A lot of research is being carried out to understand the consequences of urban development on the intricate dynamics of water within urban environments and also for examining the effects of urbanization on urban hydrological systems and processes (Chen et al., 2017; Miller and Hess, 2017; Sahoo and Sreeja, 2013; Sanyal et al., 2014; Suriya and Mudgal, 2012; Zope et al., 2016).

Accurate quantification of imperviousness plays a critical role in urban hydrologic analysis and the management of urban floods. Common examples of impervious surfaces include roads, building rooftops, parking lots, and other infrastructure elements. These impervious surfaces collectively are known as the total impervious area (TIA) in urban environments. The TIA can be further categorized into non-effective impervious area (NEIA) and directly connected impervious area (DCIA). NEIA refers to impervious surfaces that are not hydraulically connected, which do not contribute directly to stormwater drainage. On the other hand, DCIA is known as effective impervious area (EIA), representing the impervious surfaces that directly connect with stormwater drainage inlets. This means that EIA contributes directly to the flow of stormwater within the urban drainage system (Han and Burian, 2009; Sahoo and Sreeja, 2013; Yang et al., 2018).

Given the projected increase in the global urban population, the challenges posed by urban-

ization on hydrology are expected to intensify. Urban stormwater management becomes crucial to mitigate the adverse impacts of impervious surfaces, increase infiltration, and manage surface runoff effectively. Accurate quantification of imperviousness, such as distinguishing between effective and non-effective impervious areas, is essential for urban hydrologic analysis and flood management. In conclusion, the impact of LULC changes on hydrology is significant and require careful assessment and management. Urbanization, in particular, has led to numerous alterations in hydrological processes, necessitating effective urban stormwater management strategies. By adopting appropriate measures, it is possible to mitigate the negative impacts of urbanization on hydrology and promote sustainable urban development. Insufficient or inadequate management of urban water can result in a range of social, economic, and environmental issues.

2.4 Urban Flooding

In urban areas, one common type of flooding is pluvial flood, which typically occurs when the volume of runoff exceeds the capacity of the storm sewer system to convey it effectively. During heavy rainfall events, the rainfall intensity and duration lead to an increased volume of runoff. If the storm sewer system cannot handle the excessive runoff, water accumulates on the streets, sidewalks, and other urban surfaces, resulting in pluvial flooding. This type of flooding is often characterized by rapid onset and short duration (Naulin et al., 2013). Gupta and Nair (2011) observed that flooding in urban areas occurs faster due to high flow, within minutes and flood peaks are three times larger compared to rural floods.

Over the past few decades, significant efforts have been made to enhance the accuracy and efficiency of urban flood modeling methodologies (Chen et al., 2009; Guinot et al., 2017; Hénonin et al., 2013; Sreeja and Gupta, 2006). Urban flood modeling involves various complex processes and interactions between various atmospheric, surface, and sub-surface components, and it is necessary to capture various hydrologic and hydraulic processes, including rainfall-runoff transformation, overland flow routing, and pipe flows (Shrestha et al., 2022). Several models are available for urban flood modeling. However, researchers still face several challenges in urban flood modeling. The main challenge involves availability and quality of data (Horritt and Bates, 2001; Hosseinzadehtalaei et al., 2020; Rafieeinasab et al., 2015), model complexity, lack of data for calibration and validation (Fu et al., 2011; Ghosh and Mujumdar, 2006; Wang et al., 2018b; Willems et al., 2012), climate change (Denault et al., 2006; Olsson et al., 2009; Rangari et al., 2021; Vinnarasi and Dhanya, 2019; Zahmatkesh et al., 2015b), urbanization (Chen et al., 2017; Miller and Hess, 2017; Sahoo and Sreeja, 2013; Sanyal et al., 2014; Suriya and Mudgal, 2012; Zope et al., 2016) and so on. Addressing these challenges is crucial for developing robust and reliable urban flood models supporting effective flood risk management strategies, urban planning, and infrastructure design. Continued research, interdisciplinary collaboration, and stakeholder engagement are essential to enhance our understanding of urban flooding further and improve our ability to mitigate and adapt to its impacts.

2.5 Best Management Practices (BMPs)

Flooding in urban areas poses a substantial risk due to its potential for direct and indirect damages. Understanding the different sources of flood risk and implementing appropriate management strategies is crucial to minimize the socio-economic losses and environmental impacts associated with these events (Cea and Costabile, 2022). Flooding cannot be prevented, however, proper flood management strategies can reduce its impact and damage. Stormwater best management practices (BMPs) encompass engineered structures and planned actions implemented within the landscape to promote favourable hydrological conditions and improve water quality. In light of the growing global urban population, the proliferation of impermeable surfaces has led to heightened levels of stormwater runoff, posing risks to both populations and infrastructure in terms of flooding and degraded water quality.

Green infrastructure has recently gained popularity as a more sustainable and effective technique for mitigating urban floods. Green infrastructures are sustainability-based practices known by different names in different parts of the world. They are referred to as Water Sensitive Urban Design (WSUD) in Australia (Rashetnia et al., 2022), Low Impact Development (LID), Stormwater Control Measures (SCM), or Best Management Practices (BMPs) in the United States of America (USA) (Darnthamrongkul and Mozingo, 2021; Fletcher et al., 2014; de Macedo et al., 2022), Low Impact Urban Design and Development (LIUDD) in New Zealand (Zhang et al., 2022), Sponge City (SC) in China (Guan et al., 2021), Nature-based solutions (NBS) in Europe (Shkaruba et al., 2021), Compensatory Techniques (CTs) in France (Fletcher et al., 2014), and Sustainable Urban Drainage System (SUDS) in the United Kingdom (Fletcher et al., 2014). The LID aims to recreate the pre-development condition by enhancing the soil infiltration and delaying and lowering the runoff. LIDs are helpful in managing rainwater, thereby reducing the risks associated with stormwater problems. Different LIDs include green roofs, bio-retention, rain gardens, vegetative swale, permeable pavements, infiltration trenches, rain barrels, roof-top disconnection, and detention basins.

LIDs have been found to reduce the runoff volume, soil erosion, and pollutant load and improve water quality at local scales (Chen et al., 2019; Fan et al., 2022; Guo et al., 2021; Ma et al., 2019; Yang et al., 2022). In addition to these hydrological benefits, LIDs also improve the aesthetics of the city (Cheng and Wang, 2018; Ureta et al., 2021). LIDs were found to be an effective strategy for managing urban floods. Fig. 2.2 shows a conceptual sketch of a catchment with and without LID. Table 2.2 shows various studies conducted by researchers in different parts of the world in mitigating the runoff. Although LIDs are used to regulate stormwater, they indirectly contribute to increasing groundwater supplies, thereby mitigating the effects of droughts and aiding in the recycling and reuse of stormwater (Hawken et al., 2021). Azari and Tabesh (2022) has observed that LIDs have been found to increase sustainability and help in rehabilitating drainage networks. The literature review (table 2.2) clearly shows that the performance of LIDs varies with location. There is no 'one best' LID which can be recommended globally; hence, assessing the performance of LIDs on different watersheds is essential. The performance of LIDs depends on the various

local factors like topography, land use, rainfall characteristics, soil, (Kuller et al., 2019; Pour et al., 2020; Yang et al., 2022) and climate change could exacerbate this spatial heterogeneity.

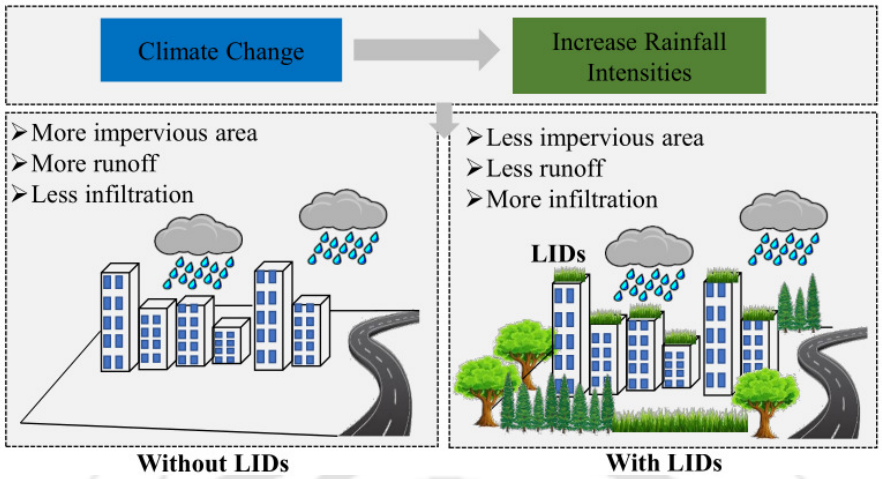

Figure 2.2: Conceptual diagram of a watershed with and without LID

Table 2.2: Synopsis of the studies on the efficacy of LID practices in the reduction in runoff

Author & Year	Study area	LIDs used	Best performing LID	Remarks
Yang et al. (2022)	Chaohu City, China	Green roof, Permeable pavement, and Bio-retention	N/A	Decreased the runoff volume and peak flow by 45–80%, 39–60% respectively.
Quichimbo-Miguitama et al. (2022)	Guayaquil, Ecuador	Green streets and Rain barrels	N/A	Reduction in peak flooding to 22% and 15% for short events and extreme events respectively.
Kumar et al. (2022b)	Qudesia Nallah watershed and Jahangirpuri drain watershed in Central Delhi, India	Green Roofs and Infiltration Trenches	N/A	22%–24% runoff reduction in the Qudesia Nallah watershed and 23%–26% in the Jahangirpuri drain watershed.
Saniei et al. (2021)	Darabad ,Tehran, Iran	Swale, Bio-retention, Permeable pavement and Detention pond	Permeable pavement	Reduction in the annual flooding by 55.96%.

Neupane et al. (2021)	Columbia, South Carolina, USA	Rain barrel, and Rain garden	Rain garden	Runoff reduction by 10%, 21%, and 32% for the rain gardens, rain barrels, and combination of the two respectively.
Abdelkebir et al. (2021)	Guelma watershed, Algeria	Permeable pavements, Rain gardens, Bioretentions, Rain barrel, and Infiltration trenches	Rain gardens	Reduced peak runoff by 54.7% and runoff volume by 75.2%.
Ömer Ekmekcioğlu et al. (2021)	Ayamama watershed, Turkey	Green roof, Bioretention, and Permeable pavements	Green roof	56.02% reduction in runoff for 10 years return period storm.
Akter et al. (2020)	Chittagong City, Bangladesh	Rain barrel	N/A	28.66% reducing in flood extent.
Palermo et al. (2020)	Paola, Italy	Permeable pavements and Green roof	N/A	45.8% and 54.3% reduction in runoff and peak flow rate respectively.
Saadatpour et al. (2020)	Tehran, Iran	Detention ponds	N/A	33% reduction in peak runoff for 10 years return period storm.
Ghodsi et al. (2020)	Tehran, Iran	Vegetated swale, Permeable pavement, Infiltration trench, and Bio-retention	N/A	18% reduction in flood volume.
de Macedo et al. (2019)	Sao Carlos, Brazil	Bio-retention	N/A	Reduced the runoff volume by 9-100%.
Zhu et al. (2019)	Nanjing, China	Permeable pavement	N/A	Reduced the surface runoff by 50%-95% and delayed the time to peak.
Taji and Regulwar (2019)	Aurangabad City, Maharashtra , India	Permeable pavements, and Rain barrel	Rain barrel	Permeable pavements performs satisfactorily in moderately urbanized areas and RWH is more effective in highly urbanised areas.

Bai et al. (2018)	Sucheng District, Jiangsu Province, China	Green roof, rain barrel, Permeable pavement, Rain garden, Infiltration trenches, Vegetable swale, and Bioretention cell	Infiltration based LIDs	Reduction in the peak flow rate by 32.5%, and flood volume by 31.8%.
Goncalves et al. (2018)	Joinville, Brazil	Infiltration trenches, Rain garden, and Detention pond	Infiltration trenches	Flood volume reduced between 30-75%.
Eckart et al. (2018)	Ontario, Canada	Bio-retention cell, Permeable pavements, Infiltration trenches, and Rain barrel	Infiltration trenches	Reduction in peak runoff by 13% and total runoff volume reduced by 29%.
Ahmed et al. (2017)	Johor, Malaysia	Infiltration trench	N/A	Reduction in peak flow in the range of 17.5–20.95%.
Ahiablame and Shakya (2016)	City of Normal-Sugar Creek Watershed, Central Illinois	Permeable pavements, Rain barrel, and Rain garden	Permeable pavement	3-47% reduction in runoff.
Palla and Gnecco (2015)	Colle Ometti,Genoa, Italy	Green roof, and Permeable pavement	N/A	Runoff peak and volume was reduced by 45% and 23% respectively.
Lee et al. (2013)	Cheon-an city, Korea	Infiltration trenches, Vegetated swales, Green roof, and Permeable pavements	N/A	6-16% reduction in peak runoff and 33–37% reduction in runoff volume.
Alfredo et al. (2010)	New York City, USA	Green roof	N/A	Reduction in peak flow by 30-78%.

Climate change has increased the intensity and frequency of precipitation, increasing the likelihood of flooding regularly. This has weakened the resilience of the cities causing damage to human life and properties (Qiao et al., 2020). Tavakol-Davani et al. (2016) has observed about a 12-18% increase in overflow in the stormwater drainage due to climate change. Kumar et al. (2021) found that a 20-year return period storm in present may become a 2-year return period storm in future due to climate change. This demonstrates the critical importance of improving the performance

of stormwater infrastructures to combat the threat of climate change. Alamdari et al. (2022) projected an increase in the annual average runoff by 10.6-28.2% for the Broad Run watershed in the city of Leesburg due to climate change. Urban areas are becoming more exposed to flooding due to climate change. Studies have identified that LIDs are tolerant to potential climate change (Li et al., 2022; Liu and Russo, 2021; Marando et al., 2022; Sohn et al., 2019), whereas few studies have found that climate change has reduced the performance of LIDs (Hathaway et al., 2014; Yang et al., 2022). Climate change has added significant uncertainty to the design and implementation of LIDs. Similar studies should be carried out in different regions to ascertain localized effects on stormwater controls because the impact of climate change varies depending on location.

2.6 Critical Appraisal of Literature Review

The vulnerability of urban areas to flooding is on the rise, resulting in severe consequences in terms of loss of life and property. It is crucial to accurately assess urban flood processes and enhance pre-disaster mitigation strategies in at-risk areas. Urban flood modelling enables users to comprehend, evaluate, and predict flood conditions and their potential impact. By utilizing such modelling techniques, stakeholders can gain valuable insights to inform decision-making, enhance preparedness, and implement effective measures to mitigate the impact of urban flooding. Figure 2.3 shows the summary of the literature review.

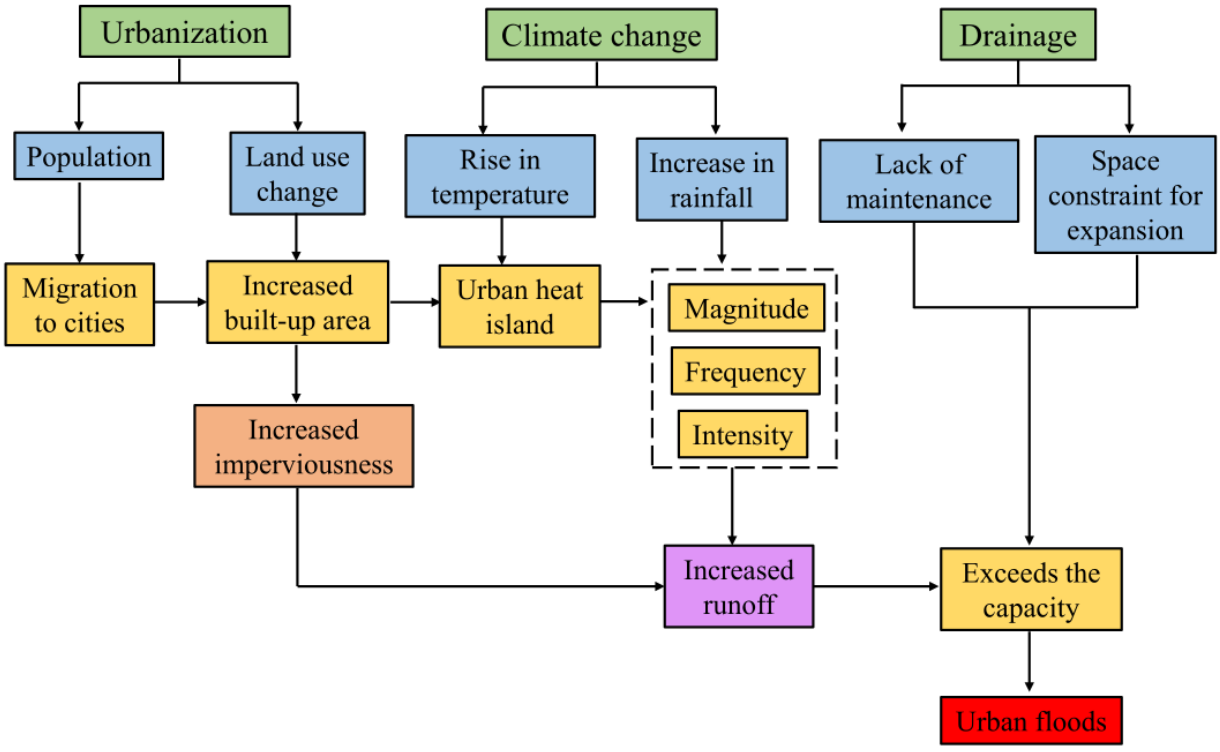

Figure 2.3: Summary of the literature review

Climate change, which is at its peak in most parts of the world can be studied using climate models. Despite the advancement in computational frameworks, the direct use of climate models

in urban applications is still limited due to their coarser resolution. Nevertheless, it is essential to note that these models exhibit high uncertainty, influenced by the choice of models and downscaling methods employed. This uncertainty is particularly pronounced when examining rainfall extremes, as the characteristics of extreme events may not necessarily align with those of average precipitation patterns.

Studies have shown that climate change has significantly escalated the intensity and frequency of short-duration extreme rainfall events. Urban impact studies use short-duration extreme rainfall incorporated in designing infrastructure through IDF curves. These curves provide a framework for considering the intensity, duration, and frequency of extreme events when designing infrastructure systems. Traditionally, IDF curves are developed based on some empirical equations or univariate analysis (considering only the rainfall intensity). But rainfall intensity and duration are interdependent so univariate analysis may underestimate the IDF curves.

Urbanization is occurring rapidly and at a faster rate globally. Urbanization is found to change the hydrological processes of an urban catchment. Urbanization in terms of imperviousness plays a crucial role in urban flood modelling, which is highly site specific and challenging to measure directly. As a result, it is not easily transferable to other cities with diverse urban sprawl characteristics. The unique characteristics and composition of urban areas, including variations in land use, infrastructure, and surface materials, make it necessary to consider site-specific data and measurements when incorporating imperviousness into flood models. The heterogeneity of urban sprawl further emphasizes the need for localized approaches and tailored data collection to assess and model the imperviousness factor in different cities accurately.

There is a growing concern regarding climate change and urbanization globally. As a result, there has been a significant increase in the number of hydrological impact studies related to land use and climate change in recent years. However, these studies predominantly assess the risks of floods and droughts at the river catchment scale. Research on the impacts of land use and climate change on urban flooding in India is currently lacking and remains relatively limited. This is partly due to the requirement for a specific focus on small urban catchment scales and also requires fine-resolution data.

Flooding in urban areas presents a significant risk, causing direct and indirect damages. To minimize the socio-economic losses and environmental impacts associated with urban floods, it is essential to understand the various sources of flood risk and implement appropriate management strategies. While flooding cannot be wholly prevented, its impact and damage can be reduced through proper flood management strategies. Stormwater best management practices (BMPs) encompass engineered structures and planned actions to improve hydrological conditions and water quality. However, the proliferation of impermeable surfaces in urban areas has led to increased stormwater runoff, aggravating the flood risk and degraded water quality. To address these challenges, green infrastructure has emerged as a sustainable and practical approach for mitigating urban floods.

Chapter 3

Description of the Study Area, Datasets, and Preliminary Rainfall Analyses

3.1 General

The present study aims to understand the impact of land use and climate change on urban flood characteristics. For this purpose, Guwahati, one of the largest and fastest-growing cities in north-east India is chosen as the study area. The city is particularly susceptible to flooding during the monsoon season. Urbanization, climate change and improper maintenance of drainage systems have increased the frequency and intensity of flooding in the city. The city lies on the bank of the Brahmaputra River, which overflows during heavy rain, causing widespread flooding in low-lying areas of the city. This chapter describes the geographic and climatic details of the study area along with the various data collected for the analysis. This chapter also includes an preliminary analysis aimed at comprehending the trends within the historical rainfall data.

3.2 Description of Study Area

The study area, which is a highly urbanized part of Guwahati, Kamrup District, Assam, North-east (NE) India, with a geographic area of 227.81 km^2 situated on the bank of river Brahmaputra, is depicted in Fig. 3.1. It is located between $26°4'45''N$ and $26°13'25''N$ Latitude and $91°34'25''E$ and $91°52'00''E$ Longitude. Guwahati is one of the most populous and rapidly growing cities in north-eastern India, located on an undulating plain at an elevation ranging from 49.5 to 55.5 m above mean sea level (MSL). The city is surrounded by hills in the southern and eastern parts. The city has several water bodies and wetlands, which are under threat due to encroachment and unplanned urban development. Guwahati has a subtropical and humid climate with an average annual rainfall of 1701 mm. The study area has been experiencing flooding due to water logging triggered by heavy rainfall.

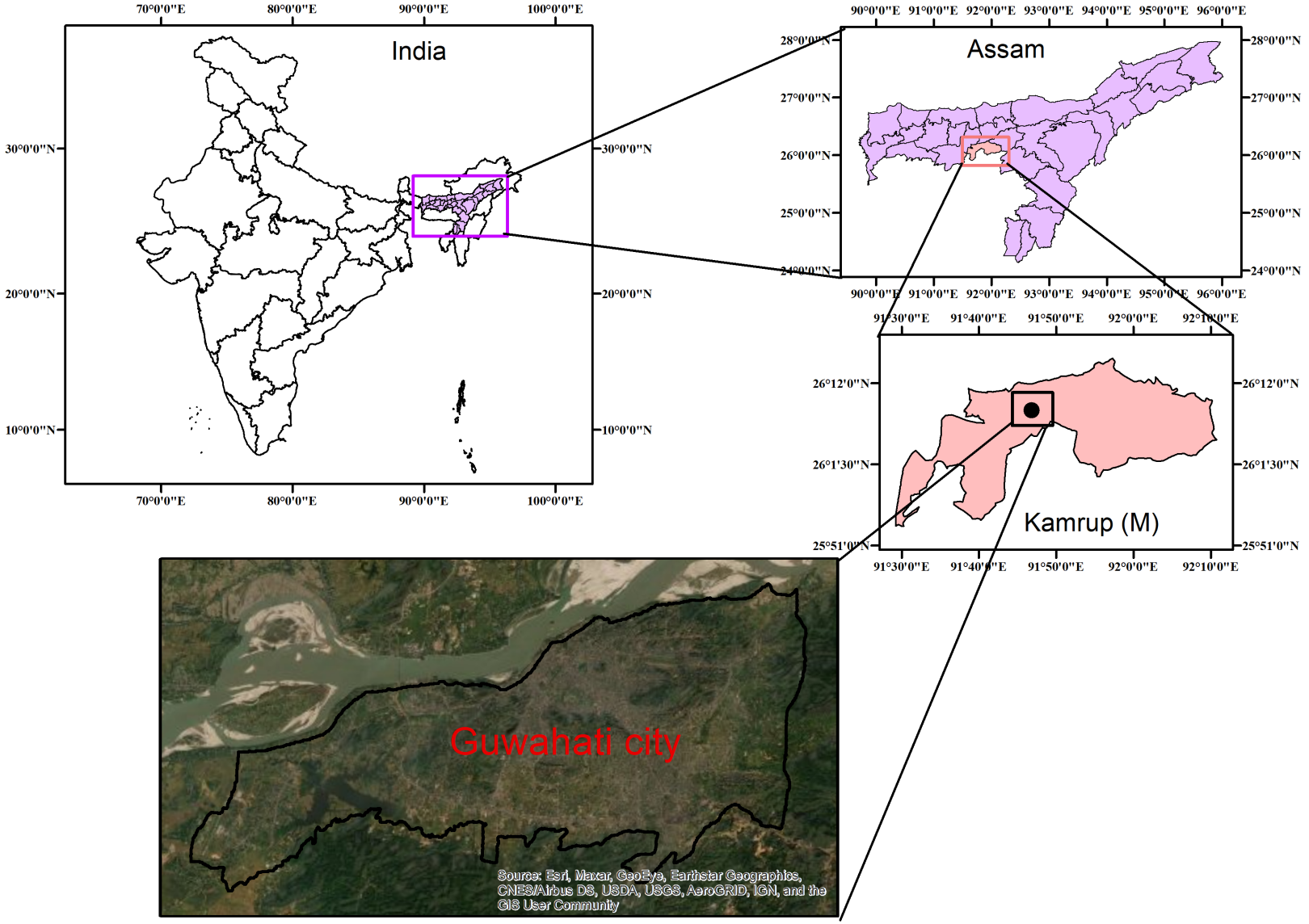

Figure 3.1: Location of Guwahati city

Figure 3.2 shows the annual maximum rainfall (AMR) of Guwahati city for a period of 37 years from 1981-2017. The AMR in the study area were categorized into three groups: (i) moderate (5-100 mm/day), (ii) heavy rain (HR) (100-150 mm/day), and (iii) Very High Rainfall (VHR) ($\geq$ 150 mm/day). The selection of boundary values for each category was based on the study of Rajeevan et al. (2008). It is evident from Fig.3.2 that Guwahati city has experienced HR about 14 times and VHR, four times (1985, 1991, 2011, and 2014), over the last 37 years. In the recent years, the pluvial flooding has increased in Guwahati, which serves as a motivation to investigate the effect of climate and land use change on flooding. The output from the study is very important while planning for the city's future expansion.

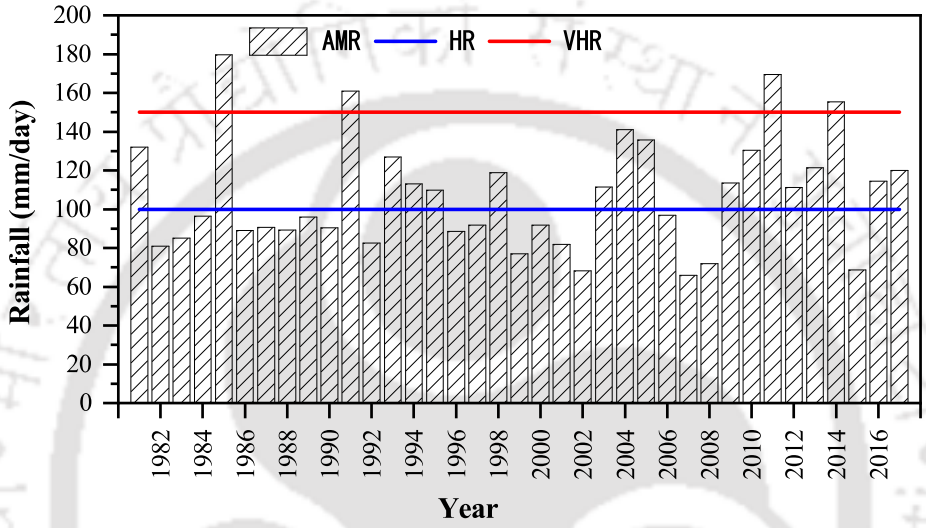

Figure 3.2: Representation of annual maximum rainfall (AMR) of the study area for 37 years period from 1981-2017 (Heavy rainfall (HR) and very high rainfall (VHR))

Extreme rainfall is influenced by natural variations in climate, large-scale factors like global warming, or local factors like urbanization (Vittal et al., 2016). Global warming is projected to cause a non-uniform increase in extreme rainfall in urban areas (IPCC, 2021). The Clausius-Clapeyron (CC) relationship suggests that a rise of 1°C in atmospheric temperature results in an approximately 7% increase in the water holding capacity of an air parcel (Trenberth, 2011). Extreme rainfall is found to exhibit temporal clustering at multi-decadal time scales, and this can be linked to the large-scale, low-frequency oscillations in atmospheric circulation (Sudharsan et al., 2020; Willems, 2013). Studies have observed that extreme rainfall is influenced by large atmospheric circulations and teleconnections, such as El Nino Southern Oscillations (ENSO), North Atlantic Oscillations (NAO), Madden-Julian Oscillation (MJO), and Indian Ocean Dipole (IOD) (Gupta et al., 2003; Lenka et al., 2022; Samantaray and Gouda, 2023). Population aggregation and the expansion of impervious surfaces associated with urbanization lead to modifications in land use or cover, thereby disrupting the wind patterns and exchanges of water, aerosol, and heat between the atmosphere and land (Golroudbary et al., 2017; Kaufmann et al., 2007; Zhang et al., 2019). These could be the possible reason for the increase in number of extreme rainfall in the study area.

3.2.1 Watershed Delineation

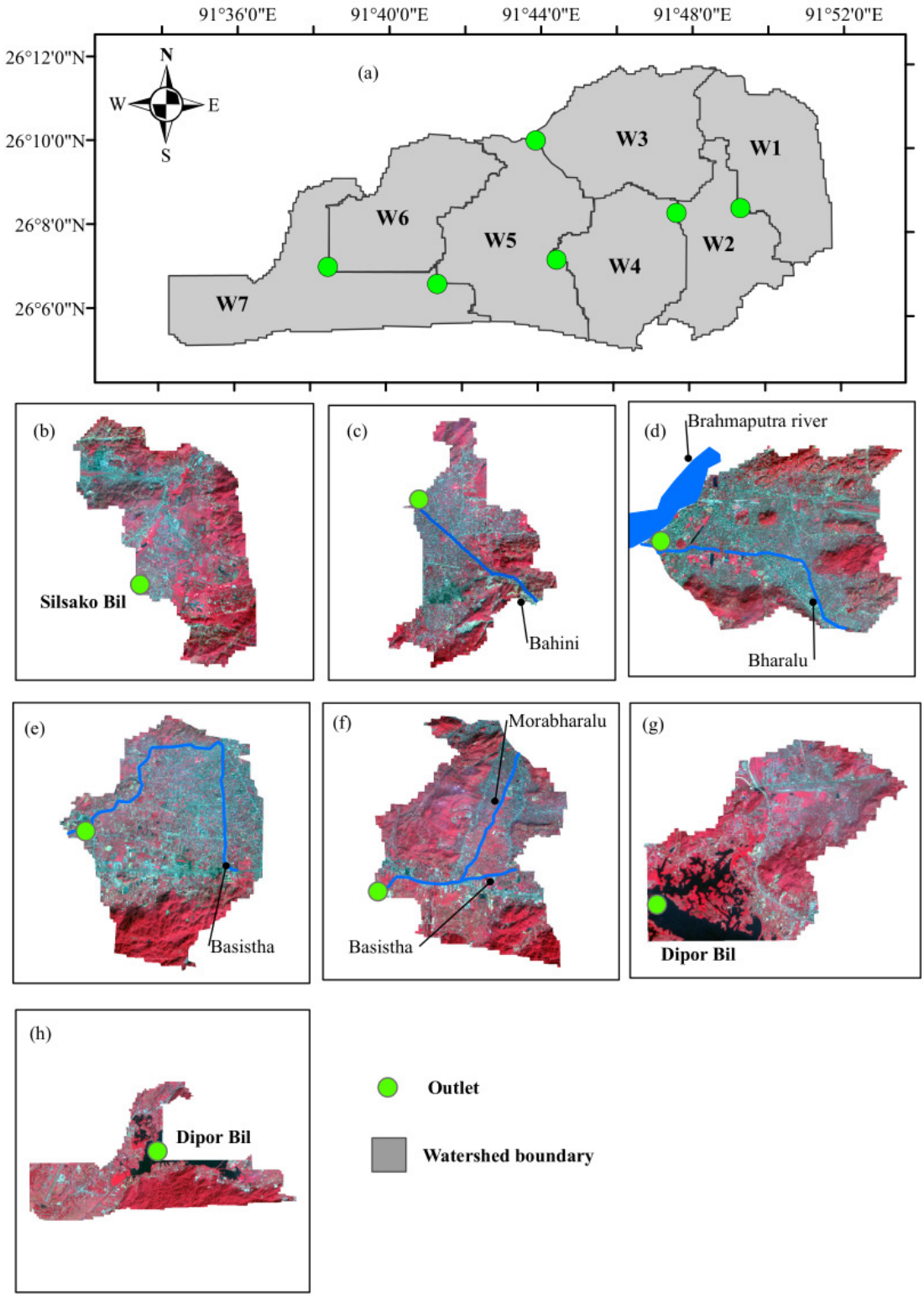

Figure 3.3: Details of watersheds of Guwahati city (a) seven watersheds of the city, (b) watershed 1, (c) watershed 2, (d) watershed 3, (e) watershed 4, (f) watershed 5, (g) watershed 6, and (h) watershed 7

The Guwahati city is delineated into seven watersheds using ArcGIS, as shown in Fig. 3.3 (a). Each watershed is again divided into 87 smaller sub-watersheds. Fig. 3.3(b) represents watershed 1, which covers an area of 28.15 km^2, includes military area, refinery, industrial townships, and substantial portions of Narkalbari and Sunsili hills. It drains into a wetland named Silsako Bil Lake, which is further subdivided into 22 sub-watersheds. Watershed 2 consists of 14 sub-watersheds with an area of 22.89 km^2 as shown in Fig. 3.3(c). Most of the storm water from this watershed is carried away by the riven Bahini, which is a tributary of river Bharalu. Fig. 3.3(d) depicts the watershed 3, which is the most urbanized and flood prone part of the study area with a catchment area of 28.3 km^2. Divided into 14 sub-watersheds, it covers residential, commercial, institutional, and business areas. River Bharalu carries the stormwater from this watershed and discharges it to river Brahmaputra. Watershed 4 having an area of 23.45 km^2 is divided into 14 sub-watersheds and is shown in Fig. 3.3(e). Watershed 5 has a catchment area of 40.2 km^2, which is subdivided into 10 sub-watersheds as shown in Fig. 3.3(f). Stormwater from watershed 4 reaches watershed 5 through the Basistha River, and it joins the river Morabharalu and finally discharges into a permanent freshwater lake, Dipor Bil. Fig. 3.3(g) shows the watershed 6 having 5 sub-watersheds, which is located in the southern part of Guwahati city with an area of 25.8 km^2 and covers a major portion of Dipor bil (outlet point). Watershed 7, divided into 8 sub-watersheds, is shown in Fig.3.3(h) with an area of 33.2 km^2. It drains into Dipor bil. It is located in the southern part of Guwahati city and Lokpriya Gopinath Bordoloi International Airport is located in this watershed.

3.3 Description of Data

The list of the collected data is given as follows:

(i) Rainfall

Daily and 15-minutes rainfall data for a period of 37 years from 1981-2017 of Guwahati city was collected from the Regional Meteorological Centre, Guwahati. The rainfall variability for all the twelve months is shown in Fig. 3.4. It is evident from the figure that Guwahati experiences the highest amount of rainfall in the month of July and lowest amount of rainfall in the month of December. Table 3.1 shows the distribution of rainfall over different seasons, and around 63% of the total rainfall in the city can be attributed to the monsoon season.

Table 3.1: Percentage of rainfall during different seasons

Season	Period	Percentage of rainfall
Premonsoon	Mar-May	28
Monsoon	Jun-Sep	63
Postmonsoon	Oct-Nov	7
Winter	Dec-Feb	2

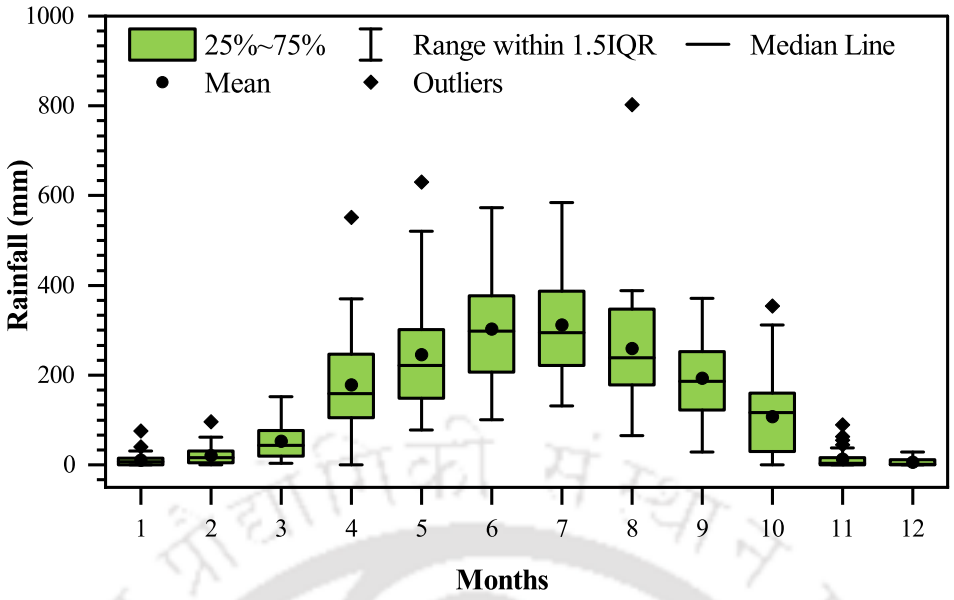

Figure 3.4: Variation of rainfall over Guwahati city in different months

Six rain events were selected from the 15-min rainfall data for event-wise rainfall-runoff analysis. The details of events are given in table 3.2, and the rainfall hyetographs for these events are shown in Fig. 3.5.

Table 3.2: Details of rainfall events

S. No.	Date	Time span (hr:min)	Designation
1	Jul-09-1985	14:00	RE-1
2	Jul-09-1990	02:00	RE-2
3	Aug-25-1994	5:15	RE-3
4	Apr-26-1997	01:30	RE-4
5	Jun-23-2013	2:00	RE-5
6	Jun-17-2016	04:45	RE-6

(ii) Global climate model (GCM) data

The CMIP5 (Coupled Model Intercomparison Project 5) GCM is a comprehensive set of experiments prepared by the World Climate Research Programme's working group on coupled modelling. The outputs were available in NetCDF format. Daily precipitation data of the 14 GCM outputs of the Coupled Model Intercomparison Project 5 (CMIP5) were downloaded from `https://esgf-data.dkrz.de/projects/esgf-dkrz/`. Table 3.3 shows the details of the GCMs used in this study. The Intergovernmental Panel on Climate Change (IPCC), in its fifth assessment report (AR5), developed the greenhouse gas scenario called representative concentration pathway (RCP). RCP is defined by four benchmark scenarios representing the concentration pathways of GHGs and the radiative forcing in 2100. Radiative forcing is the imbalance between the incoming and outgoing energy in the earth's

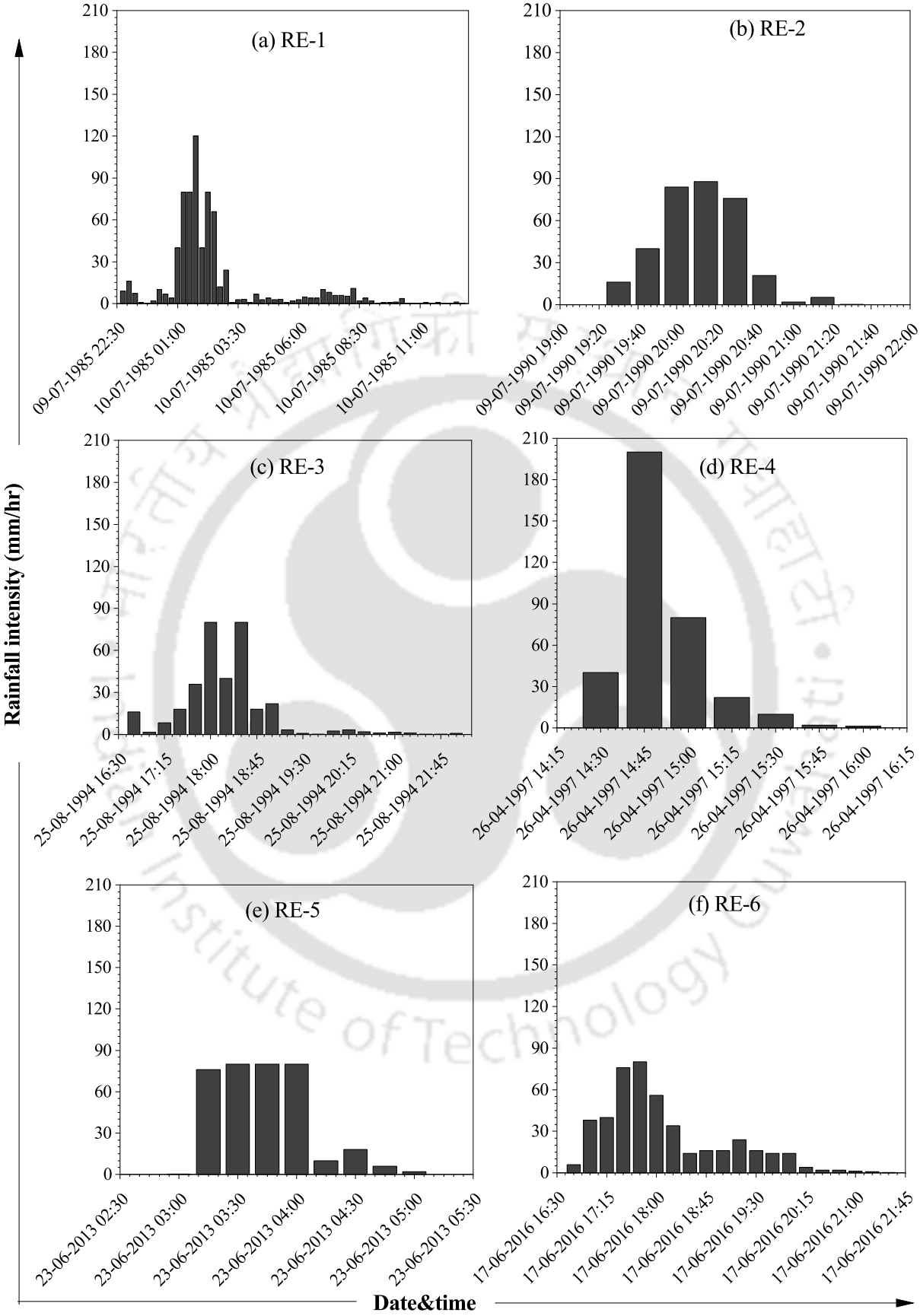

Figure 3.5: Rainfall hyetographs for (a) RE-1, (b) RE-2, (c) RE-3, (d) RE-4, (e) RE-5, and (f) RE-6

atmosphere due to climate-altering factors. The four RCP scenarios, i.e. RCP 2.6, RCP 4.5, RCP 6.0 and RCP 8.5, are summarized in table 3.4. In this study, the future rainfall scenarios are divided into three different periods: 2021-2047 (P1), 2048-2074 (P2), and 2075-2100 (P3) and four RCP scenarios are also used.

Table 3.3: Details of GCMs used for downscaling of climate data

Model Name	**Modelling Institution**	**Future Climate Scenarios**	**Spatial resolution (Lon x Lat, degree)**
BCC-CSM 1.1(m)	Beijing Climate Center, China Meteorological Administration	RCP 2.6, RCP 4.5, RCP 6.0, RCP 8.5	2.81 x 2.81
BNU-ESM	College of Global Change and Earth System Science, Beijing Normal University	RCP 2.6, RCP 4.5 RCP 8.5	2.81 x 2.81
CanESM2	Canadian Centre for Climate Modelling and Analysis, Canada	RCP 2.6, RCP 4.5 RCP 8.5	2.81 x 2.81
CMCC-CM	Euro-Mediterraneo sui Cambiamenti Climatici, Italy	RCP 4.5, RCP 8.5	0.75 x 0.75
CMCC-CMS	Euro-Mediterraneo sui Cambiamenti Climatici, Italy	RCP 4.5, RCP 8.5	1.875 x 1.8
CNRM-CM5	Centre National de Recherches Meteorologiques, Meteo-France, France	RCP 2.6, RCP 4.5, RCP 8.5	1.4 x 1.4
GFDL-ESM2G	NOAA Geophysical Fluid Dynamics Laboratory, USA	RCP 2.6, RCP 4.5, RCP 6.0, RCP 8.5	2.5 x 2.0
GFDL-ESM2M	NOAA Geophysical Fluid Dynamics Laboratory, USA	RCP 2.6, RCP 4.5, RCP 6.0, RCP 8.5	2.5 x 2.0
INM-CM4	Institute for Numerical Mathematics, Russia	RCP 4.5, RCP 8.5	2.0 x 1.5
IPSL-CM5A-LR	Institut Pierre-Simon Laplace, France	RCP 2.6, RCP 4.5, RCP 6.0, RCP 8.5	3.75 x 1.89
IPSL-CM5B-LR	Institut Pierre-Simon Laplace, France	RCP 4.5, RCP 8.5	3.75 x 1.89
MPI-ESM-LR	Max Planck Institute for Meteorology, Germany	RCP 2.6, RCP 4.5, RCP 8.5	1.875 x 1.8
MPI-ESM-MR	Max Planck Institute for Meteorology, Germany	RCP 2.6, RCP 4.5, RCP 8.5	1.875 x 1.8
NorESM1-M	Norwegian Climate Centre	RCP 2.6, RCP 4.5, RCP 6.0, RCP 8.5	2.5 x 1.89

Table 3.4: Summary of RCP scenarios

RCP scenarios	Description
RCP 8.5	Rising radiative forcing pathway leading to 8.5 W/m^2 in 2100
RCP 6.0	Stabilization without overshoot pathway to 6 W/m^2 at stabilization after 2100
RCP 4.5	Stabilization without overshoot pathway to 4.5 W/m^2 at stabilization after 2100
RCP 2.6	Stabilization without overshoot pathway to 2.6 W/m^2 at stabilization after 2100

(iii) Infiltration details

The Green Ampt model is used in this study to model the infiltration characteristics of the study area and the required details are collected from Sahoo (2014), and table 3.5 shows the parameters of the Green Ampt infiltration model.

Table 3.5: Green Ampt model infiltration parameters for Guwahati city

Watershed No	Conductivity (mm/h)	Moisture deficit
1	64.8	0.35
2	46.9	0.305
	30.24	0.314
3	19.44	0.253
	72	0.344
	75.6	0.385
4	50.4	0.232
	46.8	0.305
5	46.8	0.273
	6.48	0.272
6	61.2	0.343
	6.48	0.354
7	60.12	0.361
	25.2	0.282

(iv) Topographic data

For the quantification of the land use changes in the study area, satellite images of different years were procured from the National Remote Sensing Centre (NRSC), India, and the details are given in table 3.6.

Table 3.6: Details of satellite images

S. No.	Date of Imagery	Spatial Resolution	Satellite
1	11-Nov-2011	5.8 m	LISS-4, Resourcesat-2
2	05-Mar-2013	5.8 m	LISS-4, Resourcesat-2
3	18-Jul-2017	5.8 m	LISS-4, Resourcesat-2A
4	16-Jan-2020	5.8 m	LISS-4, Resourcesat-2A
5	10-Jan-2022	5.8 m	LISS-4, Resourcesat-2A

(v) Other data

The details of other data collected are listed in table 3.7

Table 3.7: Details of other data collected

S.No.	Data	Agency
1	Natural drainage network	Guwahati East Water Resources Division
2	Man-made drainage network	Guwahati Metropolitan Development Authority (GMDA)
3	Building footprints	GMDA
4	Contour map (5m interval)	GMDA
5	Road networks	GMDA

3.4 Trend Analysis of Historical Rainfall Data

In order to understand the climate change taking place in the study area, historical rainfall data analyses was carried out as a preliminary step. This will help in understanding the trends in past rainfall data, which aids in determining the pattern of climate changes. Various methods used for understanding the rainfall characteristics are discussed in the following sub sections.

3.4.1 Mann–Kendall Test (MK)

The Mann–Kendall test (MK) (Kendall, 1957; Mann, 1945) is used to identify any monotonic trend in the time series data. The null hypothesis is defined as the absence of a trend in the data series. The test statistics $\mathcal{S}$ is given as Eq. 3.1

$$\mathcal{S} = \sum_{j=1}^{z-1} \sum_{j=j+1}^{z} sgn(x_j - x_i) \tag{3.1}$$

where z is the number of data points, x_i and x_j are the data values in the series i and j, respectively (where $j > i$)

$sgn(x_j - x_i)$ is given as Eq. 3.2

$$\text{sign}(x_j - x_i) = \begin{cases} -1 & \text{if } (x_j - x_i) < 0 \\ 0 & \text{if } (x_j - x_i) = 0 \\ +1 & \text{if } (x_j - x_i) > 0 \end{cases} \tag{3.2}$$

The variance of S is given as Eq. 3.3

$$V(\mathcal{S}) = \frac{z(z-1)(2z+5) - \sum_{i=1}^{m} t_i(t_i-1)(2t_i+5)}{18} \tag{3.3}$$

where m is the number of tied groups (a group of sample data having the same value) and t_i is the number of ties for time-extend i.

If $z > 10$, then the data can be assumed to follows a normal distribution and the standardized test statistic Z is computed using Eq. 3.4

$$Z = \begin{cases} \dfrac{\mathcal{S}-1}{\sqrt{Var(\mathcal{S})}} & \text{if } \mathcal{S} > 0 \\ 0 & \text{if } \mathcal{S} = 0 \\ \dfrac{\mathcal{S}+1}{\sqrt{Var(\mathcal{S})}} & \text{if } \mathcal{S} < 0 \end{cases} \tag{3.4}$$

A positive/negative value of Z indicates increasing/decreasing trends. A specific significance level α_s confirms the monotonic trend in the data series.

3.4.2 Sen's Slope Estimator (SS)

Sen's slope (SS) is a simple non-parametric test developed by Sen (1968) for time series having a linear trend. This test estimates the change per unit time (true-slope). For N pairs of data, the slope (Q_i) can be calculated as Eq. 3.5

$$Q_i = \frac{x_j - x_i}{j - i}; \quad i = 1, 2, ..., N \tag{3.5}$$

where x_j and x_i denotes the data values at times j and i respectively and $j > i$.

The median of these N values of Q_i is Sen's estimator and is calculated as a two-sided test with confidence interval (in this study 95% confidence) as Eq. 3.6

$$Q_{med} = \begin{cases} Q_{\frac{N+1}{2}} & \text{if N is odd} \\ \dfrac{Q_{\frac{N}{2}} + Q_{\frac{N+1}{2}}}{2} & \text{if N is even} \end{cases} \tag{3.6}$$

Positive and negative sign of Sen's slope indicates increasing and decreasing trends, respectively. The MK test evaluates the statistical significance of Sen's slope.

3.4.3 Trend Results

The trend analysis results are presented in table 3.8. The analysis indicates that there is no significant trend in annual and seasonal rainfall, except for the winter season, where a decrease in trend is observed for both annual and extreme precipitation. The Sen's slope (SS) estimator shows a non-significant decrease in annual rainfall by 3.183 mm/year. However, pre-monsoon and post-monsoon rainfall exhibit an increasing trend. In the case of monsoon annual rainfall, there is a non-significant decrease of 4.423 mm/year. This decrease in monsoon rainfall suggests a possible shift in rainfall from the monsoon season to the pre-monsoon and post-monsoon seasons. The extreme rainfall has no trend as per the MK test and very negligible increasing trend for annual, monsoon and post-monsoon and very negligible decreasing trend for pre-monsoon season in terms of Sen's slope. However, in winter, the MK test shows a significant decreasing trend in the extreme rainfall at a rate of 0.415 mm/year. To summarize, the trend analysis indicates no significant trends in annual and seasonal rainfall, except for a decreasing trend in winter. There is a shift in rainfall from the monsoon season to the pre-monsoon and post-monsoon seasons.

Table 3.8: Trend analysis results of MK and SS

Test	Annual		Pre-monsoon		Monsoon		Post monsoon		Winter	
	Ann.	Extr.	Ann.	Extr.	Ann.	Extr.	Ann.	Extr.	Ann.	Extr.
MK	0	0	0	0	0	0	0	0	0	-1
SS	-3.183	0.178	0.779	-0.083	-4.423	0.019	2.744	0.637	-0.848	-0.415

Sen's Slope (SS in mm/year), -1 = decreasing trend, 1 = increasing trend, 0 = no trend

3.4.4 Segmentation of Rainfall Time Series Using Gath-Geva (GG) Segmentation Algorithm

The section tried to segment the time-series data to seasons based on a data-driven method instead of defining the crisp bounds. Time series segmentation is the clustering of the time series data with a time-ordered structure. The clustering method considered in this study is the modified Gath-Geva clustering algorithm (Abonyi et al., 2005) which can also be referred to the fuzzy maximum likelihood clustering with probabilistic principal component analysis. The clusters obtained from this method would be multivariate Gaussian functions. A Gaussian membership function is defined for homogeneous segmentation of the time-series data. The present study defines the shift or creep of the seasons as the movement of the centre of the segment/season with time, whereas the dispersion as the variation in the length of the segment/season with time. The trend in the monsoon season was investigated by averaging the climatic variables for each segment with a length ,where is the centre of a season and is the standard deviation at the timescale.

The fuzzy clustering algorithm was considered to segment the time series of climate data. The

clustering algorithm performs a simultaneous identification of local probabilistic principal component analysis (PPCA) models and measures the homogeneity of the segments (Abonyi et al., 2005). The algorithm favours contiguous clusters in time and can detect changes in the hidden structure of multivariate time-series. The details of the GG segmentation algorithm are as follows.

Consider a time series of n samples denoted as $T_n = x_k | 1 \leq k \leq n$ where $k = 1, 2, ..., n$ and $x_k = [x_{1,k}, x_{2,k}, ..., x_{n,k}]$ labelled by time points $t_1, t_2, ..., t_n$. The time series T is partitioned to c-segments represented as t_n where $1 \leq i \leq c$ which satisfies $1 = t_{n0} < .... < t_{nc} = t_n$. The time points $t_{n0}, t_{n1}, ..., t_{nc}$ and the interval $[t_{i=1}, t_{ni}]$ are the segment boundaries and segments respectively. The crisp segmentation cost is formulated as an optimization problem that minimises the segment's variance resulting in the following Eq. 3.7 (Abonyi et al., 2005; Wang et al., 2011a)

$$Cost_{crisp}(t) = \sum_{k=1}^{N} \sum_{i=1}^{c} \beta_i(t_k) D^2(x_k, v_i^x) \tag{3.7}$$

where $D^2(x_k, v_i^x)$ is the distance between the centre of the i^{th} cluster (v_i^x) and x_k data point. $\beta_i(t_k) \in 0, 1$ stands for the crisp membership of the k^{th} data point in the i^{th}segment and can be written as Eq. 3.8

$$\beta_i(t_k) = \begin{cases} 1 & \text{if } \; t_{n_{i-1}} < t_k < t_{n_i} \\ 0 & \textit{Otherwise} \end{cases} \tag{3.8}$$

Since defining a crisp boundary is not practical for most of the time series segmentation applications, Abonyi et al. (2005) have introduced a Gaussian membership function for the time series data. Within the Gaussian membership function $A_i(t_k)$, given by the Eq. 3.9 and the time coordinate is considered as an additional variable that divides the time series into fuzzy segments.

$$A_i(t_k) = exp\left[\frac{-1}{2} \frac{(t_k - v_i^k)^2}{\sigma_{i,t}^2}\right] \tag{3.9}$$

The new fuzzy segmentation parameter $\beta_i(t_k)$ is defined by Eq.3.10

$$\beta_i(t_k) = \frac{A_i(t_k)}{\sum_{j=1}^{c} A_j(t_k)} \in [0, 1] \tag{3.10}$$

The objective function is modified as the sum of the weighted squared distances between z_k and η_i where $z_k = [t_k, x_k^T]^T$ and η_i is the cluster prototype. The objective function (J) assumes that the data points can be modelled as a mixture of multivariate Gaussian distribution (Abonyi et al., 2005; Wang et al., 2011a). The objective function J is given by Eq. 3.11

$$J = \sum_{k=1}^{n} \sum_{i=1}^{c} (\mu_{i,k})^m \, D^2 \, (z_k, \eta_i) \tag{3.11}$$

where $\mu_{i,k}$ signifies the degree of membership of the observed data. m ($m \in [1, \infty)$) is the weighting component that decides the fuzziness of the cluster (usually $m = 2$). The distance $D^2(z_k, \eta_i)$ is inversely proportional to the probability of the data points z_k belongs to the i^{th} cluster. As the time variable t_k is independent of x_k, the distance measure $D^2(z_k, \eta_i)$ is defined as Eq. 3.12

$$p(z_k/\eta_i) = \frac{1}{D^2(z_k, \eta_i)} = \alpha_i \times p\left(t_k/\eta_i^t\right) \times p\left(x_k/\eta_i^x\right) \tag{3.12}$$

where, α_i is the priori probability of the cluster, $p(t_k/\eta_i^t)$ is the distance between k^{th} data point and the centre of the i^{th} segment (v_i^t), $p(x_k/\eta_i^x)$ is the distance between the cluster prototype (η_i) and the data in the feature space.

Abonyi et al. (2005) developed the GG clustering algorithm based time series segmentation using Lagrange multipliers, and the objective function ($\bar{J}$) is given by Eq. 3.13

$$\bar{J} = \sum_{k=1}^{n}\sum_{i=1}^{c}(\mu_{i,k})^m D^2(z_k, \eta_i) + \sum_{k=1}^{n}\lambda_k\left(\sum_{i=1}^{c}\mu_{i,k} - 1\right) \tag{3.13}$$

where λ_k is the Lagrange multiplier and $\mu_{i,k}$ is the membership degree of data point x_k to the i^{th} cluster ($i = 1, ..., c$) and $\mu_{i,k}$ is subjected to the following constraint given by Eq. 3.14

$$\mu_{i,k} \in [0, 1], \forall i, k; \;\; 0 < \sum_{k=1}^{n}\mu_{i,k}, \forall i; \;\; \sum_{i=1}^{c}\mu_{i,k} = 1, \forall k \tag{3.14}$$

3.4.4.1 Segmented Seasons Using Modified Gath-Geva Algorithm to Rainfall Data of Guwahati City

The rainfall data were averaged for every three years from 1980 to 2009. The parameters of the Gath-Geva algorithm were adjusted in such a way that the final number of segments is five for each observation period. The final segments were assumed to be the non-rainy, pre-monsoon, monsoon, post-monsoon, and non-rainy seasons. Fig. 3.6a and 3.6b shows the seasons obtained for every three years, from 1980 to 2009. For further analyses, the centre and standard deviation of each season on the time scale were determined. Corresponding to each season, the mean rainfall intensity was estimated for $\mu \pm 1.5 \times \sigma$, where μ is the centre of a season and σ is the standard deviation at the time scale and performed the trend analyses.

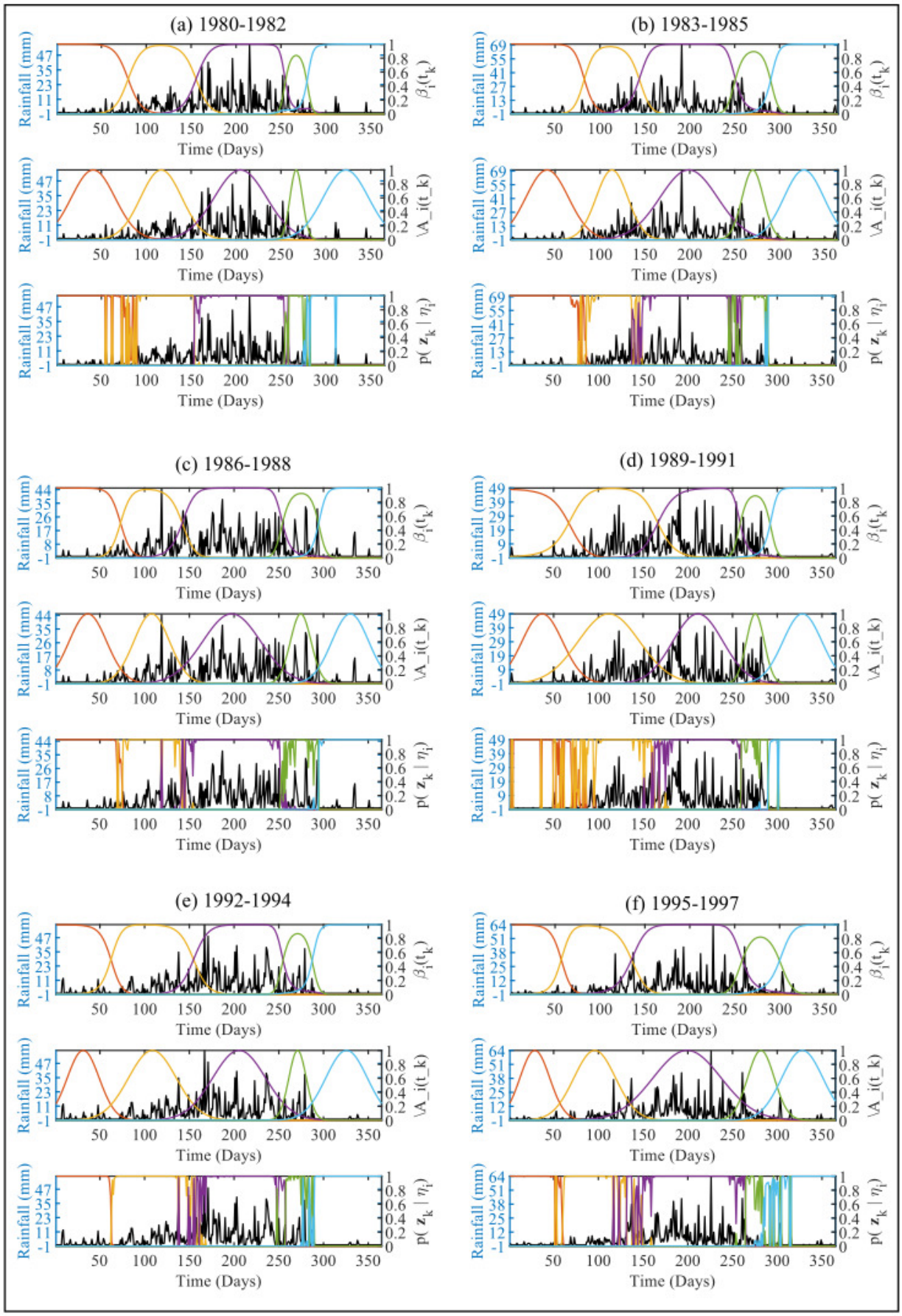

(a)

Figure 3.6: Final segments obtained after applying the modified Gath-Geva algorithm (Part 1)

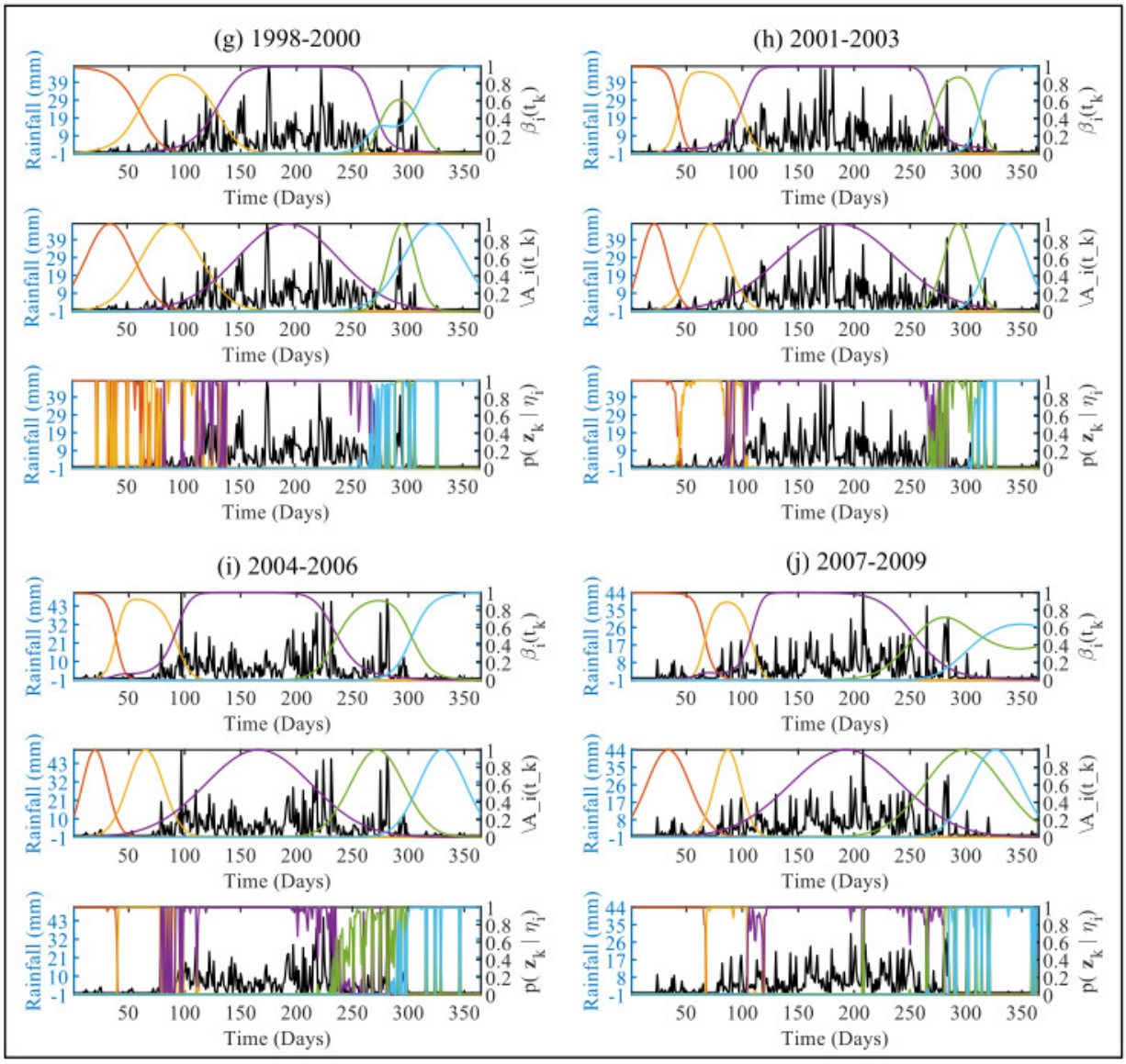

(b)

Figure 3.6: Final segments obtained after applying the modified Gath-Geva algorithm (Part 2)

The time series are segmented into five clusters and the shift, dispersion and trend in pre-monsoon, monsoon, and post-monsoon season is analyzed further. The shift is determined by tracking the movement of the position of the central tendency of the seasons over the years. The dispersion is measured through the coefficient of variation of the segment length (period of the season) over the years. The trend was also analyzed with the behaviour of the average rainfall within the segment over the years. The average was determined for a period within the segment of length, where μ is the centre of a season and σ is the standard deviation at the timescale.

The analysis of the deviation of the centre of the season with time has shown a non-significant shift of the seasons over time. Fig. 3.7 shows the shift of seasons corresponding to pre-monsoon, monsoon, and post-monsoon seasons. It is evident from the figures that the seasons are creeping into other seasons. Table 3.9 shows the statistics of the shift in the pre-monsoon, monsoon,

and post-monsoon seasons. The analysis shows a non-significant shift in every season. The pre-monsoon and monsoon season shifts backwards (i.e., early occurrence of the pre-monsoon and monsoon seasons), whereas the post-monsoon seasons shows a forward shift (i.e., the late occurrence of the post-monsoon season). The pre-monsoon occurs early by 4.236 days/3years, whereas the monsoon season occurs early by 2.306 days/3years. The post-monsoon season occurs late by 2 days/3years.

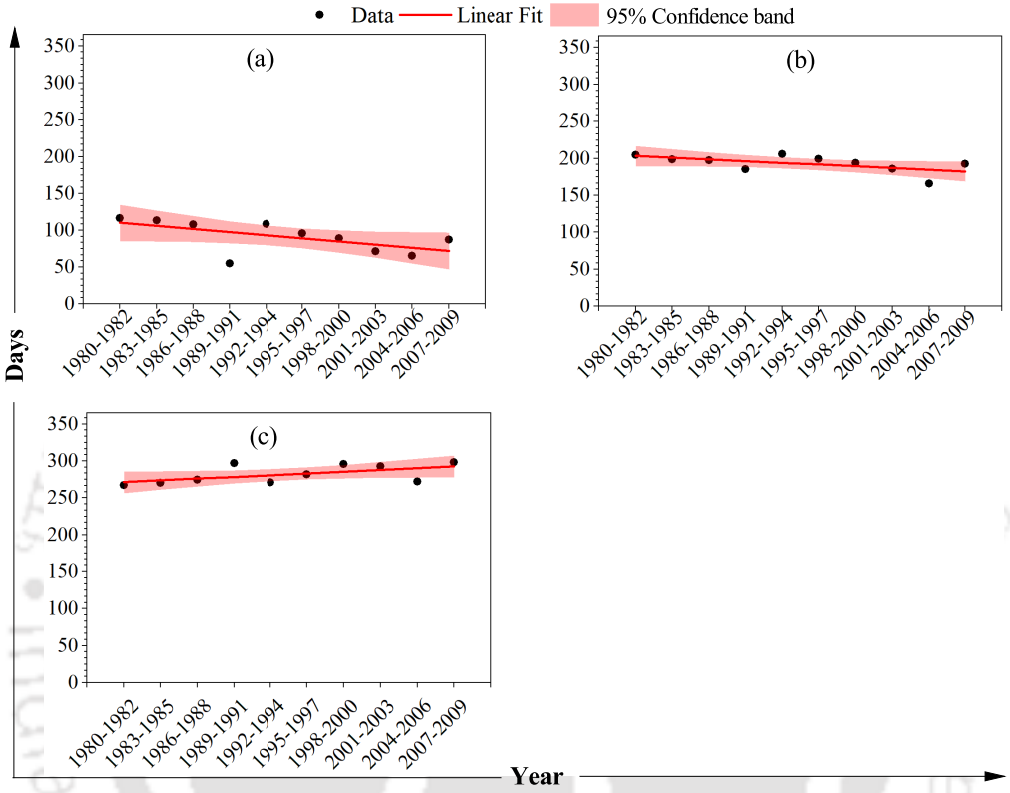

Figure 3.7: Analysis of the shift of season a) pre-monsoon b) monsoon c) post-monsoon

Table 3.9: Statistics of the season shift analysis

Season	Estimated Slope	Standard Error
Pre-Monsoon	-4.236	2.016
Monsoon	-2.306	1.101
Post-Monsoon	2.382	1.206

The dispersion of the season is measured through the coefficient of variation of the length of the segment (duration of the season) over the years. Fig. 3.8 shows the dispersion of the pre-monsoon, monsoon, and post-monsoon seasons. The monsoon and post-monsoon season show a non-significant dispersion of the seasons. Table 3.10 shows the statistics of the dispersion analysis of the seasons. All the seasons have shown positive dispersion, indicating the spread of the seasons.

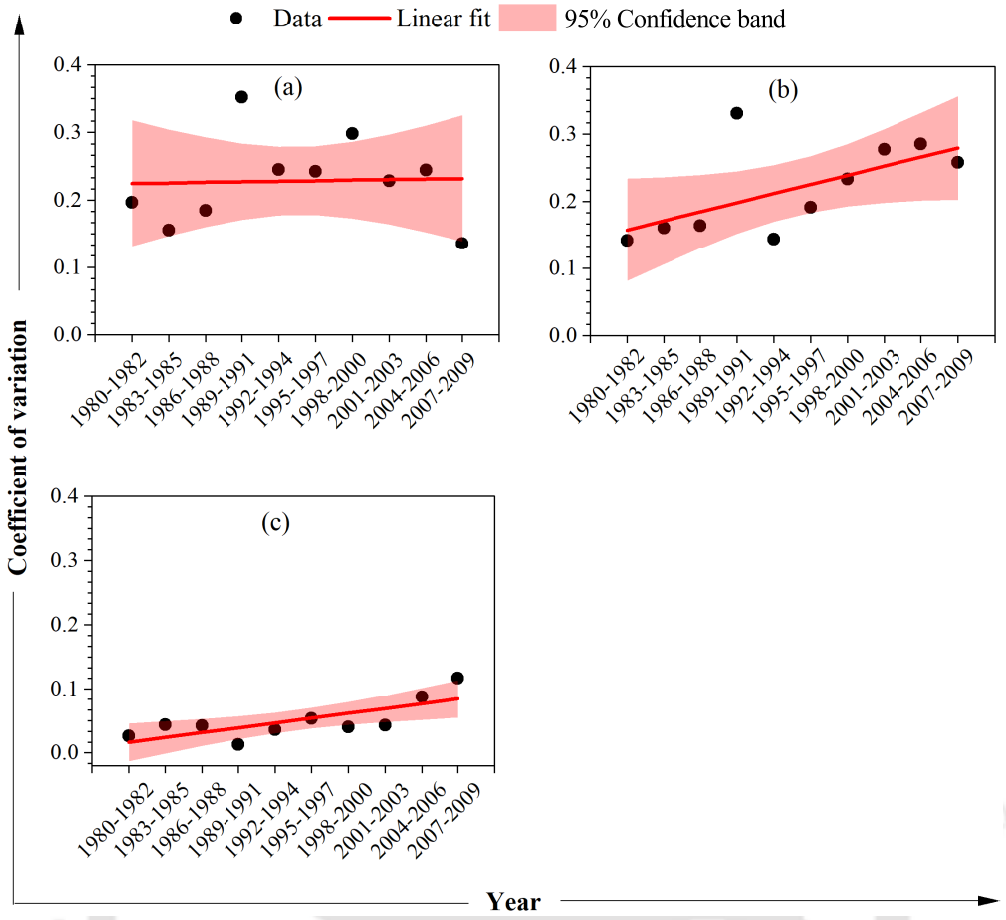

Figure 3.8: Analysis of the dispersion of the seasons a) pre-monsoon b) monsoon c) post-monsoon

Table 3.10: Statistics of season dispersion analysis

Season	Estimated Slope	Standard Error
Pre-Monsoon	0.001	0.008
Monsoon	0.014	0.006
Post-Monson	0.007	0.002

The trend in the rainfall during the pre-monsoon, monsoon, and the post-monsoon season were analyzed (Fig. 3.9), and a non-significant decrease in rainfall was observed for all the seasons. Table 3.11 shows the statistics of the rainfall trend analyses of the seasons. Pre-monsoon season shows a non-significant decrement in rainfall by 0.237 mm/3years. The monsoon season shows a decrease in rainfall by 0.170 mm/3years and the post-monsoon season shows a decreasing rate of 0.077 mm/3years. All these decrement rates are statistically insignificant.

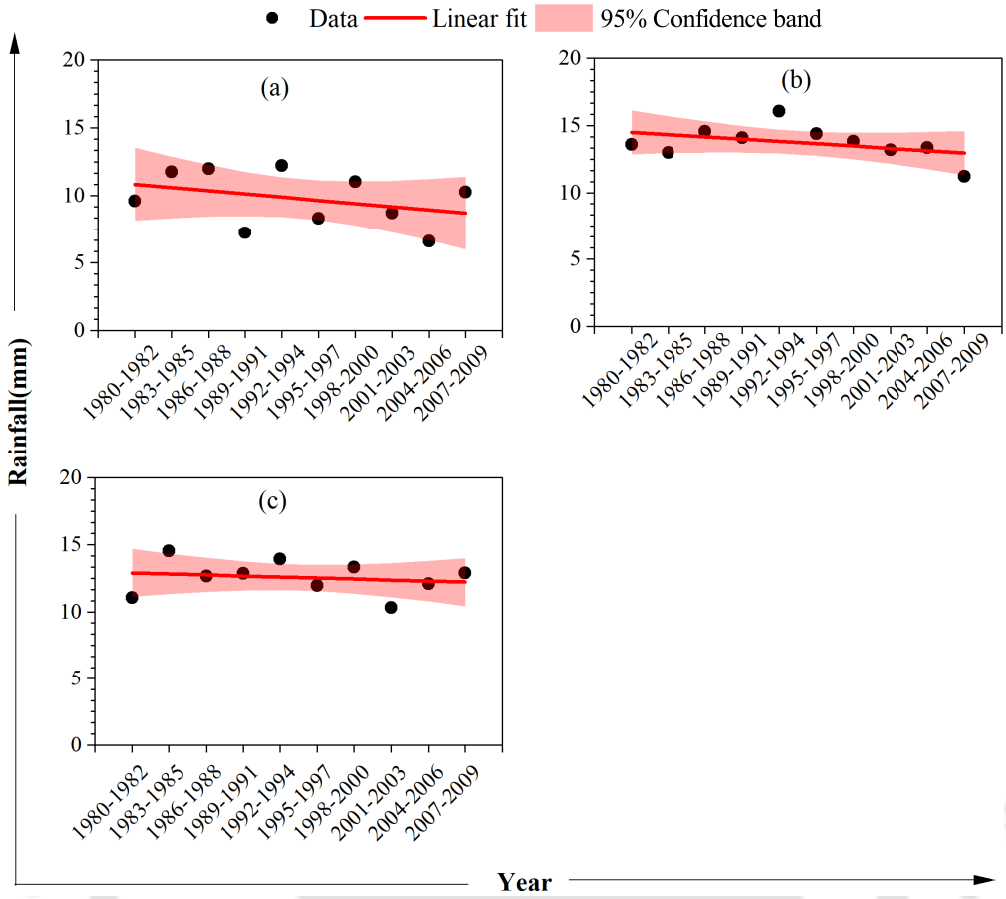

Figure 3.9: Analysis of the trend of the seasons a) pre-monsoon b) monsoon c) post-monsoon

Table 3.11: Statistics of trend analysis

Season	Estimated Slope	Standard Error
Pre-Monsoon	-0.237	0.220
Monsoon	-0.170	0.132
Post-Monsoon	-0.077	0.145

3.5 Summary

The chapter discussed about the study area and the data used for understanding the impact of land use and climate change on urban flood. Also, a preliminary rainfall analysis was carried out to understand the pattern in the time series. In this a different approach is used to analyze the shift and dispersion of seasons by using fuzzy sets instead of crisp boundaries. This method allowed for a more comprehensive understanding of the migration behavior of seasons over time. By adjusting the parameters of the GG algorithm, the climate data time-series was segmented into five distinct seasons: non-rainy season, pre-monsoon season, monsoon season, post-monsoon season, and non-rainy season. The analysis revealed several significant findings. Firstly, the pre-

monsoon and monsoon seasons were observed to occur earlier than usual, while the post-monsoon season exhibited a delayed onset, indicating a clear shift in the seasons. Furthermore, positive dispersion was observed for the pre-monsoon, monsoon, and post-monsoon seasons, indicating a wider spread of these seasons. Additionally, a non-significant decreasing trend in rainfall was noticed for all three seasons.

Based on the analysis of past rainfall data in Guwahati city, there are indications of potential changes in the rainfall pattern. These findings suggest the possibility of a shift in the local climate, which could have implications for the hydrological cycle in the region. However, it is crucial to recognize that these results are preliminary and further research is required. It is necessary to conduct further investigations utilizing climate models to validate and gain a more comprehensive understanding of future climate changes in the area. These models can provide more robust insights into the potential impacts of climate change on rainfall patterns in Guwahati city. Therefore, while the initial trend analysis of historical rainfall data highlights possible changes in the rainfall pattern, it is essential to continue research using climate models to validate these findings and obtain a more accurate understanding of the future climate changes in the region.

Chapter 4

Development of Rainfall Intensity Duration Frequency Curves Incorporating Climate Change

4.1 General

Drastic changes in climate during the last decades have resulted in frequent occurrences of extreme events/ disasters, including floods, drought, and landslides. The factors contributing to climate change has caused a sharp variations in the atmospheric variables especially an increase in the intensity and frequency of short duration extreme rainfall (Cheng and AghaKouchak, 2014; Douglas and Fairbank, 2011; Kuo et al., 2015; Westra et al., 2014). Past studies have reported that the frequency and magnitude of extreme rainfall are increasing faster than the mean rainfall in Europe, Africa, and Asia (Vinnarasi and Dhanya, 2016; Vittal et al., 2013). Such an unanticipated increase in extreme rainfall results in the malfunctioning of stormwater infrastructure systems and thereby makes the cities and major infrastructures more vulnerable than in the past (Cheng et al., 2014; Mailhot et al., 2007; Sarhadi et al., 2016).

One of the reason for the failure of stormwater infrastructure can be mainly attributed to the non-consideration of changing climate and inappropriate anticipation of future rainfall scenarios (Agilan and Umamahesh, 2016; Willems et al., 2012; Zahmatkesh et al., 2015b). The consideration of extreme events in the infrastructure design is fulfilled using the intensity duration frequency (IDF) curves. Therefore, it is essential to design the hydraulic infrastructure based on the IDF curves, capturing extreme rainfall characteristics and presumably how these extreme rainfall characteristics will change over time.

This chapter aims to develop IDF curves using point gauge rainfall data and also using the rainfall data from the climate models for quantifying the drift in the IDF curves due to climate change. The detailed methodology used for the the development of IDF curves using different approaches is schematically illustrated in Fig. 4.1. This chapter is divided into three sections.

Section 4.2 deals with the downscaling and disaggregation of rainfall data from various climate models. Section 4.3 deals with the the details about the development of IDF curves using various methods. It is believed that this study will be useful for choosing an appropriate IDF curve (with or without climate change consideration) for planning and designing of new hydraulic structures or for augmenting the existing hydraulic structures.

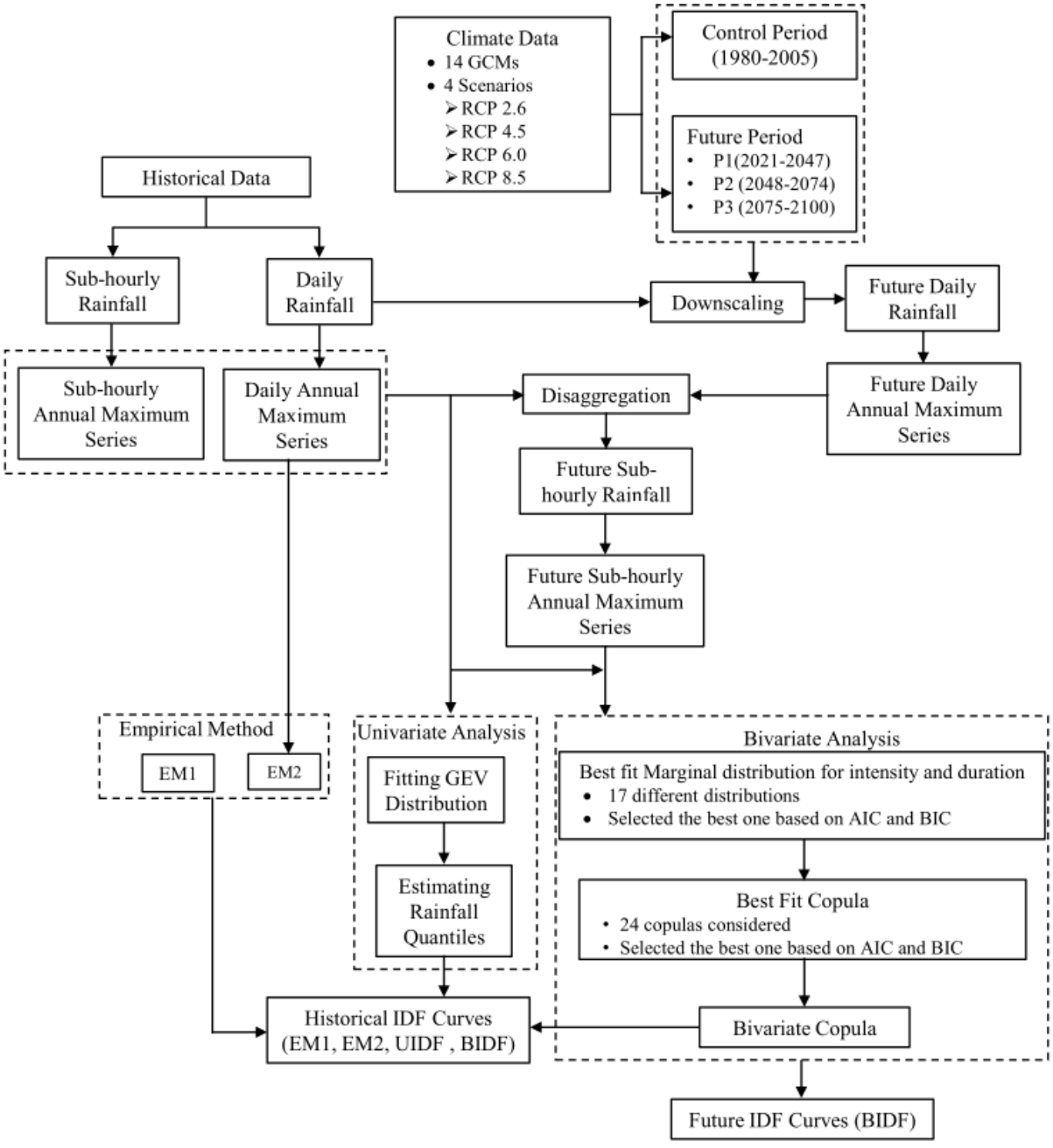

Figure 4.1: Flowchart illustrating the development of IDF curves using different approaches

4.2 Downscaling and Disaggregation of Rainfall

It is noteworthy that climate changes are well captured in the global climate models (GCMs). Though GCMs are essential for assessing climate change impacts, there are certain hurdles to estimate extreme rainfall for smaller or medium catchments from climate model outputs. Firstly, the precipitation outputs are often underestimated due to systematic errors in GCMs, especially for the annual maximum rainfall (Cannon et al., 2015; Maraun, 2013). Secondly, the temporal resolution of the GCM output is limited to daily or monthly scale (Lee and Jeong, 2014; Sharma et al., 2007). Nevertheless, rainfall at a finer time scale is essential for understanding the hydrological effects of climate change in urban catchments (Lee and Jeong, 2014; Uraba et al., 2019). To alleviate the above mentioned limitations, past studies have developed several downscaling and disaggregation techniques (Chandra et al., 2015; Nguyen and Nguyen, 2020; Soltani et al., 2020; Zahmatkesh et al., 2015a). Downscaling refers to the techniques that allow for predictions or modeling at a finer, local scale based on data or models at a larger, broader scale. This allows for more detailed and accurate predictions in areas where only coarse-scale data or models are available (Ekström et al., 2015; Hewitson and Crane, 1996). Disaggregation is a technique in which the low resolution data (daily rainfall data) is converted to high resolution data (sub-hourly rainfall data) using the information from the observed data. Disaggregation is also known as temporal downscaling (Yeo et al., 2020).

4.2.1 Downscaling

This study used delta change method to downscale the future rainfall using all the four representative concentration pathway (RCP) scenarios, i.e. RCP 2.6, RCP 4.5, RCP 6.0, and RCP 8.5. The delta change method projects the future climate based on a change factor, which is the ratio between the mean of rainfall in the future and the historical runs of the same GCM. Using this factor, the observed time series is then transformed into future series as presented by Eq. 4.1. Generally, the change factor was calculated monthly to take the effect of seasonality.

$$P_f = CF \times P_{obs} \tag{4.1}$$

where P_f is the projected future daily rainfall, P_{obs} is the observed daily rainfall and CF is the change factor, and is estimated using Eq. 4.2

$$CF = \frac{GCM_f}{GCM_b} \tag{4.2}$$

where, GCM_f and GCM_b are the mean values from GCM future and baseline scenarios respectively.

Notably, various GCM models predict precipitation in different magnitudes in the future and hence, it is difficult to determine the best GCM for projecting future climate. To overcome this dif-

ficulty, the Intergovernmental Panel on Climate Change (IPCC, 2007) and other studies (Rahmani and Zarghami, 2013) have suggested using multi-model ensembles of GCMs, instead of a single GCM for climate change impact analysis. This study also adopts the same approach to enhance the accuracy of future rainfall projections.

4.2.1.1 Reliability Ensemble Averaging

The Reliability Ensemble Average (REA) is a statistical method developed to enhance the reliability of climate model predictions. In the context of global climate models, the REA approach involves analyzing the performance of multiple climate models and producing an average prediction that is considered to be more reliable than any individual model. The REA method considers the uncertainty associated with each model's prediction and reduces the influence of poorly performing models or outliers. Giorgi and Mearns (2002, 2003) developed the REA method to model the uncertainty resulting from the use of various GCMs. To overcome the uncertainty arising from different GCMs, the REA is applied to get an ensemble of all the GCMS. By evaluating the performance of the models at the baseline climate and its ability to converge to the ensemble average at a future period, the REA method offers a quantitative measure of reliability (Galavi et al., 2022). It is important to note that the overall reliability of a model will only improve only if the following criteria are satisfies

- The model performance criterion, which is assessed based on the performance of models under present-day climate ($R_{m,i}$)
- The model convergence criterion, which is evaluated by checking the model's ability to converge to the ensemble average at a future period ($R_{c,i}$)

The REA weights, R_i of i number of GCMs are calculated by multiplying the above two criteria and are mathematically expressed as Eq. 4.3

$$R_i = R_{m,i} \times R_{c,i} \tag{4.3}$$

In this equation, the model performance is evaluated using bias in the control period of GCMs to the observed data and model convergence is assessed by the deviation of GCM simulated change from the average change predicted by the REA approach.

Thus the ensemble average (EA) of the GCMs can be calculated as Eq. 4.4

$$EA = \frac{\sum_i (R_i * GCM_i)}{\sum_i R_i} \tag{4.4}$$

where i refers to the GCM models

4.2.2 Disaggregation

The projected daily rainfall obtained after downscaling needs to be disaggregated to finer scales for the IDF curve development. The disaggregation technique used in this study is based on the scale invariance properties of the extreme rainfall series (Bairwa et al., 2016; Nguyen et al., 2007; Yeo et al., 2020). The scale invariance theory is based on the assumption that the statistical characteristics of a short duration rainfall can be inferred from the statistical properties observed at a longer time duration (Vu et al., 2018; Yeo et al., 2020).

A statistical system is said to be scale-invariant, if the statistical or the functional properties of the system are unaffected by the shift in the scale of the parameters. A scaled function exhibits the linear log-log function of the ensemble moments in the system. For instance, a function $f(z)$ of a random variable z is said to be scaled if and only if $f(z)$ is proportionate to its scaled function $f(\lambda z)$, for all positive values of scale factor λ. If $f(z)$ is scale-invariant, then there exist a function $g(\lambda)$ given by Eq. 4.5

$$f(z) = g(\lambda) f(\lambda z) \tag{4.5}$$

$g(\lambda)$ can be expressed using proportional relation as by Eq. 4.6 (Yeo et al., 2020)

$$g(\lambda) = \lambda^{-\beta} \tag{4.6}$$

Here, the quantity β means a scale exponent and is called the 'strict-sense simple scale function'. Eq. 4.5 can be expressed in terms of duration (t) as Eq.4.7 as

$$f(t) = g(\lambda) f(\lambda t) \tag{4.7}$$

The term β is a constant for a particular site and it can be written as Eq. 4.8

$$f(t) = t^{\beta} f(1) \tag{4.8}$$

Therefore, the non- central moment (NCMs) ψ of order n as a function of duration t can be expressed using Eq. 4.9

$$\psi_n = E\left\{f^n(t)\right\} = t^{\beta(n)} b(n) \tag{4.9}$$

This implies that the moments and quantiles of the distribution function at each point are also scale-invariant. Under simple scaling conditions, denoted as $b(n) = f^n(1)$ and $\beta(n) = k\beta$, it is evident that the power-form relationship between the n-order NCMs and durations t serves as a suitable representation for capturing the scaling behavior of extreme rainfall. If the Eq. 4.9 holds true, then NCMs verses duration on log-log scale gives a linear relationship and the slope of the plot gives the scaling exponent. This approach is frequently employed to examine the scaling

characteristics of a physical process like rainfall (Nguyen et al., 2007; Yeo et al., 2020). If the assumption of simple scaling is valid, the observed data points fall approximately along a straight line. This relationship is utilized to derive shorter duration rainfall from long duration rainfall even in the absence of statistical properties of short duration rainfall.

In the present study, a three-parameter Generalized Extreme Value (GEV) distribution is used and the parameters of the GEV distribution at two different time scales t and λt can be expressed as Eq. 4.10

$$\xi(\lambda t) = \lambda^{\beta}\xi(t); \quad \alpha(\lambda t) = \lambda^{\beta}\alpha(t); \quad \kappa(\lambda t) = \lambda^{\beta}\kappa(t) \tag{4.10}$$

The cumulative distribution function (CDF), $F(x)$ of the GEV is given by the Eq. 4.11

$$F(x) = exp\left\{\left(1 + \frac{\kappa(x-\xi)}{\alpha}\right)^{-\frac{1}{\kappa}}\right\}; \quad \kappa \neq 0; \quad \left\{1 + \frac{\kappa(x-\xi)}{\alpha}\right\} > 0, \alpha > 0, x, \xi \in R \tag{4.11}$$

The n^{th} order non- central moment of the GEV distribution is given by Eq. 4.12

$$\psi_n = \left(\xi + \frac{\alpha}{\kappa}\right)^n + (-1)^n \left(\frac{\alpha}{\kappa}\right)^n \Gamma(1+n\kappa) + d\sum_{i=1}^{n-1}(-1)^i \left(\frac{\alpha}{\kappa}\right)^i \left(\xi + \frac{\alpha}{\kappa}\right)^{n-i} \Gamma(1+i\kappa) \tag{4.12}$$

where ξ, κ, and α is the location parameter, shape parameter, and scale parameter of the GEV distribution respectively, and Γ is the Gamma function.

Eq. 4.13 shows the scale factor λ^{β} for two different time scale t and λt.

$$\lambda^{\beta} = \frac{\psi_1(\lambda t)}{\psi_1(t)} \tag{4.13}$$

4.3 Methods for Developing of IDF Curves

4.3.1 Empirical Models

Several empirical models are available for the development of the IDF curves. Babu et al. (1979) and Kothyari and Garde (1992) developed two widely adopted empirical models for the Indian subcontinent. To model the relationship between intensity, duration, and frequency, Babu et al. (1979) have analysed the rainfall characteristics from 42 rain gauge stations all over India and developed an empirical relation given by Eq. 4.14

$$I = \frac{KT^a}{(D+b)^n} \tag{4.14}$$

where I is the rainfall intensity in mm/h, T is the return period in years, D is the storm duration in hours, and K, a, b and n are constants that depend on the geographical properties of different cities in India. For IDF curve development, Indian subcontinent was divided into five zones: northern zone, central zone, eastern zone, western zone and southern zone. In each zone different cities were considered and for each cities, the values of the constants (K, a, b and n) were proposed.

Equation 4.15 shows the empirical relation suggested by Kothyari and Garde (1992), based on the rainfall data from 78 rain gauge stations across India.

$$I = \mathcal{C}\frac{T^{0.20}}{D^{0.7}}(R_{24}^2)^{0.33} \tag{4.15}$$

where I is the rainfall intensity in mm/h for a storm duration of D hours having a return period of T years, C is the constant which depends on the geographical location and R_{24}^2 is the 24 hour two-years rainfall. Kothyari and Garde (1992) has divided the entire India into five zones, i.e., northern, eastern, central, western and southern zones and for each zone the value of $\mathcal{C}$ is given.

From here on, Eq. 4.14 and Eq. 4.15, are designated as EM1 and EM2, respectively.

4.3.2 Univariate Frequency Analysis

In the univariate frequency analysis, the IDF curves are developed by fitting a theoretical distribution to the historical data. For different rainfall durations (0.25, 0.5, 1, 2, 3, 6, 12 and 24 hours), the annual maximum series (AMS) of rainfall intensity was fitted with a GEV distribution. The cumulative distribution function (CDF) of GEV is given by Eq. 4.11. From the CDF, the rainfall quantiles (**x**) for different return periods are estimated by using the Eq.4.16. From here on, the IDF curves developed based on univariate analysis will be termed as UIDF.

$$\mathbf{x} = F^{-1}\left(1 - \frac{1}{T}\right) \tag{4.16}$$

This study considers the return periods (T) such as 2, 5, 10, 15, 25, 50, 75, 100 years for IDF curve estimation using the univariate frequency analysis. Many researchers have used the univariate frequency analysis for constructing the IDF curves for different Indian cities like Roorkee (Singh et al., 2016), Hyderabad (Bairwa et al., 2016; Dourte et al., 2013), Delhi (Bairwa et al., 2016; Chaudhuri and Sharma, 2020), Chennai (Andimuthu et al., 2019) and Bengaluru (Bairwa et al., 2016; Chandra et al., 2015).

4.3.3 Multivariate Frequency Analysis

Some of the climatological and hydrological variables are jointly dependent, which justifies the use of multivariate methods to understand their association. This study utilizes the copula for the IDF curve development, considering the interdependency of intensity and duration of rainfall. A copula is a joint distribution function with uniformly distributed marginals that relates the marginal probabilities to the joint probability. (Genest and MacKay, 1986; Genest and Rivest, 1993; Nelsen, 1999). Copula allow independent modeling of the marginal distribution and dependence structure. Thus, a copula function helps to model the relationship between multiple dependent variables, without the assumption of normality or homogenous marginal distributions.

Consider two random variables X and Y designated as $(x_1, y_1), (x_2, y_2), ..., (x_N, y_N)$ which are drawn from a bivariate population, and let $F_X(x)$ and $F_Y(y)$ be their marginal distribution functions, respectively. The best fitted marginal distributions for intensity and duration were identified using Akaike Information Criteria (AIC) and the Bayesian Information Criteria (BIC). A lower value of AIC and BIC indicates a better model fit. AIC consider the intricacy of the model and is expressed as Eq. 4.17 (Akaike, 1974)

$$AIC = 2\mathcal{D} - 2l \tag{4.17}$$

where $\mathcal{D}$ is the number of parameters of the statistical model, l is the log-likelihood value and n is the number of observations.

Eq. 4.18 shows the expression for the BIC calculations (Schwarz, 1978).

$$BIC = \mathcal{D}ln(n) - 2l \tag{4.18}$$

Sixteen distributions are utilized, namely Beta, Exponential, Extreme Value, Birnbaum-Saunders (BS), Normal, Gamma, Log-Logistic, Generalized Extreme Value, Generalized Pareto (GP), Inverse Gaussian, Rician, Logistic, Log-Normal, Nakagami, *t* Location-scale, Rayleigh, and Weibull (Sadegh et al., 2017). Table 4.1 shows the AIC and BIC values for the different marginal distributions for rainfall intensity and duration for the observed rainfall dataset. Based on the AIC and BIC, the Birnbaum- Saunders(BS) and Generalized Pareto (GP) were found to be the best fit distribution for rainfall duration and intensity, respectively.

Table 4.1: Goodness of fit of different marginal distribution (Bold indicates best fit)

S.No.	Distribution	Duration		Intensity	
		AIC	BIC	AIC	BIC
1	Birnbaum–Saunders	**1432.76**	**1439.97**	2546.49	2553.7
2	Exponential	1529.15	1532.76	2568.86	2572.46
3	Extreme Value	2014.91	2022.12	2908.86	2916.07
4	Gamma	1496.52	1503.73	2568.72	2575.93
5	Generalized Extreem Value	1489.31	1500.13	2600.86	2611.67
6	Generalized Pareto	1439.2	1450.02	**2535.25**	**2546.07**
7	Inverse Gaussian	1463.22	1470.43	2566.27	2573.48
8	Logistic	1861.69	1868.9	2752.64	2759.85
9	Log-Logistic	1493.77	1500.98	2591.54	2598.75
10	Log-Normal	1470.74	1477.95	2569.33	2576.54
11	Nakagami	1516.9	1524.11	2582.67	2589.88
12	Normal	1885.71	1892.92	2765.37	2772.58
13	Rayleigh	2166.21	2169.82	2813.35	2816.96
14	Rician	2168.21	2175.42	2815.35	2822.56
15	t Location-Scale	1756.42	1767.24	2752.65	2763.47
16	Weibull	1488.73	1495.95	2569.53	2576.74

Accordant to Sklar's theorem (Joe, 2014; Nelsen, 1999, 2007; Schweizer, 2007), the joint probability distribution H of $F_X(x)$ and $F_Y(y)$ can be estimated using the copula C (Eq. 4.19)

$$C\left[F_X(x), F_Y(y)\right] = H_{X,Y}(x, y) = H(x, y) \tag{4.19}$$

Many distinct families of copulas are available in the literature (Nelsen, 1999). Twenty-four different copulas (Ali-Mikhail Haq, BB1, BB5, Burr, Clayton, Cuadras-Auge, Farlie–Gumbel–Morgenstern, Cubic, Fischer-Hinzmann, Fischer-Kock, Frank, Galambos, Gaussian, Gumbel, Independence, Joe, Linear-Spearman, Marshal-Olkin, Plackett, Raftery, Roch-Alegre, Shih-Louis, t, and Tawn) were used in this study for carrying out the multivariate frequency analysis (Sadegh et al., 2017). A suitable copula should be identified to model the variable's dependency structure based on the AIC and BIC criteria. Table 4.2 shows the AIC and BIC value for the copula models for the observed rainfall dataset. Based on both AIC and BIC criteria, the Frank copula, which falls under the Archimedean family is identified for performing bivariate modeling of IDF curves.

Table 4.2: Goodness of fit of different copula models (Bold indicates best fit)

S.No.	Copula	AIC	BIC	S.No.	Copula	AIC	BIC
1	Ali-Mikhail Haq	-1202.83	-1199.22	13	Gaussian	-2722.67	-2719.06
2	BB1	-1237.2	-1229.99	14	Gumbel	-1063.61	-1060
3	BB5	-1061.64	-1054.43	15	Independence	-1065.68	-1065.68
4	Burr	-1967.32	-1963.72	16	Joe	-1063.67	-1060.07
5	Clayton	-1063.65	-1060.04	17	Linear-Spearman	-2564.63	-2561.02
6	Cuadras-Auge	-1063.68	-1060.07	18	Marshal-Olkin	-1061.68	-1054.46
7	Cubic	-1091.3	-1087.7	19	Plackett	-2772.67	-2769.06
8	Farlie–Gumbel–Morgenstern	-1235.05	-1231.44	20	Raftery	-1063.68	-1060.07
9	Fischer-Hinzmann	-1061.68	-1054.46	21	Roch-Alegre	-1368.33	-1361.12
10	Fischer-Kock	-1232.77	-1225.55	22	Shih-Louis	-1437.46	-1433.85
11	Frank	**-2807.89**	**-2804.29**	23	t	-2719.91	-2712.7
12	Galambos	-1063.68	-1060.07	24	Tawn	-1059.68	-1048.86

Frank copula, which is a one parameter Archemedian copula, symmetric in nature, with the interaction function proportional to the density, is preferred for hydrologic analysis due to its simplicity (Ariff et al., 2012; Kurowicka and van Horssen, 2015; Salvadori and Michele, 2004; Singh and Zhang, 2007; Zhang and Singh, 2006). Additionally, it can be applied for positively or negatively correlated hydrological variables (Singh and Zhang, 2007; Uttarwar et al., 2020; Zhang and Singh, 2006). Table 4.3 shows the details of marginal distribution and the best fit copula along with the parameter θ of Frank copula for different datasets.

Let $U = F_X(x)$ and $V = F_Y(y)$ where U and V are uniformly distributed random variables, with u and v denoting a specific value of U and V respectively. The joint probability distribution of Frank copula (H) for the random variables can be expressed as Eq. 4.20.

$$C(u,v) = \frac{1}{\theta} ln \left\{ \frac{[1 - exp(-\theta)]}{[1 - exp(-\theta)] - [1 - exp(-\theta F_X(x))] - [1 - exp(-\theta F_Y(y))]} \right\}; \theta \neq 0 \quad (4.20)$$

where θ is the copula parameter.

Eq. 4.21 shows the generator of Frank copula

$$\phi(t) = ln \left[\frac{1 - exp(-\theta)}{1 - exp(-\theta t)} \right] \quad (4.21)$$

where t is the value of a uniformly distributed random variable U or V varying from 0 to 1.

Eq. 4.22 gives the Kendall Tau coefficient τ

Table 4.3: Details of best-fitted distributions and the copula

Data	Period	Intensity			Duration		Frank copula parameter
		Parameters of Generalized Pareto (GP) distribution			Parameters of Birnbaum Saunders (BS) distribution		
		Shape	Scale	Threshold	Scale	Shape	
Observed	-	0.014	37.90	2.75	2.45	1.73	-22.65
RCP 2.6	P1	-0.164	97.80	5.69			-26.28
	P2	-0.069	94.84	6.91			-24.24
	P3	-0.095	140.77	7.79			-19.96
RCP 4.5	P1	-0.130	98.52	5.88			-24.11
	P2	-0.104	116.52	6.92			-21.27
	P3	-0.063	135.05	7.76			-18.97
RCP 6.0	P1	0.06	105.94	4.80			-13.22
	P2	-0.024	97.33	4.99			-16.97
	P3	-0.969	118.10	6.68			-20.28
RCP 8.5	P1	-0.116	90.81	4.69			-21.20
	P2	0.111	69.40	4.49			-16.85
	P3	-0.012	141.16	8.13			-16.64

$$\tau = 1 - \frac{4}{\theta}\left[D_1(-\theta) - 1\right]; [-1, 1] \tag{4.22}$$

Here D_1 is the first-order Debye function with a negative agreement (Eq. 4.23),

$$D_1(-\theta) = \frac{1}{\theta}\int_0^{\theta} \frac{t}{exp(t) - 1} dt + \frac{\theta}{2} \tag{4.23}$$

Eq. 4.24 and Eq. 4.25 shows the conditional Frank copula function and the conditional return period respectively.

$$C_{I|D=d} = \frac{[exp(-\theta I) - 1)][exp(-\theta d)]}{[exp(-\theta d) - 1][exp(-\theta I) - 1] + [exp(-\theta) - 1]} \tag{4.24}$$

$$T(I|D = d) = \frac{1}{1 - C_{I|D=d}} \tag{4.25}$$

4.3.3.1 Paramter Estimation

In this study, the posterior distributions of the marginals and the copula function parameters are estimated using Bayesian inference. Monte Carlo Markov Chain (MCMC) simulation is used

to implement the Bayesian inference (Sadegh et al., 2017). Baye's theorem is used to calculate the posterior distribution by updating the prior information of a hypothesis and the equation for posterior distribution is given by Eq. 4.26.

$$P(\Theta|\tilde{x}) = \frac{P(\Theta)P(\tilde{x}|\Theta)}{P(\tilde{x})} \tag{4.26}$$

where, $P(\Theta)$ is the prior distribution, $P(\Theta|\tilde{x})$ is the posterior distribution and $P(\tilde{x}|\Theta) \approx L(\Theta|\tilde{x})$ is the likelihood function and $P(\tilde{x})$ is the coined evidence and it is constant for each modelling. So, 4.26 can be rewritten as Eq. 4.27

$$P(\Theta|\tilde{x}) \propto P(\Theta)L(\Theta|\tilde{x}) \tag{4.27}$$

If the prior distribution is unknown, a uniform prior can be assumed (Sadegh et al., 2017). In Bayesian analysis, it is assumed that the error residuals is uncorrelated, homoscedastic, and follow a Gaussian distribution with a mean of zero. Based on this assumption the likelihood function can be expressed as Eq. 4.28

$$L(\Theta|\tilde{x}) = \prod_{i=1}^{n} \frac{1}{\sqrt{2\pi\tilde{\sigma}^2}} \exp\left\{-\frac{1}{2}\tilde{\sigma}^{-2}[\tilde{x}_i - x_i(\Theta)]^2\right\} \tag{4.28}$$

For simplicity, Eq. 4.28 is usually expressed in logarithmic form as Eq. 4.29

$$l(\Theta|\tilde{x}) = -\frac{n}{2}ln(2\pi) - \frac{n}{2}ln(\tilde{\sigma}^2) - \frac{1}{2}\tilde{\sigma}^{-2}\sum_{i=1}^{n}[\tilde{x}_i - x_i(\Theta)]^2 \tag{4.29}$$

where $l(\Theta|\tilde{x})$ is the log-likelihood function and $\tilde{\sigma}$ is the estimate of standard deviation of measurement error and $\tilde{\sigma}$ can be estimated by Eq. 4.30

$$\tilde{\sigma}^2 = \frac{\sum_{i=1}^{n}[\tilde{x}_i - x_i(\Theta)]^2}{n} \tag{4.30}$$

Therefore, Eq. 4.29 can be simplified as Eq. 4.31

$$l(\Theta|\tilde{x}) = -\frac{n}{2}ln(2\pi) - \frac{n}{2} - \frac{n}{2}ln\frac{\sum_{i=1}^{n}|\tilde{x}_i - x_i(\Theta)|}{n} \tag{4.31}$$

It is not possible to solve Eq. 4.27 analytically, necessitating the search for alternative methods. In this study, a hybrid-evolution MCMC (HE-MCMC) which employs the intelligent prior sampling through Latin Hypercube Sampling (LHS), snooker update, Adaptive Metropolis (AM), and differential evolution (DE) was used. The entire process involves drawing samples from the prior distribution using LHS and assigning them randomly to complexes. The best sample in each complex serves as the starting point for a Markov chain. This procedure is iteratively performed.A

Snooker update is performed with a 10% probability, which involves drawing three samples from the parameter space and determining an update direction based on these samples. Along with this AM and DE update is performed with a 90% probability. Randomly selected dimensions from the parameter space are updated, and based on the iteration count, a proposal is created. This process is carried out iteratively until convergence is obtained. More details of the algorithm can be found in Sadegh et al. (2017).

From here on, the IDF curves developed based on bivariate analysis will be termed as BIDF. For the BIDF developed based on historical rainfall and climate data, the same will be termed as historical BIDF and future BIDF.

4.4 Results and Discussion

4.4.1 Downscaling and Disaggregation of Rainfall

This study used observed rainfall data (1981-2017) and 14 GCM outputs to downscale the rainfall data for Guwahati city using the delta change technique. The change factor for each month for each GCM model considered was determined and are listed in tables 4.4 and 4.5. Figure 4.2 shows the variability in the downscaled annual maximum rainfall for different GCMs for four RCP scenarios and it is noteworthy to mention that there is variability in the projected rainfall among individual climate models. For RCP 2.6 and RCP 4.5, BNU-ESM model was showing higher value, whereas fro RCP 6.0 and RCP 8.5, GFDL-ESM2G was giving the higher value of rainfall. These high values are found to be unrealistic. It is not possible to test the reliability of individual climate models for future periods since there are no observed values available for comparison. Therefore, relying on individual models for impact analysis may introduce significant uncertainty. So, in this study, the REA method was used to combine the predictions of multiple models can provide a more reliable estimate of future climate conditions, taking into account the uncertainty associated with each model.

Table 4.4: Monthly change factor for RCP 2.6 and 4.5 scenario

Month	RCP	GCMs													
		1	2	3	4	5	6	7	8	9	10	11	12	13	14
Jan	RCP 2.6	0.88	1.01	1.01	*	*	0.88	*	0.65	*	2.93	1.11	0.89	0.80	0.55
Feb		1.77	1.08	1.18	*	*	5.31	*	0.66	*	2.43	2.71	0.78	7.36	0.39
Mar		0.89	1.16	1.31	*	*	1.22	*	5.33	*	4.26	0.49	0.92	12.80	0.53
Apr		0.76	1.80	1.31	*	*	1.42	*	0.76	*	0.86	1.12	0.93	6.54	0.61
May		1.06	30.88	1.06	*	*	0.88	*	1.20	*	0.97	1.51	1.04	1.37	1.05
Jun		1.46	1.21	1.83	*	*	0.94	*	2.18	*	0.88	1.00	0.90	1.25	1.17
Jul		1.21	1.28	1.69	*	*	1.07	*	0.93	*	1.13	0.97	1.00	1.37	1.45
Aug		0.98	0.93	1.18	*	*	1.24	*	0.91	*	1.28	1.11	1.03	1.17	1.14
Sep		0.94	1.00	1.34	*	*	1.33	*	1.04	*	0.95	1.00	0.88	1.05	1.46
Oct		0.86	1.13	1.31	*	*	1.38	*	0.84	*	0.97	1.04	1.04	1.28	1.02
Nov		1.88	0.86	0.96	*	*	1.95	*	1.87	*	0.75	3.08	0.87	2.55	5.40
Dec		0.70	1.15	0.68	*	*	0.91	*	0.69	*	2.81	2.56	1.49	0.65	3.76
Jan	RCP 4.5	0.81	0.69	1.26	0.80	1.27	0.80	0.90	2.48	2.36	1.63	0.95	0.97	1.57	2.72
Feb		1.52	1.22	1.06	0.72	0.56	8.16	3.37	1.05	1.48	0.56	8.46	0.97	17.57	1.19
Mar		0.83	1.16	1.21	1.83	5.13	1.25	1.12	4.31	3.42	2.34	2.62	0.89	9.43	0.24
Apr		0.57	2.34	1.28	1.10	1.11	1.53	1.60	0.68	1.82	0.93	0.87	0.81	1.12	0.76
May		1.21	42.11	1.03	1.59	2.04	1.02	1.15	1.25	0.89	0.90	3.46	1.01	1.09	0.89
Jun		1.76	1.29	1.58	1.48	0.98	1.00	1.03	2.07	2.38	1.00	1.06	1.04	1.41	1.10
Jul		1.18	1.40	1.60	1.68	1.02	1.08	1.11	1.03	2.07	1.08	1.08	0.97	1.33	1.41
Aug		1.08	1.06	1.35	1.20	1.12	1.07	1.02	1.33	1.33	1.16	1.25	1.06	1.14	1.15
Sep		1.20	1.14	1.23	1.42	1.24	1.33	1.04	0.91	1.38	0.94	1.05	0.92	1.23	1.32
Oct		0.83	1.12	1.30	1.25	1.15	1.73	1.06	0.89	2.05	1.00	1.32	1.11	1.15	0.89
Nov		1.94	0.92	1.04	0.95	1.02	1.08	0.86	2.24	7.67	1.03	1.36	0.90	1.92	2.36
Dec		0.49	1.10	0.76	1.01	2.29	0.91	1.27	0.44	53.36	3.24	4.76	0.97	0.50	2.61

1-BCC-CSM1-1-M, 2- BNU-ESM, 3- CanESM2, 4- CMCC-CM, 5- CMCC-CM5, 6-CNRM-CM5, 7- INMCM4, 8- IPSL-CM5A-LR, 9- IPSL-CM5B-LR, 10- MPI-ESM-LR, 11- MPI-ESM-MR, 12- NorESM1-M, 13- GFDL-ESM2G, 14- GFDL-ESM2M, and *Not applicable

Table 4.5: Monthly change factor for RCP 6.0 and 8.5 scenario

Month	RCP	GCMs													
		1	2	3	4	5	6	7	8	9	10	11	12	13	14
Jan	RCP 6.0	0.81	*	*	*	*	*	*	1.42	*	*	*	0.90	0.42	0.56
Feb		1.19	*	*	*	*	*	*	0.78	*	*	*	0.97	28.97	0.46
Mar		0.91	*	*	*	*	*	*	1.40	*	*	*	1.19	43.99	0.19
Apr		0.59	*	*	*	*	*	*	0.73	*	*	*	1.00	9.65	0.36
May		1.14	*	*	*	*	*	*	1.14	*	*	*	1.03	1.13	0.77
Jun		1.62	*	*	*	*	*	*	2.50	*	*	*	0.95	1.56	1.39
Jul		1.05	*	*	*	*	*	*	1.00	*	*	*	0.99	1.32	1.55
Aug		1.07	*	*	*	*	*	*	1.32	*	*	*	0.98	1.41	1.13
Sep		1.24	*	*	*	*	*	*	1.09	*	*	*	0.91	1.17	1.33
Oct		0.70	*	*	*	*	*	*	0.87	*	*	*	1.02	1.25	0.95
Nov		1.83	*	*	*	*	*	*	1.10	*	*	*	1.00	1.79	2.37
Dec		0.87	*	*	*	*	*	*	0.48	*	*	*	1.27	0.76	2.32
Jan	RCP 8.5	0.99	0.52	1.40	1.06	0.61	1.33	0.90	0.93	1.46	1.44	0.32	0.77	0.53	0.51
Feb		1.60	1.17	1.16	2.53	0.36	5.88	2.26	0.73	1.04	0.62	11.99	0.89	93.36	1.03
Mar		0.93	1.05	1.13	1.25	1.80	1.23	1.32	11.30	2.86	2.18	1.10	0.91	27.94	0.40
Apr		0.65	0.90	1.52	1.11	1.13	1.43	1.98	0.65	1.88	0.48	0.72	0.99	1.46	0.55
May		1.17	13.63	1.25	2.35	2.53	1.06	1.23	1.35	1.25	0.97	1.20	1.01	1.56	1.06
Jun		1.78	1.35	1.99	1.90	1.11	1.13	1.04	2.53	1.73	1.06	1.02	1.05	1.74	1.30
Jul		1.36	1.30	1.73	2.00	1.10	1.19	1.14	1.12	1.75	1.23	1.17	1.18	1.84	1.86
Aug		1.07	1.02	1.76	1.38	1.41	1.31	1.08	1.46	1.56	1.30	1.45	1.10	1.72	1.61
Sep		1.20	1.10	1.61	1.26	1.34	1.71	1.09	1.28	1.02	1.06	1.13	0.91	1.28	1.42
Oct		0.72	1.22	1.44	1.27	0.95	1.46	1.00	1.03	2.12	1.03	1.32	1.07	1.16	0.87
Nov		1.26	0.97	1.18	1.23	0.97	1.05	0.81	0.65	1.39	0.43	1.44	0.81	1.57	2.08
Dec		0.92	0.65	0.74	0.98	0.80	1.26	1.17	0.66	9.08	1.08	6.08	1.23	0.79	1.57

1-BCC-CSM1-1-M, 2- BNU-ESM, 3- CanESM2, 4- CMCC-CM, 5- CMCC-CM5, 6-CNRM-CM5, 7- INMCM4, 8- IPSL-CM5A-LR, 9- IPSL-CM5B-LR, 10- MPI-ESM-LR, 11- MPI-ESM-MR, 12- NorESM1-M, 13- GFDL-ESM2G, 14- GFDL-ESM2M, and *Not applicable

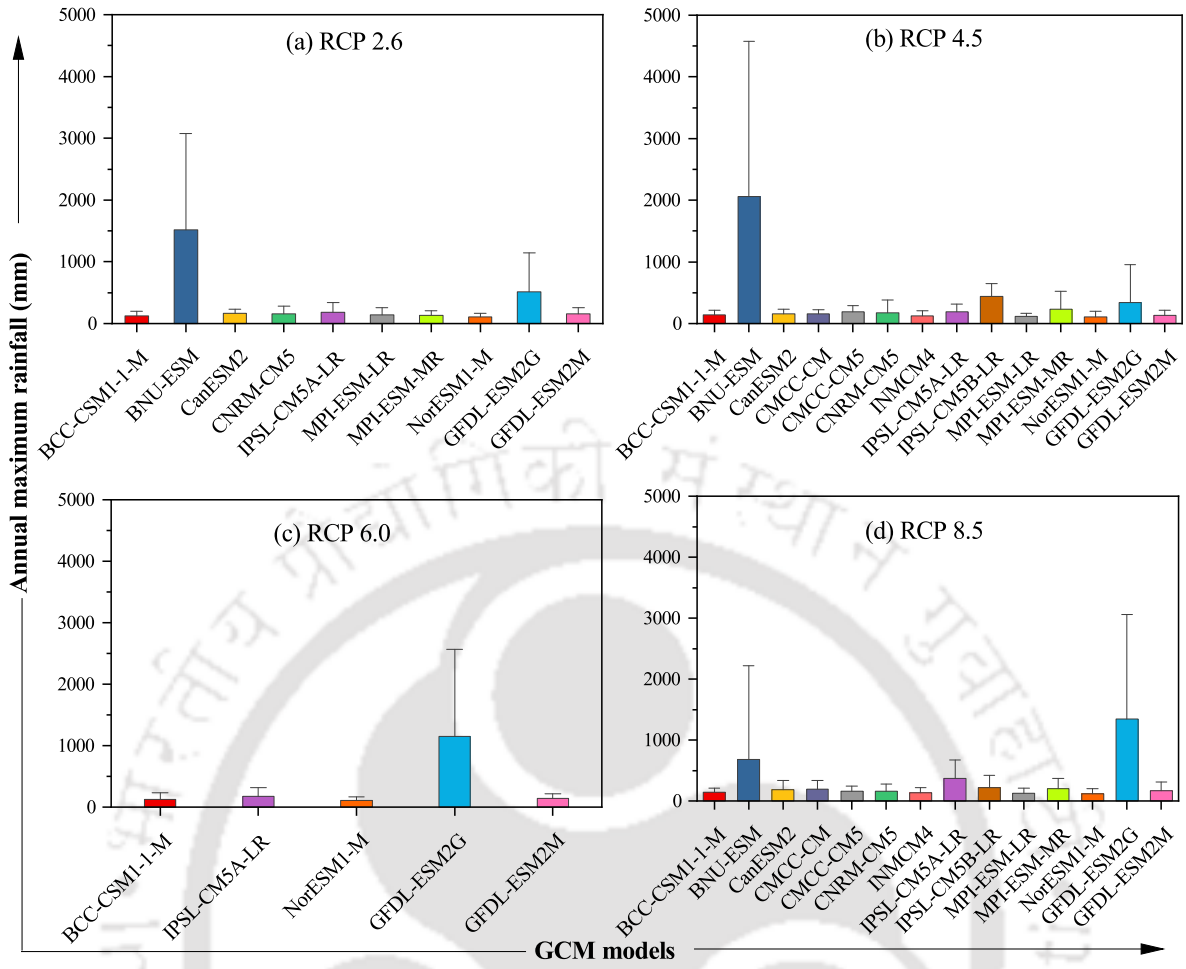

Figure 4.2: Variability in the downscaled rainfall for Guwahati city from different GCMs

4.4.1.1 Reliability Ensemble Averaging

It is clear from the above discussion that different GCMs behave differently, and choosing a single GCM for climate change analysis may result in significant uncertainties. Hence, in order to overcome this limitation, the REA method is used in this study. REA approach reduces the influence of poorly performing models, aiming to produce more accurate and reliable projections, which can inform decision-making processes related to climate change. The weights assigned to different GCMs is listed in table 4.6. It can be observed that the values for the weights are different corresponding to different climate models. This is mainly because of the calculated bias in performance term, and the distance from the ensemble average to the individual models in convergence term. Using the REA weights, the rainfall from different GCMs was combined to get an ensemble average of the rainfall for Guwahati City. The REA weight of each GCM was calculated, and Fig. 4.3 shows the annual maximum rainfall after REA for different RCPs. All four scenarios showed an increase in rainfall in the future compared to the observed rainfall. The figure displays the mean of each dataset along with the distribution of individual data points, allowing for a visual assessment of data spread and density. The rain cloud plot confirms that all RCP scenarios exhibit an upward trend in annual maximum rainfall for the future period. Notably, RCP 8.5 demonstrates a higher

spread in data points, indicating increased variability, while RCP 2.6 shows the least dispersion. Also, more number of extreme rainfall was shown in RCP 8.5 scenario.

Table 4.6: Weights assigned to GCMs using REA technique

GCM	Weights			
	RCP 2.6	RCP 4.5	RCP 6.0	RCP 8.5
BCC-CSM1-1-M	0.144	0.105	0.271	0.085
BNUESM	0.075	0.059	-	0.043
CanESM2	0.100	0.077	-	0.057
CMCCCM	-	0.079	-	0.059
CMCCCM5	-	0.068	-	0.050
CNRMCM5	0.129	0.095	-	0.075
INMCM4	-	0.054	-	0.039
IPSLCM5ALR	0.074	0.058	0.154	0.043
IPSLCM5BLR	-	0.066	-	0.049
MPIESMLR	0.082	0.064	-	0.047
MPIESMMR	0.082	0.064	-	0.047
NorESM1M	0.083	0.064	0.170	0.047
GFDLESM2G	0.075	0.058	0.154	0.043
GFDLESM2M	0.156	0.089	0.250	0.316

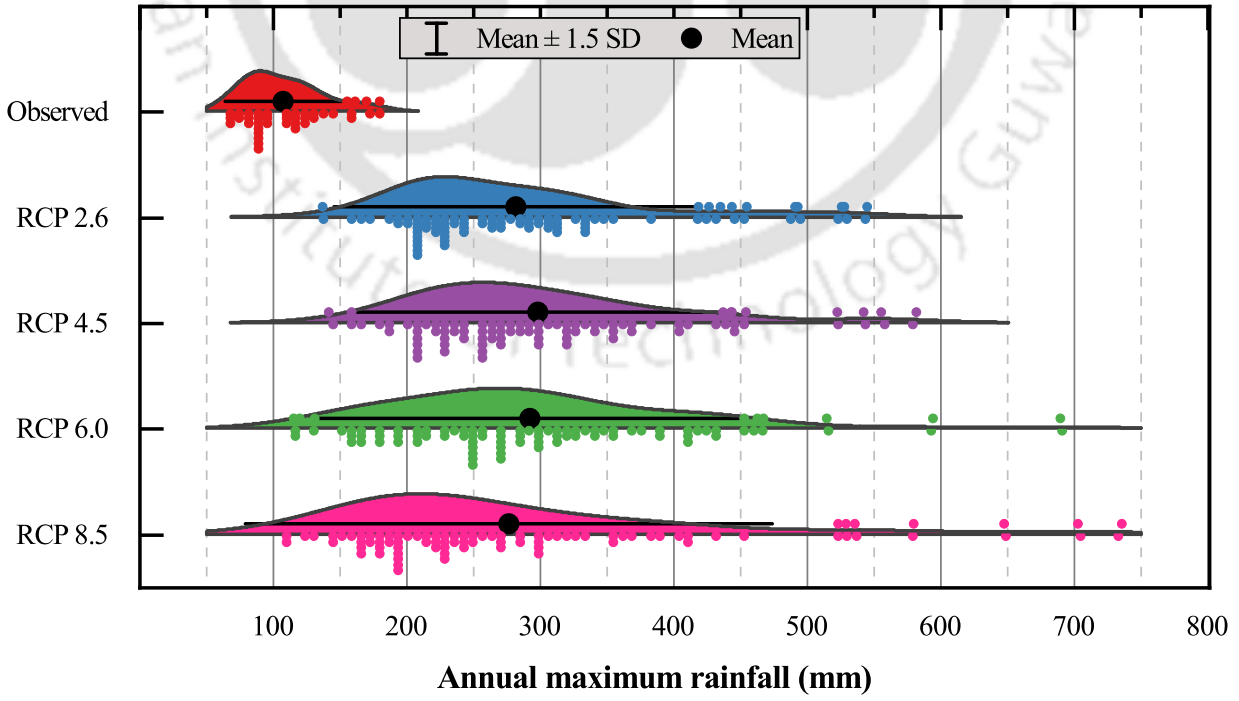

Figure 4.3: Rain cloud plot of annual maximum rainfall after reliable ensemble averaging for Guwahati city for different RCPs

4.4.1.2 Dissagregation Using Scale Invariance Theory

The Generalized extreme value (GEV) scaling method is used to disaggregate maximum rainfall to shorter durations. The rainfall durations considered are 15 and 30 minutes, 1, 2, 3, 6, 12 and 24 hours. The parameter of GEV distribution are described in table 4.7.

Table 4.7: Estimated parameter of GEV distribution

Duration	**15min**	**30min**	**1hr**	**2hr**	**3hr**	**6hr**	**12hr**	**24hr**
Shape	0.188	0.275	-0.148	-0.064	-0.094	0.101	-0.004	0.028
Scale	19.739	12.343	13.465	7.743	6.402	2.718	1.514	0.922
Location	96.741	67.362	48.548	29.835	21.169	11.799	6.962	3.904

The first three non-central moments (NCMs) of observed data are calculated from the fitted parameters of the distribution. It is observed that the moments decrease with an increase in duration, and also, the moments increase with an increase in the order of moments. The rainfall duration is plotted against the NCMs on a log-log scale to check whether the duration has a linear or non-linear relationship with NCMs as shown in Fig. 4.4. It can be observed that a linear relationship exists between the moments and the duration in the log scale with two different slopes, the first one for 15 minutes to 1-hour duration, and the second one for 1 hour to 24-hour duration with a break point at 1 hour. This implies a transition in the rainfall dynamics from long to short duration, indicating high variability in the shorter duration rainfalls. Fig. 4.5 shows the plot between order of moment and scaling exponent. This figure is used to check the linearity between scaling exponent and the order of the moment. R^2 value obtained for 15-min to 1-hr and 1-hr to 24-hr are 1 and 0.99 respectively. Higher value R^2 confirms the strong linear relationship between the order of moment and scaling exponent. Moreover, the observed linearity of the scaling exponent with the moment order confirms that a simple scaling assumption holds true for extreme rainfall. Hence, it is possible to determine the short-duration rainfall using observed long-duration rainfall data. Table 4.8 shows the scaling factor for a different duration. The scaling factor is a ratio between the moments at two different time scale t and λt. So, for 24-hr duration the scaling factor will be one. Since two different slopes exist, the scaling factor will be calculated as 24-hr to 1-hr and then 1-hr to 15-min. This break point implies a transition in the rainfall dynamics from long to short duration, indicating high variability in the shorter duration rainfalls. Short duration rainfall events often result from convective processes which are highly variable, whereas long-duration rainfall events are often linked to synoptic and mesoscale processes (Yeo et al., 2020).

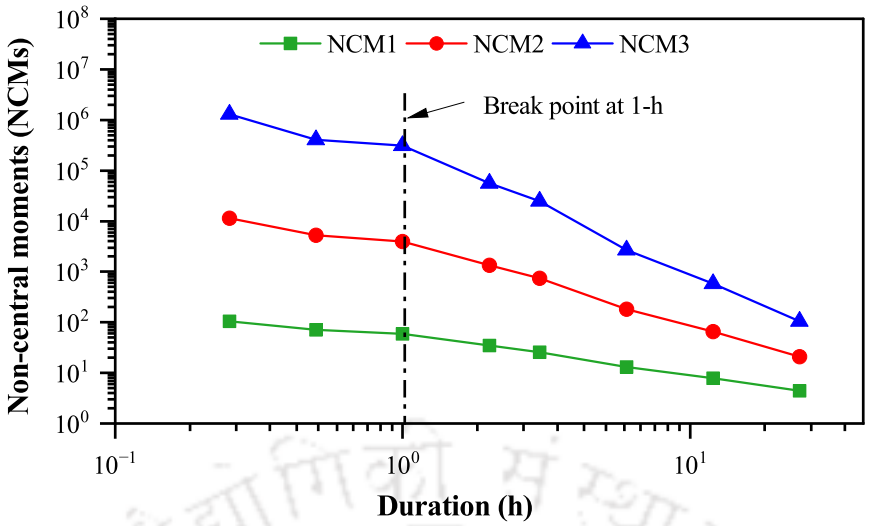

Figure 4.4: Non-central moments (NCMs) of the first three orders plotted on a log-log scale against various durations

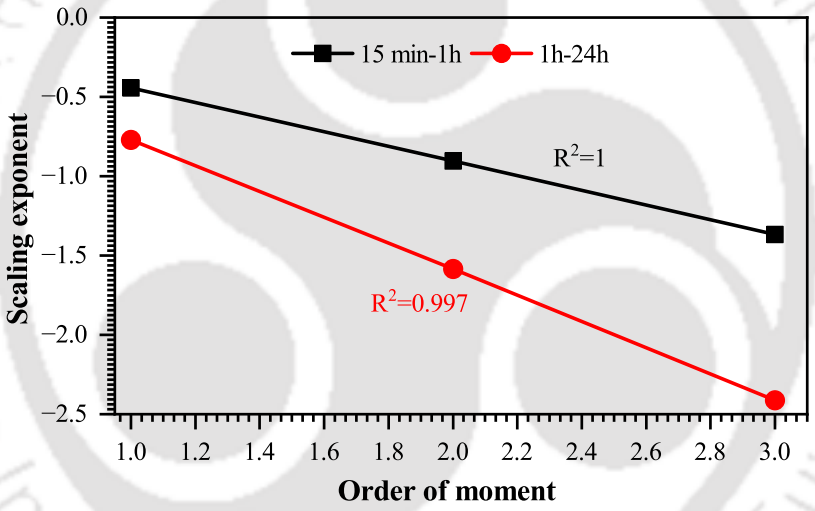

Figure 4.5: Relationship between the scaling exponents and the order of non-central moments (NCMs) of annual maximum rainfall

Table 4.8: Scaling factor for different durations

Duration (h)	0.25	0.5	1	2	3	6	12	24
Scaling factor	1.79	1.22	13.28	7.89	5.78	2.97	1.78	1.00

Finally with these scaling factors, the rainfall is disaggregated for different RCPs. Fig. 4.6 shows the AMS for future period from 2021-2100 for different RCPs and durations and these AMS will be used to develop future climate based IDF curves.

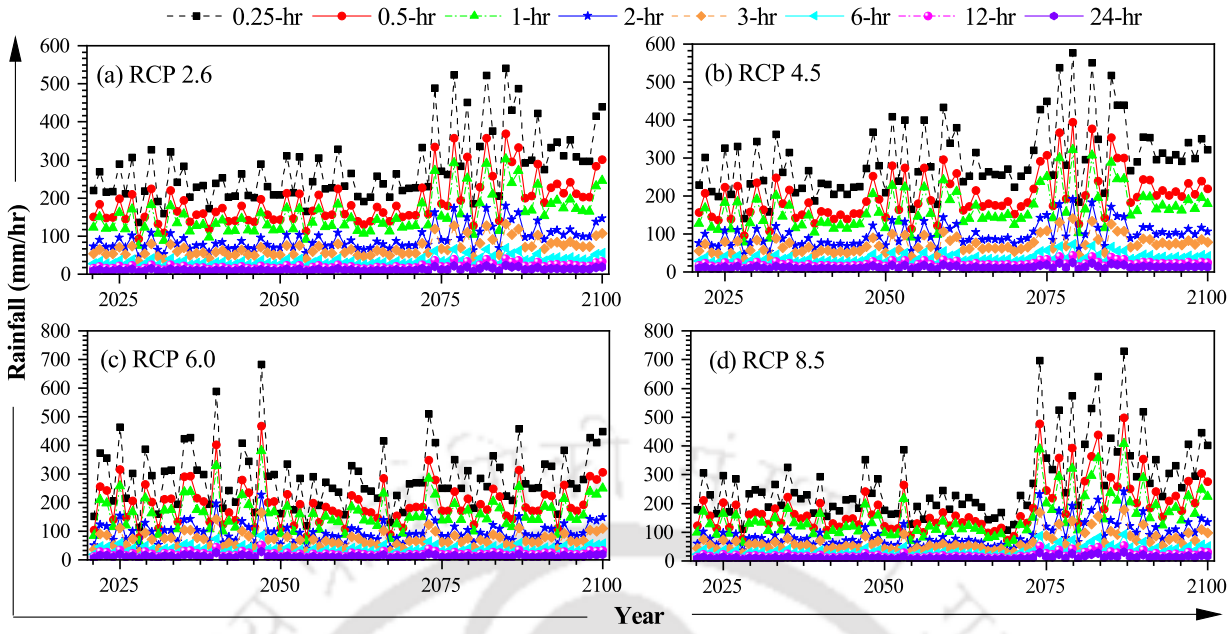

Figure 4.6: Disaggregated annual maximum rainfall for Guwahati city for 2021-2100 period

4.4.2 Interrelationship Between Rainfall Characteristics

The future rainfall scenarios are divided into three different periods: 2021-2047 (P1), 2048-2074 (P2) and 2075-2100 (P3), to investigate the future evolution of IDF curves. Figure 4.7 shows the scatter plot of rainfall intensity, duration, and their respective marginal distribution for the historical and climate data for the study area. The figure clearly demonstrates that rainfall duration and intensity exhibit distinct marginal distributions, highlighting the need to differentiate between these distributions and the dependence structure within the joint distribution of the rainfall characteristics. It is evident from Fig. 4.7 that there exists a negative correlation between rainfall intensity and duration i.e., larger the rainfall duration, the smaller the rainfall intensity. It is noteworthy that for rainfall duration less than 12 hours, the correlation between intensities and duration was high.

The correlation between rainfall intensity and duration for the historical data and climate data is given in table 4.9 in terms of Kendall's rank correlation coefficient (τ). Kendall's rank correlation coefficient is used to quantitatively measure the dependence between rainfall duration and intensity. τ measures the concordance between random variables along with the direction of the relationship. The value of Kendall's rank correlation coefficient ranges from [-1, 1] where 1 denotes total concordance, 0 denotes no concordance and -1 implies total discordance between the variables which is indicative of the negative correlation between the variables (Kao and Govindaraju, 2008). The results indicate that rainfall intensity has a strong negative relationship with rainfall duration. The magnitude of the correlation varies among RCP scenarios, suggesting potential differences in the strength of the negative correlation under different climate change pathways. Also, the observed negative correlation between rainfall characteristics, as indicated by Kendall's tau coefficients, plays a crucial role in the selection of an appropriate copula.

Table 4.9: Kendall's rank correlation coefficient between rainfall intensity and duration

Data	Kendall Coefficient		
	P1	P2	P3
Observed	-0.88		
RCP 2.6	-0.90	-0.89	-0.86
RCP 4.5	-0.89	-0.87	-0.86
RCP 6.0	-0.78	-0.83	-0.87
RCP 8.5	-0.87	-0.83	-0.83

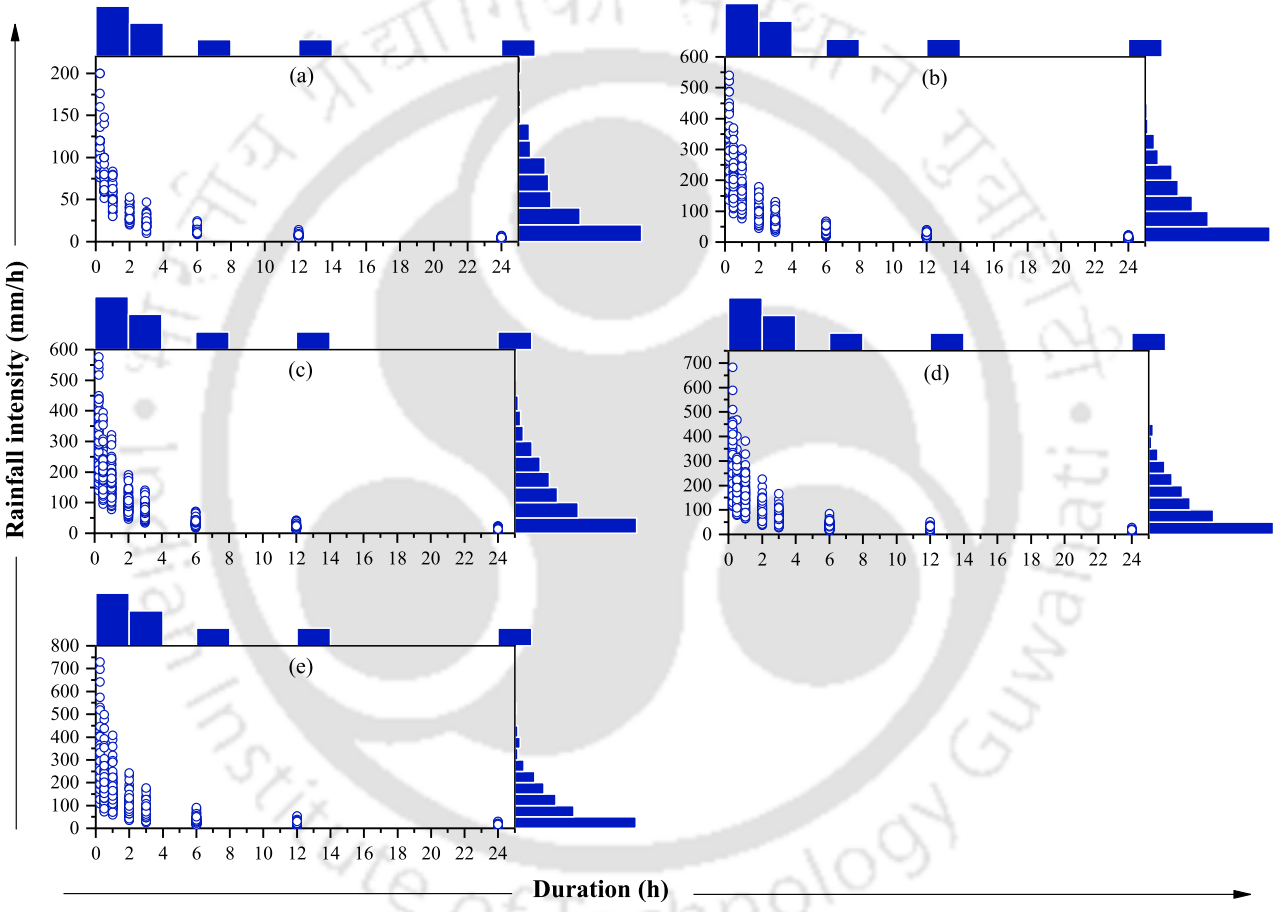

Figure 4.7: Rainfall intensity versus storm duration scatter plots, along with their marginal distributions (a) historical, (b) RCP 2.6, (c) RCP 4.5, (d) RCP 6.0, and (e) RCP 8.5

4.4.3 Comparison of IDF Curve Development Techniques

4.4.3.1 Relationship Between Rainfall Intensity and Duration for Different Return Periods

The IDF curves were developed for 0.25, 0.5, 1, 2, 3, 6, 12, and 24 hours duration for return periods of 2, 5, 10, 15, 25, 50, 75 and 100 years. Fig. 4.8 illustrates a comparison of historical IDF curves corresponding to empirical models, EM1 and EM2 (Eqs. 4.14 and 4.15), and univariate

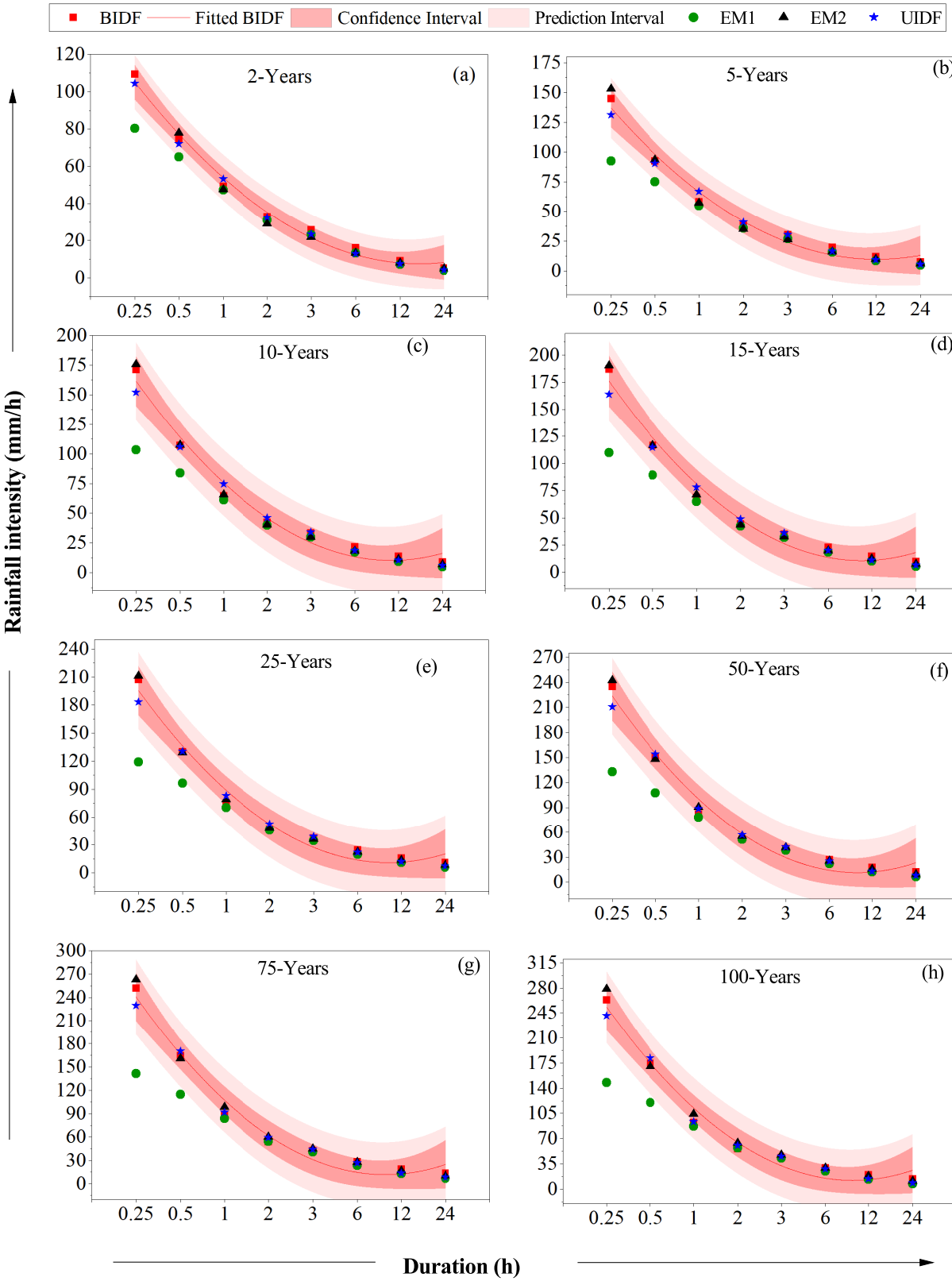

Figure 4.8: Comparison of IDF curves developed using empirical models (EM1 and EM2), and univariate analysis (UIDF) with the IDF curves developed using bivariate analysis (BIDF)

analysis using GEV model (UIDF) with the copula based bivariate IDF (historical BIDF) curve. A second order polynomial was fitted to the historical BIDF curves for determining a 95% confidence interval and prediction interval as shown in Fig. 4.8. The parameters of EM1 adopted for the study area (K = 7.206; a = 0.156; b = 0.75; and b = 0.94) resulted in an underestimation of rainfall intensity for duration between 0.25 h to 1 h. Beyond that, the rainfall intensities are within the 95% confidence interval. It may be noted that the lower durations < 1h is used for carrying out impact studies in urban catchments (Willems et al., 2012). Hence, EM1 is not able to capture the historical changes in the rainfall and may not be suitable for considering short duration events for the given urban catchment.

On the other hand, the IDF curves developed using EM2 (with its parameter $\mathcal{C} = 9.1$) deviated from the historical BIDF curve but remained within the 95% confidence interval for almost all duration-return period combinations. In comparison with BIDF, EM2 showed an increase in rainfall intensities for short durations (0.25 h and 0.5 h) for 2 years and 5 years return periods and showed a slight decrease in the intensities for durations of 1 h, 2 h, 3 h and 6 h. For durations of 0.25 h and 1 h, an increase in rainfall intensities was found over a 10 years, 15 years, 25 years, and 50 years return periods, while 2 h, 3 h, and 6 h durations showed a decrease. For 75 years and 100 years, durations of 0.25 h, 1 h and 2 h showed an increase in the rainfall intensities compared to BIDF. It can be summarized that the IDF curve developed using EM2 adequately represents the historical rainfall data of the urban catchment considered in this study. Furthermore, the IDF curve developed using univariate analysis using the GEV model, i.e., the UIDF falls within the 95% confidence interval. Another interesting observation is that for longer durations, the EM1, EM2 and UIDF appear more similar to each other than the bivariate approach.

4.4.3.2 Relationship Between Rainfall Intensity and Return Periods for Different Duration

The scale of the rainfall intensity presented in Fig. 4.8 is large, making it difficult to interpret the difference for a particular duration obtained from different methods of IDF curve generation. This understanding is mandatory for urban catchments where the short durations of rainfall are more prominent. For elucidating this better, the data from Fig. 4.8 was re-plotted as shown in Fig. 4.9, where the rainfall intensity obtained from different methods were plotted with return period for a particular duration. In this manner, the difference in rainfall intensity, if any, corresponding to the specific duration can be assessed for various IDF curve development methods considered in this study. It is explicit from Fig. 4.9 that the rainfall intensity is different for empirical models (EM1 and EM2) and GEV based univariate analysis (UIDF) in comparison with the bivariate copula model (BIDF).

4.4.3.3 Quantitative Assessment of Change in the Rainfall Intensity

For appreciating the difference better, Fig. 4.10 illustrates the percentage variation in rainfall intensity (corresponding to different durations and return periods) obtained from different methods

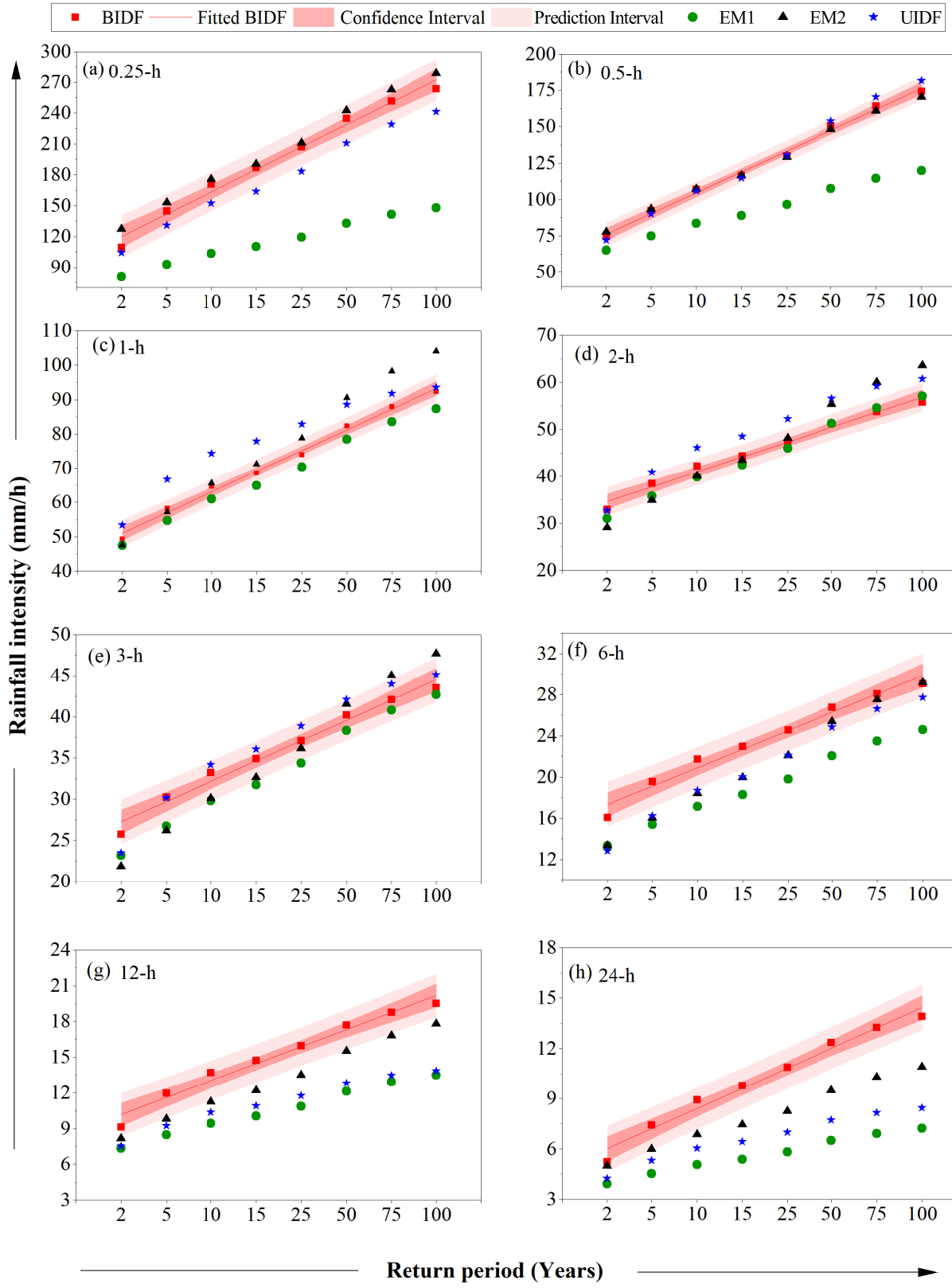

Figure 4.9: Comparison of rainfall intensities for different durations using empirical models (EM1 and EM2), and univariate analysis (UIDF) with the bivariate analysis (BIDF)

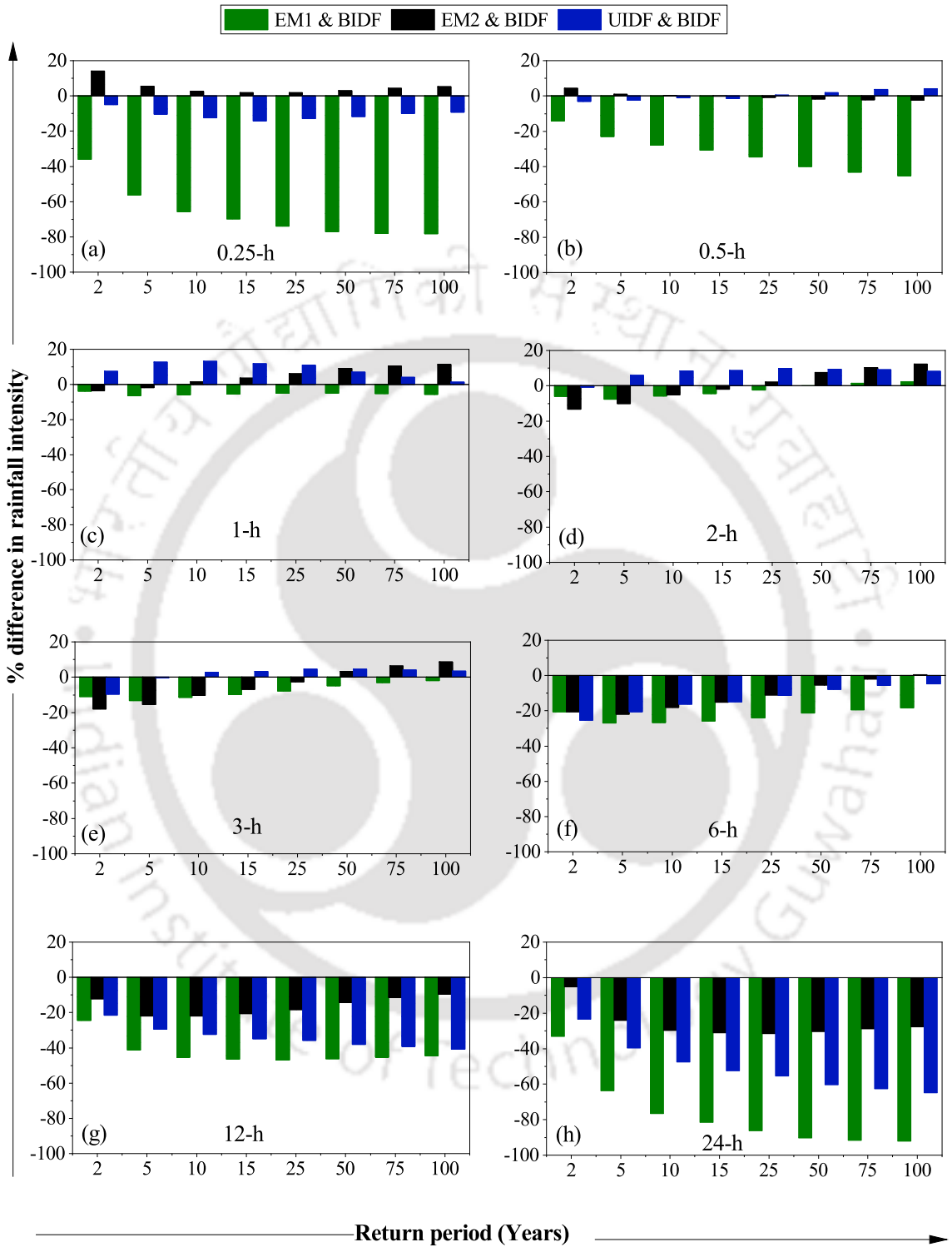

Figure 4.10: Variation in rainfall intensity estimated using empirical models (EM1 and EM2) and univariate analysis (UIDF) in comparison with the historical IDF curves developed using bivariate analysis (BIDF)

(EM1, EM2, and UIDF) and bivariate method (BIDF). It can be noted from Figs. 4.9 and 4.10 that the EM1 (Eq. 4.14) consistently underestimated the rainfall intensity with an exception for 2 h and 3 h durations. The under/over estimation is compared to other approaches. It is interesting to note that all the methods compared well with the results of the bivariate method for 2 h and 3 h durations with a percentage difference less than 20%. For all other durations, the results from EM1 falls outside the prediction interval with an underprediction varying from a marginal 2 % to as high as 80 %.

The rainfall intensity obtained from EM2 (Eq. 4.15) compared well with the bivariate results for short durations with majority of the data falling within the prediction interval. However, the deviation increases as the duration exceeds 3 h with the underestimation varying from 20% to 30%. Except for 0.5 h duration, the univariate rainfall intensity is beyond the confidence interval for majority of the cases. Similar to EM2, the percentage difference of univariate results (UIDF) increased for duration > 3h reaching a maximum of 60 %. For short duration, the historical UIDF curve compared well with the historical BIDF curve with marginal under and over estimations. Hence, both EM2 and UIDF curves can be confidently used for urban catchment considered in this study for short durations ($\leq$ 3h) but may not be considered robust for duration > 3h. These aspects could not be figured out from the discussion of Fig. 4.8. Hence, a bivariate approach may be more appropriate for such cases.

Previous studies have noted such difference between the IDF curves developed using empirical models and bivariate analysis (Ariff et al., 2012; Singh and Zhang, 2007). Given the variation in the IDF curves developed using empirical models and univariate analysis, a bivariate copula based IDF curve needs to be adopted for the design of hydraulic structures in the urban catchment. However, the present study also indicates that selective empirical model and univariate IDF curve may also fair well for specific durations, which will depend upon the study area, nature of historical rainfall data and hence cannot be generalized. Given the association between the storm intensities and duration, only the bivariate copula approach was adopted for deriving the future climate data based IDF curve.

4.4.4 Bivariate IDF Curve Based on Climate Data

Figure 4.11 presents the bivariate IDF (BIDF) curve considering the future climate data for three different time periods designated by P1 (2021-2047), P2 (2048-2074) and P3 (2075-2100). As stated earlier, four different RCPs with their features listed in table 4.10 has been used. Among all the RCPs, the RCP 2.6 represents the low emission scenario whereas RCP 8.5 represents the high emission scenario. This study attempts to understand how these climate scenarios translate to the changes in predicted future IDF curves (Future BIDF) as compared to the historical rainfall based bivariate IDF (historical BIDF) curve. While Fig. 4.11 gives an overall understanding of the future climate data based IDF curve, for urban hydrologic analysis, the effects of different RCPs on rainfall intensity for shorter durations needs to be analysed in detail. For this purpose, Fig. 4.12 depicts the rainfall intensity plotted against return period for durations $\leq$ 1 h corresponding to dif-

ferent RCPs and future time periods. Rainfall intensity obtained from bivariate copula modeling of historical rainfall (historical BIDF) data was used as the reference for understanding the influence of future climate data. This would help to assess the drift in rainfall intensity associated with future climate data imposing different scenarios listed in table 4.10.

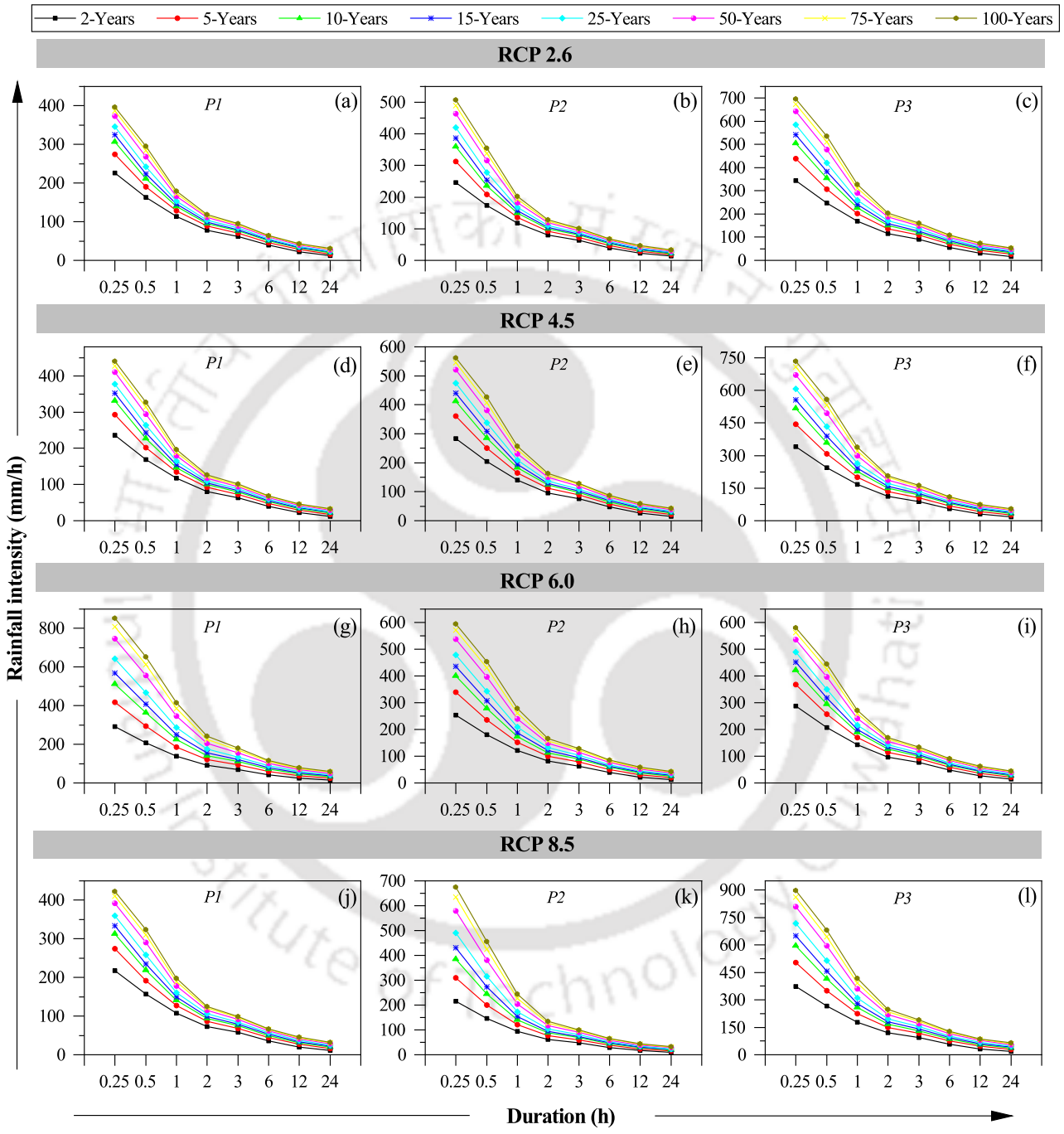

Figure 4.11: Future IDF curves developed using bivariate analysis (BIDFs) for different climate scenarios and different time periods (P1, P2, and P3)

Table 4.10: Summary of different scenarios considered in this study (IPCC, 2014)

Scenario	Special Considerations by IPCC
RCP 2.6	• Stringent mitigation scenario • Radiative forcing peaks to 3 W/m² before 2100 and afterward decline to 2.6 W/m² at stabilization after 2100 • Global mean surface temperatures and sea level are expected to rise by 0.3°C to 1.7°C and 0.26-0.55 m respectively between 2081 - 2100, compared to 1986–2005 • In comparison to the 20th century, the annual global flood exposure increases by 1-7 times over the century
RCP 4.5	• Intermediate scenario • Stabilization of radative forcing at 4.5 W/m² in the year 2100 • Global mean surface temperatures and sea level are expected to rise by 1.1°C to 2.6°C and 0.32-0.63 m respectively between 2081-2100, compared to 1986–2005 • In comparison to the 20th century, annual global flood exposure increases by 2-12 times over the century
RCP 6.0	• Intermediate scenario • Stabilization of radative forcing at 6 W/m² in the year 2100 • Global mean surface temperatures and sea level are expected to rise by 1.4°C to 3.1°C and 0.33-0.63m respectively between 2081-2100, compared to 1986–2005 • In comparison to the 20th century, annual global flood exposure increases by 1-13 times over the century
RCP 8.5	• Very high Green house gas (GHG) emissions • Radiative forcing pathway leading to 8.5 W/m² in 2100 • Global mean surface temperatures and sea level are expected to rise by 2.6°C to 4.8°C and 0.45-0.82 m respectively between 2081-2100, compared to 1986–2005 • In comparison to the 20th century, annual global flood exposure increases by 4-24 times over the century • Increase in the annual average rainfall at high latitudes, equatorial Pacific, and mid-latitude wet regions while decreasing in mid-latitude and subtropical dry regions. • Frequent and intense extreme rainfall events over the mid-latitude land masses and the wet tropical regions.

4.4.4.1 Comparison of Climate Based BIDF Curve with Historical BIDF Curve

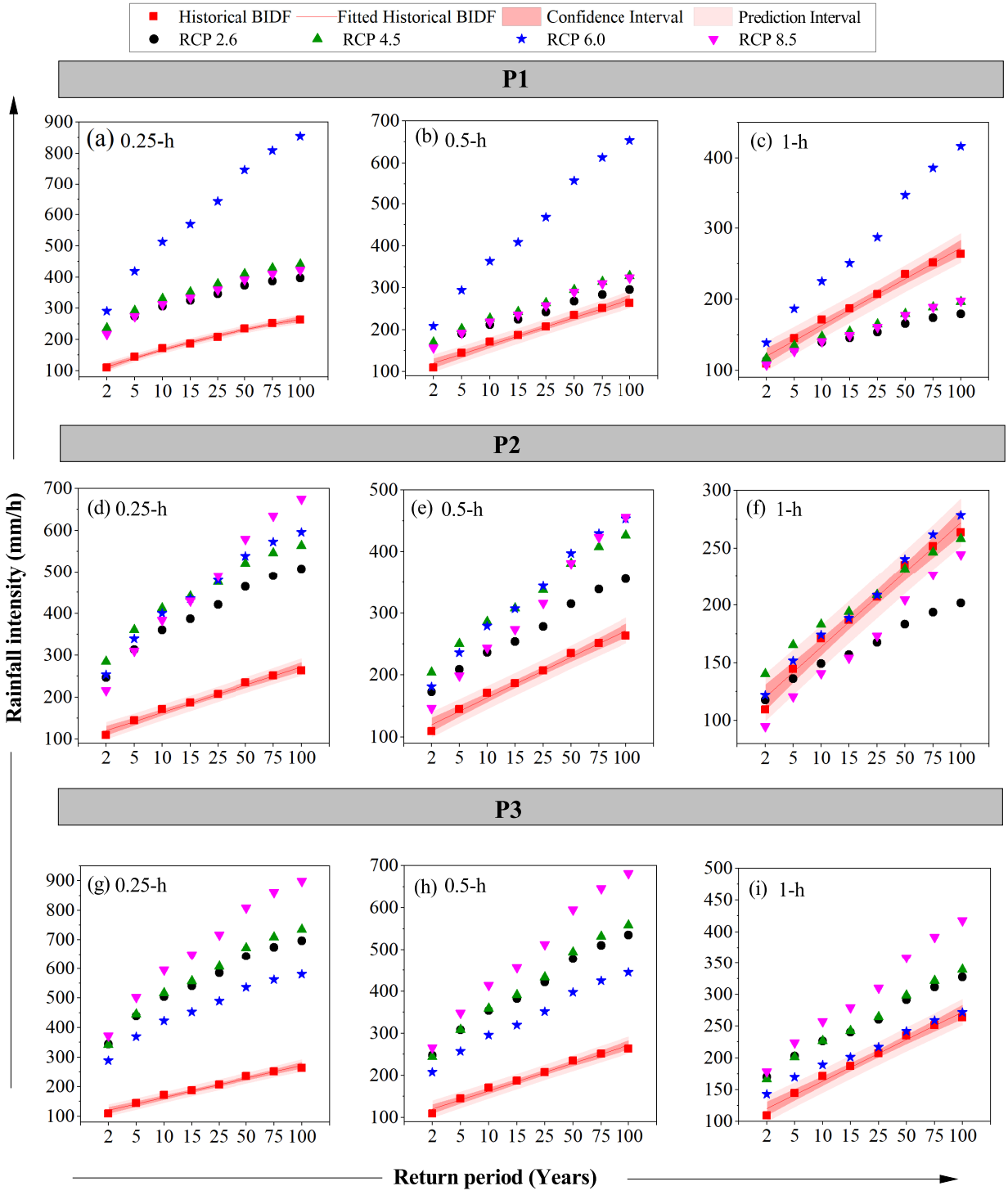

Figure 4.12: Comparison of historical and future BIDF curves for different RCP scenarios for different time periods (P1, P2, and P3)

The data presented in Fig.4.12 indicates that the rainfall intensity obtained from the future BIDF curve is far from the confidence interval of the historical BIDF curve except for one particular case of P2 – 1 h duration. For 0.25 h and 0.5 h durations, the rainfall intensity corresponding to all

the climate scenarios and time periods exhibited a significant increase from the historical data. A closer look at Fig. 4.12 reveals that different time periods considered in this study also induces variability in rainfall intensity and portray different trends. For the near future (P1), the rainfall intensity determined from RCP 6.0 scenario was consistently much higher than other scenarios. For P1-1hr, except RCP 6.0 all other scenarios were showing a decrease in the rainfall intensities when compared with the historical rainfall intensities. For the intermittent period P2 (2048-2074), all the scenarios were showing an increasing trend in the rainfall intensities except for P2-1hr. For P2-1 h duration, the rainfall intensities from all the climate scenarios were close to the historical reference data and RCP 2.6 and RCP 8.5 was showing a decrease in rainfall intensity compared to the historical. For the extreme time period P3 (2075-2100), the rainfall intensity obtained from RCP 8.5 was predominantly higher than all other data for all the durations. This shows that the severe climate change conditions imposed in RCP 8.5 become more impactful as time progresses. Strangely, the rainfall intensity determined from RCP 6.0 gave a minimum value (still higher than the historical reference data) among all the climate scenarios. Both RCPs 2.6 and 4.5 gave identical rainfall intensity higher than RCP 6.0. The reasons for such trends could not be explored in this study.

4.4.5 Comparison of the Variability in the Mean Rainfall Intensities

One aspect that is not clear from the above discussion is the overall comparison of rainfall intensities for all the methods considered in this study. For this purpose, the mean rainfall intensity and its variability were calculated by considering all the durations corresponding to a particular IDF curve development method and return period as depicted in Fig. 4.13. The box plot compares the mean rainfall intensity and its variability for two empirical models, univariate, bivariate historical rainfall data, four future climate scenarios corresponding to three different time periods (EM1, EM2, UIDF, historical BIDF and future BIDF for all the RCP scenarios for different periods). The overall trend for mean rainfall intensity and its variation is identical for all the return periods. All the climate based scenarios and time periods gave mean rainfall intensity higher than the historical rainfall intensity.

For RCP 2.6 and 4.5, the mean rainfall intensity progressively increased with the advancement in time period. For RCP 6.0, the mean rainfall intensity was highest in the near future and comparable for P2 and P3. Among all the scenarios considered, RCP 8.5 – P3 gave the highest mean rainfall intensity. The RCP 2.6 exhibited the least increase in rainfall intensities and can be attributed to the mitigation scenario leading to a very low forcing level. It is clear from the study that for considering the influence of near future climate change on infrastructure with design life < 50 years, the RCP 6.0 scenario would yield the worst case IDF curve for the study area. For long term planning with a design life > 50 years for this area, it is desirable to consider the IDF curve based on the RCP 8.5 scenario.

This study indicates that the future IDF curves considering the effect of climate change (future BIDFs) is drastically different from the IDF curves developed using the historical rainfall data.

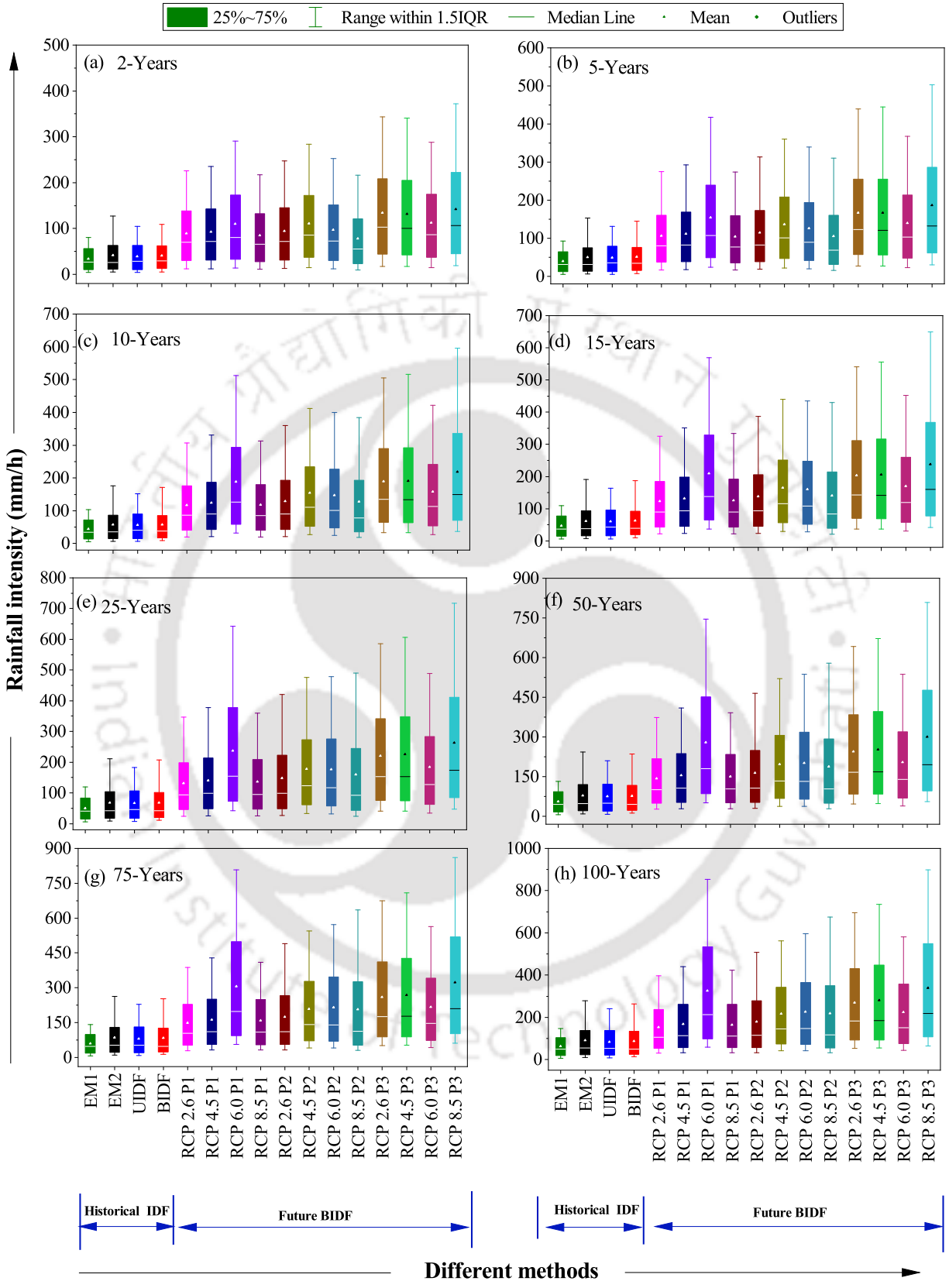

Figure 4.13: Variability in the rainfall intensities of different historical and future IDF curves

The results from the existing literature confirm that the IDF curve of different regions portrays varying trends when the effect of climate change is considered. Singh et al. (2016) observed that with intensifying RCP scenarios, the rainfall intensities were also increasing for Roorkee, India. Hosseinzadehtalaei et al. (2020) have developed IDF curves for the entire continent of Europe on the basis of two climate scenarios, namely RCP 8.5 and RCP 4.5. The authors found that the RCP8.5 was giving higher increase in the intensities in comparison to RCP 4.5. The authors also concluded that the change in intensities is higher for distant future than the near or medium term. Soltani et al. (2020) observed a reduction in the rainfall intensity under both RCP 4.5 and RCP 8.5 scenarios for southwest Iran. The analysis presented in this study also encompasses some of the trends reported in the literature. The present study and the literature confirm that in order to comprehend the impact of climate change, particularly extreme rainfall, comprehensive studies must be conducted on a local scale, as it is not a "one size fits all process" (Cook et al., 2020; Lee et al., 2020).

4.5 Summary

This study explored the importance of copula based bivariate rainfall intensity duration frequency (BIDF) curves for a prominent urban catchment of northeast India incorporating the effects of future climate change. The possible drift in the IDF curve from the reference historical rainfall data associated with the climate change impact is quantified. The bivariate copula based approach was used to develop IDF curves from historical rainfall data, which were compared with two conventional empirical models (Babu et al., 1979; Kothyari and Garde, 1992) and a univariate frequency analysis. The empirical model, EM1 proposed by Babu et al. (1979) for Indian catchments did not perform well for short durations whereas EM2 proposed by Kothyari and Garde (1992) was found to adequately capture the trends of historical rainfall when compared with the BIDF curves. The under/over estimation is compared to other approaches. Both EM2 and univariate IDF (UIDF) curves can be confidently used for urban catchment considered in this study for short durations ($\leq$ 3h) and may not be considered for duration > 3h as the percentage differences are significantly high when compared with bivariate historic rainfall intensity. Given the variation in the results obtained from empirical and UIDF curves, a bivariate copula based IDF (BIDF) curve is highly recommended for the design of new hydraulic structures and/or augmentation of drainage facilities in an urban catchment. The BIDF would also depend upon the study area, nature of historical rainfall data, and hence cannot be generalized.

Further, this study attempts to understand how the different climate scenarios translate to the changes in predicted future BIDF curves as compared to the historical rainfall based BIDF curves. It is also understood that BIDF is a better choice for encompassing the bivariate association of rainfall intensity and duration specifically for long return periods. For this purpose, four climate scenarios (RCP 2.6, 4.5, 6.0, and 8.5) spanning over three time periods (P1 2021-2047; P2 2048-2074; P3 2075-2100) were considered. The rainfall intensity corresponding to all the climate scenarios and time periods exhibited a significant increase from the historical rainfall data espe-

cially for short duration. RCP 6.0 was showing higher rainfall intensities for the near future and both RCP 6.0 and 8.5 exhibited a similar trend for the intermittent period. RCP 8.5 was predominantly higher than all other data for all the durations in the distant future. This shows that the severe climate change conditions imposed on RCP 8.5 (high baseline emission) become more impactful as time progresses. For considering the influence of near future climate change on infrastructure with design life of $\leq$ 50 years, the RCP 6.0 scenario would yield the critical IDF curve. For long term planning with a design life of > 50 years, it is desirable to consider the IDF curve based on the RCP 8.5 scenario.

The results presented in this study and the literature highlights the importance of conducting comprehensive studies on a local scale for incorporating the impact of climate change on IDF curves. This is specifically true for urban catchments in developing countries like India, where the infrastructure growth and augmentation of hydraulic structures are happening at a great pace. The updated IDF curve incorporating the changing pattern of rainfall due to climate change is very important for the efficient design of hydraulic structures with adequate capacity.

Chapter 5

Quantification of Land Use/ Land Cover and Imperviousness

5.1 General

Urbanization is the conversion of natural landscapes to urban environments such as residential, road, commercial, and other paved areas, which can drastically alter a watershed's hydrology. Rapid urbanization has become a significant concern for urban planners as it directly impacts the hydrological processes. Urbanization increases the imperviousness of the surface and decreases the infiltration of water into the soil, thereby increasing surface runoff and flood risk and decreasing hydrologic reaction time. Studies have shown that a detailed analysis of urbanization can improve the design of the stormwater drainage system as imperviousness reduces the efficiency of the stormwater drainage (Bibi et al., 2023; Hussain et al., 2021; Neupane et al., 2021). Therefore, quantifying imperviousness, especially for an urban watershed, is extremely important.

Imperviousness especially the built-up area, can be commonly determined using field surveys, aerial photographs, or satellite images. Field surveys give actual results; however, they are labour-intensive, costly, and tedious. In recent years, remote sensing techniques and geographic information system (GIS) analysis have gained popularity due to the easy availability of high-resolution satellite images, which can be processed using image processing softwares, like ENVI (Environment for Visualising Images), ERDAS IMAGINE, ArcGIS, and Quantum Geographic Information System (QGIS). This study used ArcGIS and matrix laboratory (Matlab) to visualize, analyze and process images.

This chapter deals with the quantification of LULC changes that has taken place during the period 2011-2022 in the study area. From the LULC details, the imperviousness of the study area is determined, which will be used as an input for the flood modeling. The detailed procedure of estimating the imperviousness from fine-resolution imageries is also described in this chapter. The overall methodology used for the classification of satellite images for the quantification of LULC changes is shown in Fig. 5.1.

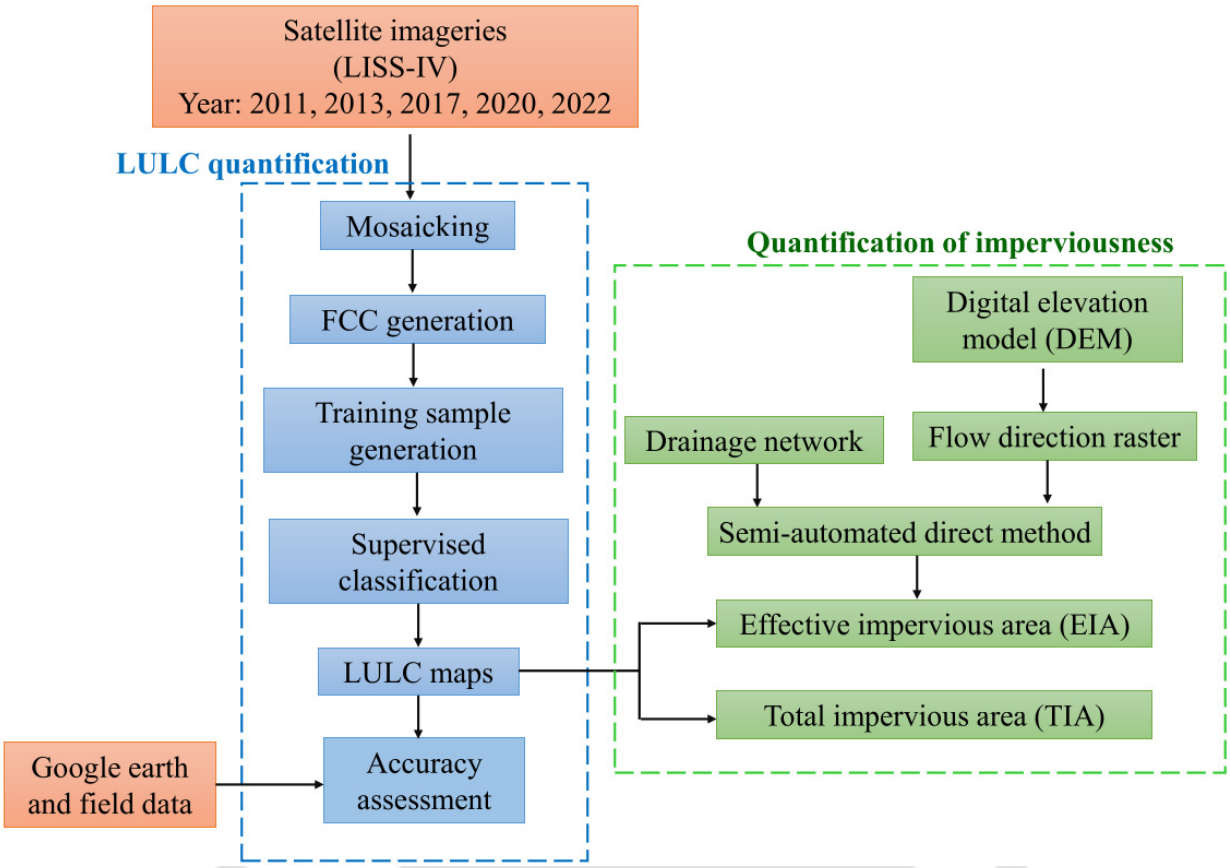

Figure 5.1: Schematic of the landuse classification framework used to generate the imperviousness of the study area

5.2 Determination of LULC Changes

5.2.1 Overview of Classification

Image classification is the process of categorising each pixel in a remotely sensed image according to a LULC classification system. The LULC changes were analysed using the high-resolution multi-spectral LISS-IV images obtained from the National remote sensing centre (NRSC), India. The details of the images used in this study are described in table 3.6 of chapter 3. Individual bands of LISS-IV give the images in different shades of grey. These bands can be combined to form coloured images called as true colour composite (TCC). In remote sensing data analysis, the combination of green, red, and near-infrared bands, which correspond to the blue, green, and red spectral regions, respectively, can produce a colored image known as a false color composite (FCC). An FCC image enhances the objects that are undetectable or poorly visible to the human eye.

The fundamental principle of classification is that different features or objects have unique spectral signatures, and distinct properties are associated with specific digital number (DN). Based on training data, classification techniques can be grouped into two types: unsupervised and super-

vised, as shown in Fig. 5.2. The basic assumption involved in these two types of classification is that each pixel in the image is homogeneous and can be assigned to only one class (Li et al., 2014). In other words, it is assumed that each pixel represents a single land cover or land use class and does not contain mixtures of different materials or spectral signatures. In unsupervised classification, the remote sensing image is categorised into different classes based on the DN and prior knowledge of the study area is not required (Joseph, 2005; Lillesand et al., 2015). Supervised classification is based on training data generated from field surveys and knowledge about the study area. The algorithm then compares the spectral properties of each pixel with the training samples and then classifies each pixel to the appropriate class type using decision rules (Joseph, 2005; Lillesand et al., 2015). Supervised classification is more reliable and accurate as compared to unsupervised classification (Dadashpoor et al., 2019; Wang et al., 2018a). So, in this study, the supervised classification was used to quantify the LULC in the study area.

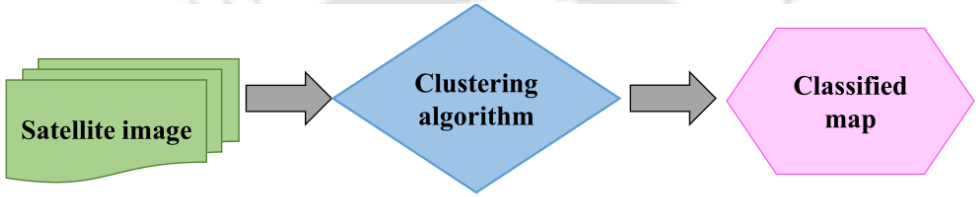

(a) Unsupervised classification

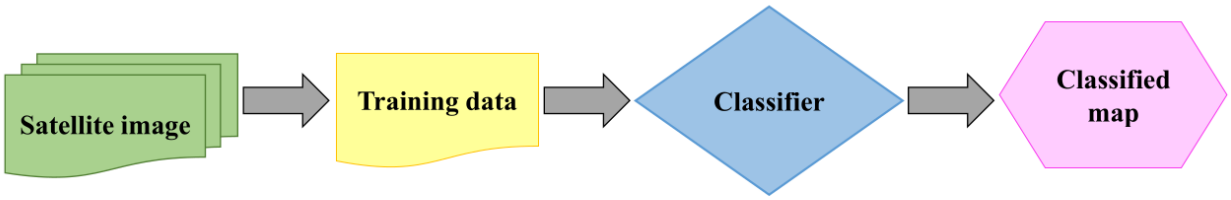

(b) Supervised classification

Figure 5.2: Types of classification algorithm (a) unsupervised classification and (b) supervised classification

5.2.1.1 Maximum Likelihood Classifier

The Maximum likelihood classifier (MLC) approach is the most extensively used supervised classification algorithm for LULC extraction (Dadashpoor et al., 2019; Wang et al., 2018a). MLC is based on the Bayes theorem, and it states that the probability that a pixel belongs to feature vector **v** belongs to a class n is given as Eq. 5.1

$$P(n|\mathbf{v}) = \frac{P(\mathbf{v}|n)P(n)}{P(\mathbf{v})} \tag{5.1}$$

where $P(n|\mathbf{v})$ is the posterior distribution, $P(\mathbf{v}|n)$ is the class specific probability density function, $P(n)$ is the prior probability and $n = 1, 2, ...N$, and $P(\mathbf{v})$ is the probability that **v** is observed and it is given by Eq. 5.2

$$P(\mathbf{v}) = \sum_{n=1}^{N} P(\mathbf{v}|j)P(j) \tag{5.2}$$

Suppose there are two classes n and j, and $P(\mathbf{v})$ is independent of n, then the decision rule for $\mathbf{v}$ is in class n can be written as Eq. 5.3

$$P(\mathbf{v}|n)P(n) \geq P(\mathbf{v}|j)P(j) \ \ \forall \ \ j = 1, 2, ...K \tag{5.3}$$

As each class is assumed to follow a normal distribution, it is easy to define the discriminant function, $d_n(\mathbf{v})$ of MLC as Eq. 5.4 (Canty, 2009)

$$d_n(\mathbf{v}) = log\ P(n) - \frac{1}{2}\ log\ |C_n| - \frac{1}{2}(x - \mu_n)^T C_n^{-1}(x - \mu_n) \tag{5.4}$$

where μ_n is mean vector, x is the M-dimensional data and M is the number of bands, C_n is the covariance matrix.

Thus, the maximum likelihood classifier can be obtained as given by Eq. 5.5

$$d_n(\mathbf{v}) > d_j(\mathbf{v}) \ \ \forall \ \ j = 1, 2, ...K \tag{5.5}$$

5.2.2 Accuracy Assessment

Accuracy assessment is used to validate the classified map, which assesses the quality of acquired information by justifying whether remotely sensed data are correctly classified or misclassified. This can be performed by comparing the classified LULC map and ground truth points or using Google Earth photos, which is vital for generating outcomes assessment and decision-making (Chughtai et al., 2021). A confusion matrix, also referred to as an error matrix, is a widely used method for evaluating the accuracy of classified maps and quantifying the misclassification of pixels. The confusion matrix provides a tabular representation of the relationship between the actual and classified values of the pixels in the map. In this study, the user accuracy (UA), producer accuracy (PA), overall accuracy (OA), and Kappa coefficient ($\mathcal{K}$) (Islami et al., 2022; Singh and Pandey, 2021) was used.

User's Accuracy (UA) refers to the probability of correctly classifying a pixel into a specific class, and is calculated by dividing the number of correctly classified pixels in that class by the total number of pixels classified in that class (Eq. 5.6) and is also called a Type I error.

$$\text{UA} = \frac{\text{Total number of correctly classified pixel in each class}}{\text{Sum of reference pixels in that class (Row)}} \tag{5.6}$$

PA is the probability that the predicted values actually belong to the class they have been as-

signed to. It is calculated by dividing the number of correctly classified pixels in a specific class by the total number of pixels in the ground truth data for that class (Eq. 5.7) and is also called a Type II error.

$$\text{PA} = \frac{\text{Total number of correctly classified pixel in each class}}{\text{Sum of reference pixels in that class (Column)}} \tag{5.7}$$

OA is an accuracy metric used to evaluate the accuracy of a classified map as a whole. It is defined as the ratio of the total number of correctly classified pixels to the total number of reference pixels in the map as given in Eq. 5.8. The reference pixels refer to the ground truth data used to evaluate the classification results, and the diagonal values in the confusion matrix represent the number of correctly classified pixels.

$$\text{OA} = \frac{\text{Total number of correctly classified pixel (Diagonal)}}{\text{Sum of reference pixels}} \tag{5.8}$$

Kappa coefficient ($\mathcal{K}$) is used to understand the agreement of the classified image with that of the reference image, and mathematically $\mathcal{K}$ is represented as Eq. 5.9. Table 5.1 shows the range of the Kappa coefficient and the strength of agreement.

$$\mathcal{K} = \frac{N \sum_{p=1}^{q}(X_{pp}) - \sum_{p=1}^{q}(X_{p+}\, X_{+p})}{N^2 - \sum_{p=1}^{q}(X_{p+}\, X_{+p})} \tag{5.9}$$

where, q is the number of rows in the confusion matrix, N is the total number of points considered, X_{pp}, X_{p+}, X_{+p} are correctly classified diagonal points, total number of points in row $+p$ and total number of points in column $p+$ respectively.

Table 5.1: Rating criteria of kappa statistics (Islami et al., 2022)

Kappa Statistics (%)	**Strength of Agreement**
<0	Poor
0-20	Slight
21-40	Fair
41-60	Moderate
61-80	Substantial
81-100	Almost perfect

5.3 Quantification of Imperviousness

Urbanization has increased the imperviousness of urban watersheds, thereby reducing the infiltration and increasing the surface runoff. So, quantification of imperviousness is essential for urban hydrologic analysis and urban flood management. Roads, building rooftops, parking lots, and

other infrastructures fall under the impervious category (Sahoo, 2014; Yang et al., 2018), which are termed as total impervious area (TIA) (Han and Burian, 2009; Sahoo and Sreeja, 2013). TIA is further subdivided into two types: impervious area that is not hydraulically connected, known as non-effective impervious area (NEIA), and directly connected impervious area (DCIA). The DCIA is also known as effective impervious area (EIA) (Han and Burian, 2009; Sahoo and Sreeja, 2013). EIA has a direct connection with the stormwater drainage inlets. Examples of EIA are gutters, parking lots, and streets with a curb which drains onto the streets, whereas examples of NEIA include rooftops that drain to a pervious area (Alley and Veenhuis, 1983). TIA can be mathematically expressed using Eq. 5.10.

$$\text{TIA} = \text{NEIA} + \text{EIA} \tag{5.10}$$

Even though TIA can easily be determined using remote sensing satellite images, it overestimates runoff from the urban flood modelling perspective (Alley and Veenhuis, 1983; Booth and Jackson, 1997; Han and Burian, 2009; Sahoo and Sreeja, 2013). Usually, EIA should be less than TIA, but due to increase in urbanization, it can go up to a value of TIA. Determination of EIA requires information about drainage networks and fine-resolution satellite images. EIA has been found to give a better result for hydrologic studies as compared to TIA. Sahoo and Sreeja (2016) has shown that EIA is more appropriate for urban flood studies. In this study, EIA is considered for the flood modelling, which can be determined using fine-resolution images.

5.3.1 Determination of TIA

TIA can be considered as a surrogate indicator of urbanization. However, the determination of TIA using direct methods are tedious, indirect methods have to be utilized for obtaining an approximate estimate. But with the advancement in remote sensing techniques, TIA can be accurately determined using the satellite images. In this study, TIA is estimated using fine-resolution LISS-IV images. The images are classified into two different classes using the maximum likelihood classifier (MLC) algorithm, namely pervious and impervious as shown in Fig. 5.3. The impervious class is extracted and designated as TIA.

5.3.2 Determination of EIA Using Semi-Automated Direct Method

Effective impervious area (EIA) gives a fair estimate of the imperviousness of the urban catchment. Techniques to determine EIA can be broadly grouped into two: direct and indirect methods. Direct approaches, like field surveys, can be used to estimate EIA; however, they are time-consuming. Another technique involves using different empirical equations which establish a relationship between the density of the population, LULC (Kauffman et al., 2006), TIA (Alley and Veenhuis, 1983; Sutherland, 1995), and using rainfall-runoff data (Ebrahimian et al., 2016). These empirical methods are easy to apply; however, they are less accurate as they are primarily de-

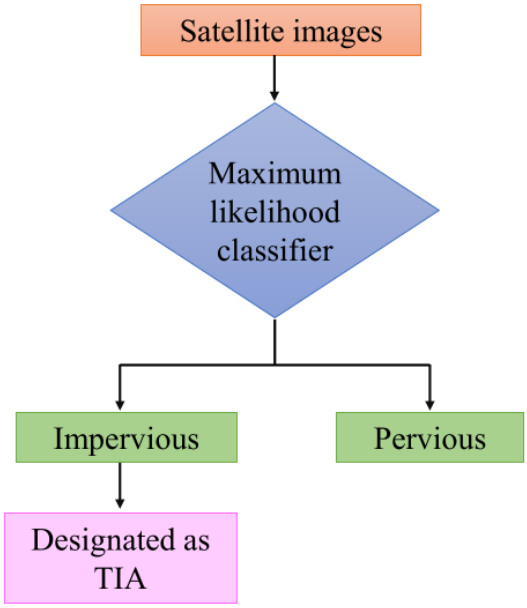

Figure 5.3: Flow chart for determining the TIA from fine resolution images

veloped or derived for a particular location and lack the spatial distribution of impervious surfaces required to anticipate stormwater runoff effectively. Several recent studies have combined remote sensing and GIS techniques to estimate EIA. Han and Burian (2009) developed a semi-automated identification of the EIA using geospatial analysis.

This study estimates EIA from fine-resolution images using a semi-automated direct method (Han and Burian, 2009; Sahoo and Sreeja, 2013). The method involves classifying the image into two categories: pervious and impervious classes, using the MLC algorithm. The digital elevation model (DEM), drainage network, and classified maps are digitized and converted to a common coordinate system. The classified image is superimposed on the drainage network layer of the study area, and the pixel through which the drainage network passes is selected. If a selected pixel is impervious, it is chosen, and its nearby pixels are examined. If the nearby pixels are also impervious, they are chosen, but if they are pervious, they are ignored. The flow direction was checked in these selected pixels. The flow direction is determined using the DEM, and if the flow direction is from impermeable pixels to the pixel under consideration, they are labeled as EIA; otherwise, they are ignored. The assumption made in this study is that the drainage network is open throughout the study area, as the precise locations of manholes and gutters were unknown. The entire methodology is summarized in a flowchart as shown in Fig. 5.4.

5.4 Results and Discussion

This section describes the result obtained from this study. It is divided into two sections. The first section provides a quantitative analysis of the observed changes in land use and land cover (LULC) in the study area, while the second section focuses on quantifying imperviousness in terms of both TIA and EIA.

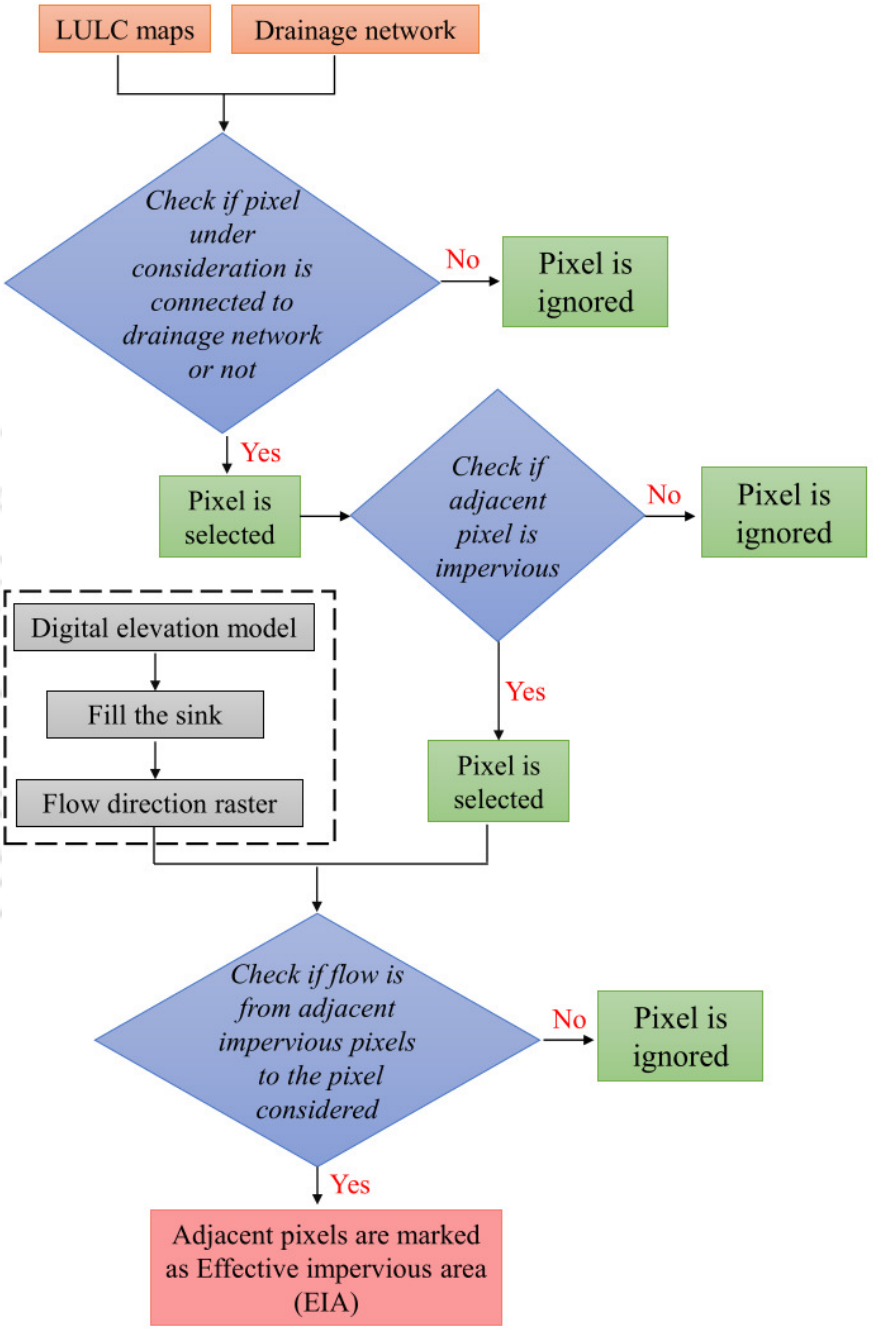

Figure 5.4: Semi-automated method for determining the EIA from fine resolution images

5.4.1 Quantification of LULC Changes

The quantification of LULC changes was achieved using the image analysis using remote sensing techniques. The satellite images of the study area for different years spanning from the year 2011 to 2022 were collected for studying the LULC changes. After identifying the various LULC classes, the built-up area is utilised to determine the imperviousness (TIA and EIA) of the study area. The false colour composites (FCC) of the images were developed as shown in Fig. 5.5. These images show that the built-up area (cyan colour) is increasing with the year.

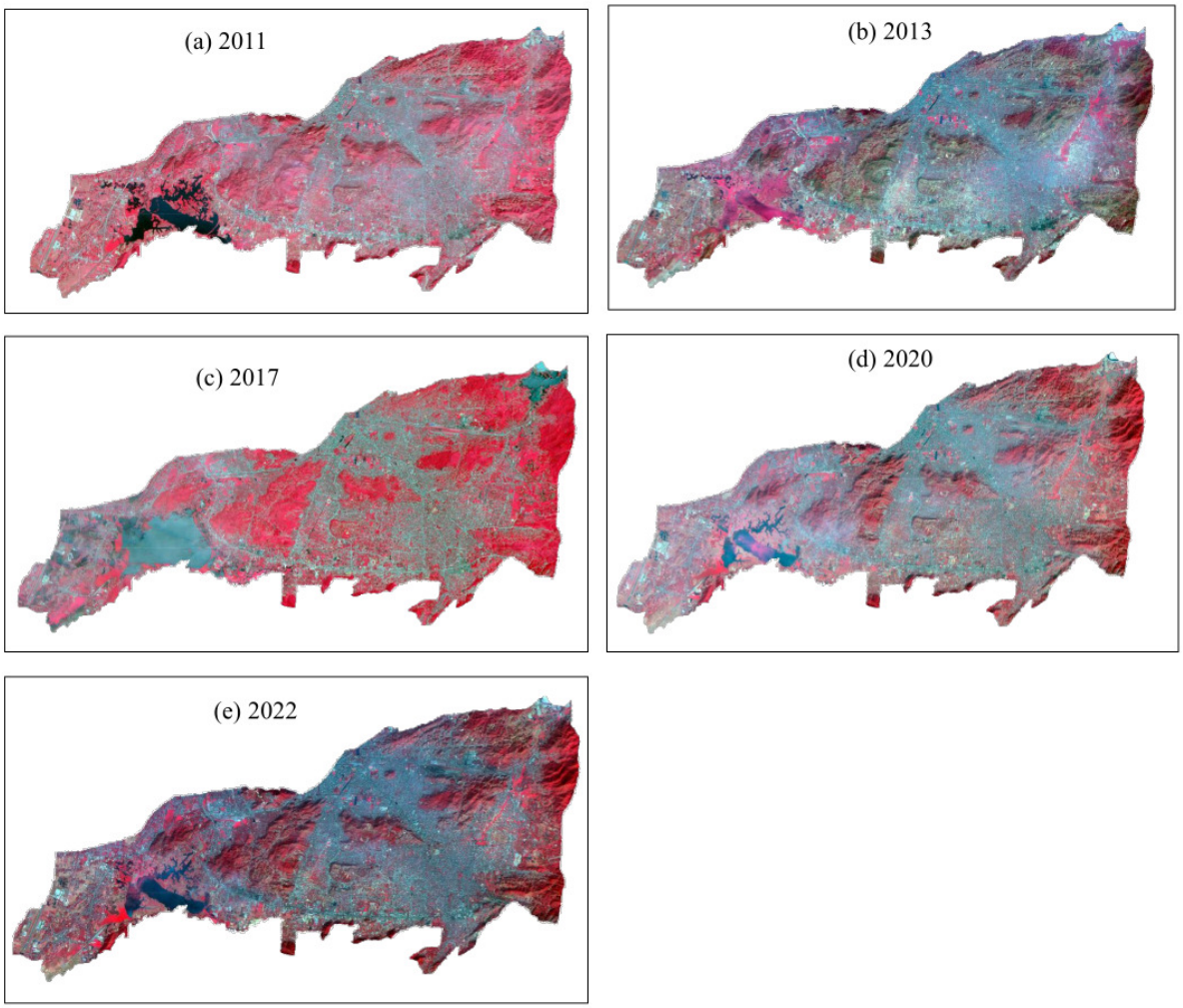

Figure 5.5: False colour composite of satellite imageries for different years (a) 2011, (b) 2013, (c) 2017, (d) 2020, and (e) 2022

The training samples are generated from the FCC images, with the knowledge of study area by means of field data and visual interpretation. Then, the supervised classification was performed using the training samples. The LULC maps for the study area for 2011, 2013, 2017, 2020, and 2022 are shown in Fig. 5.6. Table 5.2 gives the details of the different LULC classes for different years considered. The entire study area is divided into five classes: built-up, water body, forest, swampy land, and vegetation. Vegetation includes cropland, scrub land, and fallow land. From

Fig. 5.6 and table 5.2, it is clear that the built-up area is showing an increasing trend. The forest area and vegetation are found to decrease from 2011 to 2022. For 2013, forest area was found to be low (7.98 km^2) compared to the year 2011 (22.93 km^2) due to the mis-classification of the image as some of the forest area during that year was dry. This is confirmed by comparing the previous images and those from google earth. These areas were mis-classified as swampy land due to the colour code. The water body is showing a slight decrease for the years considered. As seen from the Fig. 5.6 (b), for the year 2013, the primary water body in the study area (Dipor bil) is classified as swampy land since the water body was covered with water hyacinth. This has been accounted for and corrected in table 5.2. The image acquisition date for the year 2017 was during the monsoon period due to the nonavailability of good quality cloud-free images. As a result of this, the area of waterbody was found to be more in comparison with other years, which can be observed in Fig. 5.6 (c). Minor mis-classification of vegetation as built-up areas and water bodies has been rectified in table 5.2 by comparing with the previous year image and google earth images for different months of the same year.

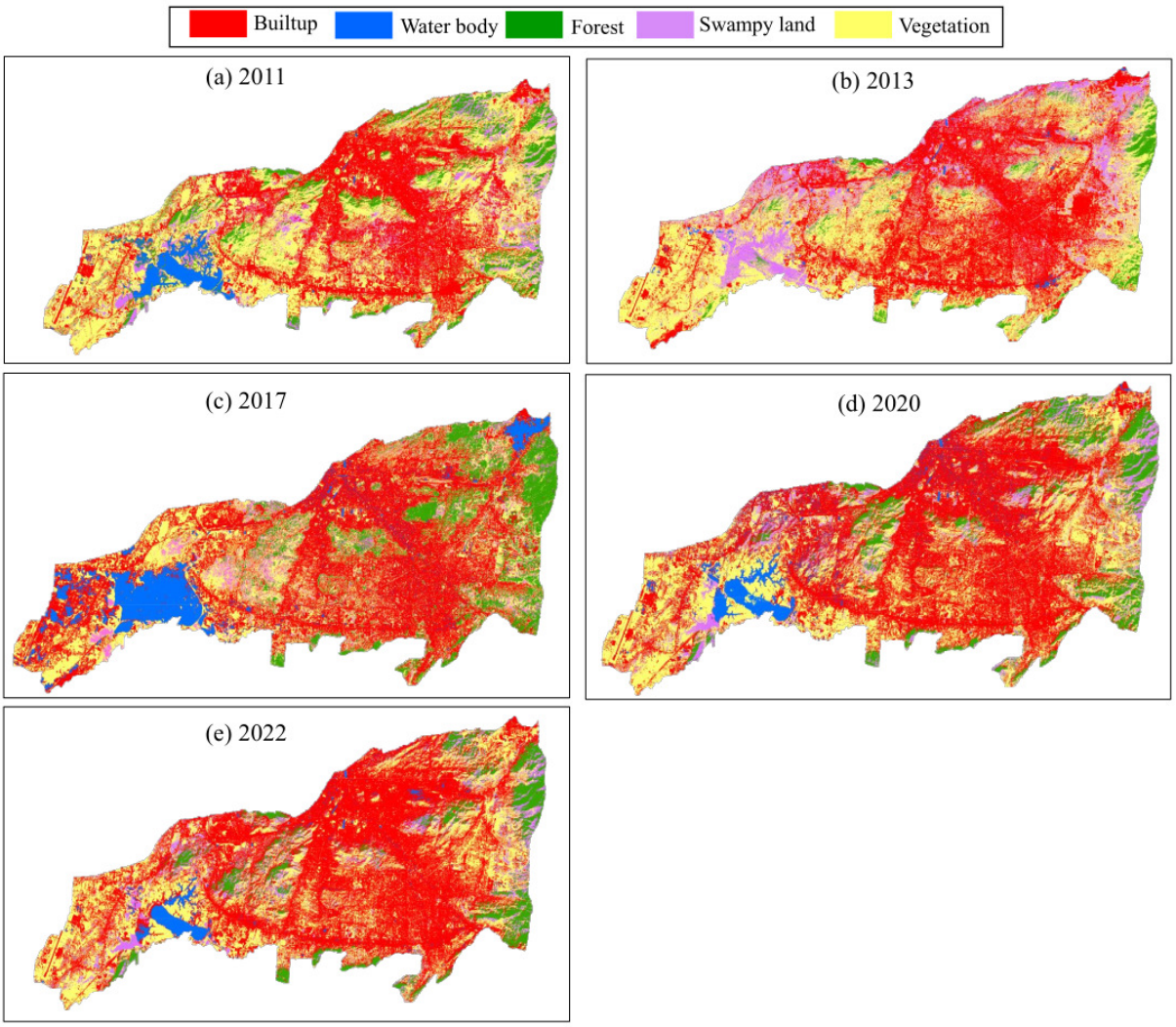

Figure 5.6: LULC map of the study area for different years (a) 2011, (b) 2013, (c) 2017, (d) 2020, and (e) 2022

Table 5.2: Land use land cover distribution over Guwahati from 2011 to 2022

Class type	Colour code	Area (km^2)				
		2011	2013	2017	2020	2022
Builtup	Red	81.88	89.38	100.08	106.76	115.01
Forest	Green	22.93	7.98	21.72	19.18	18.24
Swampy land	Purple	23.67	30.49	22.52	21.93	20.49
Vegetation	Yellow	91.82	92.39	76.32	72.72	68.35
Water body	Blue	7.17	7.22	6.81	6.17	5.37

Figure 5.7 shows the temporal changes in the LULC classes from 2011 to 2022. It can be observed that the increase in the built-up area is occurring at the expense of converting the agricultural area, swampy land and forest area. Table 5.3 shows the changing pattern in the different classes from 2011 to 2022. A positive value indicates an increase in the area, which is seen only for the built-up class, and a negative value indicates a decrease in the area. A 20.26% increase in built-up area was observed from 2011 to 2022 for the study area.

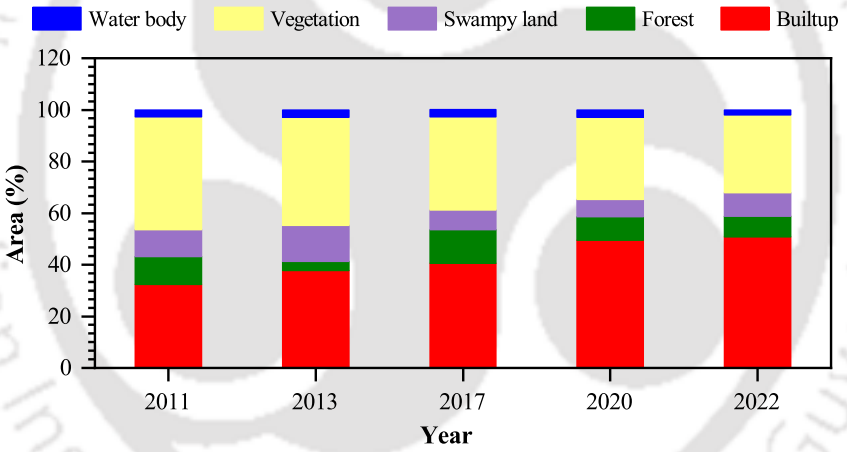

Figure 5.7: Temporal change of different land classes

Table 5.3: Change detection of various land covers from 2011 to 2022

Class type	2011		2022		Change in area from 2011 to 2022	
	Area (km^2)	% of total area	Area (km^2)	% of total area	Area (km^2)	% of total area
Builtup	81.88	36.00	115.01	50.56	33.13	14.57
Forest	22.93	10.08	18.24	8.02	-4.68	-2.06
Swampy land	23.67	10.40	20.49	9.01	-3.18	-1.40
Vegetation	91.82	40.37	68.35	30.05	-23.47	-10.32
Water body	7.17	3.15	5.37	2.36	-1.79	-0.79

+ve value shows an increase in area; -ve value shows a decrease in area

Figure 5.8 shows the conversion of different land-use classes to built-up land. It is clear from the figure that, from 2011 to 2022, the land-use classes such as vegetation, swampy, and forest land have been converted into built-up areas.

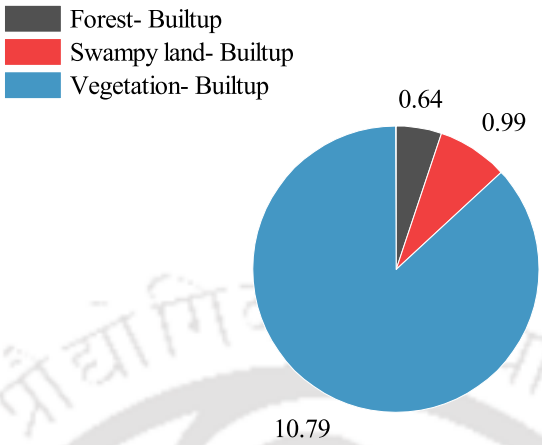

Figure 5.8: Change in LULC classes to built-up from 2011 to 2022

5.4.1.1 Accuracy Assessment of Classified Maps

The accuracy of the classified map is determined by taking random points in the classified map and then comparing them with the ground points through google earth images of the same year. Accuracy assessment is done by calculating the UA, PA, OA, and Kappa coefficients. Fig. 5.9 shows the overall accuracy (OA) and Kappa coefficient values of the classified maps for the years 2011, 2013, 2017, 2020, and 2022. The Kappa coefficient ($\mathcal{K}$) of the LULC maps for all the years is above 80%, which falls under substantial and almost perfect as per table 5.1. Table 5.4 shows the different accuracy values (UA and PA) of the classified LULC map. All the classes offered good accuracy value except for the swampy class for 2011 (UA = 44%). From the accuracy assessment results, it can be concluded that the classified maps are in good agreement with the ground truth points. So these maps can be used for further analysis.

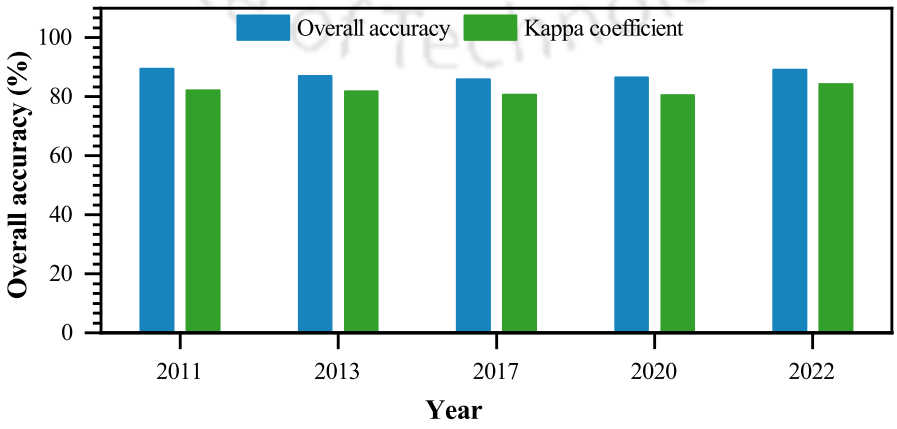

Figure 5.9: Overall accuracy and kappa coefficient of the classified maps for different years

Table 5.4: Accuracy assessment calculation of land use land cover classified maps

Year/Class	Builtup		Water body		Forest		Swampy land		Vegetation	
	UA (%)	PA (%)	UA (%)	PA (%)	UA (%)	PA (%)	UA (%)	PA (%)	UA (%)	PA (%)
2011	86.10	100.00	90.00	90.00	80.00	100.00	44.00	67.70	100.00	80.00
2013	86.84	91.67	60.00	75.00	80.00	80.00	81.25	100.00	97.62	83.67
2017	77.50	93.94	80.00	88.89	92.31	100.00	80.00	88.89	97.06	75.00
2020	85.71	89.36	70.00	77.78	100.00	100.00	70.00	100.00	93.75	78.95
2022	92.16	94.00	80.00	100.00	100.00	90.91	60.00	85.71	93.33	80.00

5.4.2 Determination of Urbanization Growth of the Study Area

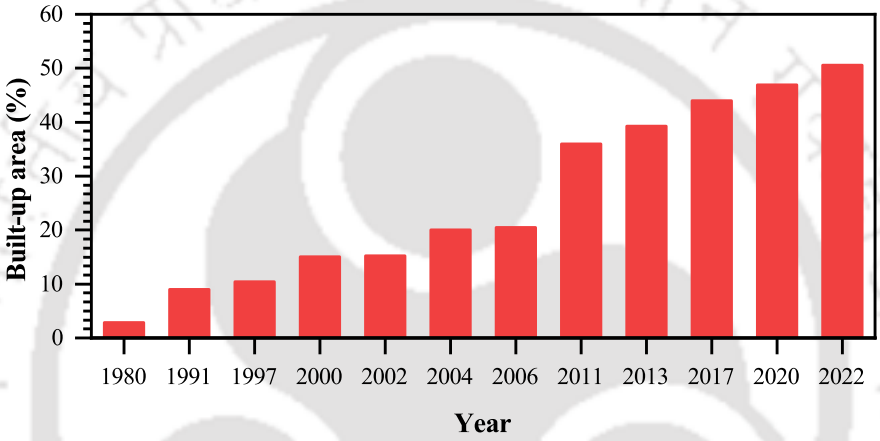

Figure 5.10: Urbanization growth from 1980 to 2022 for Guwahati city

In this study, the urbanization growth in terms of built-up area was studied from the year 1980 to 2022 and is shown in Fig. 5.10 and Fig. 5.11. The percentage of built-up area for the years 1980, 1991, 1997, 2000, 2002, 2004, and 2006 are taken from Sahoo and Pekkat (2014). Fig. 5.10 and Fig. 5.11 shows an increasing trend in the percentage of the built-up area from 1980 to 2022 (2.85% to 50.56%). A drastic increase in the percentage of built-up area was noticed from 2006 to 2011, and this can be attributed to the migration of people from rural areas to cities in search of jobs and better livelihood (Sahoo, 2014). From 2011 to 2022, a gradual increase in the built-up area is observed in Guwahati city. A modest increase in the percentage of built-up area is noticed for the years 2017-2022.

5.4.3 Quantification of Imperviousness

In this section, the findings and analysis regarding the imperviousness of the area under investigation in terms of total impervious area (TIA) and effective impervious area (EIA) are presented.

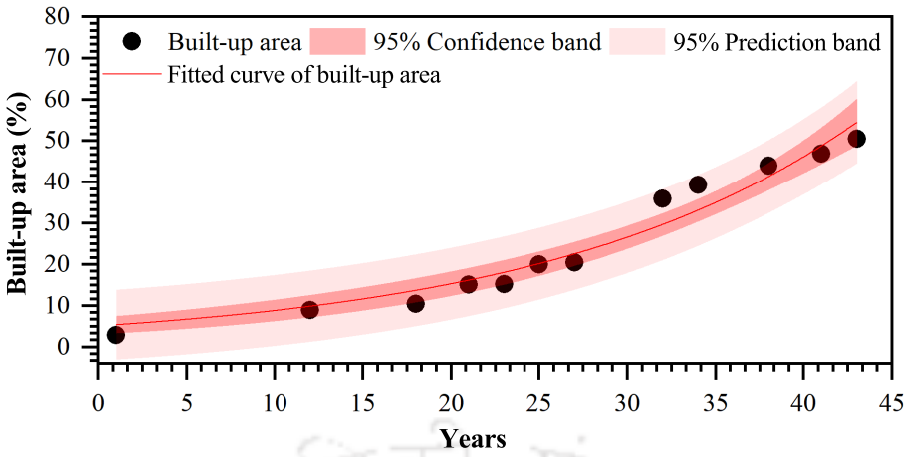

Figure 5.11: Trend in the urbanization growth from 1980 to 2022 for Guwahati city

5.4.3.1 Total Impervious Area of Guwahati City

Figure 5.12 shows the percentage of TIA determined for the seven watersheds of the study area. Watershed 3 showed the highest percentage of imperviousness of 56.90%, 57.78%, 61.13%, 68.71%, and 75.69% of the total area for the years 2011, 2013, 2017, 2020, and 2022 respectively. Watershed 7 shows the least percentage of imperviousness of 9.72%, 10.09%, 14.79%, 16.57%, and 19.87%, of the total area respectively, for the years 2011, 2013, 2017, 2020, and 2022 in terms of TIA. Table 5.5 shows the percentage values of TIA for the different watersheds for different years.

Figure 5.13 shows the percentage of TIA for sub-watersheds of all the 7 watersheds for 2011, 2013, 2017, 2020, and 2022. The percentage of imperviousness in terms of TIA was observed to increase with the years.

Table 5.5: Percentage of TIA for different watersheds of the study area

Watershed No	TIA (%)				
	2011	2013	2017	2020	2022
W1	23.41	26.29	29.79	31.73	33.74
W2	40.94	48.55	48.79	49.07	55.14
W3	56.90	57.78	61.31	68.71	75.69
W4	46.46	49.32	51.60	53.99	56.24
W5	34.24	35.80	39.94	48.11	49.65
W6	23.35	24.94	30.78	41.16	43.73
W7	9.72	10.09	14.79	16.57	19.87

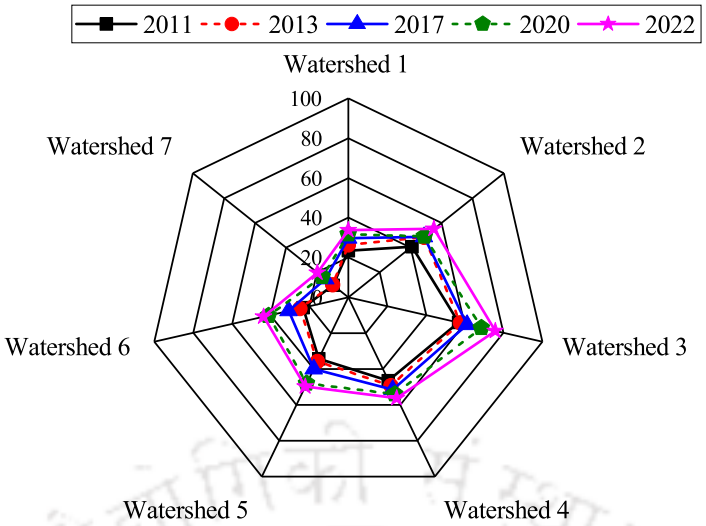

Figure 5.12: Percentage of TIA estimated for the study area for different watersheds

5.4.3.2 Effective Impervious Area of Guwahati City

The percentage of EIA determined for the seven watersheds of the study area is depicted in Fig.5.14. Watershed 3 showed the highest percentage of imperviousness of 12.06%, 13.22%, 13.74%, 15.10%, and 22.37% for the years 2011, 2013, 2017, 2020, and 2022 respectively. Watershed 7 has the least percentage of imperviousness for the years 2011, 2013, and 2020, whereas, for the years 2017 and 2022, watershed 6 has the least percentage of EIA. The respective percentage values of EIA for the different watersheds for different years is listed in table 5.6.

5.4.3.3 Change in TIA and EIA of Sub-Watersheds

Figure 5.16 (a) and (b) presents the percentage of TIA and EIA, respectively, for the seven watersheds. From the results, it is clear that there is a consistent increase in TIA and EIA for all the watersheds for all the years. The rise in impervious areas could be attributed to various factors,

Table 5.6: Percentage of EIA for different watersheds of the study area

Watershed No	EIA (%)				
	2011	2013	2017	2020	2022
W1	2.13	3.63	4.10	4.69	5.48
W2	3.45	4.88	5.76	6.22	7.09
W3	12.06	13.22	13.74	15.10	22.37
W4	3.29	4.74	5.36	6.07	7.22
W5	2.48	3.33	3.70	4.43	5.96
W6	0.45	0.80	1.19	1.45	1.71
W7	0.40	0.55	1.22	1.39	1.76

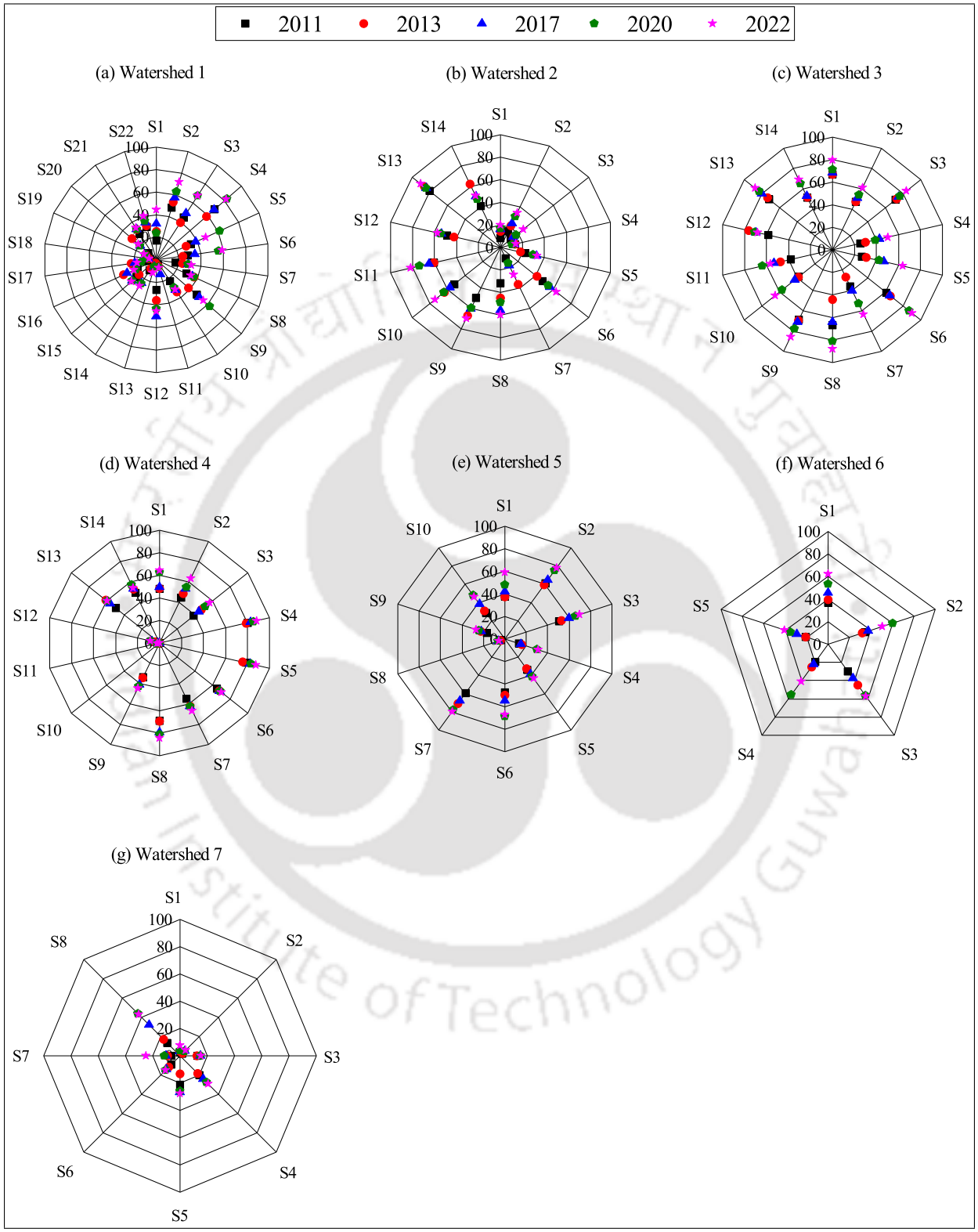

Figure 5.13: Percentage of TIA estimated for the study area for different sub-watersheds

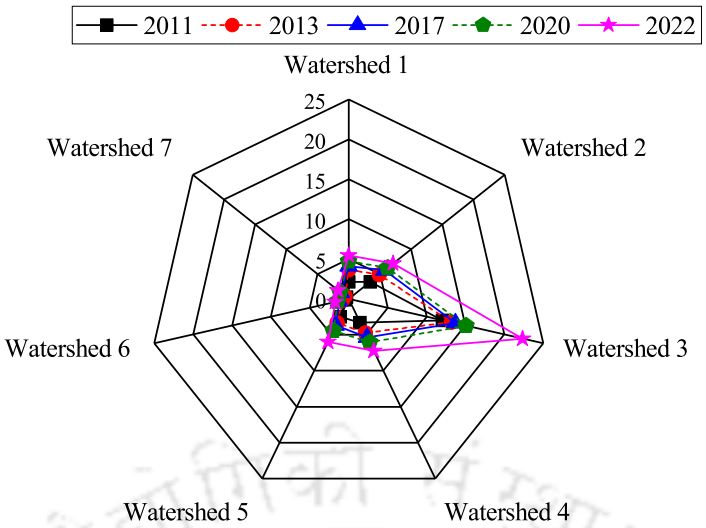

Figure 5.14: Percentage of EIA estimated for the study area for different watersheds

such as urbanization, population growth, and land development, which replaces the natural lands with buildings, roads, and parking lots. The results suggest that watershed 3 has the highest percentage of imperviousness, which can be attributed to the fact that it encompasses a significant portion of the city. In contrast, watersheds 6 and 7 have the lowest percentage of imperviousness compared to the other watersheds. This is likely because these two watersheds consist mainly of wetlands and have less built-up areas. Figure 5.16 (c) and (d) shows the percentage of TIA and EIA respectively for different years. Watershed 3 was showing a steep increase in TIA from 2017 to 2022. Similarly, watershed 6 is showing a steep increase in TIA from 2017 to 2020. In terms of EIA, watershed 3 is showing a drastic increase from the year 2020 to 2022.All other watersheds was showing only gradual increase in EIA.

5.4.3.4 Comparison of TIA and EIA for the Study Area

The percentage of TIA and EIA obtained for the study area for different years is shown in Fig. 5.17 and the same are listed in table 5.7. It is clear that both TIA and EIA is increasing with years, indicating that urbanization has increased the imperviousness of the area. This will reduce the infiltration capacity of the land and thereby increases the surface runoff. It is also clear from the Fig. 5.17 that TIA value is more as compared to EIA. TIA in the entire study area was found to be 10.43 times more than the directly estimated EIA for the year 2011 and 2013, and it was 10.58, 11.21, and 8.11 times more than estimated EIA for the year 2017, 2020, and 2022 respectively.

5.5 Summary

Guwahati is an important city in northeast India. As per the 2011 Census, the population of urban Guwahati was 962334 and was projected to grow approximately by 41% by 2024. Guwahati has become one of the most poorly planned cities in India due to uncontrolled population growth, lack

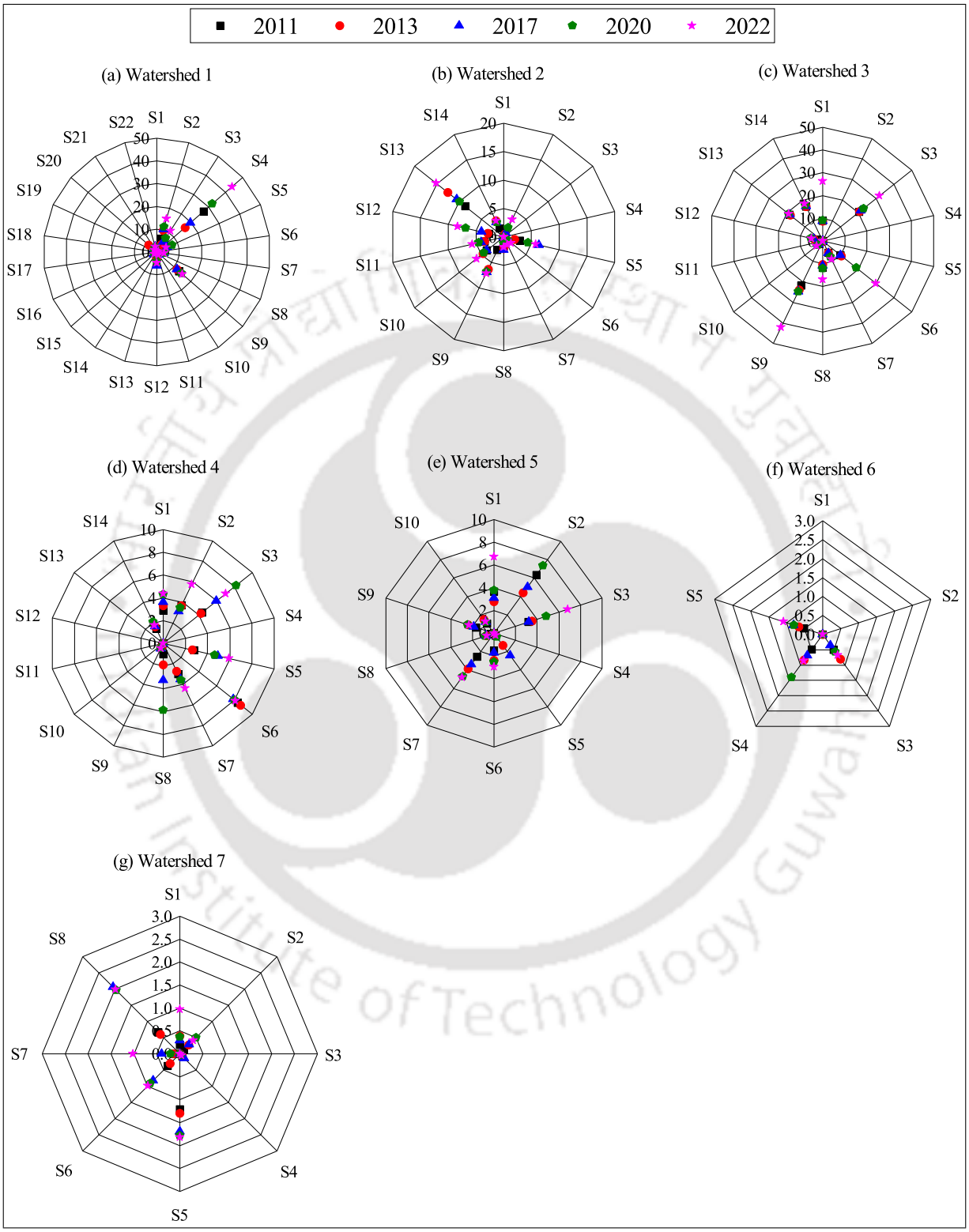

Figure 5.15: Percentage of EIA estimated for the study area for different sub-watersheds

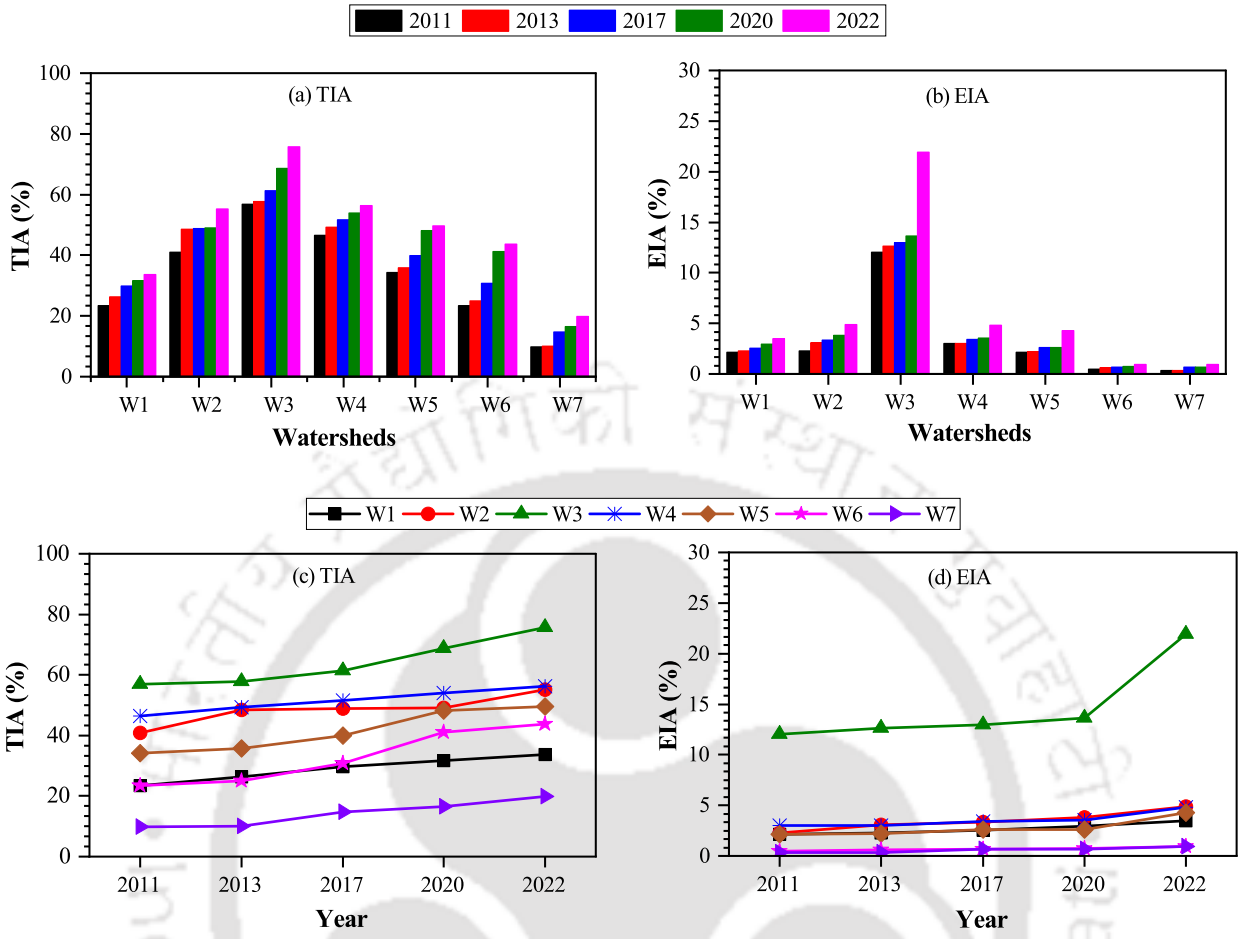

Figure 5.16: Comparison of TIA and EIA for the different watersheds for different time periods (a) TIA verses watersheds, (b) EIA verses watersheds, (c) TIA verses years, and (d) EIA verses years

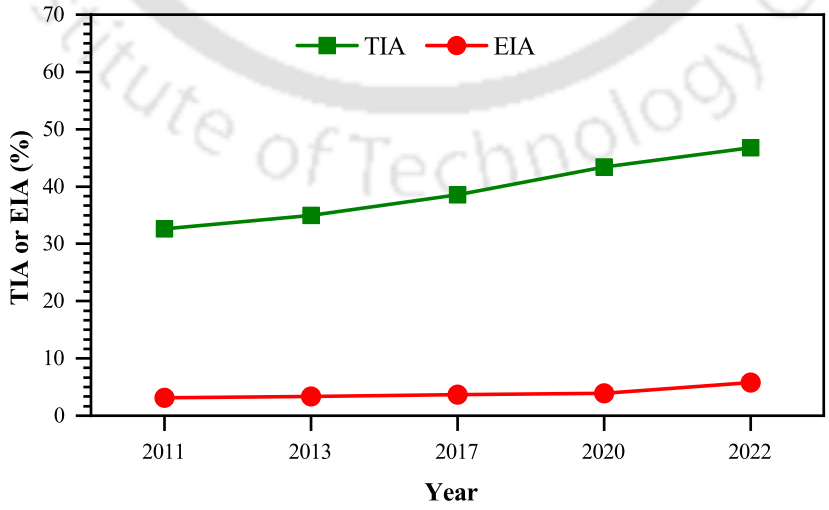

Figure 5.17: Comparison of TIA and EIA estimated for the study area

Table 5.7: Percentage imperviousness for Guwahati city

Year	TIA(%)	EIA(%)
2011	32.64	3.13
2013	34.94	3.35
2017	38.56	3.64
2020	43.42	3.87
2022	46.80	5.77

of coordination among different planning departments, absence of efficient planning and management policies, low monetary funds and so on. People from rural areas have migrated to the city in search of better employment and a better livelihood. This has led to the encroachment of forests and hills to construct buildings. Also, due to the uncontrolled growth of population and to meet food demands, many swampy lands, forests and hills are also converted to agricultural land. There has been a shift from subsistence farming to large-scale farming to meet the growing demand. Developments in transportation facilities has led to a rise in land prices and a change in the land use pattern. Also, deforestation has become predominant to meet the demand for wood for construction activities. All these contributed to the increase in built-up area in the city.

The increase in impervious surfaces due to urbanization will lead to decreased infiltration and increased surface runoff in urban watersheds. Therefore, accurately measuring the impervious areas is crucial for effective urban flood management. This chapter focused on examining the changes in land use and land cover and quantifying imperviousness using TIA and EIA of the study area. The LULC map of the study area was developed for the years 2011, 2013, 2017, 2020, and 2022 using the LISS-IV images, and quantification of the LULC changes has been carried out from 2011 to 2022. The maximum likelihood classifier approach is used to classify the LISS IV remote sensing images into five different classes (built-up, forest, vegetation, water body, and swampy land). The studied observed an increase in built-up area at the expense of the vegetated regions, swampy land and forest area. The trend in urbanization was also analysed and it was observed that from 1980 to 2022 there has been an increase in built-up area from 2.85% to 50.56%.

Urbanization has led to a rise in impervious surfaces within urban watersheds, resulting in decreased infiltration capacity and a subsequent increase in surface runoff. Therefore, accurately quantifying imperviousness becomes crucial for conducting urban hydrologic analysis and effective urban flood management. In this study the quantification of imperviousness is carried out. The imperviousness of the study area in terms of TIA and EIA was determined from the fine-resolution remote sensing images using geospatial analysis. A semi-automated direct method was used to estimate the EIA in this study. It was observed that TIA and EIA was showing an increase from 2011 to 2022 for all the watersheds. Watershed 3, the most urbanized part of Guwahati city, gave the highest percentage of imperviousness (in terms of TIA and EIA) for all the years. In terms of TIA, watershed 7 was showing the least percentage of imperviousness for all the years. However,

in terms of EIA, watershed 7 showed the least percentage of EIA for the years 2011, 2013, and 2020, whereas watershed 6 has shown the least percentage for 2017 and 2022. The imperviousness of sub-watersheds was also determined and was showing similar trends. This rise in impervious areas could be attributed to various factors, such as urbanization, population growth, and land development, which replaces the natural lands with buildings, roads, and parking lots. The study revealed a significant difference between TIA and EIA in the entire study area, with TIA being ten times greater than EIA. So, in urban flood applications it is recommended to use EIA instead of TIA, as TIA may overestimate the runoff.

Chapter 6

Quantification of the Impact of Land Use and Climate Change on Urban Flood

6.1 General

Extreme rainfall is influenced by natural variations in climate, large-scale factors like global warming, or local factors like urbanization (Vittal et al. 2016). Global warming is projected to cause a non-uniform increase in extreme rainfall in urban areas (IPCC 2021). The Clausius-Clapeyron (CC) relationship suggests that a rise of 1°C in atmospheric temperature results in an approximately 7% increase in the water holding capacity of an air parcel Trenberth (2011). Population aggregation and the expansion of impervious surfaces associated with urbanization lead to modifications in land use or cover, thereby disrupting the wind patterns and exchanges of water, aerosol, and heat between the atmosphere and land (Golroudbary et al., 2017; Kaufmann et al., 2007; Zhang et al., 2019).

The recent increase in urban flooding and its associated damages has become a primary global concern. Urbanization and climate change are considered as the major drivers of urban flooding. Urbanization causes a rise in impervious surfaces, which leads to the reduction in infiltration, thus leads to an increase in surface runoff. Climate change has affected the intensity and frequency of precipitation, which made the urban catchments more vulnerable to flooding. The combined effects of climate change and urbanization have increased the risk of flooding in cities. These factors have led to the changes in flood characteristics, such as the magnitude, frequency, and duration of floods leading to devastating impacts on urban areas. Comprehending the effects of climate and land use/cover change on urban flood characteristics is critical. This understanding is necessary for effective planning and management of urban infrastructures and developing mitigation strategies to reduce the risk of flooding.

This chapter investigates the role of land use and climate change on urban floods. This objective is achieved through three scenarios. The first scenario is to understand the impact of different rainfall events on urban floods. In the second scenario, the impact of land use change on urban

flood is studied, keeping the climate variables constant. In the third scenario, the individual impact of climate change is investigated, keeping the land use as time-invariant. The overview of this chapter is shown in Fig. 6.1.

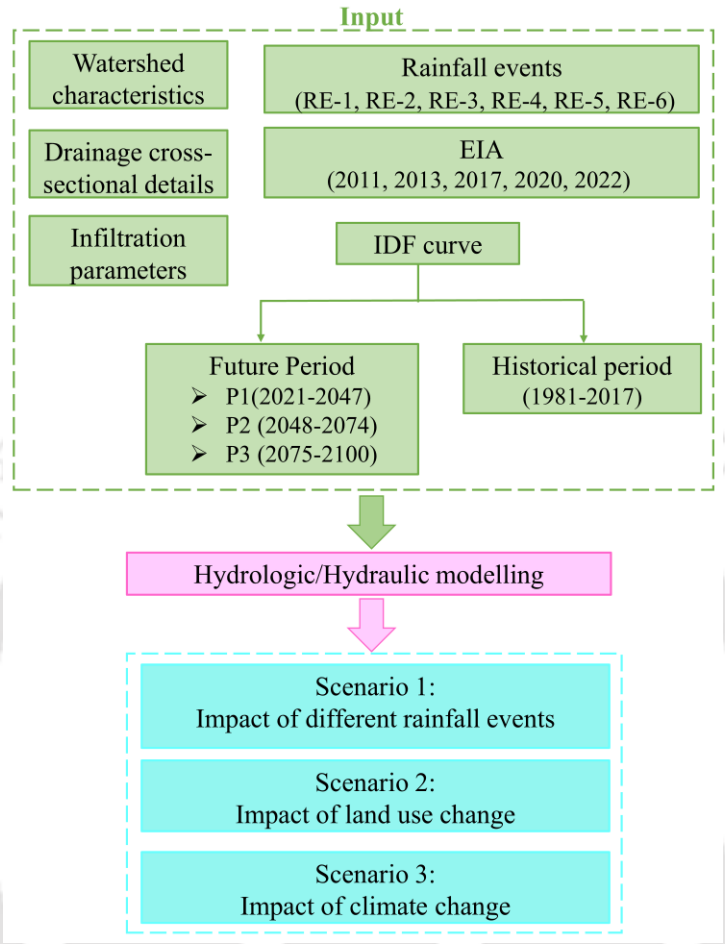

Figure 6.1: Overall methodology

6.2 Description of the Simulation Model

6.2.1 Stormwater Management Model (SWMM)

Several hydrologic models are available for runoff modelling, which differ in input variables, representation of hydrologic processes, etc. Furthermore, the characteristics of the watershed, the availability of data, and the intended results influence the choice of a hydrologic model. In the present study, the SWMM is used because of its applicability in the hydrologic modelling of urban catchments (Morsy et al., 2016; Rossman and Huber, 2016b; Wang et al., 2022; Yang et al., 2023; Zahmatkesh et al., 2015a). SWMM is a dynamic rainfall-runoff simulation model developed by the U.S. Environmental Protection Agency (EPA) and is used in various urban watersheds for quantitative and qualitative estimation of surface runoff during single or continuous events (Rossman and Huber, 2016b). SWMM consists of two components; i) hydrological component and ii) hy-

draulic component. The hydrological module models the watershed as a nonlinear reservoir with rainfall as input to generate the runoff. The overland flow is modelled using the mass conservation equation given by

$$\frac{\partial d}{\partial t} = I - e - f - q_s \tag{6.1}$$

where I is the rainfall intensity, e is the rate of evaporation, f is the infiltration rate and q_s is the surface runoff. All these values are expressed as flux (flow rates per unit area).

The sub-catchments are assumed to be rectangular in shape and also the flow across the sub-catchments are assumed to be uniform flow. The Manning's equation given by Eq. 6.2 is used to find the volumetric flow of runoff (Rossman and Huber, 2016b). The Q_s is updated for each time step for ponded depth d

$$Q_s = w\frac{1}{n}(d - d_s)^{5/2}S^{1/2} \tag{6.2}$$

where Q_s is the surface runoff, w is the width of the sub-catchment, S is the slope, n is the Manning's roughness coefficient, d is the depth and d_s is the maximum depression storage depth. The surface runoff occurs only when $d > d_s$.

SWMM allows the watersheds to be divided into any number of sub-watersheds, thereby considering the variability in the sub-watersheds. The basin and infiltration parameters considered in the SWMM would differ for watersheds but are assumed to be homogeneous within a watershed (Sahoo and Sreeja, 2013, 2017). Physical characteristics such as watershed area, width, slope and hydrological parameters like evaporation, rainfall, etc., are inputs to the model for each sub-watershed. SWMM has different methods, such as Horton, Green-Ampt and Curve Number, to compute the infiltration loss for the pervious area. This study used the Green-Ampt method to find the infiltration loss from catchments.

The runoff simulated by the hydrological module is routed to the hydraulic module through a network system consisting of pipes, channels, storage/treatment devices, pumps, and regulators. The input parameters required for the hydraulic module include the cross-sectional details of the drainage, shape of conduit, roughness invert elevation, etc. The routing is based on the Saint-Venant continuity and momentum equations as given by Eq. 6.3 and 6.4. SWMM can perform hydraulic routing by three different methods, namely, steady flow routing, kinematic wave routing and dynamic wave routing. This study uses dynamic wave routing, which solves the complete one-dimensional Saint-Venant continuity and momentum equations.

$$\frac{\partial Q}{\partial x} + \frac{\partial A}{\partial t} = 0 \tag{6.3}$$

$$\frac{1}{A}\frac{\partial Q}{\partial t} + \frac{1}{A}\frac{\partial (Q^2/A)}{\partial x} + g\frac{\partial y}{\partial x} - g(S_0 - S_f) = 0 \tag{6.4}$$

where Q is the flow rate in the channel, A is the cross-sectional area of the channel, y is the flow

depth, g is the acceleration due to gravity, x is the distance in the direction of flow, t is the time, S_0 is the channel bottom slope, and S_f is the friction slope. Figure 6.2 shows the working mechanism of the SWMM.

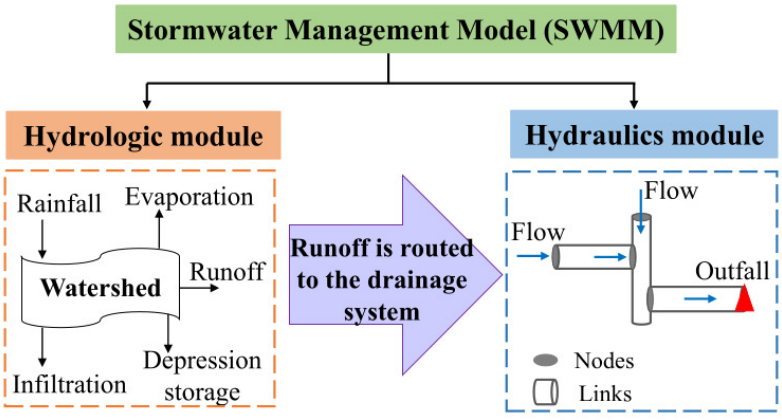

Figure 6.2: Working mechanism of SWMM

6.2.2 Validation of Storm Water Management Model

The SWMM was validated using the observed water level measured at the three different locations in the waterhseds and the details are shown in table 6.1. The model was able to simulated the water levels with a reasonable degree of accuracy.

Table 6.1: Validation of SWMM

Location	Observed water level (mm)	Simulated water level (mm)
Location 1	400	360
Location 2	120	130
Location 3	300	400

6.3 Scenario Development

Table 6.2 shows different scenarios considered for the quantification of urban flood in the study area. Flood modeling is carried out using six 15-minutes rainfall events to understand the characteristics of runoff generated in the urban catchments with varying EIA considerations. Also to understand the impact of land use and climate change on urban runoff, the flood modeling is carried out for different rainfall intensity values obtained using the historical and future IDF curves. These scenarios collectively aim to enhance our understanding of the complex interactions between rainfall events, urban catchments, LULC, and climate change in the context of urban flooding. Researchers and policymakers can make informed decisions regarding urban planning, flood management strategies, and climate change adaptation measures by studying these aspects.

Table 6.2: Details of different scenarios

S.No	Scenario	EIA	Climate	Purpose
1	I	2011, 2013, 2017, 2020, 2022	RE-1, RE-2, RE-3, RE-4, RE-5, RE-6	Impact of different rainfall events on urban flood
2	II	2011, 2013, 2017, 2020, 2022	IDF curves (UIDF and BIDF)	Impact of LULC on urban flood
3	III	2022	Future climate: P1 (2021-2047), P2 (2048-2074), P3 (2075-2100)	Impact of climate change on urban flood

The choice of using short-duration rainfall data is common in urban studies because it is often more efficient and practical for assessing the urban drainage systems performance. It is important to note that urban drainage systems are typically designed to handle rainfall events with return periods ranging from 2 to 10 years (ASCE, 1992; CPHEEO, 2019). This range is considered suitable for most urban areas in terms of managing stormwater runoff and preventing flooding. However, it is worth mentioning that certain critical urban structures, such as airports, may require additional considerations. In these cases, rainfall events with longer return periods, typically between 50 to 100 years (CPHEEO, 2019), need to be taken into account during the design phase. This is because airports and other similar structures require higher resilience and greater capacity to handle more extreme rainfall events. Therefore, in this study, the rainfall intensity chosen for a 15-minute duration with a 10-year return period from various IDF curves (design rainfall) is appropriate for analyzing and understanding the impacts of landuse and climate change on urban flooding.

6.4 Results and Discussion

6.4.1 Impact of Different Rainfall Events on Urban Flood Characteristics

In this section, the impact of various observed rainfall events (RE-1, RE-2, RE-3, RE-4, RE-5, and RE-6) on the runoff patterns for different EIA conditions was investigated. Figures 6.3 to 6.7 shows the simulated runoff data for all seven watersheds with different EIA corresponding to the years, 2011, 2013, 2017, 2020, and 2022. From the figures, it is evident that different rainfall events exhibit diverse behaviors across the various watersheds. Specifically, it is observed that for most of the watersheds (excluding watershed 5 and 6), the rainfall event RE-4 results in the highest amount of runoff. However, for watershed 5 and 6, the rainfall event RE-1 produces a higher runoff volume. RE-3 was giving the lowest amount of runoff for all the watersheds for all the years.

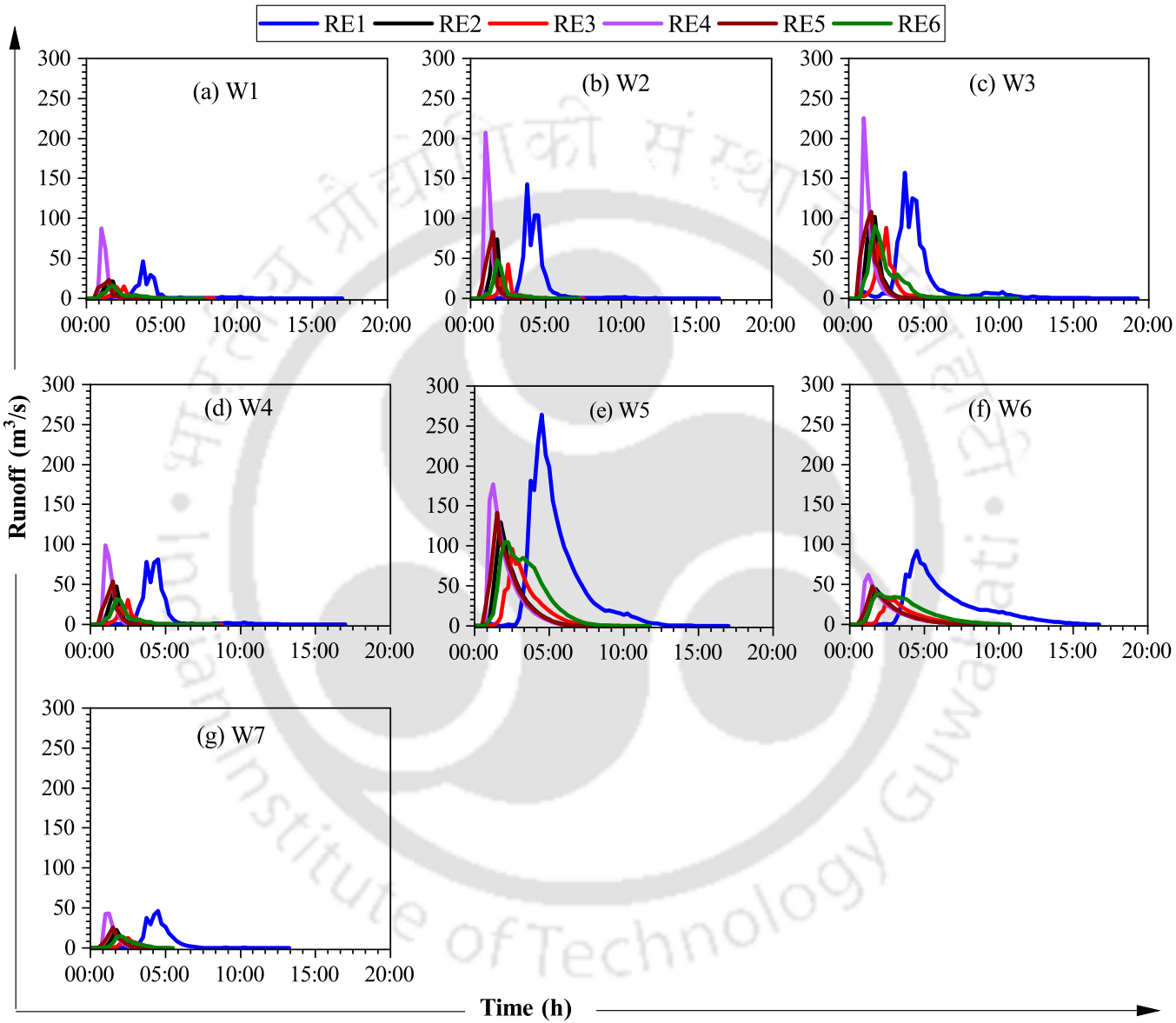

Figure 6.3: Simulated runoff for all the watersheds for 2011 EIA

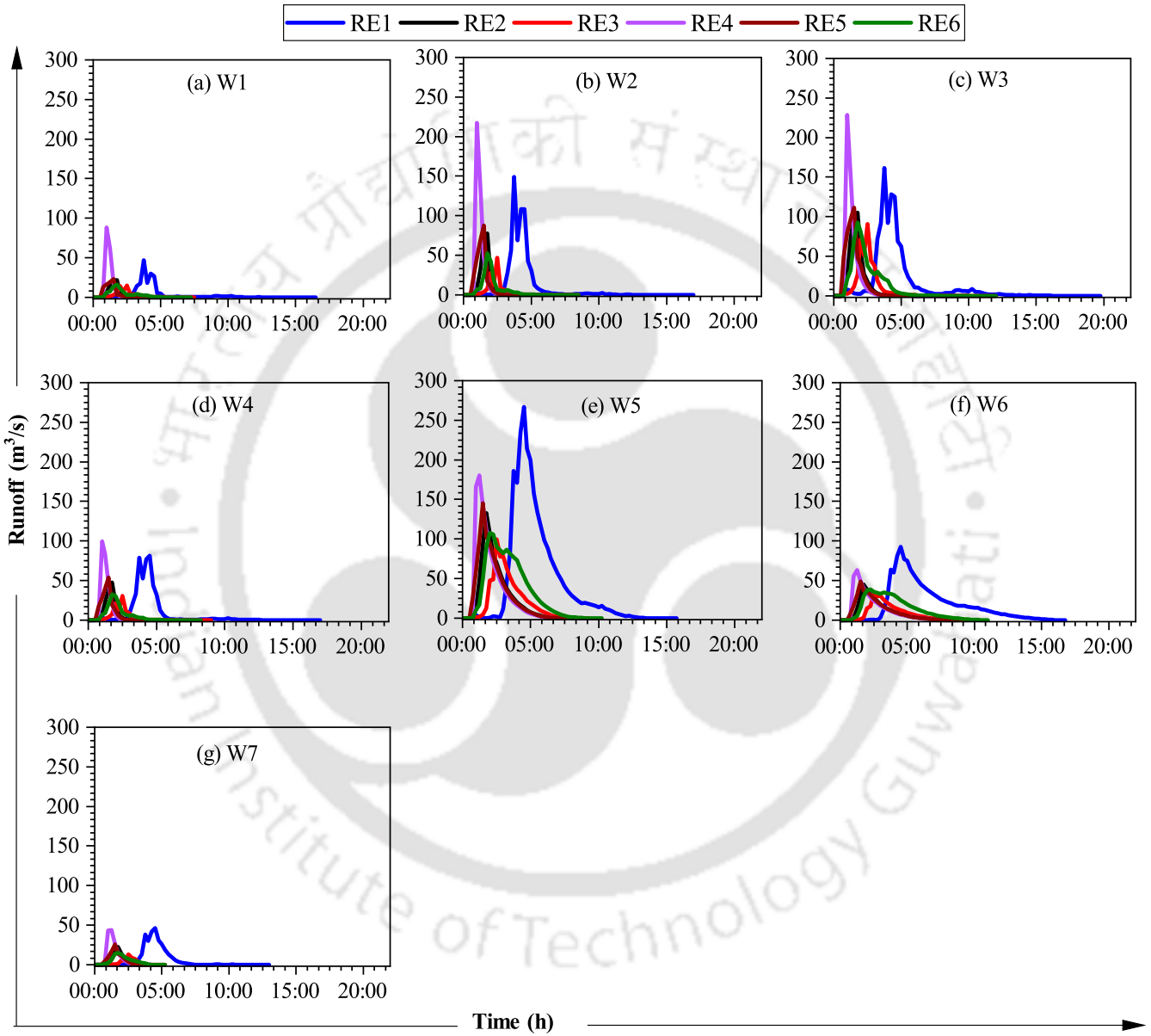

Figure 6.4: Simulated runoff for all the watersheds for 2013 EIA

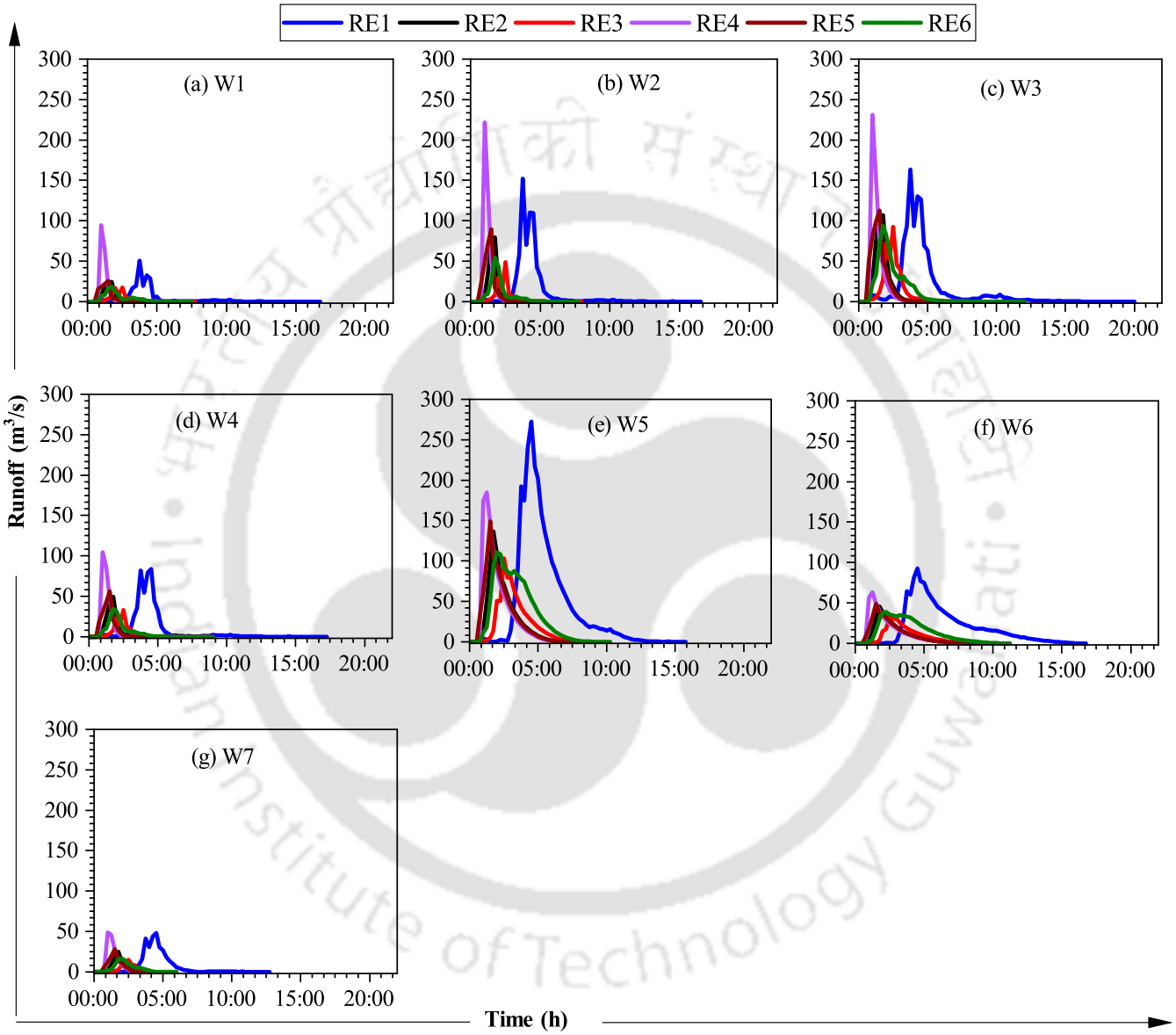

Figure 6.5: Simulated runoff for all the watersheds for 2017 EIA

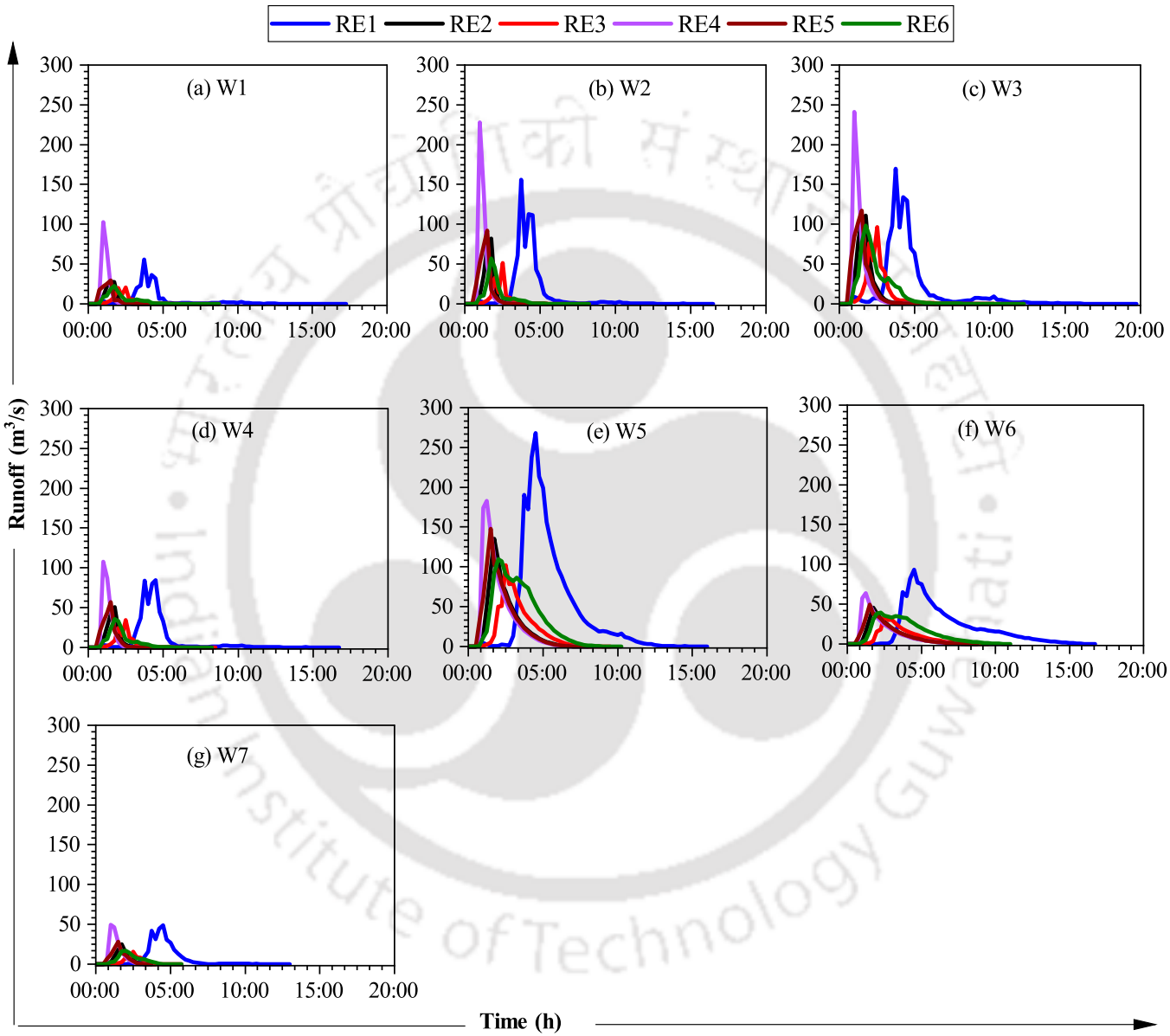

Figure 6.6: Simulated runoff for all the watersheds for 2020 EIA

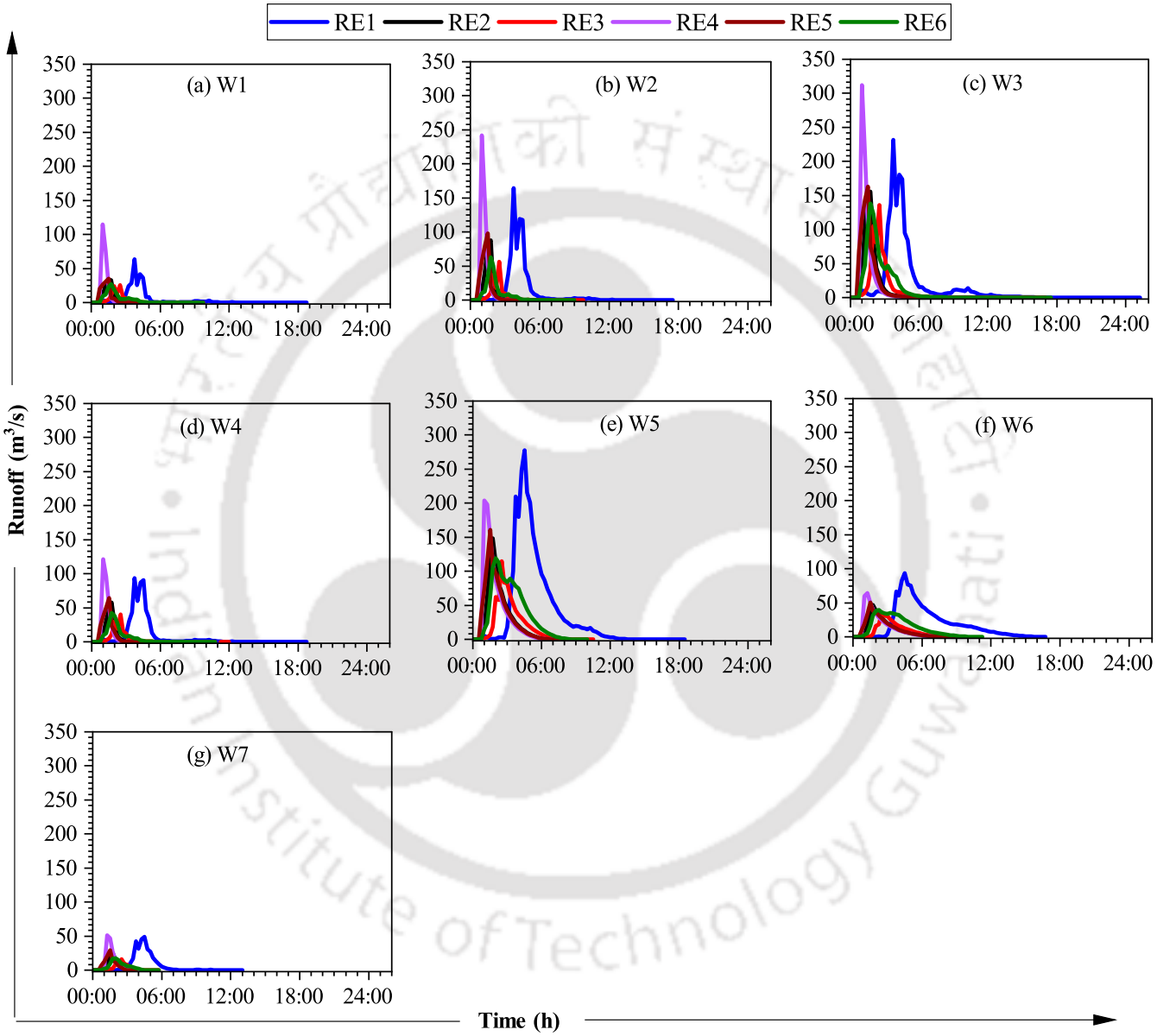

Figure 6.7: Simulated runoff for all the watersheds for 2022 EIA

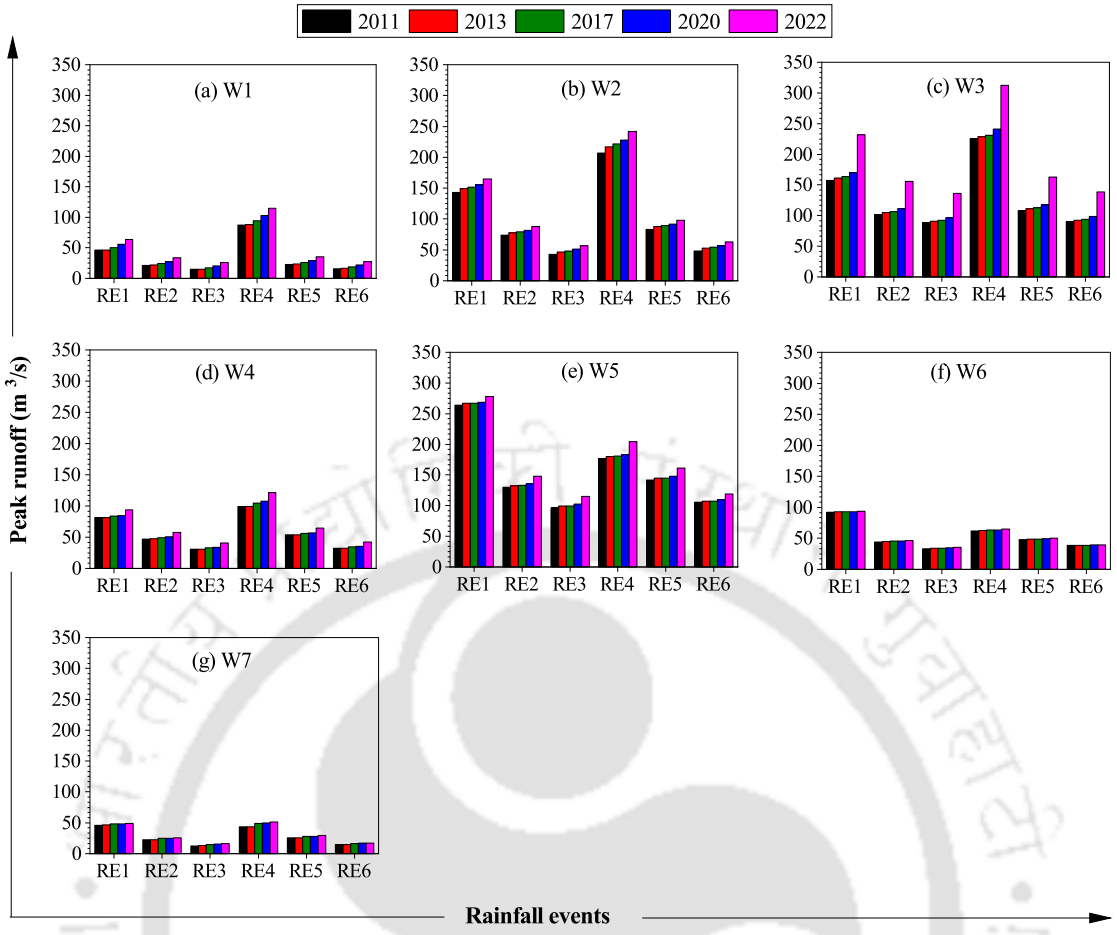

Figure 6.8: Comparison of simulated peak runoff for all the watersheds for different rainfall events

Figure 6.8 illustrates the comparison of simulated peak runoff for different rainfall events. The graph reveals a clear trend: as imperviousness increases (as indicated by the EIA), the peak runoff also increases. Among the different rainfall events, RE-4 consistently generates the highest peak runoff for most of the watersheds, with the exception of watersheds 5 and 6. For watersheds 5 and 6, RE-1 produces the highest peak runoff values. It is worth noting that watershed 7 consistently exhibits the lowest peak runoff values for all rainfall events, indicating that it is the least affected by the observed rainfall events.

The spatial distribution of runoff variation across different watersheds for different rainfall events is shown in figures 6.9 to 6.14. From the figures, it is clear that watersheds 2, 3, and 5 are more vulnerable to flooding during all the rainy events. The runoff exhibited a consistent upward trend of 17.5%, 26.2%, 34%, 23.2%, 24.7%, and 29.7% for rainfall events RE1, RE2, RE3, RE4, RE5, and RE6, respectively, as the EIA changed from 2011 to 2022.

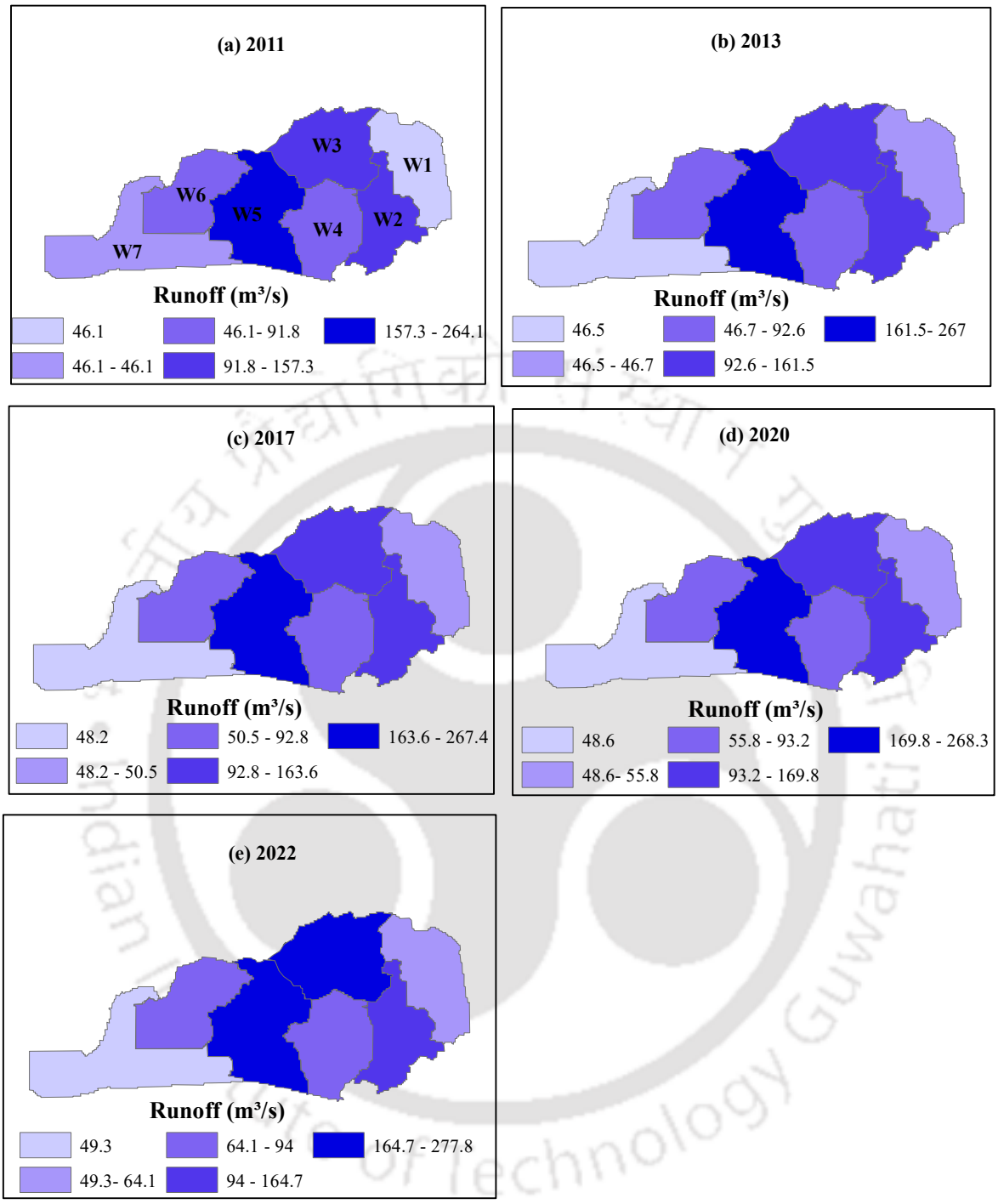

Figure 6.9: Spatial variation of peak runoff across different watersheds for RE1

The response of different rainfall events for the the EIAs of different years 2011, 2013, 2017, 2020 and 2022 are analyzed. Table 6.3 presents the response of different rainfall events for the EIA of the year 2022 in terms of peak runoff, duration of flooding, and the number of flooded

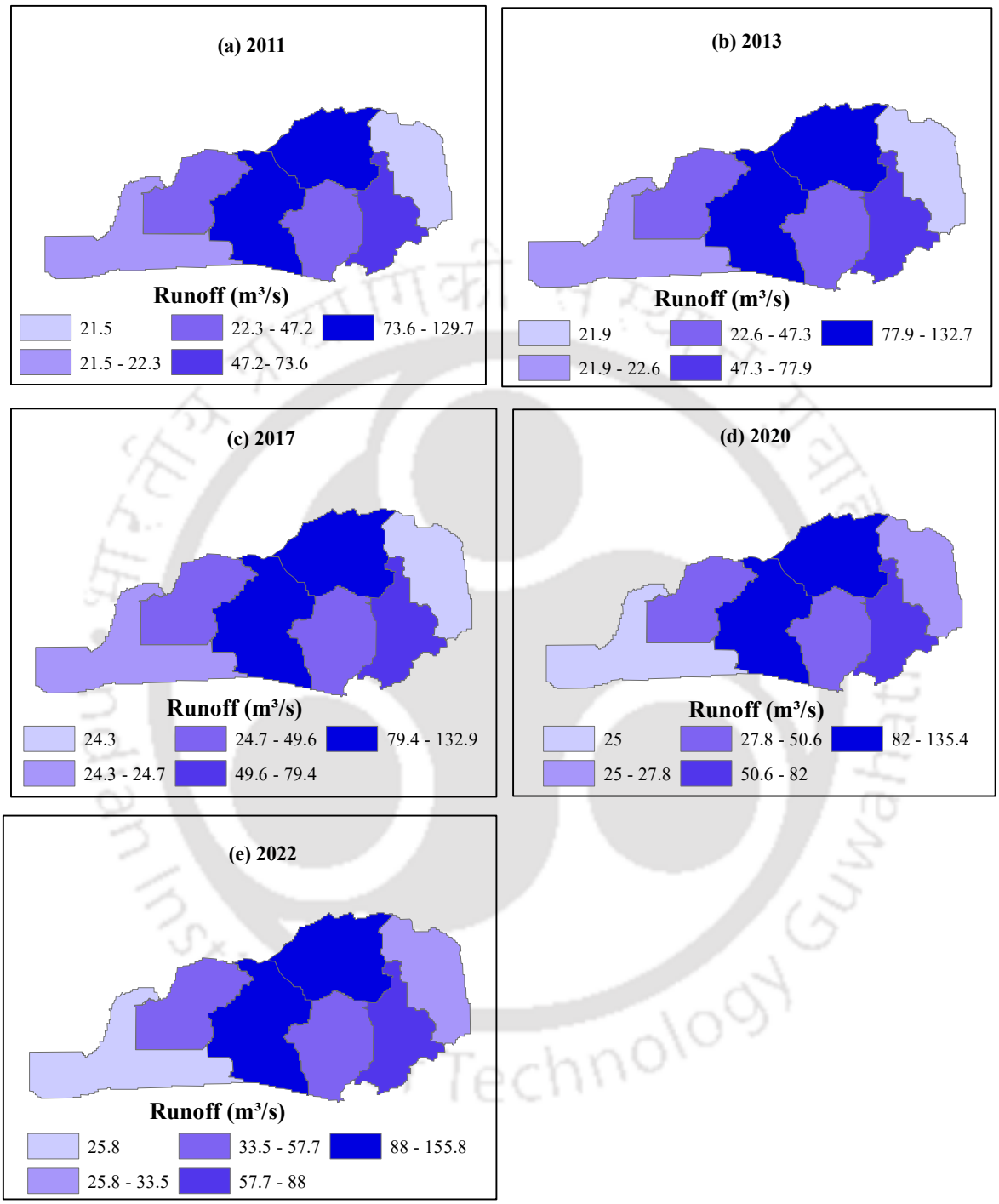

Figure 6.10: Spatial variation of peak runoff across different watersheds for RE2

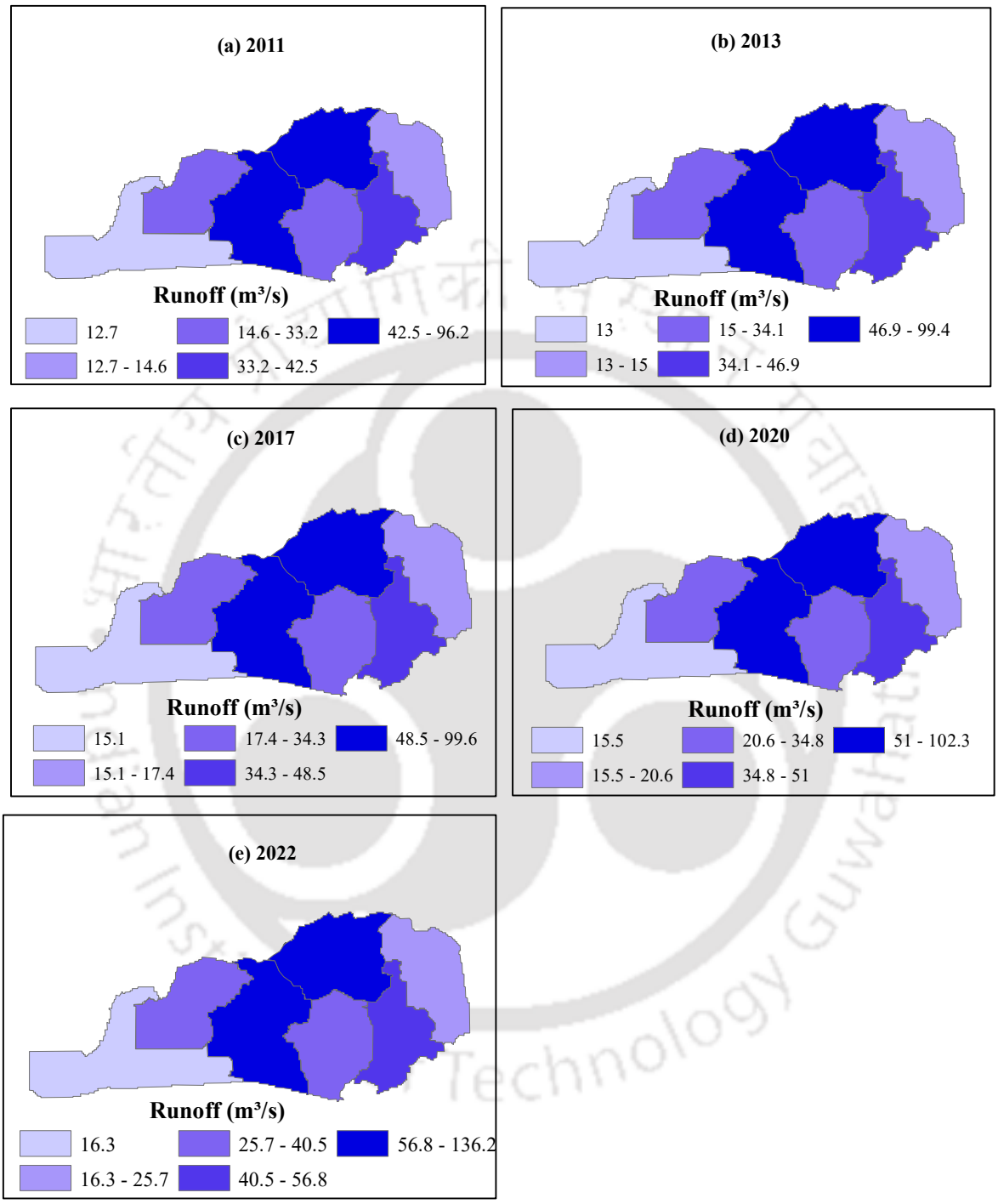

Figure 6.11: Spatial variation of peak runoff across different watersheds for RE3

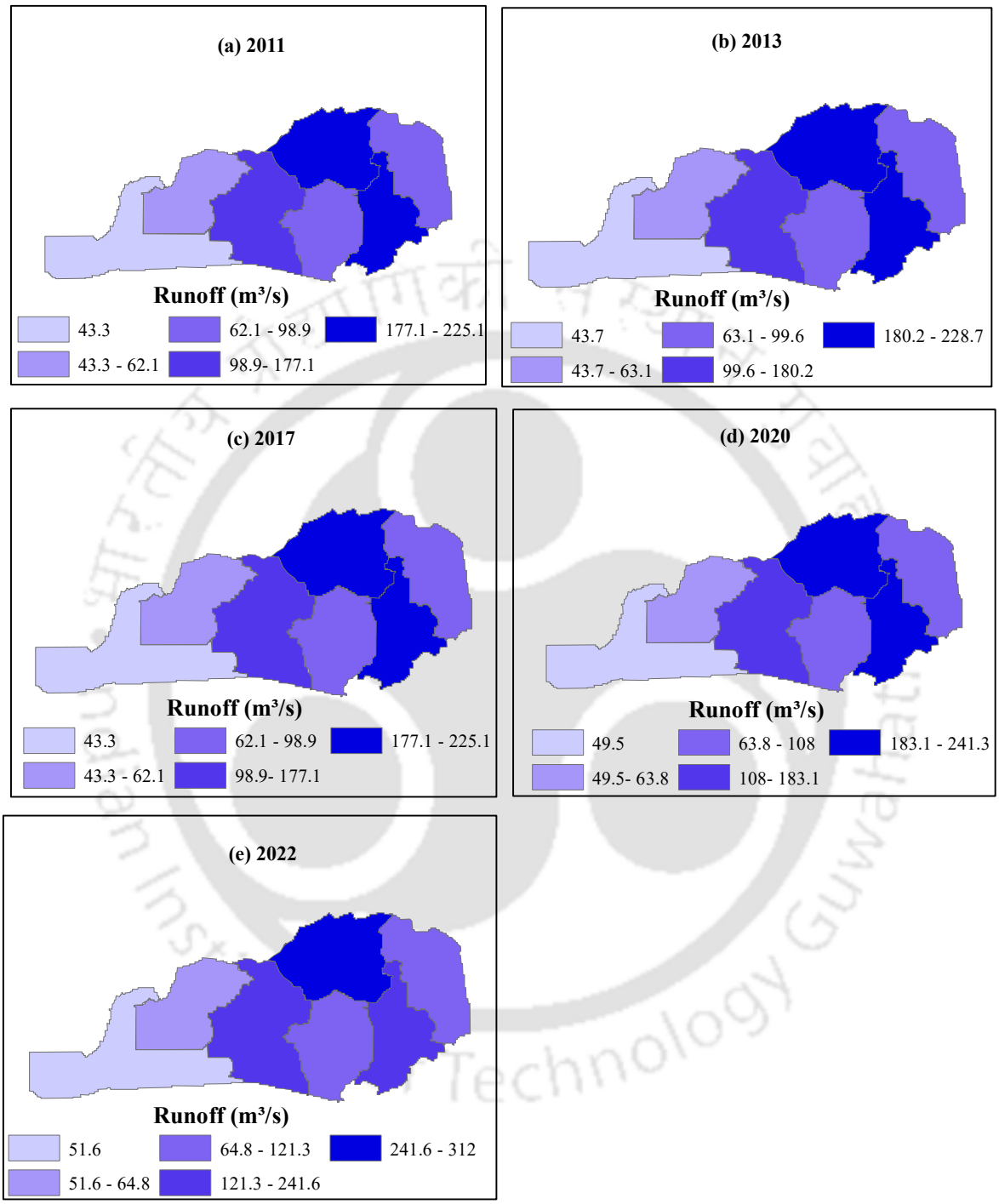

Figure 6.12: Spatial variation of peak runoff across different watersheds for RE4

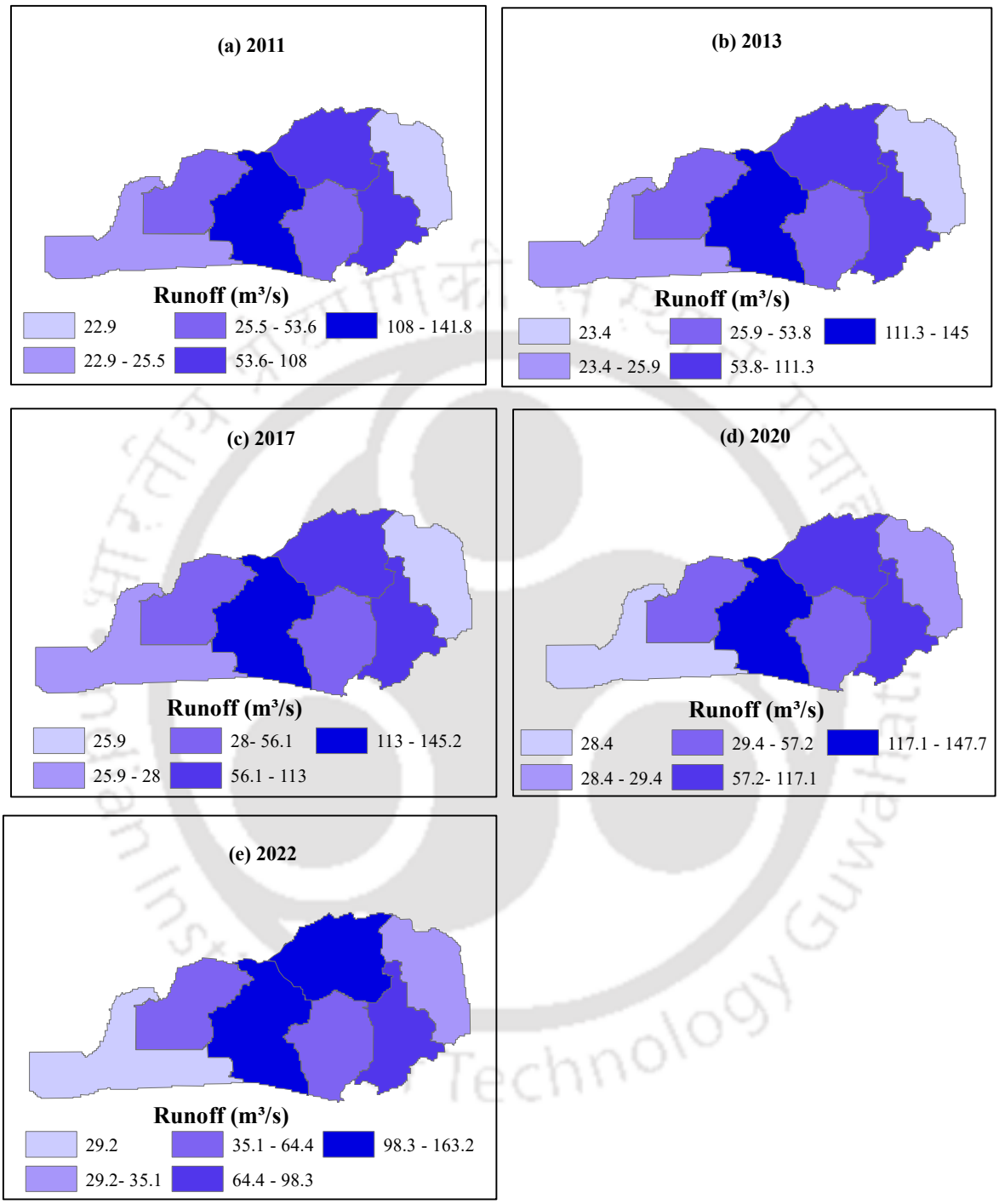

Figure 6.13: Spatial variation of peak runoff across different watersheds for RE5

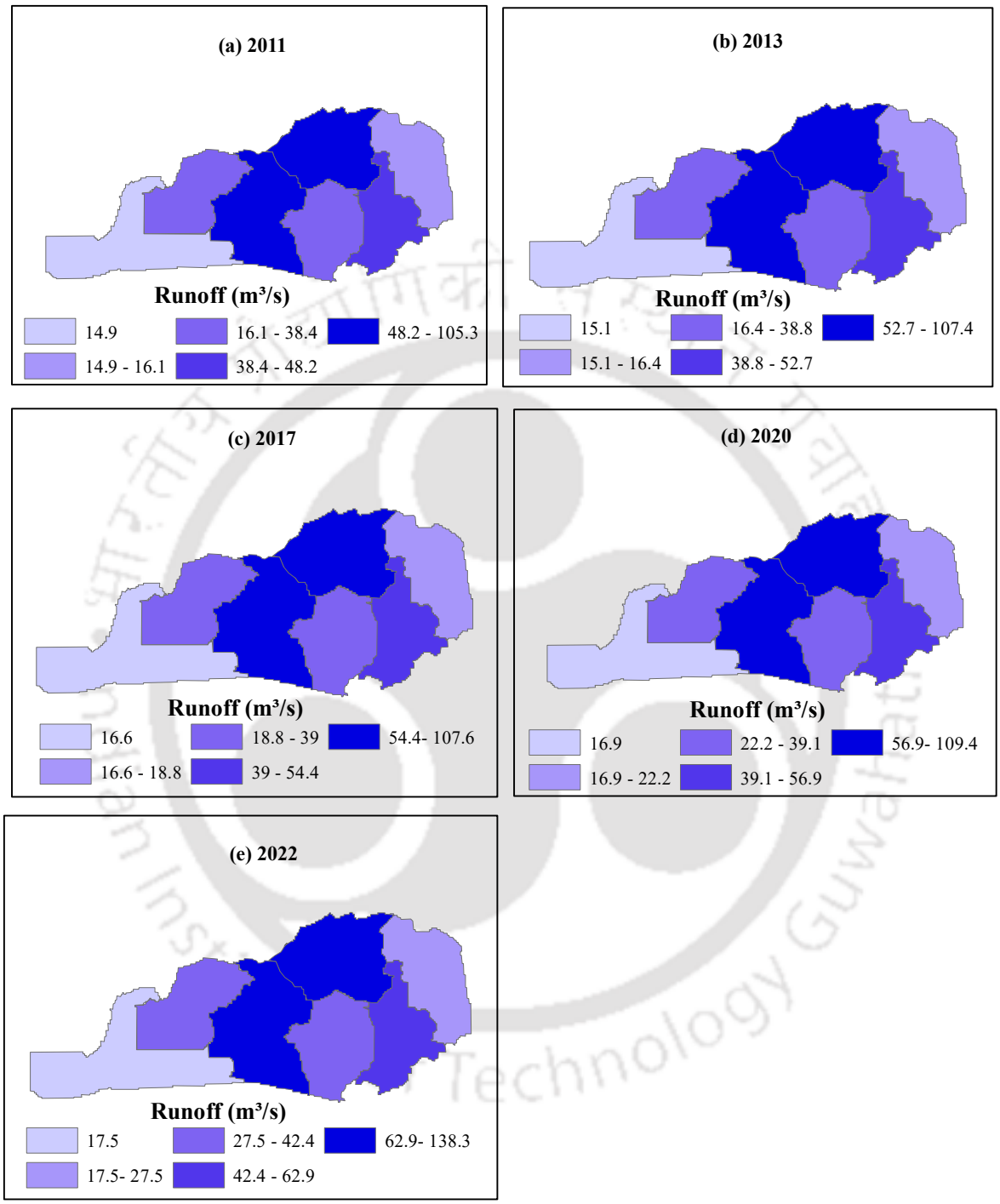

Figure 6.14: Spatial variation of peak runoff across different watersheds for RE6

nodes. Similar response patterns were observed for EIA corresponding to the years 2011, 2013, 2017, and 2020. The results indicate that for the majority of watersheds, RE-4 leads to higher peak runoff values. However, when considering the duration of flooding, RE-1 exhibits longer duration compared to other rainfall events. It is important to note that the duration of flooding mentioned here refers to the entire watershed, and the duration at individual nodes may differ. It is also interesting to note that only RE-1 and RE-4 was causing flooding in watershed 7. From these observations, it becomes clear that RE-1 is more critical in terms of flooding duration.

Table 6.4 specifically displays the duration of flooding for different EIAs. Watershed 2, 3, and 5 show longer duration of flooding compared to other watersheds.

6.4.2 Impact of Land Use Change on Urban Runoff

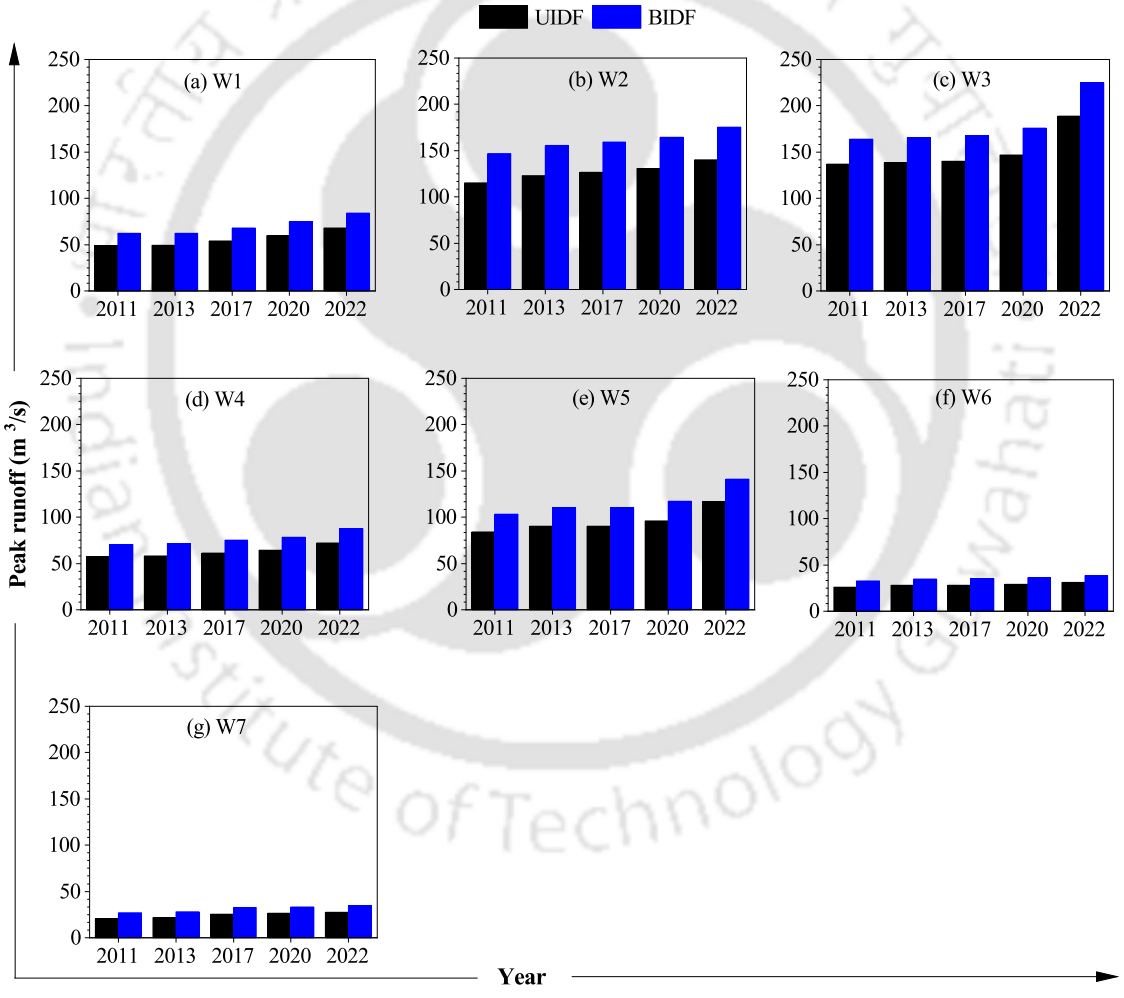

Figure 6.15: Simulated peak runoff for all the watersheds for 15-min duration and 10 year return period for UIDF and BIDF for different LULC

Figure 6.15 shows the comparison of simulated peak runoff for the rainfall intensities corresponding to 15-min duration and 10 year return period with historical UIDF and BIDF for all the watersheds. It is clear from the figure that UIDF underestimate the runoff. The difference in peak runoff

Table 6.3: Response of different rainfall events for 2022 EIA

Rainfall	**W1**			**W2**			**W3**			**W4**			**W5**			**W6**			**W7**		
event	**R**	**D**	**N**	**R**	**D**	**N**	**R**	**D**	**N**	**R**	**D**	**N**	**R**	**D**	**N**	**R**	**D**	**N**	**R**	**D**	**N**
RE-1	64.05	2.5	4	164.71	18.5	3	231.45	12	15	93.53	3.25	7	277.83	14.5	8	93.99	6	3	49.34	1.25	1
RE-2	33.54	1.5	4	88.01	9.25	1	155.8	3.25	11	57.68	2	4	148.23	7.75	8	46.83	3	2	25.83	*	*
RE-3	25.66	1.75	3	56.76	11	1	136.16	4.5	10	40.47	1.25	4	114.8	8.5	7	35.81	3.25	2	16.29	*	*
RE-4	115.2	1.25	5	241.58	9.5	4	312.04	3.25	16	121.29	2	7	204.27	7.5	8	64.8	3	3	51.58	1	1
RE-5	35.13	1.75	4	98.31	9.5	2	163.21	3.5	13	64.42	2	5	160.95	8	8	50.32	3.25	2	29.23	*	*
RE-6	27.46	3.25	3	62.89	11.25	1	138.34	5	11	42.42	2.5	4	119.25	9.25	8	39.58	4.5	2	17.49	*	*

R is the peak runoff (m^3/s)
D is the duration of flooding (h)
N is the number of flooded nodes
*- No flooding

Table 6.4: Duration of flooding for RE-1 for different EIA

Year	Duration of flooding (h)						
	W1	W2	W3	W4	W5	W6	W7
2011	2	15.75	9	3	12.25	5.75	1.5
2013	2	16.25	11.75	3	12.5	6	1.75
2017	2.25	16.75	11.75	2.75	12.75	6	2.25
2020	2.5	17.25	12	3	12.75	6	1
2022	2.5	18.5	12	3.25	14.5	6	1.25

between BIDF and UIDF was 14.5 m^3/s, 33.3 m^3/s, 29.3 m^3/s, 14.1 m^3/s, 20.9 m^3/s, 7.2 m^3/s, and 6.8 m^3/s, for watershed 1, 2, 3, 4, 5, 6, and 7, respectively. Since the runoff obtained using the rainfall intensity of UIDF is less, further analysis is carried out using the rainfall intensity from BIDF.

The spatial distribution of runoff across different watersheds using UIDF and BIDF is shown in Fig. 6.16 and Fig. 6.17, respectively. From the figures, it is clear that watersheds 2, 3, and 5 are more vulnerable to flooding, followed by watersheds 1, 4, and 6, and watershed 7 showed the least runoff. The runoff exhibited a consistent upward trend of 31.9% and 29.6% for rainfall events UIDF and BIDF, respectively, as the EIA changed from 2011 to 2022.

The impact of land use and land cover (LULC) on urban flooding was examined as depicted in Fig. 6.18. The effects of different EIA scenarios from 2011, 2013, 2017, 2020, and 2022 was analysed using the 15-minute duration and 10-year return period rainfall intensity from the historical BIDF. The findings revealed that the peak runoff increased as the percentage of impervious area (EIA) increased. Table 6.5 shows the details of the change in peak runoff corresponding to the change in EIA for all the watersheds. Among all the watersheds, watershed 3 exhibited the highest percentage increase in impervious area (EIA) and consequently showed the largest increase in peak runoff. Specifically, in 2011, the peak runoff for watershed 3 was recorded at 163.7 m^3/s. However, by 2022, the peak runoff in the same watershed had risen to 224.9 m^3/s. During this period, the percentage of impervious area (EIA) in watershed 3 increased from 12.1% to 22.4%. These findings emphasize the strong relationship between land use changes and urban flooding. The study demonstrates that as urban areas experience more development and increased impervious surface coverage, such as roads, parking lots, and buildings, the potential for peak runoff and subsequent flood risks also amplifies.

The findings emphasize significant influence of imperviousness on peak runoff in the study area. As imperviousness of the region increases with changes in land use patterns, such as urbanization, deforestation, or agricultural practices, there is a corresponding rise in peak runoff. The analysis specifically indicates that EIA-related changes from 2011 to 2022 have caused a 1.3 times increase in peak runoff. Such insights are crucial for decision-makers to implement effective measures that mitigate the adverse effects of increased peak runoff and enhance the flood resilience.

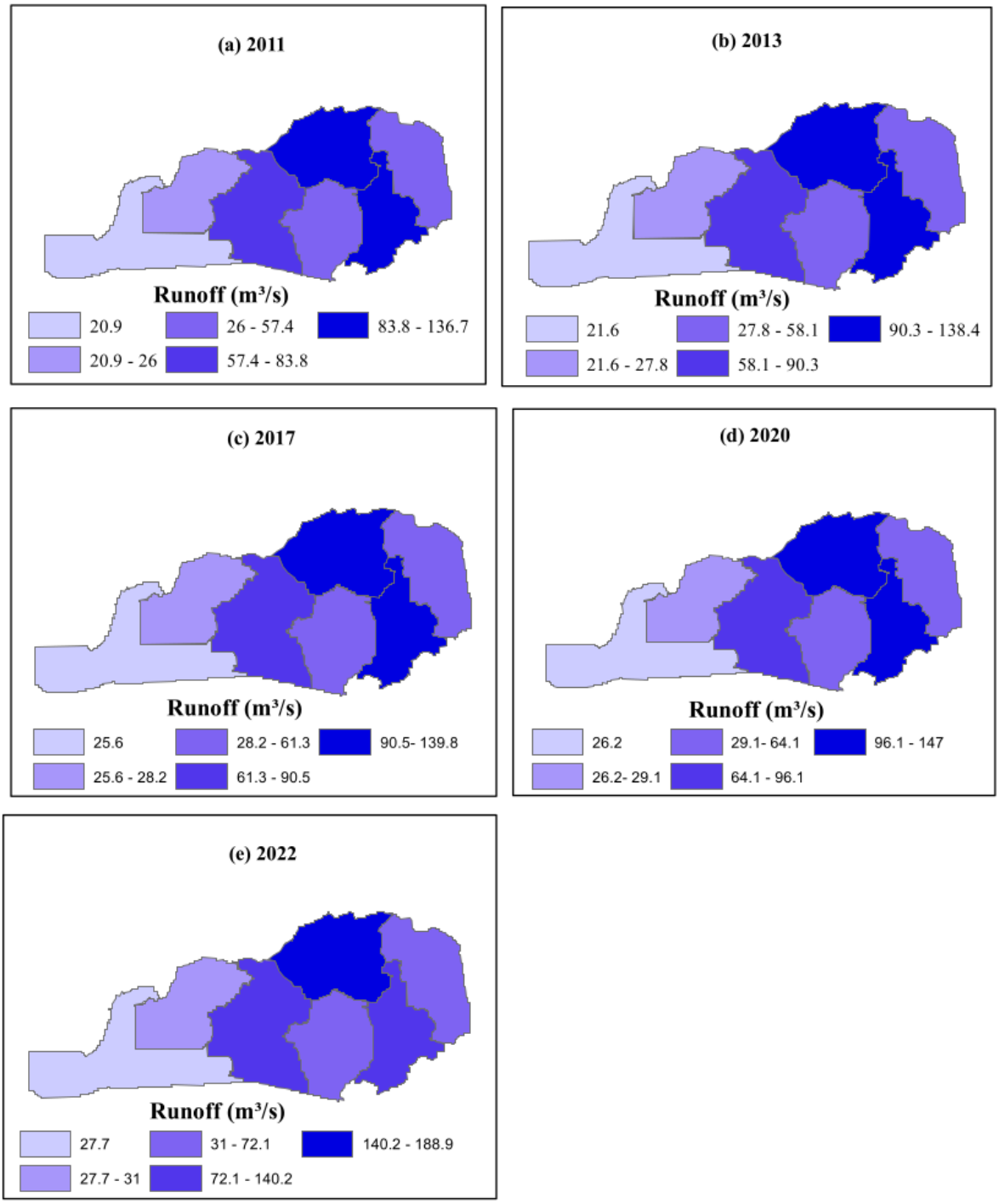

Figure 6.16: Spatial variation of peak runoff across different watersheds for UIDF

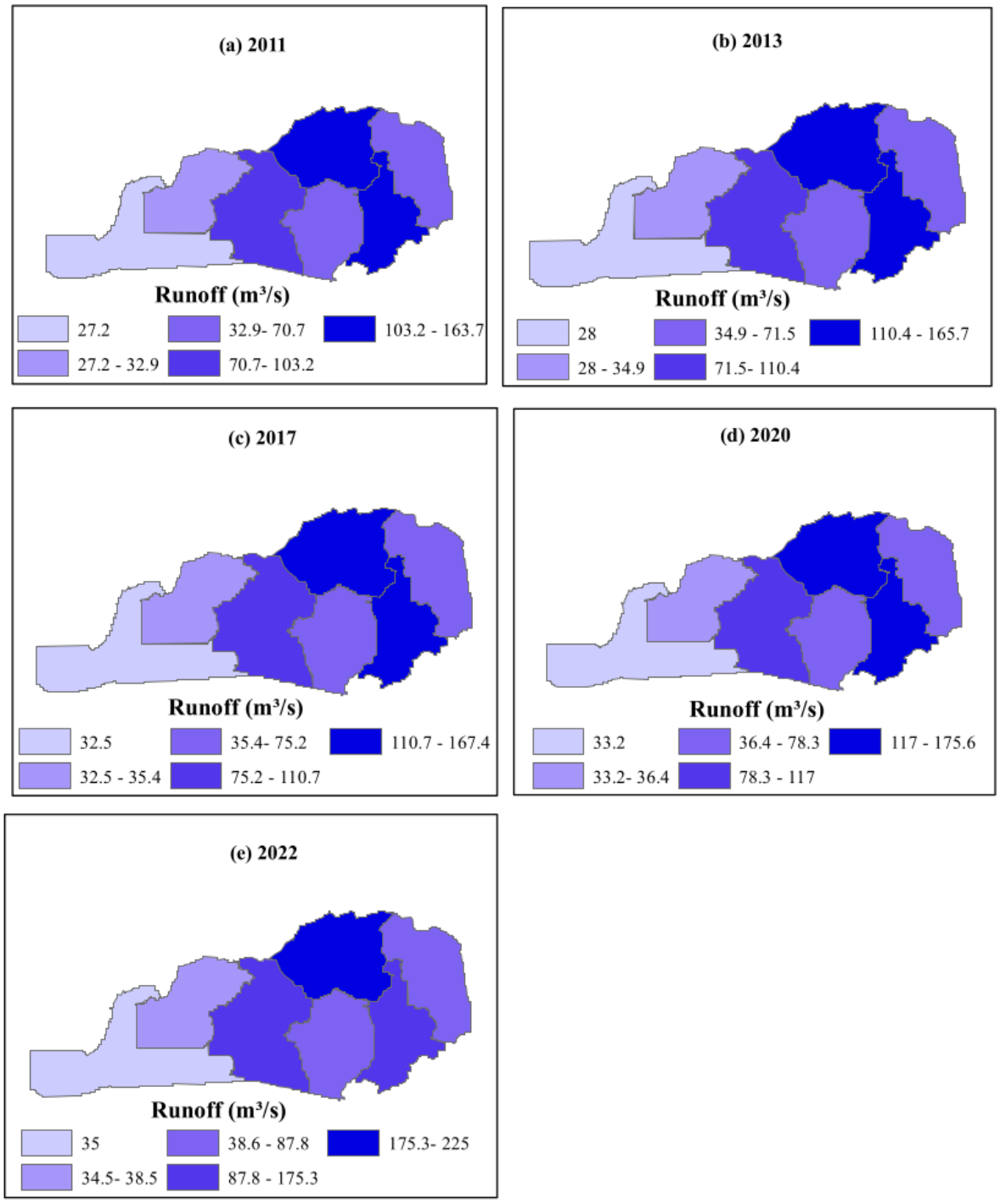

Figure 6.17: Spatial variation of peak runoff across different watersheds for BIDF

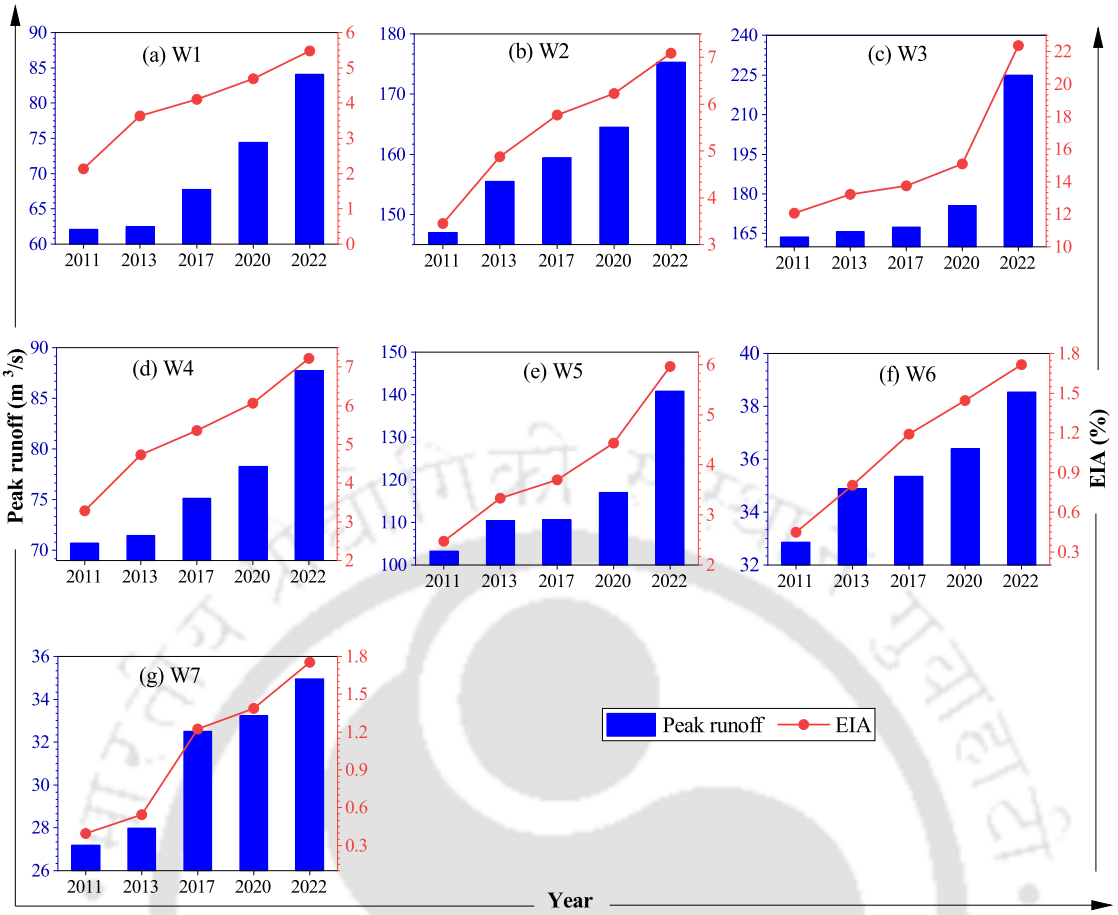

Figure 6.18: Simulated peak runoff for all the watersheds for 15-min duration and 10 year return period for UIDF and BIDF for different LULC

Table 6.5: Percentage change in peak runoff and EIA from 2011 to 2022

Watershed	Percentage change in peak runoff	Increase in EIA (%)
W1	35.4	3.35
W2	19.3	3.64
W3	37.5	10.31
W4	24.1	3.93
W5	36.4	3.48
W6	17.3	1.26
W7	28.5	1.36

6.4.3 Impact of Climate Change on Urban Runoff

In order to investigate the separate impact of climate change on urban runoff, the LULC for the year 2022 has been fixed, and the climate period is divided into three periods 2021-2047 (P1), 2048-2074 (P2), and 2075-2100 (P3).

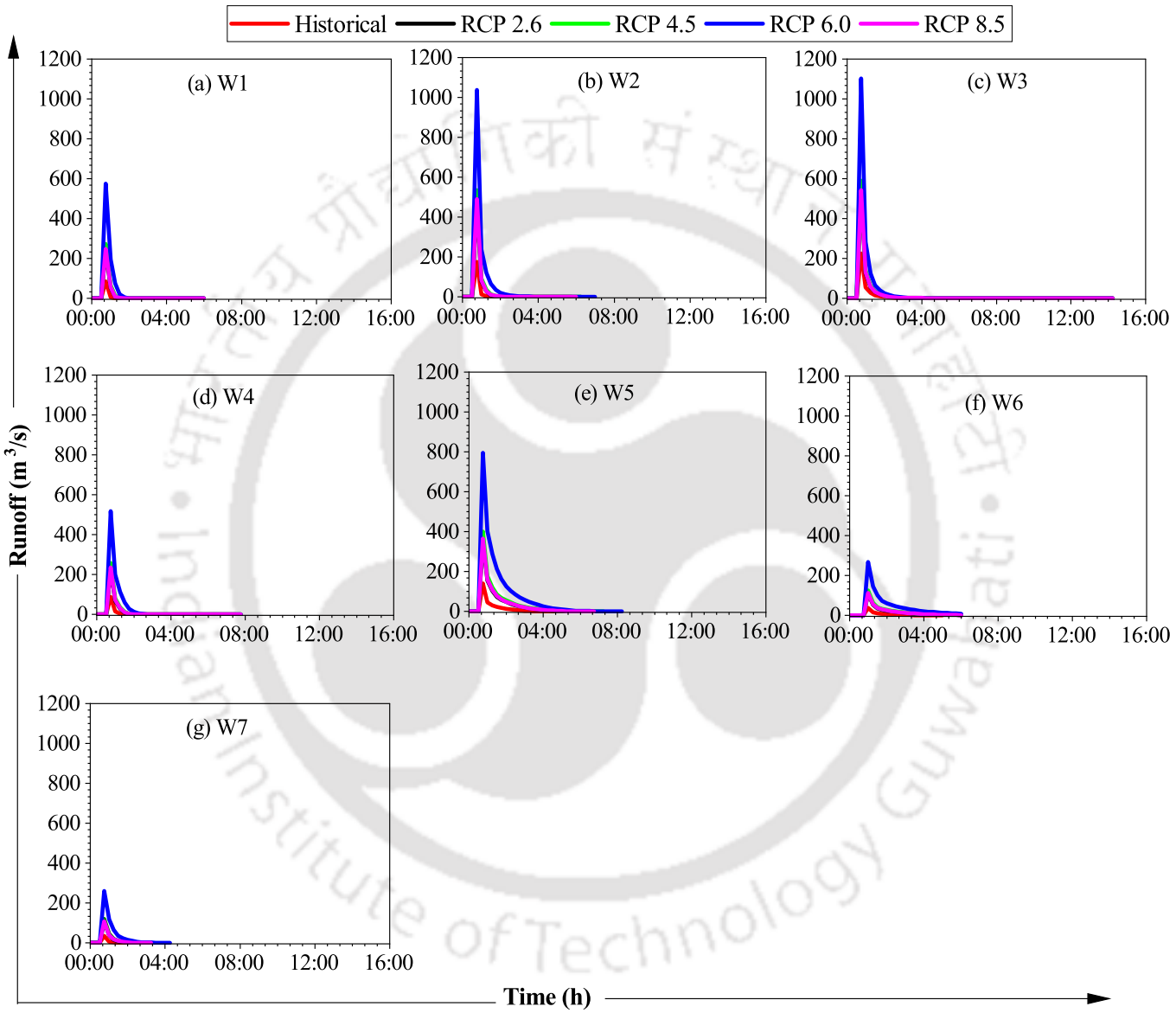

Figure 6.19: Comparison of simulated runoff for historical and different RCP scenarios for period P1 across all watersheds for rainfall intensities of 15-min duration and 10 year return period

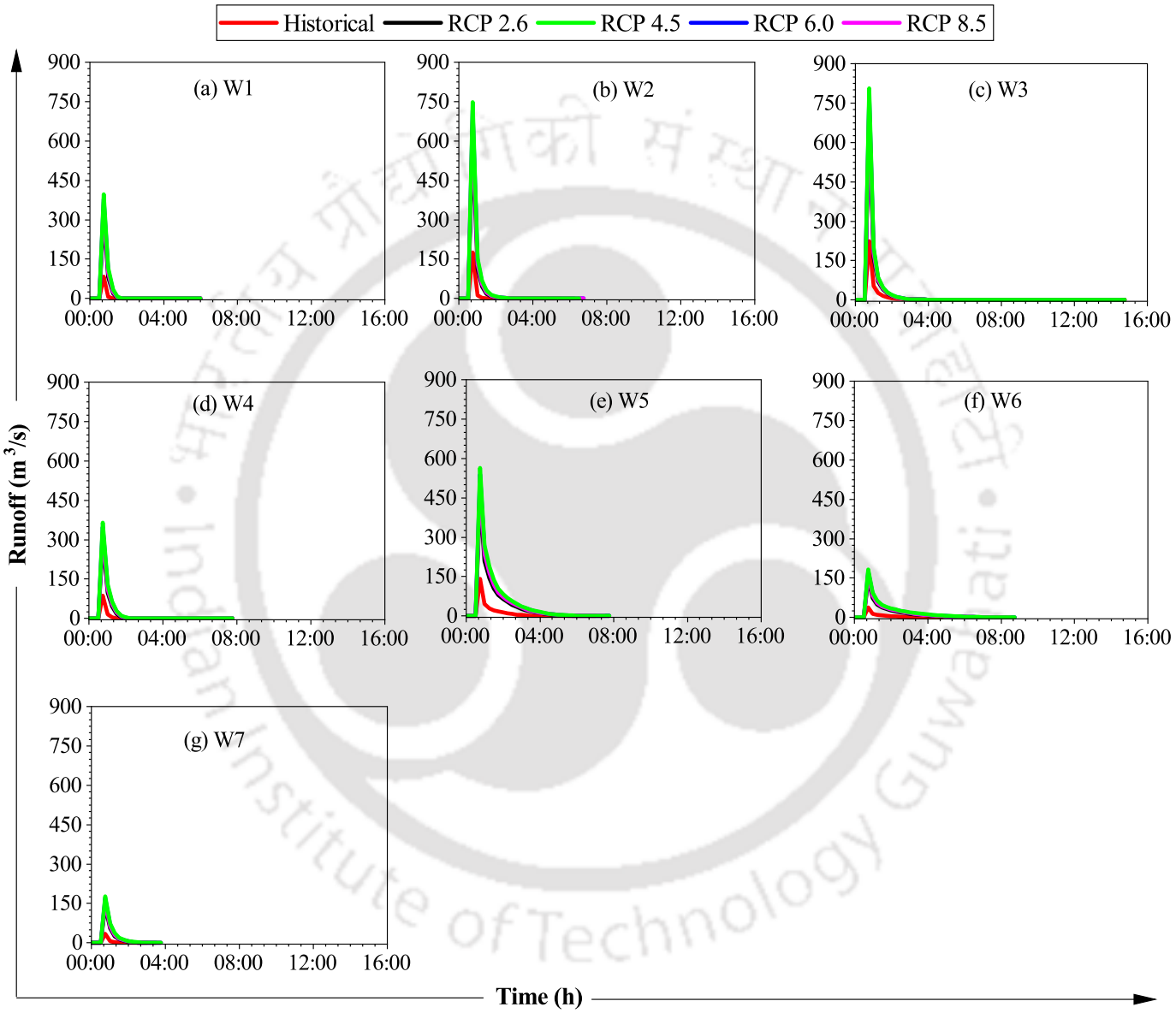

Figure 6.20: Comparison of simulated runoff for historical and different RCP scenarios for period P2 across all watersheds for rainfall intensities of 15-min duration and 10 year return period

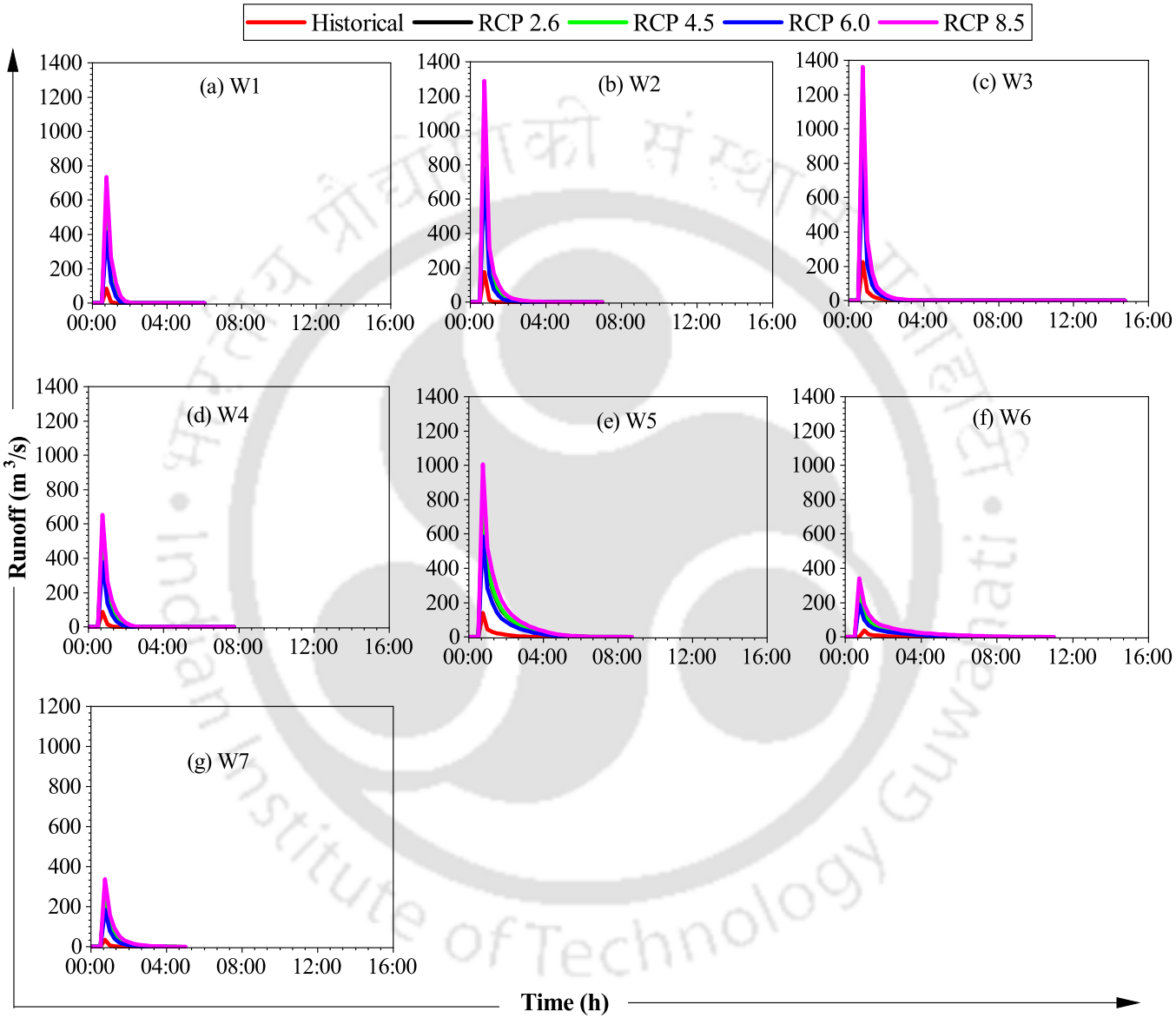

Figure 6.21: Comparison of simulated runoff for historical and different RCP scenarios for period P3 across all watersheds for rainfall intensities of 15-min duration and 10 year return period

Figures 6.19 to 6.21 show the comparison of simulated runoff for historical and different RCP scenarios for the P1, P2, and P3 respectively, for all the watersheds with a rainfall intensity corresponding to 15-min duration and 10 year return period. For the near future (P1), the rainfall intensity determined from RCP 6.0 scenario was consistently much higher than other scenarios. This high intensity is reflected in the runoff trend also. RCP 6.0 scenario gives the highest runoff compared to other scenarios for P1 period. For P2 and P3 periods, RCP 4.5 and RCP 8.5, respectively, give the higher rainfall intensities and the same is seen in terms of runoff i.e., RCP 4.5 was giving higher runoff for P2 and, RCP 8.5 was showing higher runoff for P3. The figures show that the simulated runoff values for all the three periods are more significant than the historical runoff values.

Figures 6.22 to 6.25 shows the spatial distribution of runoff for the watersheds for different climate periods. Watersheds 2,3, and 5 shows the higher runoff compared to other watersheds. From the figures, it is clear that watersheds 2, 3, and 5 are more vulnerable to flooding, followed by watersheds 1, 4, and 6, and watershed 7 showed the least runoff. The percentage change in runoff from P1 to P2 was 28.7% for RCP 2.6, 41.1% for RCP 4.5, -31.9% for RCP 6.0, and 38.3% for RCP 8.5. Similarly, the change from P2 to P3 was 68.9%, 41.7%, 8.7%, and 96.8% for RCP 2.6, RCP 4.5, RCP 6.0, and RCP 8.5, respectively. The overall percentage change from P1 to P3 for RCP 2.6, RCP 4.5, RCP 6.0, and RCP 8.5 was 117.4%, 99.9%, -26%, and 172.1% respectively. A decrease in rainfall was observed from P1 to P2 and P1 to P3 for the RCP 6.0 scenario.

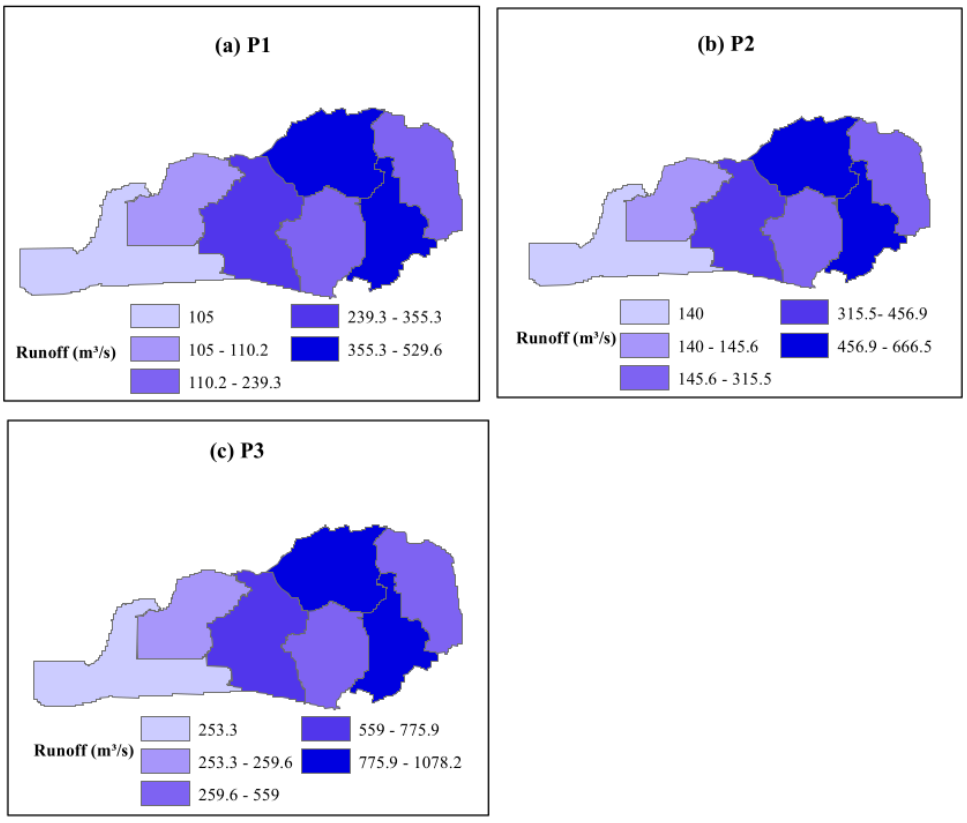

Figure 6.22: Spatial variation of peak runoff across different watersheds for RCP 2.6

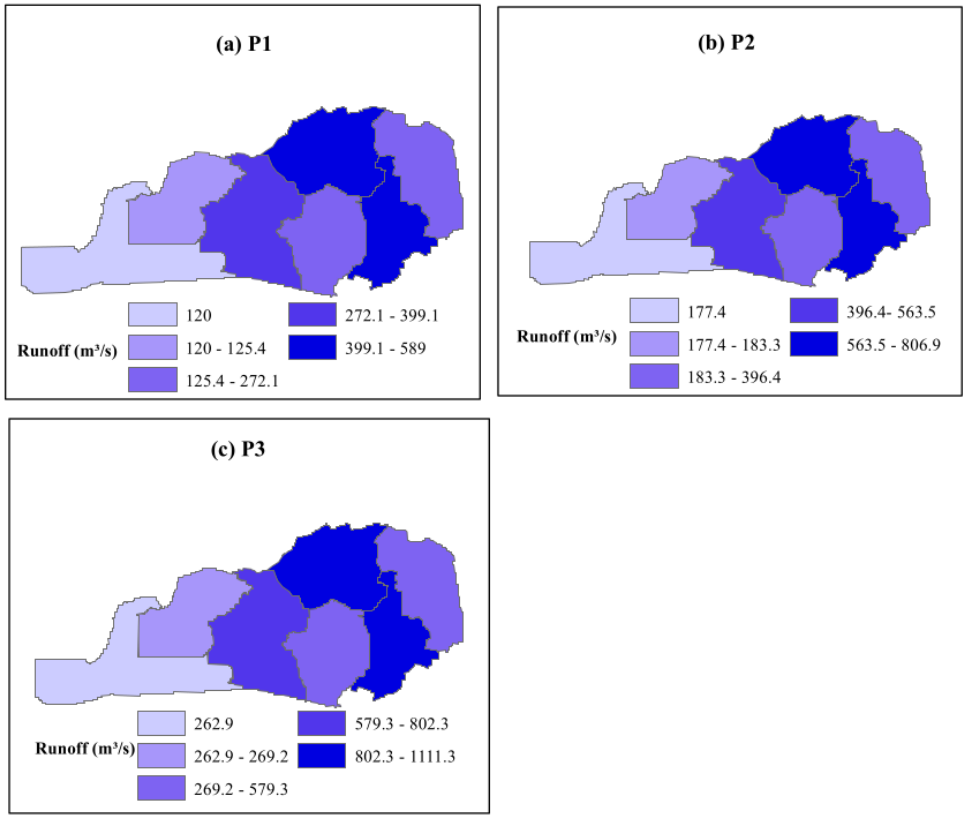

Figure 6.23: Spatial variation of peak runoff across different watersheds for RCP 4.5

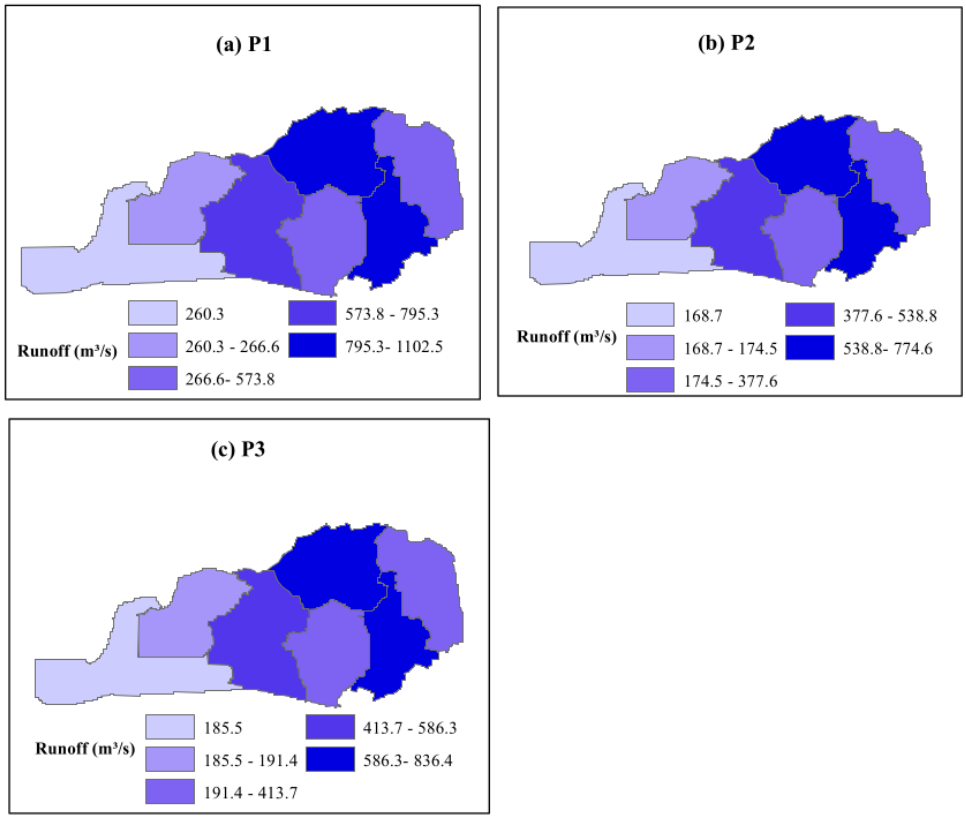

Figure 6.24: Spatial variation of peak runoff across different watersheds for RCP 6.0

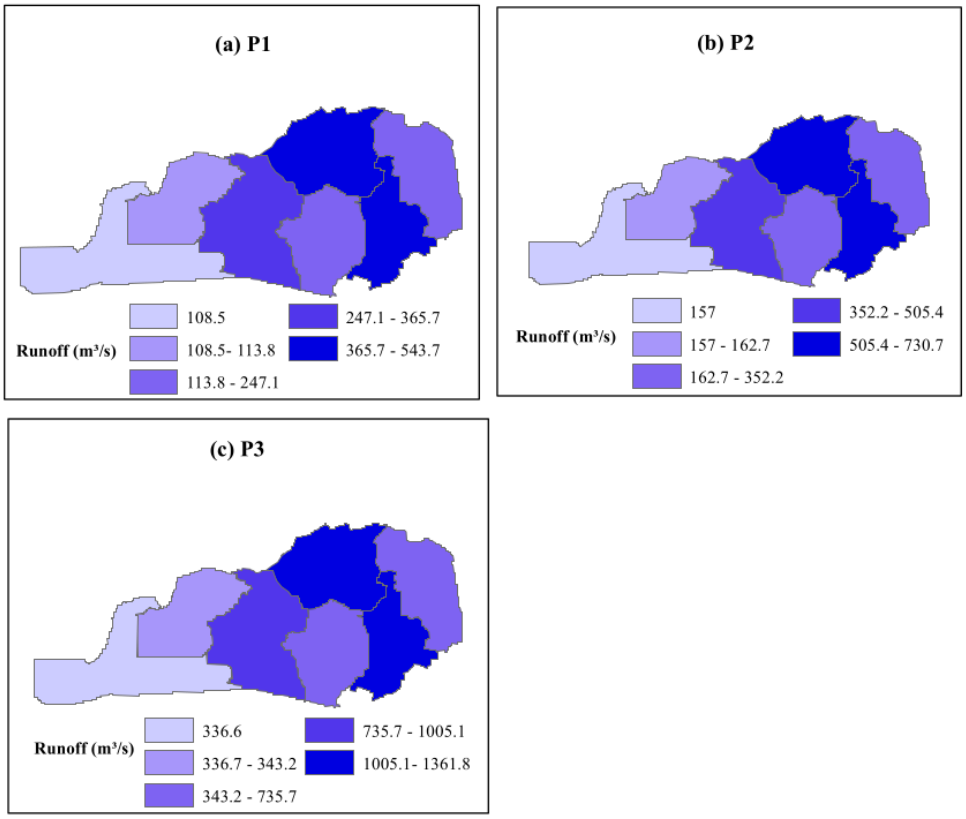

Figure 6.25: Spatial variation of peak runoff across different watersheds for RCP 8.5

This study attempts to understand how these climate scenarios translate to the changes in simulated runoff as compared to the historical runoff for Guwahati city. This finding suggests that climate change exerts a noteworthy influence on the amount of runoff experienced in urban catchment areas. By keeping the land use characteristics constant and carrying out the analysis for different periods, it was observed that climate change scenarios resulted in substantially higher runoff than historical conditions.

Figure 6.26 shows the comparison of simulated peak runoff for different future periods and table 6.6 lists out the corresponding changes in the peak runoff for different periods with respect to the observed peak runoff. The figure demonstrates that RCP 2.6, RCP 4.5, and RCP 8.5 scenarios display an increase in peak runoff from P1 to P3. On the other hand, RCP 6.0 exhibits a higher peak runoff during the P1 period, followed by a decrease in peak runoff during the P2 period, and finally an increase again during the P3 period. Among all the scenarios, RCP 8.5 during the P3 period shows the highest peak runoff value. It is worth noting that all four RCP scenarios and the three periods show higher peak runoff values compared to the observed period for the seven watersheds examined. The figure makes it evident that RCP 6.0 yields a higher peak runoff value during the P1 period, RCP 4.5 during the P2 period, and RCP 8.5 during the P3 period. The results indicate an overall increase in peak runoff from P1 to P3 for most of the scenarios, with RCP 8.5 during the P3 period showing the highest peak runoff value. This suggests that future climate scenarios have the potential to contribute to higher peak runoff in comparison to the observed historical period for

the studied watersheds. This emphasizes the considerable effect of climate change on the runoff observed in urban catchments.

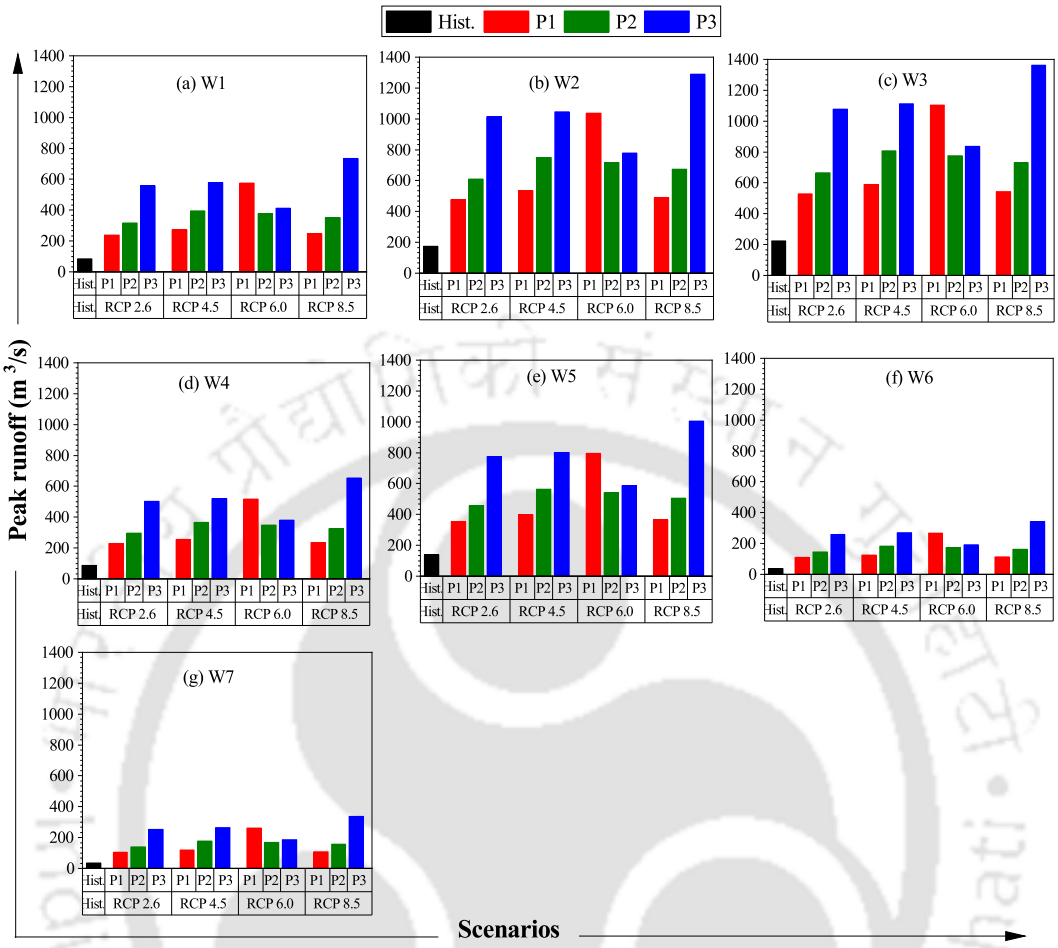

Figure 6.26: Comparison of simulated peak runoff for different scenarios for all the watersheds

Table 6.6: Change in peak runoff with respect to observed runoff

Period	Change in peak runoff (m^3/s)			
	RCP 2.6	**RCP 4.5**	**RCP 6.0**	**RCP 8.5**
P1	304.6	364.1	877.5	318.7
P2	441.5	581.9	549.6	505.7
P3	853.2	886.3	611.4	1136.6

Figure 6.27 shows the simulated peak runoff corresponding to the EIA of the year 2022. This graph provides insights into the influence of climate change on urban runoff. Notably, it is evident that the far-end future period (P3) and the near-future period (P1) exhibit higher runoff values compared to the mid-future period (P2). The graph demonstrates that as it move further into the future, specifically to the far-end future period (P3), the peak runoff values tend to increase. Similarly, in the near-future period (P1), there is a noticeable rise in peak runoff. On the other hand, during the mid-future period (P2), the peak runoff values are relatively lower compared to P1 and

P3. This implies that the impact of climate change on urban runoff becomes more pronounced as it progress towards the far-end future, while the immediate future also experiences substantial runoff changes. The mid-future period appears to have a comparatively lesser impact on peak runoff.

The future runoff projections under different RCPs reveal that RCP 6.0 will experience 4.9 times greater runoff compared to historical levels, RCP 4.5 will have 3.6 times greater runoff, and RCP 8.5 will encounter 6.1 times greater runoff. These findings align with the findings from the IPCC (2014) report, which states that annual global flood exposure could increase by 2-12 times for RCP 4.5, 1-13 times for RCP 6.0, and 4-24 times for RCP 8.5 scenarios. The findings suggest that urban flood characteristics are likely to be significantly impacted by climate change.

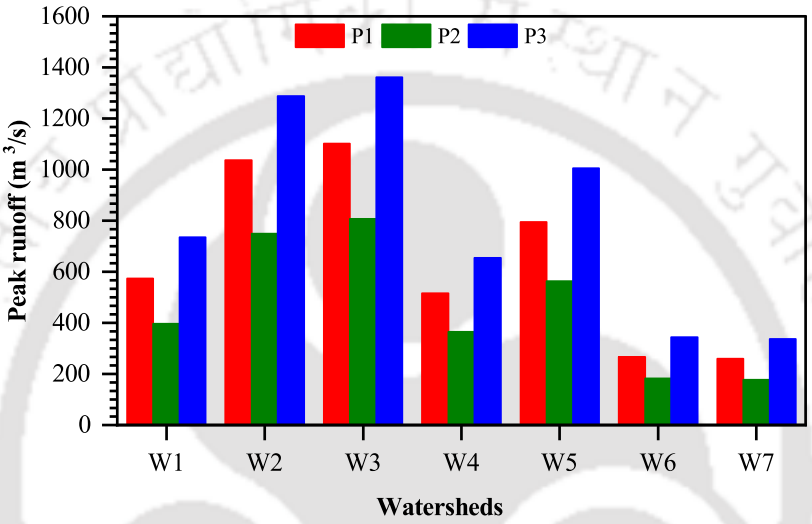

Figure 6.27: Comparison of simulated peak runoff for different periods for 2022 EIA

6.5 Summary

This chapter discussed the impact of LULC and climate change on urban runoff characteristics in Guwahati city. The analysis was divided into three different scenarios. In the first scenario, the influence of different rainfall events having 15-minute duration on runoff in the different sub watersheds of Guwahati was studied. The second scenario tried to understand the impact of LULC alone on the urban runoff. This is studied by varying the EIA from the year 2011 to 2022 and keeping the rainfall intensity constant. The findings showed that peak runoff increased with an increase in the percentage of impervious area. Among all the watersheds, watershed 3 experienced the highest percentage increase in EIA, leading to the higher peak runoff i.e., for 10.3% increase in EIA, the peak runoff increase was 37.5%. The third scenario of the study focused on investigating the impact of climate change on urban flooding. In this scenario, the LULC was kept constant as that of the year 2022, while the rainfall intensity corresponding to different RCPs (RCP 2.6, RCP 4.5, RCP 6.0, and RCP 8.5) during the P1 to P3 periods were changed. The comparison of simulated runoff for historical and different RCP scenarios revealed that RCP 6.0 showed consistently higher rainfall intensity and runoff for the near future (P1) compared to other scenarios. For P2 and P3

periods, RCP 4.5 and RCP 8.5, respectively, exhibited higher rainfall intensity and corresponding runoff. Overall, the findings demonstrate that climate change scenarios lead to significantly higher runoff than historical conditions, emphasizing the substantial influence of climate change on urban runoff in Guwahati city.

This study shows that both LULC and climate can significantly affect urban flood characteristics. It was observed that climate change has more impact than LULC. The analysis demonstrated that the changes in EIA from 2011 to 2022 led to 1.3 times increase in peak runoff. Whereas the future runoff projections under different RCPs indicated that RCP 6.0 will experience 4.9 times greater runoff, RCP 4.5 will have 3.6 times greater runoff, and RCP 8.5 will encounter 6.1 times greater runoff than historical runoff. This study will be helpful for urban planners to take appropriate measures for flood mitigation in cities. By comprehending the relationships between land use changes, climate change, and runoff patterns, decision-makers can develop effective strategies to manage stormwater and improve their flood resilience.

Chapter 7

Best Management Practices for Urban Flood Mitigation in a Changing Climate

7.1 General

Rapid and unplanned urbanization, climate change, and inadequate drainage systems are the reason for urban flooding. As far as Guwahati city is concerned, the detailed investigation on the impact of land use and climate change on flooding is studied and it was observed that there is a need to adopt suitable best management practices for the mitigation of flooding. Conventionally, the grey infrastructure, like expanding the capacity/ constructing a new drainage system, was believed to control the floods effectively. However, this solution has become unsustainable and infeasible due to economic constraints and the space limitation in cities (Li et al., 2020b).

An emerging solution to address these challenges involves the growing adoption of green infrastructure controls, also known as low impact developments (LIDs). LIDs have gained significant recognition as a more sustainable and efficient approach for mitigating urban floods. These measures aid in restoring urban watersheds to their pre-development state essentially imitating natural water cycles. Assessing the efficacy of LIDs on a watershed scale is difficult due to the non availability of high resolution data for the entire watershed. Hence, for the implementation of LIDs to any watershed, there is a need to identify the best performing LIDs on micro watershed scale, which are small-scale drainage areas. By studying these small-scale drainage areas, researchers can better understand the best suited LIDs for a particular watershed and develop effective flood management strategies.

In this study, four micro-watersheds in Guwahati are chosen for understanding the efficacy of LIDs. This chapter deals with the selection of suitable best management practices for urban flood mitigation under a changing climate scenario. For this purpose, flood modeling is carried out in these four micro-watersheds by considering grey and green infrastructural measures. Figure 7.1 shows the schematic representation of the overall methodology followed in computing the runoff from the micro watersheds with and without LIDs for historic and climatic rainfall data.

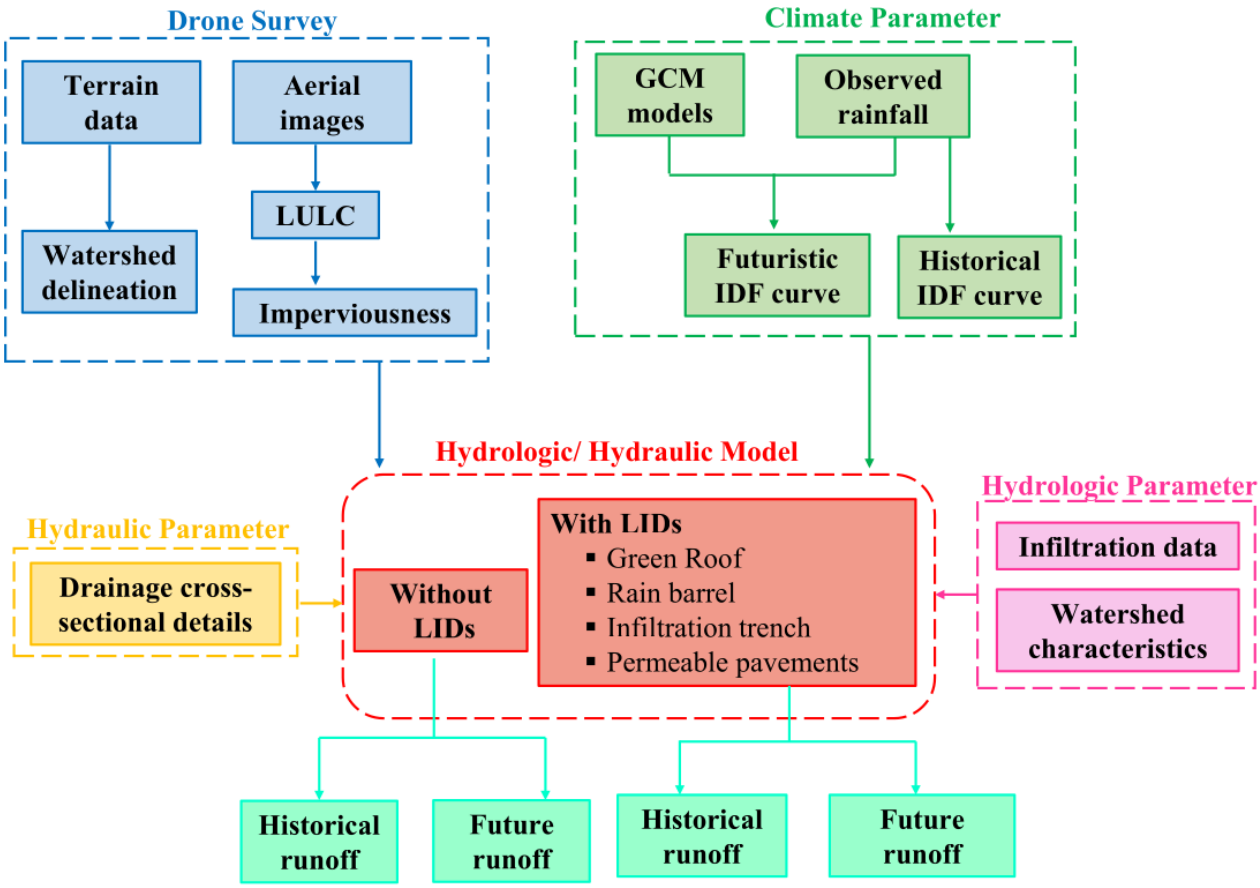

Figure 7.1: Schematic representation of the flow simulation with and without LIDs in micro-watersheds

This chapter is divided into four sections. Detailed description of the micro-watersheds and the input data used for modeling is discussed in the first section. Second section discusses about the commonly used LIDs for the flood mitigation. In the third section, the modeling aspects considering various scenario generation is discussed and in the last section, the performance evaluation of different LIDs in managing runoff is carried out for the selection of the best-performing LID. Also, the efficacy of the selected LID in reducing flooding on watershed scale is studied for the most urbanized watershed in Guwahati city.

7.2 Description of the Micro-Watersheds

In this study, the efficacy of various approaches for minimizing urban flooding was demonstrated by considering four different micro-watersheds located in Guwahati, which experience flooding every year. A drone survey was conducted to capture the fine-resolution data of the micro watersheds for better understanding of the topographical features. Fig. 7.2 illustrates the procedure followed in the drone survey, which is broadly divided into four stages, namely, preparation stage, acquisition stage, post-processing stage, and analysis stage.

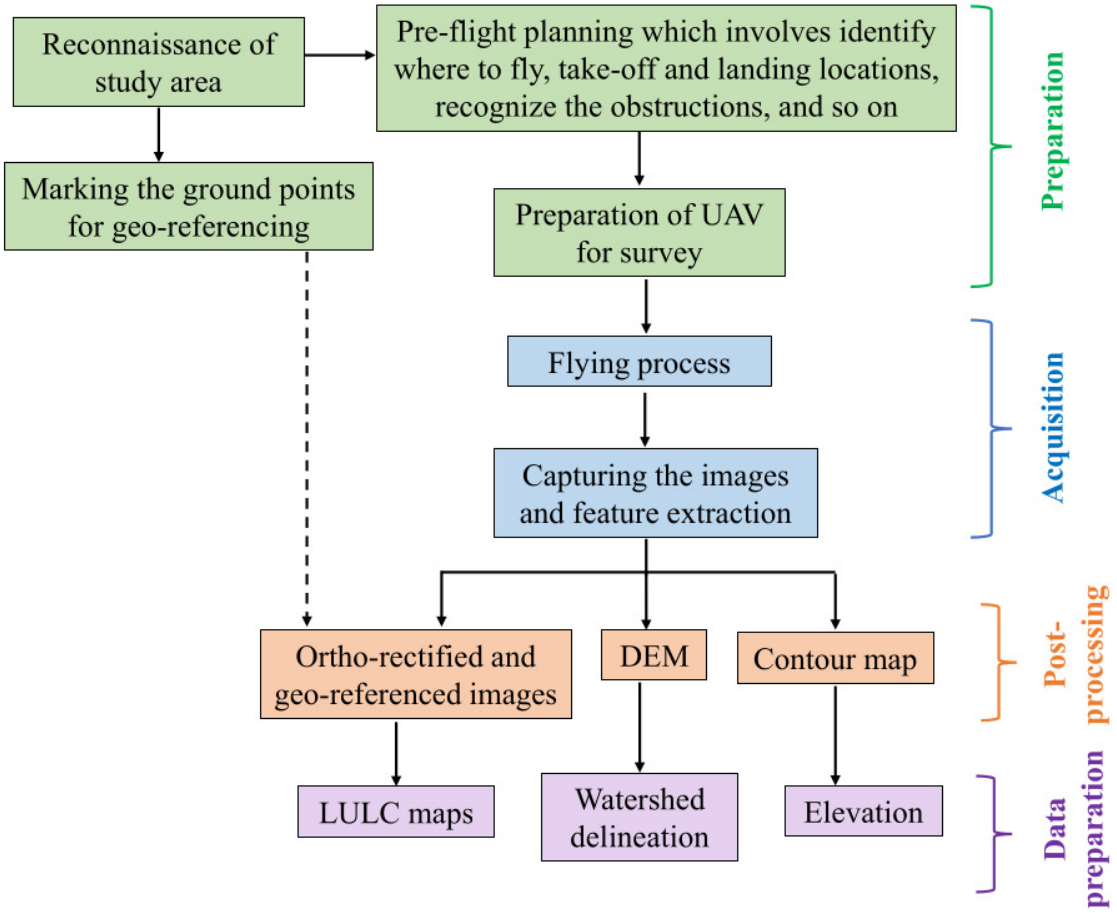

Figure 7.2: Flowchart of the data acquisition procedures

The drone survey yielded an ortho-rectified and geo-referenced image (0.023m resolution), a contour map (0.2 m accuracy) and a digital elevation model (0.045 m resolution) of the micro watersheds. The four micro watersheds, named as watershed A, B, C and D, respectively, are depicted in Fig. 7.3. Different land use classes of the micro watersheds are identified by carrying out the aerial image analysis with ArcGIS software by manual classification technique. The slopes were calculated from the contour maps. The cross-sectional details of the drainage were obtained by carrying out the field survey and using aerial images. The micro-watersheds are further delineated into sub-watersheds, and the details are listed in table 7.1. The elevation of watershed A ranges from 51.27- 59.07 m, watershed B is from 50.07- 59.14 m, watershed C is 40.09- 59.03 m, and watershed D is 42.06- 58.57 m. All four micro-watersheds are low-lying areas, having clayey silt type of soil. The infiltration parameters used in the study are suction head (0.29 m), hydraulic conductivity (0.5 mm/hr), and initial deficit (0.279 mm). The existing drainage network present in these four micro-watersheds was insufficient to manage the stormwater in the area. Also, during the monsoon season, stormwater from surrounding areas flows to these micro-watersheds resulting in heavy flooding.

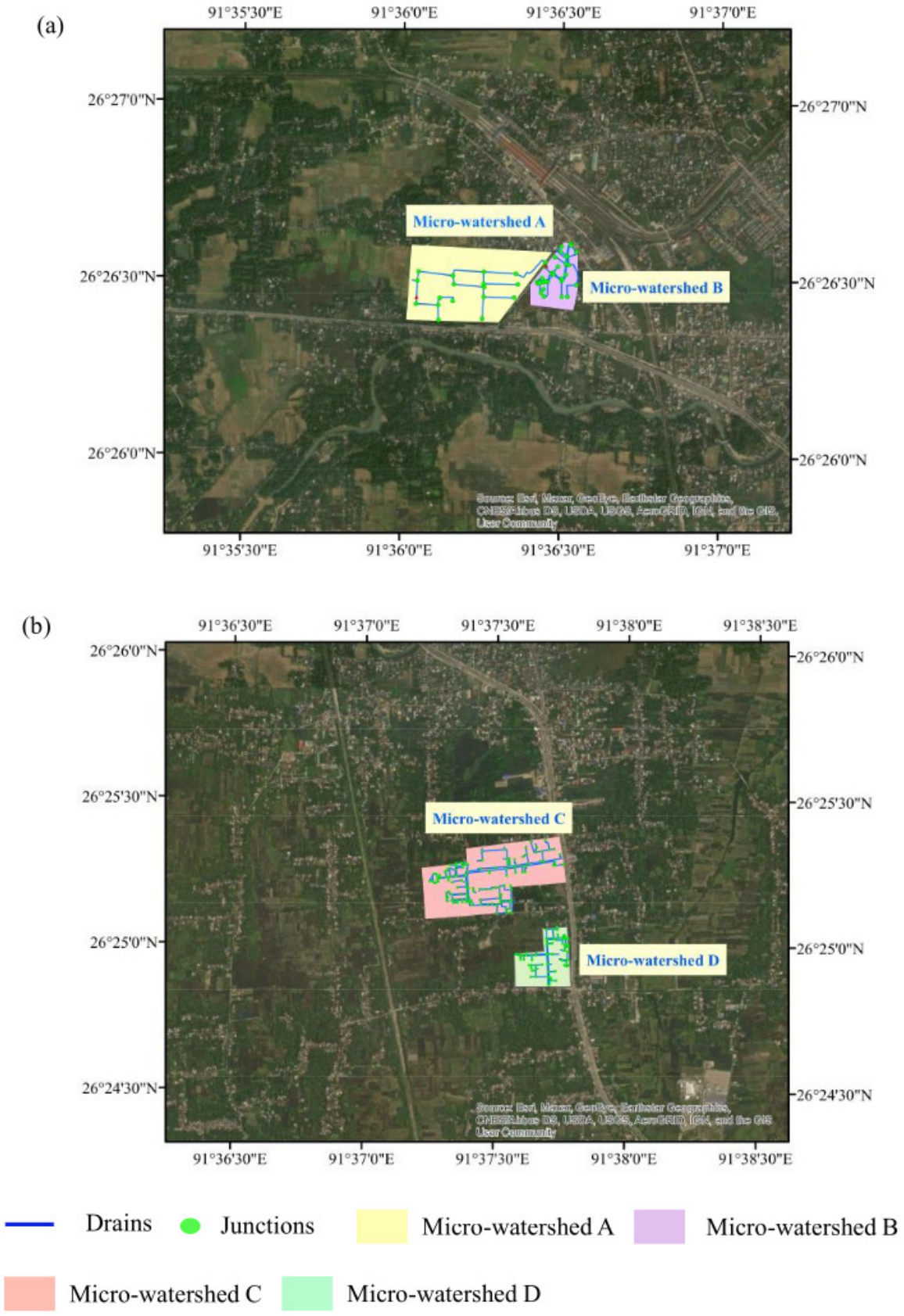

Figure 7.3: Location of four micro-watersheds for LID analysis

Table 7.1: Details of the micro-watershed

Name	A	B	C	D
Total area (Ha)	21.42	5.17	17.24	7.61
No. of sub-watersheds	22	15	75	52
No. of nodes	25	29	144	81
No. of conduits	36	35	166	88

7.2.1 Land Use Classification of the Micro-Watersheds

The aerial image obtained from the drone survey were classified manually into different land use classes. The area designated for each land use class is shown in table 7.2. The percentage imperviousness of micro-watersheds A, B, C, and D are 11.7%, 36.3%, 40.9%, and 33.1%, respectively.

The reason for choosing these four micro-watersheds are:

- For micro-watershed A, about 50% of the LULC is marshy land. In this study, attempts are made to utilize these areas and understand how they can be used to mitigate floods.
- For micro-watersheds B, C, and D, the imperviousness in terms of built-up area is high.
- Implementation of LIDs over a larger area (city scale) may not be feasible. So it is better to implement the LIDs over small areas like micro-watersheds, which can give a better understanding of the problems and solutions.

Table 7.2: Land use details of the micro-watersheds

Name	Area (%)			
	A	B	C	D
Builtup	11.7	36.3	40.7	32.9
Marshy land	49.1	0.2	0.1	3.2
Openland	29.1	48.0	38.4	44.8
Water body	0.1	2.0	7.8	6.5
Vegetation	10.1	13.5	13.0	12.6

7.3 Low Impact Developments (LIDs)

LIDs are the mitigation measures designed to capture and hold stormwater that would otherwise become runoff and cause flooding on the site (Rossman and Huber, 2016a). The latest version of SWMM (version 5) is used to understand the hydrologic performance of LIDs for managing runoff. The various LIDs available in SWMM5 to simulate runoff include rain barrels, bio-retention cells, vegetative swales, green roofs, rooftop disconnections, infiltration trenches, permeable pavements,

and rain gardens. Figure 7.4 shows the working mechanism of LIDs. A portion of the rain that falls on the impervious portion of the urban area may flow to the pervious region of the watersheds, where the majority will be converted to runoff, resulting in a flood. When LID is implemented in an urban area, a portion of the water falling on impervious surfaces is routed to the LID, where it can be stored or infiltrated, thereby reducing runoff and flooding. Based on the site characteristics, four different types of LIDs, namely, green roofs (GR), infiltration trenches (IT), rain barrels (RB), and permeable pavements (PP) were chosen in this study. The characterization of different types, installation locations, and primary functions of different LIDs used in the study are given in table 7.3.

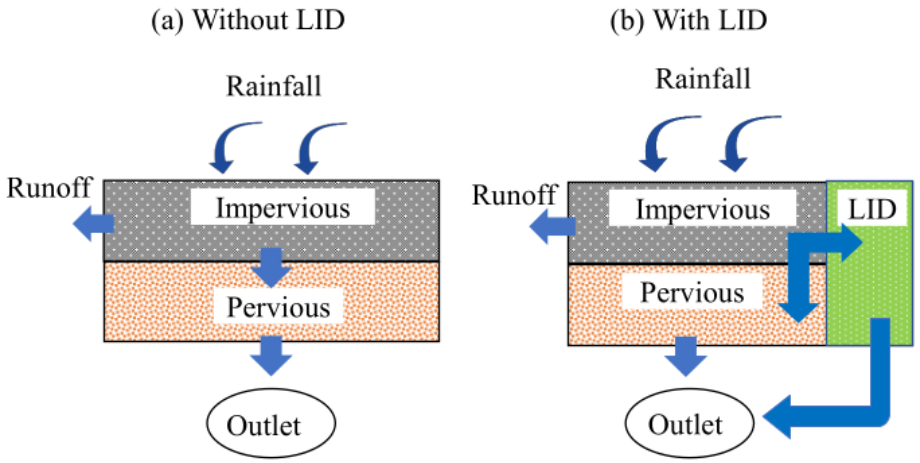

Figure 7.4: Schematic representation of mechanism of LIDs (a) without LID and (b) with LID

Table 7.3: Characterization of LIDs used in this study

LID type	**Function**	**Installation location**	**Layers & Equations**
Green Roof	Retention	Rooftops	• Surface layer: $\phi_1 \frac{\partial d_1}{\partial t} = i - e_1 - f_1 - q_1$ • Soil layer: $D_2 \frac{\partial \theta_2}{\partial t} = f_1 - e_2 - f_2$ • Drainage layer: $\phi_3 \frac{\partial d_3}{\partial t} = f_2 - e_3 - q_3$
Rain barrel	Retention	Rooftops	• Storage layer: $\frac{\partial d_3}{\partial t} = s_1 - q_1 - q_3$
Permeable pavements	Infiltration	Parking lots	• Surface layer: $\frac{\partial d_1}{\partial t} = i + q_0 - e_1 - f_1 - q_1$ • Pavement layer: $D_4(1 - F_4) \frac{\partial \theta_4}{\partial t} = f_1 - e_4 - q_3$ • Storage layer: $\phi_3 \frac{\partial d_3}{\partial t} = f_2 - e_3 - f_3 - q_3$

Infiltration trenches	Infiltration	Open space	• Surface layer: $\frac{\partial d_1}{\partial t} = i + q_0 - e_1 - f_1 - f_3 - q_1$ • Storage layer: $\phi_3 \frac{\partial d_3}{\partial t} = f_1 - e_3 - f_3 - q_3$

i - Rate of precipitation falling on the surface directly, q_0 - Inflow from other areas to the surface layer, q_1 - Overflow rate in the surface layer, q_3 - Outflow rate of storage layer underdrain, f_1 - Infiltration rate of surface water into soil layer, f_2 - percolation rate into the storage layer from the soil layer, f_3 - exfiltration rate into the native soil from the storage layer, f_4 - Draining rate of water out of the pavement layer, e_1, e_2, e_3, e_4 – evapotranspiration rate of surface, soil, storage , and pavement layer respectively, θ_2, θ_4-Moisture content of soil and permeable pavement layer respectively, d_1, d_3- Depth of water on the surface and storage layer respectively, D_2, D_4 -Thickness of the soil and pavement layer respectively, ϕ_1, ϕ_3- Void fraction of surface volume and storage layer respectively, F_4 - Fraction of the surface area taken by the impermeable paver blocks

All four types of LIDs were implemented in the four micro-watersheds separately, and the impact of each LID on runoff mitigation was studied. A brief description of the LIDs used in this study is given below. Unlike developed countries such as Singapore and the United States, which have well-established LID manuals guiding the modeling and parameter selection process, developing countries like India often lack such comprehensive documentation. So, in this study, the authors had to rely on a preliminary analysis of the site conditions and on-site visits to determine the most appropriate LID parameters. This approach is particularly crucial given the absence of readily available standards, and it underscores the need for a more context-specific understanding of LID implementation in diverse regions. The alternative, conducting exhaustive experiments to ascertain LID parameters, would indeed be a laborious and resource-intensive task. So, in this study, the parameters of different LIDs were adopted from the literature, and the same is mentioned below.

7.3.1 Green Roof (GR)

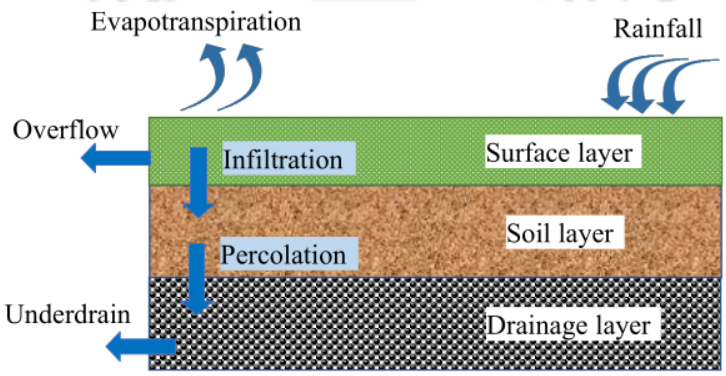

Figure 7.5: Schematic representation of green roof

Green roofs are roofs of buildings covered with vegetation. It comprises of three layers: i) the surface layer, ii) the soil layer, and iii) the drainage layer that drains excess water. A schematic representation of GR is shown in Fig.7.5. The parameters of the GR were taken from Bai et al. (2018) and is shown in table 7.4.

Table 7.4: Parameters of green roof

Layer	Parameters (units)	Value
Surface Layer	Storage Depth (mm)	100
	Vegetation Volume fraction	0.4
	Roughness of Surface	0.03
	Slope of surface (%)	1
	The slope of Swale Side	0
Soil Layer	Thickness (mm)	100
	Porosity	0.5
	Field capacity	0.2
	Point of wilting	0.1
	Hydraulic conductivity(mm/hr)	0.3
	Conductivity slope	10
	Head of suction (mm)	88.9
Drain	Coefficient of Drain (mm/ hr)	4
	Exponent of Drain	0.5
	Offset height of Drain (mm)	0.2

7.3.2 Rain Barrel (RB)

The rain barrels collect water from the roofs, which can either be stored for later use, such as gardening, or released afterwards. A typical schematic representation of a rain barrel is shown in Fig.7.6. SWMM models the rain barrels as a storage layer consisting of a drain valve that can be closed before and opened after the rainfall ends. The parameters of the RB were taken from Cho et al. (2013) as shown in table 7.5.

Table 7.5: Parameters of rain barrel

Layer	Parameters (units)	Value
Storage Layer	Height (mm)	1500
Underdrain	Drain Coefficient (mm/hr)	25.4
	Drain Exponent	0.5
	Drain Offset Height (mm)	10
	Drain Delay (hours)	6

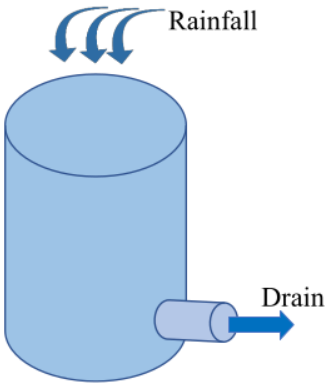

Figure 7.6: Schematic representation of rain barrel

7.3.3 Permeable Pavements (PP)

Permeable pavements are streets or parking lots that are surfaced with a porous concrete or asphalt mixture above a gravel storage layer. Rainfall penetrates through the paving and enters the storage layer, seeping into the natural soil. A schematic representation of PP is shown in Fig.7.7. PP has four layers: (1) surface layer, (2) pavement layer, (3) storage layer, and (4) underdrain layer. The parameters of the PP were taken from Ahiablame and Shakya (2016) as shown in table 7.6.

Table 7.6: Parameters of permeable pavement

Layer	Parameter (units)	Value
Surface	Storage Depth (mm)	20
	Surface Roughness (Manning's n)	0.02
	Surface Slope (%)	1
Pavement	Thickness (mm)	150
	Void Ratio (voids/solids)	0.21
	Impervious Surface Fraction (fraction)	0
	Permeability (mm/hr)	2000
	Clogging Factor	0
Storage	Height (mm)	300
	Void Ratio (fraction)	0.75
	Filtration Rate (mm/hr)	10
	Clogging Factor	0
Underdrain	Drain Coefficient (mm/hr)	0.2
	Drain Exponent	0.5
	Drain Offset Height (mm)	30

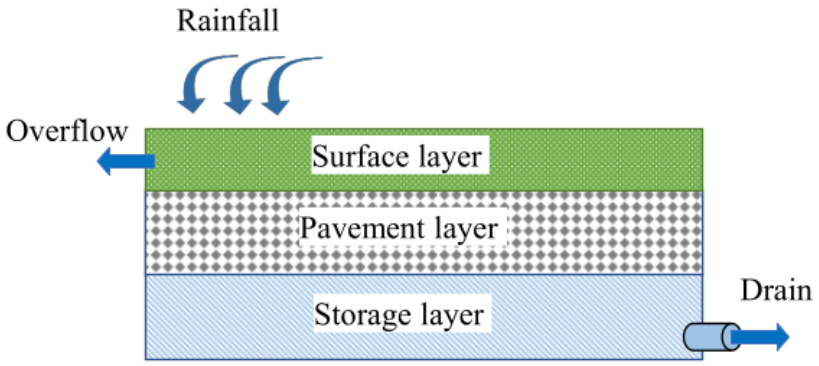

Figure 7.7: Schematic representation of permeable pavements

7.3.4 Infiltration Trench (IT)

Infiltration trenches are narrow ditches that collect stormwater from adjacent areas. IT consists of two layers, a surface layer and a storage layer, as represented in Fig.7.8. The storage layer provides additional time for the captured runoff to infiltrate into the soil. The parameters of the IT were taken from Cho et al. (2013) and is shown in table 7.7.

Table 7.7: Parameters of infiltration trench

Layer	Parameters (units)	Infiltration Trench
Surface Layer	Storage Depth (mm)	200
	Vegetation Volume fraction	0.4
	Roughness of Surface	0.02
	Slope of surface (%)	1
	The slope of Swale Side	0
Storage Layer	Height (mm)	400
	Void Ratio	0.5
	Conductivity(mm/hr)	10
	Clogging factor	0

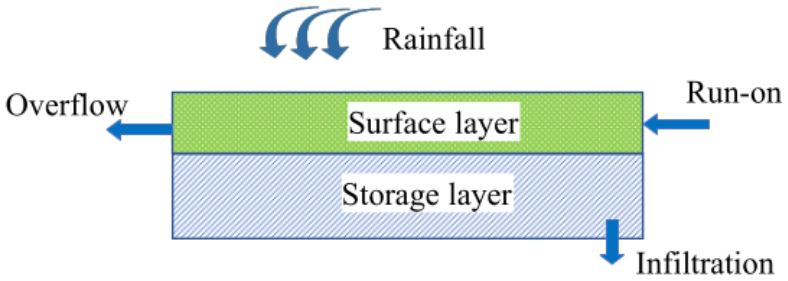

Figure 7.8: Schematic representation of infiltration trench

7.4 Modeling the Effects of Grey and Green Infrastructures

Modeling the effects of grey and green infrastructures on flood mitigation at micro-watershed scale is carried out using the dynamic wave routing present in the storm water management model (SWMM) under climate change. The rainfall intensities used for the analysis are taken from the derived intensity duration frequency curves which are explained in Chapter 4. While deriving the IDF curves, the future rainfall data were divided into three different periods: 2021-2047 (P1), 2048-2074 (P2) and 2075-2100 (P3). It was observed that the RCP 6.0 scenario gave higher rainfall intensities for P1, RCP 4.5 scenario for P2 and RCP 8.5 scenario for P3. So, in this chapter, these three climate periods and RCPs will be used for the simulation. It may be noted that the lower duration < 1h is more prominent for urban watersheds, and the design periods used for urban areas must be equal to or less than 10 years (ASCE, 1992; CPHEEO, 2019). So in this study, the IDF curves developed for the 15-minute duration and return periods of 2-years, 5-years and 10-years are utilized. This approach acknowledges that shorter return periods can have a more significant effect on these smaller-scale watersheds. Infiltration was calculated using the Green-Ampt method, and the Manning's equation was used to estimate the overland flow.

The simulation was carried by considering the redesigned drainage systems and various LIDs, for identifying the suitable flood mitigation measures. Redesigning drainage systems fall under the grey infrastructure, which includes changing the drainage system's cross-section, materials and parameters. This study has attempted to understand how redesigning the existing drainage system will affect the runoff generated in the watersheds along with various LIDs. The modeling was carried out under various scenarios, which are discussed in the following subsection.

7.4.1 Scenario Analysis

Different scenarios were analysed to understand how the LIDs help to reduce surface runoff. Different scenarios considered in this study are:

- S1: Observed rainfall with no LID
- S2: Observed rainfall with redesigned drainage
- S3: Observed rainfall with IT
- S4: Observed rainfall with GR
- S5: Observed rainfall with PP
- S6: Observed rainfall with RB
- S7: Future rainfall with no LID
    a. S7-P1: Climate period P1
    b. S7-P2: Climate period P2

c. S7-P3: Climate period P3

- S8: Future rainfall with best performing LID

a. S8-P1: Climate period P1

b. S8-P2: Climate period P2

c. S8-P3: Climate period P3

Scenarios S1 to S6 were analysed with the observed rainfall, and from these, the best-performing LID was chosen, which will be used for further analysis of future rainfall. Scenarios S7 and S8 are for future rainfall intensities. The workflow of the methodology is shown in Fig.7.9

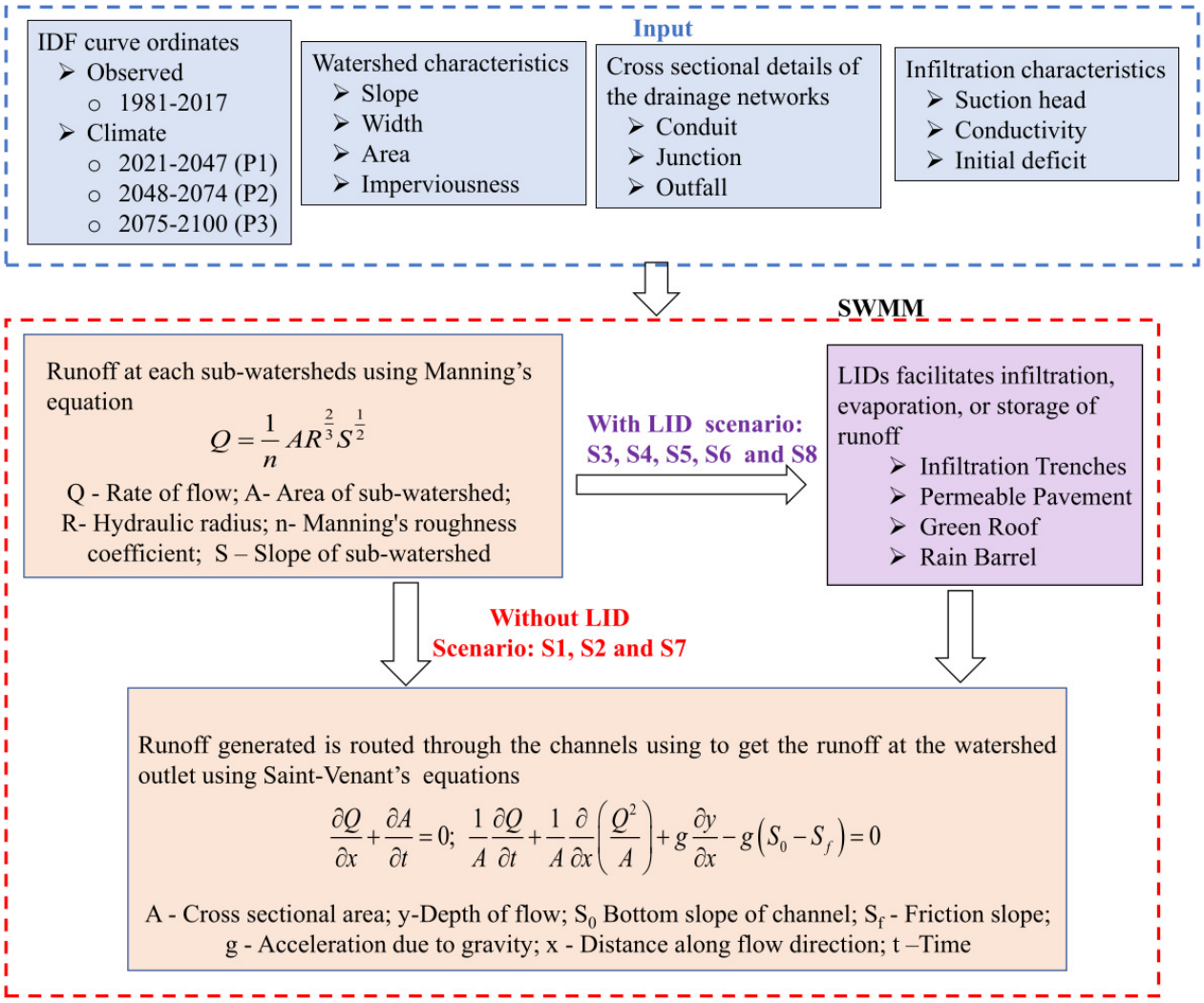

Figure 7.9: Workflow of the methodology

The effectiveness of LID in preventing flooding was evaluated by calculating the percentage change in the captured component (including runoff depth and peak runoff), as shown in Eq. 7.1

$$C_i = \frac{R_{noLID} - R_{LID}}{R_{noLID}} * 100 \tag{7.1}$$

where, C_i is the percentage change in the captured component for i indicator (runoff depth and peak runoff), R_{noLID} is the indicator without LID, and R_{LID} is the indicator after LID implementation.

7.4.2 Runoff Coefficient

The impact of LID on runoff coefficient is also assessed in the micro watershed scale. The runoff coefficient is the ratio between total runoff depth and rainfall. Mathematically it can be written as

$$C_R = \frac{R_{total}}{P_{total}} \tag{7.2}$$

where, C_R is the runoff coefficient, R_{total} is the total runoff depth in the micro-watershed, and P_{total} is the total rainfall depth in the micro-watershed.

7.5 Results and Discussions

7.5.1 Performance Evaluation of Grey Infrastructure in Runoff Reduction

This section discusses the result obtained after redesigning the existing drainage system for the micro-watersheds. Redesigning the drainage system includes changing the cross-section, materials and parameters of the drainage network. It is clear from Fig. 7.10 that there is not much reduction in the runoff depth after modifying the existing drainage system. The percentage reduction in the runoff is shown in table 7.8. For micro-watershed A, a decrease of 3.16%, 2.74%, and 2.53% in runoff depth for the return periods 2-years, 5-years and 10-years, respectively, was observed. Similarly, for micro-watershed B, the percentage reduction in runoff depth was 3.05%, 2.95%, and 2.89%, respectively, for return periods 2-years, 5-years and 10-years. For watershed C, the percentage reduction in the runoff for 2-years, 5-years and 10-years return period was 3.24%, 3.09%, and 3.02%, respectively. The runoff depth reduction for watershed D was 3.55% for 2-years, 3.31% for 5-years, and 3.19% for 10-year return period.

In the case of peak runoff (Fig. 7.10), only micro-watershed A showed a reduction after re-designing the drainage. A 2% decrease in peak runoff for all three return periods was observed in micro-watershed A. Micro-watersheds B, C, and D showed an increased peak runoff for the modified drainage networks. Micro-watershed B showed an increase in peak runoff by 5.59%, 5.47%, and 5.10%, respectively, for the 2-year, 5-year and 10-year return periods. Similarly, watershed C showed an increase in peak runoff by 3.46% for 2-years, 3.50% for 5-years, and 3.55% for 10-years. Again, the peak runoff of micro-watershed D increased by 1.24%, 1.78%, 1.82% for the three return periods.

The time to drain the water in each micro-watershed for existing and redesigned drainage is given in table 7.8. The draining time for runoff has increased to 30 min for a 2-year return period, 45 min for a 5-year return period and 60 min for a 10-year return period for micro-watersheds A

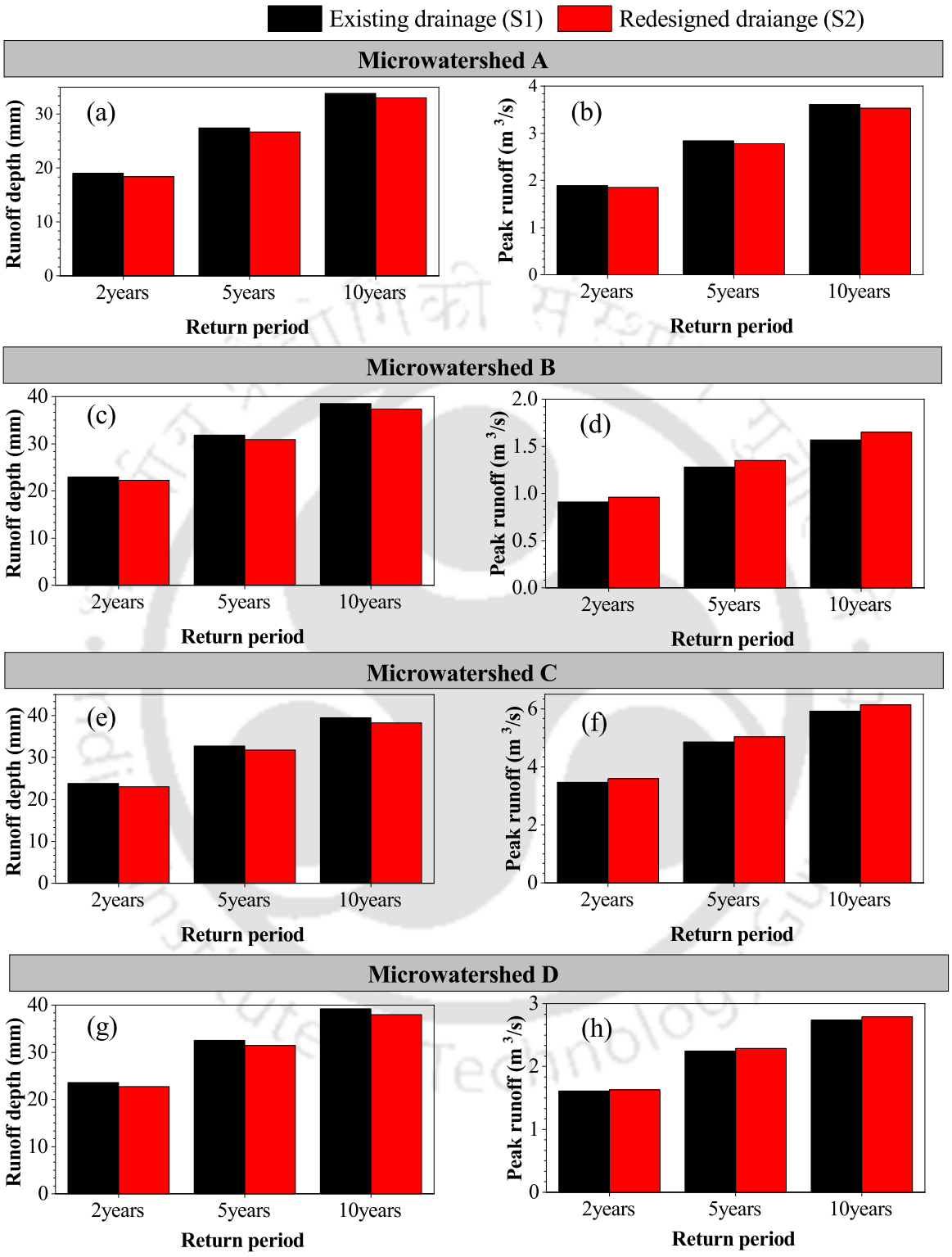

Figure 7.10: Runoff characteristics for existing and redesigned drainage for historical data: (a), (c), (e), (g) represents the runoff depth for micro-watersheds A, B, C, and D, respectively and (b), (d), (f), (h) represents the peak runoff for micro-watersheds A, B, C, and D, respectively

and 15 min for micro-watershed B and C. In contrast, there was no change in the time to drain runoff in micro-watershed D. These observations show that drainage redesign is not effective in controlling the runoff in these watersheds.

Table 7.8: Details of percentage change in the runoff generated and draining time for the redesigned drainage

Pockets	**Return period**	**Percentage change in captured component**		**Draining time (h)**	
		Runoff depth	**Peak runoff**	**Existing drainage**	**Redesigned drainage**
A	2-year	3.16	2.12	06:30	07:00
	5-year	2.74	2.11	07:00	07:45
	10-year	2.53	2.22	07:15	08:15
B	2-year	3.05	-5.49	03:00	03:15
	5-year	2.95	-5.47	03:15	03:30
	10-year	2.89	-5.10	03:15	03:30
C	2-year	3.24	-3.46	03:45	04:00
	5-year	3.09	-3.50	04:00	04:15
	10-year	3.02	-3.55	04:15	04:15
D	2-year	3.55	-1.24	02:45	02:45
	5-year	3.31	-1.78	03:00	03:00
	10-year	3.19	-1.82	03:00	03:00

-ve sign indicates an increase in peak runoff.

The results of redesigning the existing drainage system for the micro-watersheds show a minor reduction in runoff depth for various return periods. Although the percentage reduction in runoff depth appears to be minor, even a slight decrease in runoff can significantly reduce the risk of flooding and its associated damages. However, redesigning the drainage system may only be feasible in some cases due to space limitations and the economic feasibility of redesigning the drainage system. The cost of redesigning the drainage system may outweigh the benefits of reducing runoff depth. Additionally, climate change may increase the flood volume, which may exceed the capacity of drainage system. In such scenarios, it may be essential to investigate other flood mitigation techniques. Adopting low impact development (LID) strategies could be one such strategy.

7.5.2 Performance Evaluation of Green Infrastructures (LIDs) in Runoff Reduction

Figure 7.11 compares the runoff depth obtained for the observed rainfall intensities of the four micro-watersheds with and without LIDs. It is clear from the figure that implementing LIDs has reduced runoff depth in all four micro-watersheds. From Fig. 7.11, it is clear that GR was showing a higher reduction in runoff depth for all the micro-watersheds. For micro-watershed A, IT also gave better results in reducing the runoff depth. Similarly, a reduction in peak runoff for the four

micro-watersheds was also observed. Regarding peak runoff reduction, GR performed better for all four watersheds.

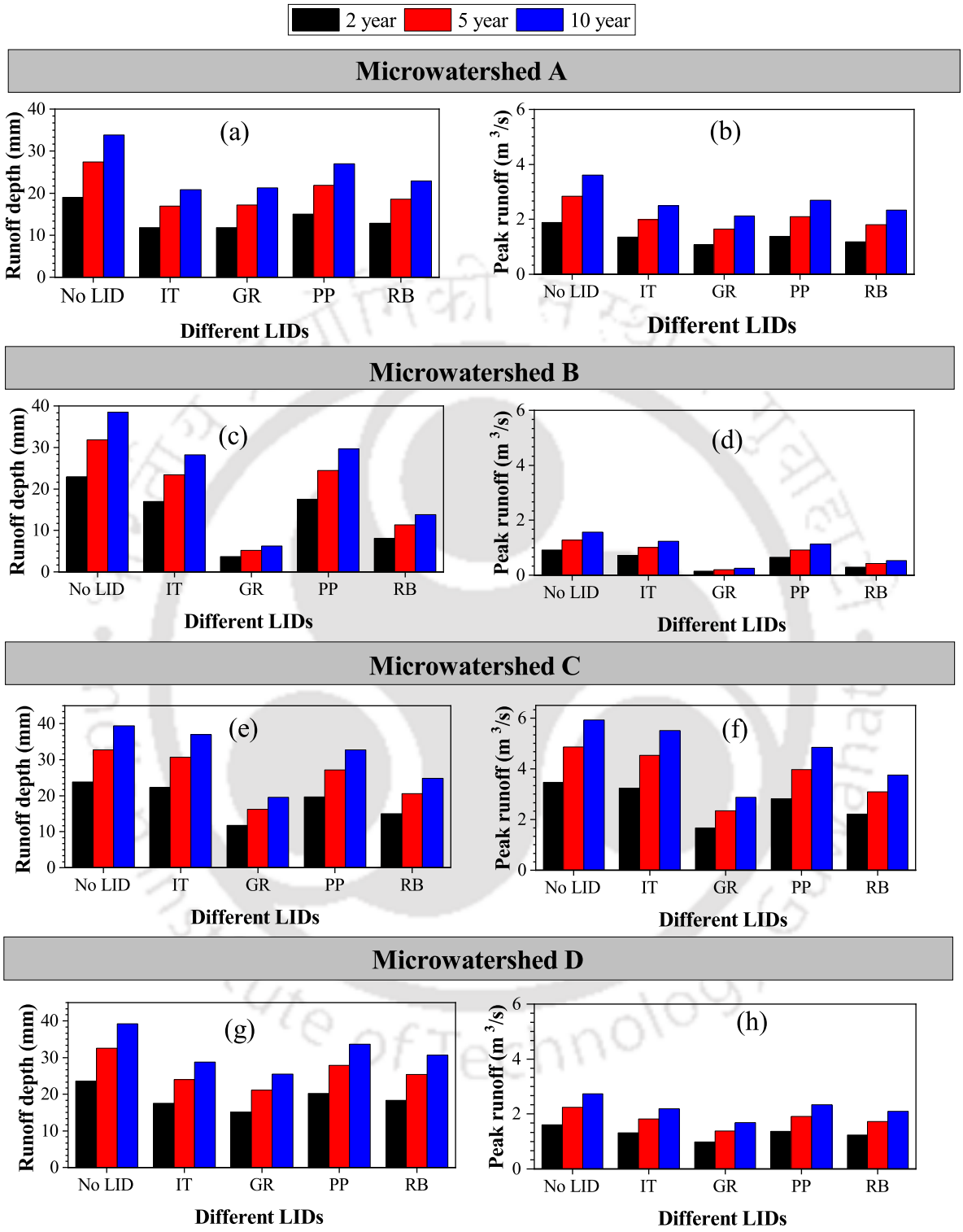

Figure 7.11: Runoff generated for the four micro-watershed without and without LIDs for historical data:(a), (c), (e), (g) represents the runoff depth for micro-watersheds A, B, C, and D, respectively and (b), (d), (f), (h) represents the peak runoff for micro-watersheds A, B, C, and D, respectively

Fig. 7.12 shows the percentage reduction in the captured components for the four micro-

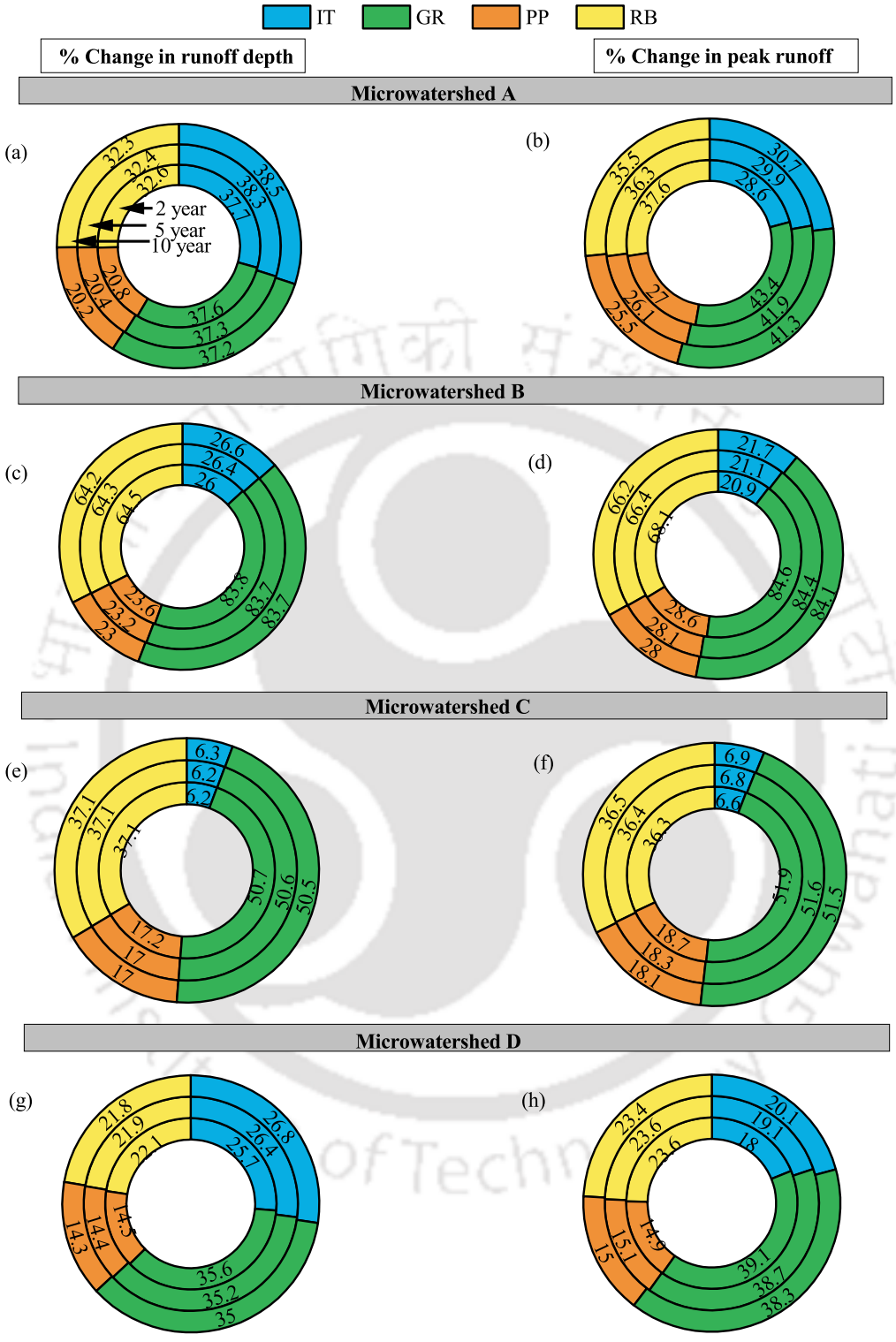

Figure 7.12: Percentage change in runoff depth and peak runoff for different LIDs for historical data: (a), (c), (e), (g) represents the percentage change in runoff depth for micro-watersheds A, B, C, and D, respectively and (b), (d), (f), (h) represents the percentage change in peak runoff for micro-watersheds A, B, C, and D, respectively

watersheds. In the micro-watershed A, a decrease in the runoff depth of around 38%, 37%, 33%, and 21% was observed while using IT, GR, RB, and PP, respectively. Similarly, for micro-watershed B, the percentage reduction in runoff depth is as follows: 83% for GR, 65% for RB, 26% for IT, and 23% for PP. For micro-watershed C, the percentage of reduction for GR, RB, PP, and IT are 51%, 37%, 17%, and 6%, respectively, and for micro-watershed D, around 36% for GR, 27% for IT, 22% for RB, and 14% for PP.

It is clear from the Fig. 7.12 that the micro-watershed A showed a reduction in peak runoff around 41-43% for GR, 36-38% for RB, 29-31% for IT, and 25-27% for PP. In micro-watershed B, around 85%, 66-68%, 28-29%, and 21-22% reductions in peak runoff were observed for GR, RB, PP, and IT, respectively. Similarly, for micro-watershed C, the percentage reduction in peak runoff is as follows: 52% for GR, 36% RB, 18% for PP, and 7% for IT. For micro-watershed C, the percentage reduction in peak runoff for GR, RB, IT, and PP are 39%, 24%, 18-20%, and 15%, respectively and for micro-watershed D, around 36% for GR, 27% for IT, 22% for RB, and 14% for PP.

Figure 7.13: Potential location of green roof

It is clear from the above discussions that the effectiveness of different LIDs varied across the four micro-watersheds. For instance, micro-watershed A showed the highest reduction in runoff depth when using IT, whereas micro-watershed B showed the highest reduction when using GR. The difference in the performance of LIDs on mitigating the runoff depth can be sequentially represented as micro-watershed A- IT>GR>RB>PP; micro-watershed B- GR> RB>IT>PP; micro-watershed C- GR> RB>PP>IT; and micro-watershed D- GR> IT>RB>PP. Similarly, in terms of peak runoff: micro-watershed A- GR>RB>IT>PP; micro-watershed B- GR>RB>PP>IT; micro-watershed C- GR> RB>PP>IT; and micro-watershed D- GR> RB>IT>PP. These results demonstrate that the performance of LIDs is site-specific and depends on several factors, such as the type of LID, rainfall intensity, soil type, and topography. Moreover, the discussion indicates that GR outperformed other LIDs in reducing both runoff depth and peak runoff in most micro-watersheds. The potential location of GR for the micro-watersheds is shown in Fig. 7.13. So in the further analysis to study how climate change affects the performance of LIDs on these micro-watersheds, only GR will be used.

7.5.3 Efficacy of LIDs on Reduction of Flooding and Runoff Coefficient Incorporating Climate Change

Table 7.9: Percentage increase in the future runoff characteristics with respect to observed runoff

Micro-watersheds	Climate periods	Percentage change in runoff characteristics					
		Runoff depth			Peak runoff		
		2 year	5 year	10 year	2 year	5 year	10 year
A	P1	233.4	246.3	250.9	301.1	339.1	354.8
	P2	225.0	193.7	176.1	288.9	258.8	238.2
	P3	340.5	323.8	312.5	463.5	463.4	454.8
B	P1	200.2	218.2	225.8	223.1	251.6	262.4
	P2	193.1	171.9	158.9	215.4	195.3	181.5
	P3	290.9	286.2	280.8	331.9	334.4	329.9
C	P1	194.1	213.0	221.2	215.0	238.9	249.0
	P2	187.2	167.8	155.6	206.9	186.6	173.3
	P3	281.8	279.3	275.0	316.7	316.0	311.7
D	P1	195.7	214.2	222.2	212.4	235.1	244.5
	P2	188.7	168.8	156.3	204.3	184.0	170.8
	P3	284.1	280.8	276.2	311.8	311.1	305.8

Initially, the flow simulation was carried out without implementing GR in all the four micro watersheds using the details from the observed IDF curves and the future IDF curves in order to understand the impact of climate change on runoff depth and peak runoff. Figure 7.14 compares the runoff depth and peak runoff generated for observed and future rainfall intensities for three

return periods (2-years, 5-years, and 10-years). The future climate data was divided into three periods: P1, P2, and P3. Runoff depth increased for all three periods compared with the observed runoff. P3 showed the highest runoff depth, followed by P1 and P2 for all the micro-watersheds. Table 7.9 shows the percentage increase in the runoff characteristics due to climate change.

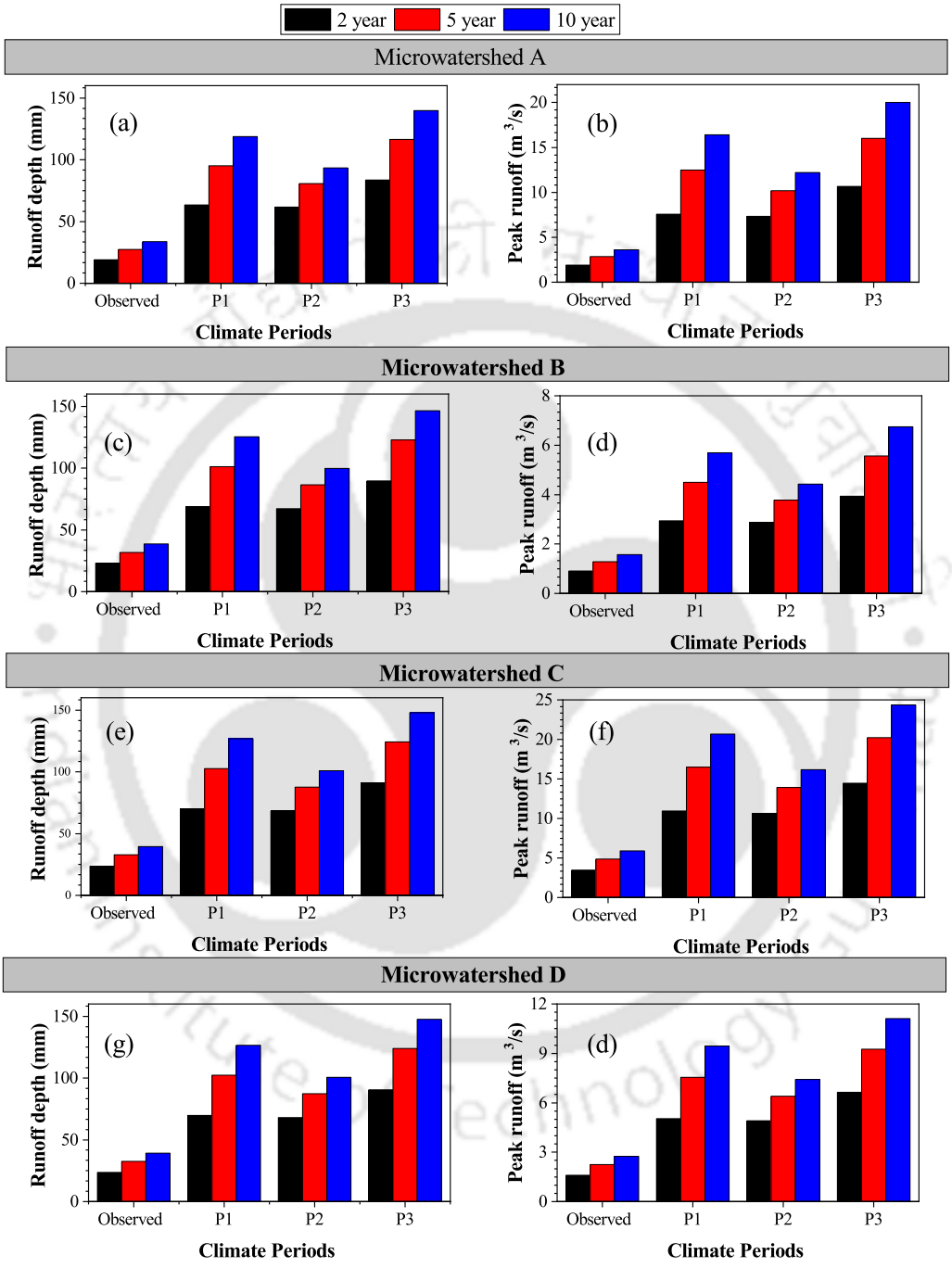

Figure 7.14: Runoff depth and peak runoff generated for observed and future climate rainfall intensities without LIDs for different return periods: (a), (c), (e), (g) represents the runoff depth for micro-watersheds A, B, C, and D, respectively and (b), (d), (f), (h) represents the peak runoff for micro-watersheds A, B, C, and D, respectively

Figure 7.15 shows the reduction in the runoff depth and peak runoff generated after the imple-

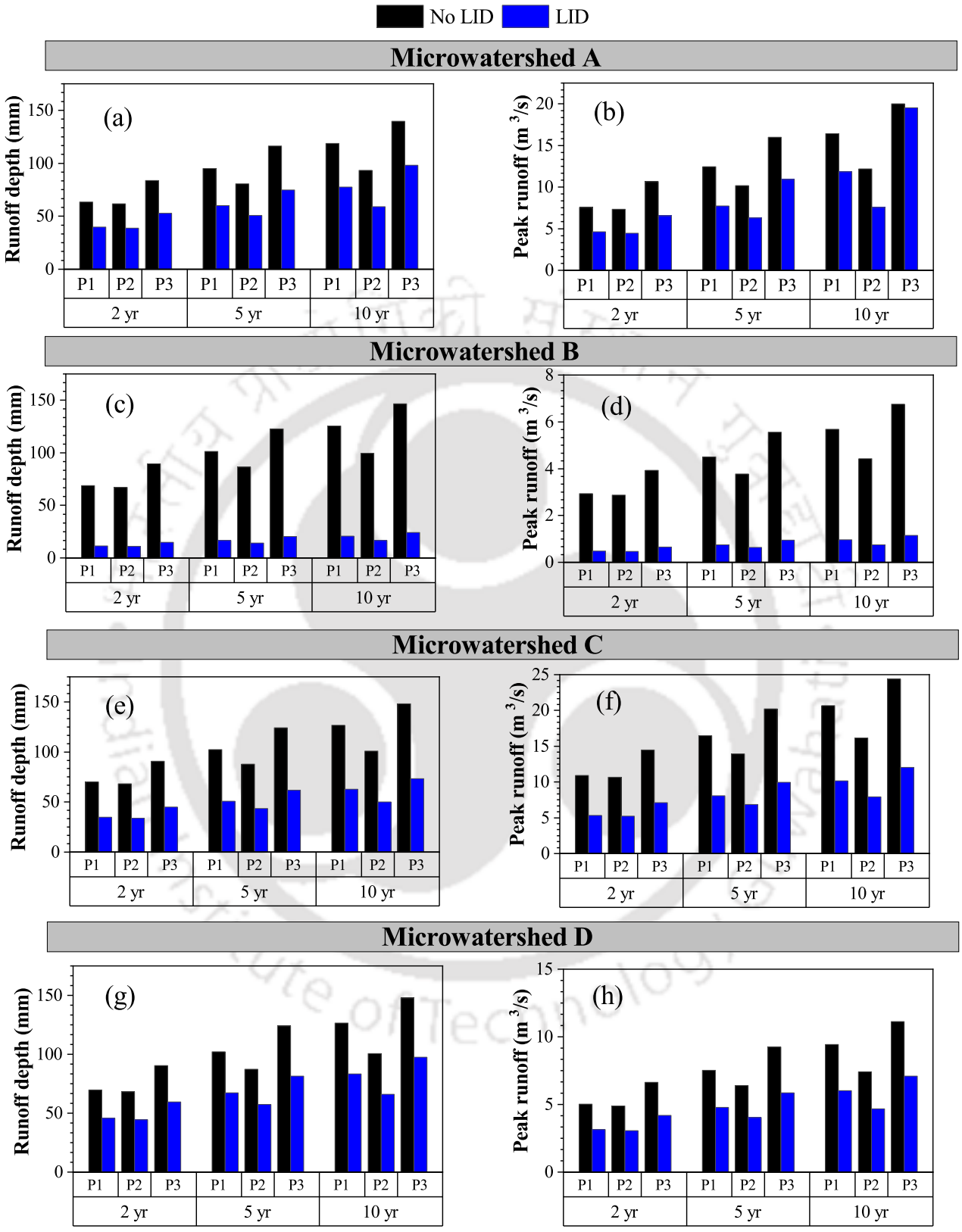

Figure 7.15: Reduction in the runoff depth and peak runoff with green roof for future rainfall intensities and different return periods: (a), (c), (e), (g) represents the runoff depth for micro-watersheds A, B, C, and D, respectively and (b), (d), (f), (h) represents the peak runoff for micro-watersheds A, B, C, and D, respectively

mentation of GR for different climate periods and return periods. GR reduced the captured components for different climate periods and return periods. For micro-watershed A, around 30-38% and 28-39% reductions in runoff depth and peak runoff were observed. However, for the 10-year return period and the P3 period, only a 2.5% decrease in peak runoff was observed. For micro-watersheds B, C, and D, it was observed that GR was able to reduce the runoff depth by 83%, 50%, and 34%, respectively. Similarly, the percentage reduction in peak runoff for micro-watersheds B, C, and D was 83-84%, 51%, and 36-37%, respectively.

Table 7.10 shows the comparison of the efficacy of different LIDs in mitigating runoff. The reduction in runoff varies depending on the study area and LID proportions. In this study, the total area covered by the best-performing LID (i.e., the GR) for micro-watershed A was 2.2%, and the corresponding reduction in runoff depth and peak runoff was 37.6% and 43.4%. For watershed B, the reduction rates are 83.8% and 84.6% for 5.7% of the LID area. Similarly, for C and D, the respective area occupied by GR was 3.3% and 3.2%, and with this occupancy percentage, watershed C has achieved a 50.7% and 51.9% reduction in runoff depth and peak runoff and a 35.6% and 39.1% reduction for watershed D.

Table 7.10: Review of efficacy of different LIDs

Author & Year	**LID type**	**$\frac{\text{LID area}}{\text{Total area}}$(%)**	**% Reduction in runoff depth**	**% Reduction in peak runoff**
Quichimbo-Miguitama et al. (2022)	Bio-retention cells	1.4	-	22
Ömer Ekmekcioğlu et al. (2021)	Green Roof	8.9	56.02	-
Akter et al. (2020)	Rain barrel	33.1	28.7	-
Zhu et al. (2019)	Permeable pavements	72.7	72.5	-
Bai et al. (2018)	Infiltration based LIDs	28.6	31.8	32.5
Goncalves et al. (2018)	Infiltration trenches	0.5	39.7	-
Goncalves et al. (2018)	Infiltration trenches	1	55.9	-
Micro-watershed A	Green roof	2.2	37.6	43.4
Micro-watershed B	Green roof	5.7	83.8	84.6
Micro-watershed C	Green roof	3.3	50.7	51.9
Micro-watershed D	Green roof	3.2	35.6	39.1

Figure 7.16 shows the runoff coefficient for different scenarios (as discussed in 7.4.1) for four micro-watersheds. It is clear from Fig. 7.16 that the runoff coefficient was high for observed and climate-based data. However, when LIDs were implemented, there was a significant reduction

in the runoff coefficient for all the micro-watersheds. GR has shown a reduced value of runoff coefficient for all the micro-watersheds. This indicates that LIDs have helped in reducing the runoff coefficient of the study area.

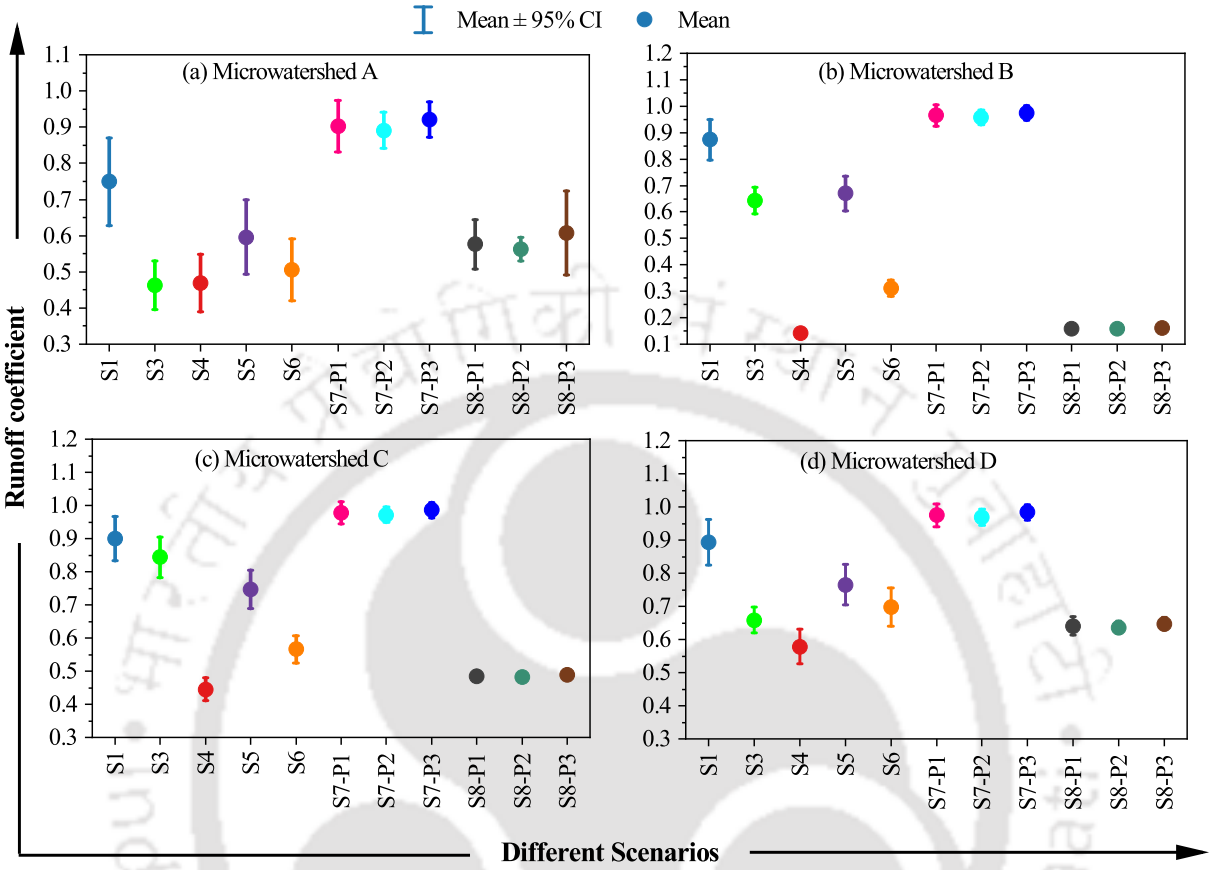

Figure 7.16: Interval plot showing runoff coefficient for different scenarios

From the analysis carried out using grey and green infrastructures, it was observed that re-designing the existing drainage helps only to a minimal reduction in runoff depth for all the four micro watersheds. Regarding green infrastucture, the efficiency of four different LIDs scenarios, namely green roof, rain barrel, infiltration trench, and permeable pavements, in reducing the runoff depth, peak runoff, and runoff coefficient was studied. The green roof was found to be relatively more efficient in reducing the urban flooding. The effect of climate change on the implementation of green roofs was examined, and it was found that green roof has significantly reduced the runoff. Hence, green roof was considered as the LID for Urban Guwahati city.

7.6 LIDs for Flood Mitigation in Urban Guwahati

This section aims to evaluate the effectiveness of different best management practices for the reduction of flooding in Guwahati city, with a specific focus on watershed 3, which is characterized by high levels of urbanization. In previous sections, a comprehensive examination of the efficacy of various LIDs in mitigating runoff was conducted in four micro-watersheds. The results

consistently indicated that the green roof technique outperformed other LIDs in terms of runoff mitigation. Building upon these findings, the primary objective of this section is to implement the green roof approach in watershed 3 and evaluate its effectiveness in mitigating runoff.

7.6.1 Mitigation of Runoff Using Green Roof for Guwahati City

The implementation of best management practices, will be carried out in the most urbanized watershed of the study area, Guwahati city. Hence, watershed 3 is chosen and green roofs (GR) at various percentages of the built-up area was implemented. Specifically, the scenarios considered were that 5%, 10%, 15%, 20%, and 25% of the built-up area were equipped with green roofs. Figure 7.17 presents a comparison of simulated peak runoff for different scenarios: no LID and the different percentages of green roof implementation. The figure includes results for historical and future scenarios, using a 15-minute rainfall duration, 10-year return period and 2022 effective impervious area (EIA). The future scenarios were based on different representative concentration pathways: RCP 6.0 for the P1 period, RCP 4.5 for P2, and RCP 8.5 for P3. The results indicate that implementing green roofs led to a reduction in peak runoff for both historical and future periods.

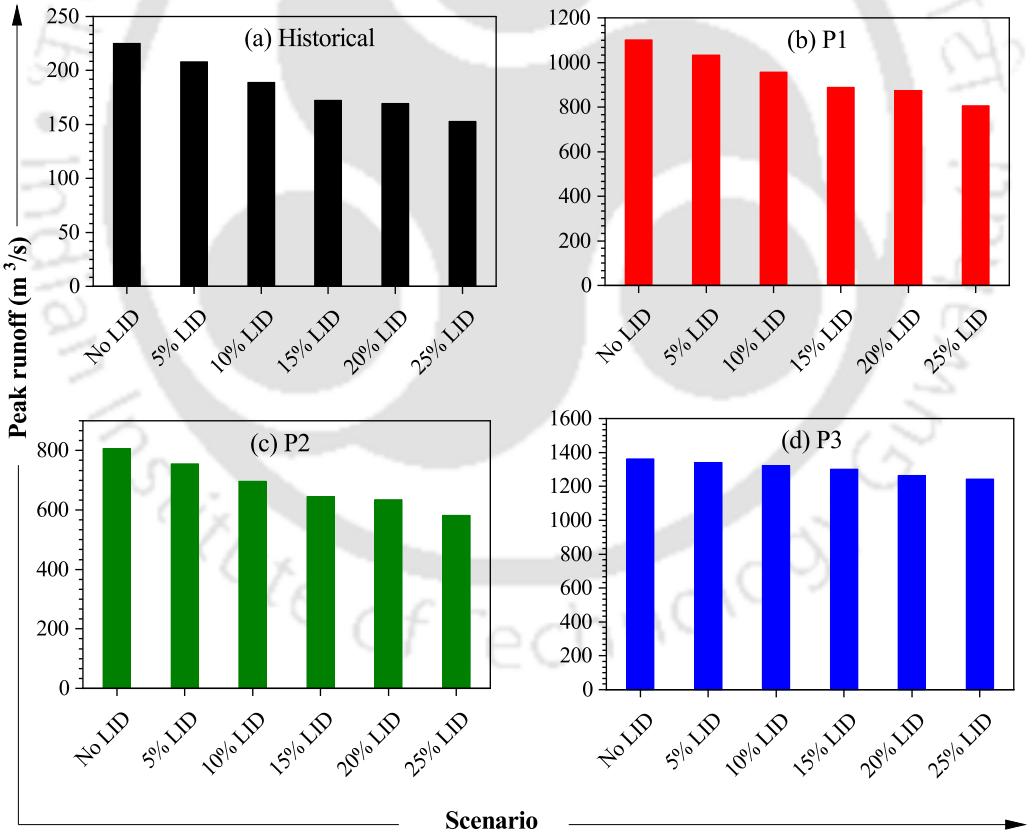

Figure 7.17: Comparison of simulated peak runoff for different scenarios

For the historical period, the peak runoff in Guwahati city without green roofs (GR) reached 224.99 m^3/s. However, with the implementation of GR covering 25% of the built-up area, the peak runoff significantly reduced to 152.79 m^3/s. Looking ahead to the future period P1, the peak runoff

decreased from 1102.48 m^3/s to 805.44 m^3/s when GR covering 25% of the built-up area were employed. Similarly, in period P2, the peak runoff dropped from 806.88 m^3/s to 582.3 m^3/s with the same LID implementation. Furthermore, in period P3, the peak runoff decreased from 1361.74 m^3/s to 1241.79 m^3/s. These results emphasize the positive impact of integrating green roofs in mitigating runoff and managing stormwater in Guwahati city.

The presented results, illustrated in Fig. 7.18 and table 7.11, highlight the percentage change in simulated peak runoff for different scenarios. Notably, a consistent decrease in peak runoff was observed across all analysed periods, including the historical and future climate periods (P1, P2, and P3). However, it is important to note that the percentage decrease in runoff was generally lower for the future climate periods than the historical period. Among the future climate periods, P2 exhibited the highest reduction in peak runoff, followed by P1 and P3. The rainfall intensities were found to intensify in P3 (details provided in Chapter 4).

For historical period 5% implementation of LID has led to 7.48% reduction in runoff. For the future periods, a decrease in efficacy of GR was observed with 6.24%, 6.43%, and 1.56% respectively for P1, P2, and P3. For 10% implementation of LID, the respective percentage of reduction for historical, P1, P2, and P3 are 15.95%, 13.21%, 13.65%, and 2.87%. For 15% implementation, the reduction in runoff has drop down from 23.43% to 4.43%. Similarly for 20% and 25%, the percentage change in runoff has reduced from 24.61% to 7.25% and 32.09% to 8.81% respectively. This implies that the effectiveness of green roofs (GR) in mitigating urban floods may be influenced by climate change, as the reduction in peak runoff is relatively less pronounced in future climate scenarios. In order to mitigate the floods resulting from climate change, a higher percentage of the built-up area should be transformed into LIDs

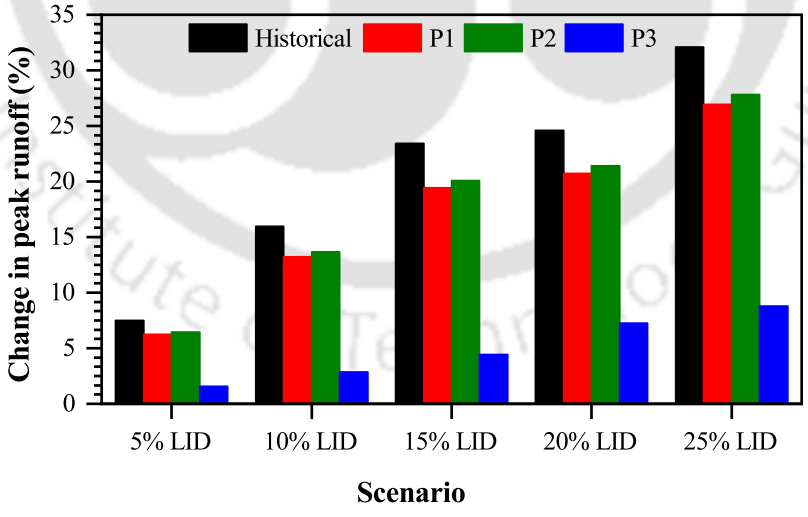

Figure 7.18: Percentage change in simulated peak runoff with green roof for different scenarios

Table 7.11: Percentage change in runoff due to green roof

Scenario	Change in runoff (%)			
	Historical	P1	P2	P3
5% LID	7.48	6.24	6.43	1.56
10% LID	15.95	13.21	13.65	2.87
15% LID	23.43	19.45	20.08	4.43
20% LID	24.61	20.71	21.40	7.25
25% LID	32.09	26.94	27.83	8.81

Expanding on these findings, the efficacy of green roofs in managing stormwater and mitigating urban floods may be impacted by climate change. The observed decrease in peak runoff is likely influenced by changing precipitation patterns, intensity, and duration, which may differ in future climate scenarios. These findings emphasize the need to consider climate change projections when designing and implementing LID strategies like green roofs to ensure their continued effectiveness in a changing climate.

7.7 Summary

This study tried to understand the effect of LIDs on mitigating floods in four micro-urban watersheds in northeast India. The efficiency of four different LIDs scenarios, namely green roof, rain barrel, infiltration trench, and permeable pavements, in reducing the runoff depth, peak runoff, and runoff coefficients was studied on four different micro-watersheds. The result implies that LIDs are effective methods that can be used to mitigate floods in urban areas. The green roof gave the maximum runoff reduction based on the analysis of different LIDs for the four watersheds. Moreover, it was found that all four watersheds behave differently with different LIDs. So the performance of LIDs varies with site and watershed, so it is necessary to explore different LIDs to achieve flood reduction goals.

Also, attempts have been made to see how redesigning the existing drainage helps to mitigate the runoff in the study area. Results indicate that redesigning the existing drainage system has led to a minimal reduction in runoff depth for the four micro-watersheds. In contrast, only watershed A showed a decrease in peak runoff, whereas watersheds B, C, and D exhibited an increase of around 1.24-5.59%. Climate change has increased rainfall intensities for future periods (P1, P2, and P3) for the study areas. All four watersheds showed a considerable increase in surface runoff due to climate change. Therefore, the effect of climate change on the implementation of green roofs was examined, and it was found that GR has significantly reduced the runoff.

Analysis of LID requires fine-resolution data, which may not be available on a city scale. So, from the analysis of micro-watersheds, it has been identified that the green roof was performing better in mitigating floods. So, green roof has been implemented at different percentage of built-

up area to the most urbanized watershed of Guwahati city. Implementing green roofs at various percentages of the built-up area in the highly urbanized watershed 3 of Guwahati city reduced peak runoff for both historical and future scenarios. The peak runoff decreased significantly, with the highest reduction observed when 25% of the built-up area was equipped with green roofs, leading to better city stormwater management and runoff mitigation. However, it was observed that the reduction in runoff is less for future periods indicating that more percentage of built-up area is required to be converted to green roofs.

In the context of climate change, this study provides essential information to decision-makers about the effectiveness of LID measures in reducing flood risk. However, this choice may not be valid for other watersheds. Therefore it is recommended to do site-specific studies to get a better understanding of the choice of LIDs.

The effectiveness of LIDs depends on various factors such as geographical location, soil characteristics, land use, climate, and slope. Choice of LIDs should consider the land use of the area. In residential areas, practices like rain gardens, rainwater harvesting, and permeable pavements are often applicable for efficient stormwater management. Commercial spaces may benefit from the implementation of green roofs, rainwater harvesting systems, and permeable pavements. Open spaces, when transformed into vegetation swales and bioretention cells, not only contribute to stormwater control but also enhance the overall aesthetics of the city. Tailoring LID strategies based on specific LULC characteristics ensures a more nuanced and effective approach to sustainable urban development (Hu et al., 2017; Martin-Mikle et al., 2015).

Low impact developments can be a sustainable solution to mitigate floods in urban areas. Urban planners and policymakers, along with the government, can help promote and make awareness among the public about the use and benefits of LIDs. LIDs not only help in flood mitigation but can also be used to control water pollution and improve the air quality in urban areas. LIDs can reduce the urban heat island issues prevailing in cities. For instance, the green roof can control humidity issues in a hot and humid environment and provide cooling effects to the building. LIDs can also help to improve the aesthetic of the area.

Urban planners and government authorities can work together to prompt the LIDs. Government authorities can develop regulations like mandatory inclusion of LID components in the design of new buildings and efforts to upgrade existing infrastructure with LIDs, providing incentives for implementation, sanctions for non-compliance, providing tax-benefits and so on. Policymakers can collaborate with private and non-governmental organizations for the implementation, particularly in low-income areas where flooding is most common. There is a need of codal provision outlining design practices, maintenance procedures, and implementation guidelines for LID tailored to the specific geographical conditions of each region. Policymakers and scientists must work together to conduct more research to determine effective LIDs for different areas and develop guidelines and norms for applying and implementing LIDs. Ultimately, LIDs can help in creating more resilient and sustainable cities in the face of accelerating urbanization and climate change through smart policy and urban planning.

Chapter 8

Conclusions and Future Scope of Work

8.1 General

This study delved into the effects of climate and land use changes on urban flooding, revealing their significant impact on urban flood characteristics. Urban areas are particularly vulnerable to these changes, and understanding their impact is crucial for developing effective flood management strategies. Additionally, the study tried to understand the drift in the intensity duration frequency curve due to change in extreme rainfall caused by climate change. Another important factor that contributes to urban flooding is the imperviousness. Impervious surfaces, such as roads, pavements, and buildings, prevent water from being absorbed into the ground, leading to increased surface runoff during rainfall events. As a result, urban areas with higher imperviousness tend to experience more severe and frequent flooding. Understanding the effects of climate change and imperviousness on urban runoff is crucial for devising effective flood mitigation and management strategies. In the pursuit of flood management solutions, the study evaluated the efficacy of low impact developments (LIDs) and concluded that they hold promise in fostering more resilient and sustainable cities amidst the challenges posed by rapid urbanization and climate change. Implementing smart policies and urban planning that incorporate LIDs can play a vital role in achieving this goal.

This chapter presents a list of significant findings obtained from this study, accompanied by its major contributions. The final section of this chapter explores the potential avenues for future research.

8.2 Conclusions

The major conclusions drawn from this study includes:

- The study quantified the potential drift in the intensity-duration-frequency (IDF) curve from historical rainfall data due to climate change.

- Historical bivariate copula-based IDF curves were compared with two conventional empirical models (EM1 and EM2) and univariate frequency analysis. It was observed that EM1, proposed for Indian catchments, performed poorly for short durations, while EM2 adequately captured historical rainfall trends compared to the BIDF curves.
- EM2 and univariate IDF (UIDF) curves were found to be suitable for short durations ($\geq$3h) in the urban catchment, but not for longer durations due to significant percentage differences from bivariate historic rainfall intensity.
- The study explored various climate scenarios (RCP 2.6, RCP 4.5, RCP 6.0, and RCP 8.5) and time periods (P1 2021-2047; P2 2048-2074; P3 2075-2100) to understand changes in future BIDF curves compared to historical rainfall-based BIDF curves.
- The climate scenarios showed a significant increase in rainfall intensity for short durations, with RCP 6.0 exhibiting higher intensities for the near future and RCP 8.5 showing the highest intensities for distant future periods.
- The study emphasized the importance of conducting comprehensive local-scale studies in developing countries like India, where infrastructure growth and hydraulic structure augmentation are rapid, to incorporate climate change impacts on IDF curves.
- The study observed a significant increasing trend in the built-up area from 1980 to 2022, growing from 2.85% to 50.56%. This expansion occurred at the expense of vegetated regions, swampy land, and forest areas.
- The EIA was quantified using geospatial analysis on fine-resolution remote sensing images, and a significant increase in EIA was observed in all watersheds from 2011 to 2022.
- Watershed 3, was the most urbanized part of Guwahati city, exhibited the highest percentage of imperviousness throughout the studied years.
- During the years 2011, 2013, and 2020, watershed 7 exhibited the lowest percentage of EIA, while watershed 6 showed the lowest percentage for 2017 and 2022.
- The study investigated the influence of LULC and climate change on urban runoff, revealing that both factors substantially impact flood characteristics in urban areas.
- The study examined the influence of various historical short-duration rainfall events and observed that each event exhibited unique behaviour. Among the different rainfall events (RE-1, RE-2, RE-3, RE-4, RE-5, and RE-6), RE-1 and RE-4 had a more pronounced impact on the study area. RE-1 resulted in a longer duration runoff, while RE-4 had a higher peak runoff.
- The study compared the runoff generated using historical BIDF and univariate IDF curves and found that the univariate IDF curve consistently underestimated the runoff.

- The impact of LULC on urban flood is studied by varying the LULC from 2011 to 2022 and keeping the rainfall intensity constant. The findings revealed that an increase in imperviousness within urban catchments led to higher surface runoff, consequently raising the flood risk. Specifically, there was a 37.5% increase in runoff when the effective impervious area (EIA) increased from 12.1% to 22.4%.
- LULC changes have resulted in a 1.3 times higher runoff in the study area from 2011 to 2022.
- The study examined the impact of climate change on urban flood characteristics by varying the rainfall intensity across three future periods (P1, P2, and P3) while maintaining a constant land use scenario corresponding to the year 2022.
- The results demonstrate that RCP 6.0 produces a higher peak runoff value during the P1 period, RCP 4.5 during the P2 period, and RCP 8.5 during the P3 period. Overall, there is an evident increase in peak runoff from P1 to P3.
- Climate change has led to a significant increase in runoff, with values ranging from approximately 3.6 to 6.1 times higher compared to the runoff from the historical rainfall.
- Suitability of LIDs on reducing urban runoff was investigated in four micro-watersheds.
- The study examined four different LID options: green roof, permeable pavement, infiltration trench, and rain barrel. The results indicated that among these LIDs, the green roof demonstrated superior performance in mitigating runoff compared to the other options.
- The knowledge acquired about LIDs was then put into practice and implemented in the most urbanized watershed (watershed 3) of Guwahati city. Specifically, green roofs were implemented at various percentages of the built-up area (5%, 10%, 15%, 20%, and 25%) within watershed 3. The implementation demonstrated that green roofs can effectively reduce runoff. However, it was observed that the effectiveness of green roofs alone in mitigating urban floods is influenced by climate change, as the reduction in peak runoff is relatively less pronounced in future climate scenarios.
- Governments can develop regulations mandating LID components in new building designs and upgrading existing infrastructure with LIDs. They can also provide incentives for implementation and impose sanctions for non-compliance.
- Policymakers and scientists should conduct more research to identify effective LIDs for different areas and establish guidelines and norms for their application and implementation.

8.3 Major Contributions of the Study

- The study explored the application of copula-based BIDF curves for a prominent urban catchment in northeast India, considering the effects of future climate change. This provided valuable insights into the significance of this approach for hydrological analysis and design.

- Considering the variation in results from empirical and UIDF curves, the study highly recommended using a bivariate copula-based IDF (BIDF) curve for designing new hydraulic structures and drainage facilities in urban catchments.
- For considering the influence of near-future climate change on infrastructure with design life $\leq$50 years, the RCP 6.0 scenario would yield the critical IDF curve.
- For long-term planning with a design life > 50 years, it is desirable to consider the IDF curve based on the RCP 8.5 scenario.
- A semi-automated direct method along with high-resolution satellite imagery was utilized to determine the effective imperviousness within the study area.
- The study examined the impact of LULC changes and climate change on urban runoff. It was observed that climate change has more impact on urban floods than LULC.
- Quantified the increase in urban runoff associated with climate change and compared it with the historical data.
- The importance of low impact developments (LIDs) as a sustainable solution to mitigate floods in urban areas was demonstrated in this study. The study provides decision-makers with important insights, emphasizing the need to consider climate change projections for the efficacy of LID strategies.

8.4 Uncertainties and Limitations of the Study

This study acknowledges several sources of uncertainties and limitations.

- The utilization of different Global Climate Models (GCMs) introduces model-based uncertainty, given the inherent variability in their structures and assumptions.
- This study is based on single rain gauge thereby neglecting the spatial variability in rainfall patterns, prompting the need for incorporating spatially distributed rainfall data for a more comprehensive understanding of the hydrological processes under consideration.
- The effectiveness of Low Impact Developments (LID) in reducing floods is noted to be inherently site-specific. While this study offers a preliminary analysis, it is emphasized that conducting site-specific studies is crucial to precisely measure the efficacy of LID measures in diverse geographical and environmental settings.

8.5 Future Scope

- The study can be extended to quantify the flood risk of the study area by incorporating various factors such as LULC changes, climate projections, hydrological modeling, population data and topographic data.

- Machine learning / deep learning techniques can be used for determining and predicting land use and land cover (LULC) changes and relating it to urban runoff.
- The impact of low impact development(LID) on reducing flood risk can be extended by adding an optimization framework based on the severity of the flooding, climate change, willingness of house owners in implementing LIDs, cost of LID implementation and the availability of resources.

References

Abbaspour, K.C., Faramarzi, M., Ghasemi, S.S., Yang, H., 2009. Assessing the impact of climate change on water resources in iran. Water Resources Research 45. URL: https://doi.org/10.1029%2F2008wr007615, doi:10.1029/2008wr007615.

Abdelkebir, B., Maoui, A., Mokhtari, E., Engel, B., Chen, J., Aboelnour, M., 2021. Evaluating low-impact development practice performance to reduce runoff volume in an urban watershed in algeria. Arabian Journal of Geosciences 14. URL: https://doi.org/10.1007%2Fs12517-021-07178-0, doi:10.1007/s12517-021-07178-0.

Abonyi, J., Feil, B., Nemeth, S., Arva, P., 2005. Modified gath–geva clustering for fuzzy segmentation of multivariate time-series. Fuzzy Sets and Systems 149, 39–56. URL: https://doi.org/10.1016%2Fj.fss.2004.07.008, doi:10.1016/j.fss.2004.07.008.

Agilan, V., Umamahesh, N., 2016. Is the covariate based non-stationary rainfall IDF curve capable of encompassing future rainfall changes? Journal of Hydrology 541, 1441–1455. URL: https://doi.org/10.1016%2Fj.jhydrol.2016.08.052, doi:10.1016/j.jhydrol.2016.08.052.

Agilan, V., Umamahesh, N.V., 2017. Non-stationary rainfall intensity-duration-frequency relationship: a comparison between annual maximum and partial duration series. Water Resources Management 31, 1825–1841. URL: https://doi.org/10.1007%2Fs11269-017-1614-9, doi:10.1007/s11269-017-1614-9.

Ahiablame, L., Shakya, R., 2016. Modeling flood reduction effects of low impact development at a watershed scale. Journal of Environmental Management 171, 81–91. URL: https://doi.org/10.1016%2Fj.jenvman.2016.01.036, doi:10.1016/j.jenvman.2016.01.036.

Ahmed, K., Chung, E.S., Song, J.Y., Shahid, S., 2017. Effective design and planning specification of low impact development practices using water management analysis module (WMAM): Case of malaysia. Water 9, 173. URL: https://doi.org/10.3390%2Fw9030173, doi:10.3390/w9030173.

Akaike, H., 1974. A new look at the statistical model identification. IEEE Transactions on Automatic Control 19, 716–723. URL: https://doi.org/10.1109%2Ftac.1974.1100705, doi:10.1109/tac.1974.1100705.

Akhtar, M., Ahmad, N., Booij, M., 2008. The impact of climate change on the water resources of hindukush–karakorum–himalaya region under different glacier coverage scenarios. Journal of Hydrology 355, 148–163. URL: https://doi.org/10.1016%2Fj.jhydrol.2008.03.015, doi:10.1016/j.jhydrol.2008.03.015.

Akpoti, K., Antwi, E., Kabo-bah, A., 2016. Impacts of rainfall variability, land use and land cover change on stream flow of the black volta basin, west africa. Hydrology 3, 26. URL: https://doi.org/10.3390%2Fhydrology3030026, doi:10.3390/hydrology3030026.

Akter, A., Tanim, A.H., Islam, M.K., 2020. Possibilities of urban flood reduction through distributed-scale rainwater harvesting. Water Science and Engineering 13, 95–105. URL: https://doi.org/10.1016%2Fj.wse.2020.06.001, doi:10.1016/j.wse.2020.06.001.

Alamdari, N., Claggett, P., Sample, D.J., Easton, Z.M., Yazdi, M.N., 2022. Evaluating the joint effects of climate and land use change on runoff and pollutant loading in a rapidly developing watershed. Journal of Cleaner Production 330, 129953. URL: https://doi.org/10.1016%2Fj.jclepro.2021.129953, doi:10.1016/j.jclepro.2021.129953.

Alfieri, L., Feyen, L., Baldassarre, G.D., 2016. Increasing flood risk under climate change: a pan-european assessment of the benefits of four adaptation strategies. Climatic Change 136, 507–521. URL: https://doi.org/10.1007%2Fs10584-016-1641-1, doi:10.1007/s10584-016-1641-1.

Alfredo, K., Montalto, F., Goldstein, A., 2010. Observed and modeled performances of prototype green roof test plots subjected to simulated low- and high-intensity precipitations in a laboratory experiment. Journal of Hydrologic Engineering 15, 444–457. URL: https://doi.org/10.1061%2F%28asce%29he.1943-5584.0000135, doi:10.1061/(asce)he.1943-5584.0000135.

Alley, W.M., Veenhuis, J.E., 1983. Effective impervious area in urban runoff modeling. Journal of Hydraulic Engineering 109, 313–319. URL: https://doi.org/10.1061%2F%28asce%290733-9429%281983%29109%3A2%28313%29, doi:10.1061/(asce)0733-9429(1983)109:2(313).

Andimuthu, R., Kandasamy, P., Mudgal, B.V., Jeganathan, A., Balu, A., Sankar, G., 2019. Performance of urban storm drainage network under changing climate scenarios: Flood mitigation in indian coastal city. Scientific Reports 9. URL: https://doi.org/10.1038%2Fs41598-019-43859-3, doi:10.1038/s41598-019-43859-3.

Arif, M., Sengupta, S., Mohinuddin, S.K., Gupta, K., 2023. Dynamics of land use and land cover change in peri urban area of burdwan city, india: a remote sensing and GIS based approach. GeoJournal URL: https://doi.org/10.1007%2Fs10708-023-10860-3, doi:10.1007/s10708-023-10860-3.

Ariff, N., Jemain, A., Ibrahim, K., Zin, W.W., 2012. IDF relationships using bivariate copula for storm events in peninsular malaysia. Journal of Hydrology 470-471, 158–171. URL: https://doi.org/10.1016%2Fj.jhydrol.2012.08.045, doi:10.1016/j.jhydrol.2012.08.045.

Arnell, N., 1999. Climate change and global water resources. Global Environmental Change 9, S31–S49. URL: https://doi.org/10.1016%2Fs0959-3780%2899%2900017-5, doi:10.1016/s0959-3780(99)00017-5.

Arnell, N.W., Gosling, S.N., 2014. The impacts of climate change on river flood risk at the global scale. Climatic Change 134, 387–401. URL: https://doi.org/10.1007%2Fs10584-014-1084-5, doi:10.1007/s10584-014-1084-5.

Arnone, E., Pumo, D., Francipane, A., Loggia, G.L., Noto, L.V., 2018. The role of urban growth, climate change, and their interplay in altering runoff extremes. Hydrological Processes 32, 1755–1770. URL: https://doi.org/10.1002%2Fhyp.13141, doi:10.1002/hyp.13141.

ASCE, 1992. Design and construction of urban stormwater management systems.

Azari, B., Tabesh, M., 2022. Urban storm water drainage system optimization using a sustainability index and LID/BMPs. Sustainable Cities and Society 76, 103500. URL: https://doi.org/10.1016%2Fj.scs.2021.103500, doi:10.1016/j.scs.2021.103500.

Babu, R., Tejwani, K., Agarwal, M., Bhushan, L., 1979. Rainfall intensity-duration-return period equations and nomographs of india. Bulletin No. 3, Central Soil and Water Conservation Research and Training Institute, ICAR, Dehradun, India .

Bai, Y., Zhao, N., Zhang, R., Zeng, X., 2018. Storm water management of low impact development in urban areas based on SWMM. Water 11, 33. URL: https://doi.org/10.3390%2Fw11010033, doi:10.3390/w11010033.

Bairwa, A.K., Khosa, R., Maheswaran, R., 2016. Developing intensity duration frequency curves based on scaling theory using linear probability weighted moments: A case study from india. Journal of Hydrology 542, 850–859. URL: https://doi.org/10.1016%2Fj.jhydrol.2016.09.056, doi:10.1016/j.jhydrol.2016.09.056.

Barron, O.V., Donn, M.J., Barr, A.D., 2012. Urbanisation and shallow groundwater: Predicting changes in catchment hydrological responses. Water Resources Management 27, 95–115. URL: https://doi.org/10.1007%2Fs11269-012-0168-0, doi:10.1007/s11269-012-0168-0.

Belay, T., Mengistu, D.A., 2021. Impacts of land use/land cover and climate changes on soil erosion in muga watershed, upper blue nile basin (abay), ethiopia. Ecological Processes 10. URL: https://doi.org/10.1186%2Fs13717-021-00339-9, doi:10.1186/s13717-021-00339-9.

Berihun, M.L., Tsunekawa, A., Haregeweyn, N., Meshesha, D.T., Adgo, E., Tsubo, M., Masunaga, T., Fenta, A.A., Sultan, D., Yibeltal, M., Ebabu, K., 2019. Hydrological responses to land use/land cover change and climate variability in contrasting agro-ecological environments of the upper blue nile basin, ethiopia. Science of The Total Environment 689, 347–365. URL: https://doi.org/10.1016%2Fj.scitotenv.2019.06.338, doi:10.1016/j.scitotenv.2019.06.338.

Bernard, M.M., 1932. Formulas for rainfall intensities of long duration. Transactions of the American Society of Civil Engineers 96, 592–606.

Bevacqua, E., Maraun, D., Haff, I.H., Widmann, M., Vrac, M., 2017. Multivariate statistical modelling of compound events via pair-copula constructions: analysis of floods in ravenna (italy). Hydrology and Earth System Sciences 21, 2701–2723. URL: https://doi.org/10.5194%2Fhess-21-2701-2017, doi:10.5194/hess-21-2701-2017.

Bezak, N., Šraj, M., Mikoš, M., 2016. Copula-based IDF curves and empirical rainfall thresholds for flash floods and rainfall-induced landslides. Journal of Hydrology 541, 272–284. URL: https://doi.org/10.1016%2Fj.jhydrol.2016.02.058, doi:10.1016/j.jhydrol.2016.02.058.

Bibi, T.S., Kara, K.G., Bedada, H.J., Bededa, R.D., 2023. Application of PCSWMM for assessing the impacts of urbanization and climate changes on the efficiency of stormwater drainage systems in managing urban flooding in robe town, ethiopia. Journal of Hydrology: Regional Studies 45, 101291. URL: https://doi.org/10.1016%2Fj.ejrh.2022.101291, doi:10.1016/j.ejrh.2022.101291.

Booth, D.B., Jackson, C.R., 1997. Urbanization of aquatic systems: degradation thresholds, stormwater detection, and the limits of mitigation. Journal of the American Water Resources Association 33, 1077–1090.

Bottyán, Z., Kircsi, A., Szegedi, S., Unger, J., 2005. The relationship between built-up areas and the spatial development of the mean maximum urban heat island in debrecen, hungary. International Journal of Climatology 25, 405–418. URL: https://doi.org/10.1002%2Fjoc.1138, doi:10.1002/joc.1138.

Camici, S., Brocca, L., Melone, F., Moramarco, T., 2014. Impact of climate change on flood frequency using different climate models and downscaling approaches. Journal of Hydrologic Engineering 19. URL: https://doi.org/10.1061%2F%28asce%29he.1943-5584.0000959, doi:10.1061/(asce)he.1943-5584.0000959.

Cancelliere, A., 2017. Non stationary analysis of extreme events. Water Resources Management 31, 3097–3110. URL: https://doi.org/10.1007%2Fs11269-017-1724-4, doi:10.1007/s11269-017-1724-4.

Cannon, A.J., Sobie, S.R., Murdock, T.Q., 2015. Bias correction of GCM precipitation by quantile mapping: How well do methods preserve changes in quantiles and extremes? Journal of Climate 28, 6938–6959. URL: https://doi.org/10.1175%2Fjcli-d-14-00754.1, doi:10.1175/jcli-d-14-00754.1.

Canty, M.J., 2009. Image Analysis, Classification, and Change Detection in Remote Sensing. CRC Press. URL: https://doi.org/10.1201%2F9781420087147, doi:10.1201/9781420087147.

Cea, L., Costabile, P., 2022. Flood risk in urban areas: Modelling, management and adaptation to climate change. a review. Hydrology 9, 50. URL: https://doi.org/10.3390%2Fhydrology9030050, doi:10.3390/hydrology9030050.

Chanapathi, T., Thatikonda, S., 2020. Investigating the impact of climate and land-use land cover changes on hydrological predictions over the krishna river basin under present and future scenarios. Science of The Total Environment 721, 137736. URL: https://doi.org/10.1016%2Fj.scitotenv.2020.137736, doi:10.1016/j.scitotenv.2020.137736.

Chandra, R., Saha, U., Mujumdar, P., 2015. Model and parameter uncertainty in IDF relationships under climate change. Advances in Water Resources 79, 127–139. URL: https://doi.org/10.1016%2Fj.advwatres.2015.02.011, doi:10.1016/j.advwatres.2015.02.011.

Chang, H., Jung, I.W., 2010. Spatial and temporal changes in runoff caused by climate change in a complex large river basin in oregon. Journal of Hydrology 388, 186–207. URL: https://doi.org/10.1016%2Fj.jhydrol.2010.04.040, doi:10.1016/j.jhydrol.2010.04.040.

Chaudhuri, R.R., Sharma, P., 2020. Addressing uncertainty in extreme rainfall intensity for semi-arid urban regions: case study of delhi, india. Natural Hazards 104, 2307–2324. URL: https://doi.org/10.1007%2Fs11069-020-04273-5, doi:10.1007/s11069-020-04273-5.

Chawla, I., Mujumdar, P.P., 2015. Isolating the impacts of land use and climate change on streamflow. Hydrology and Earth System Sciences 19, 3633–3651. URL: https://doi.org/10.5194%2Fhess-19-3633-2015, doi:10.5194/hess-19-3633-2015.

Chen, J., Hill, A.A., Urbano, L.D., 2009. A GIS-based model for urban flood inundation. Journal of Hydrology 373, 184–192. URL: https://doi.org/10.1016%2Fj.jhydrol.2009.04.021, doi:10.1016/j.jhydrol.2009.04.021.

Chen, J., Liu, Y., Gitau, M.W., Engel, B.A., Flanagan, D.C., Harbor, J.M., 2019. Evaluation of the effectiveness of green infrastructure on hydrology and water quality in a combined sewer overflow community. Science of The Total Environment 665, 69–79. URL: https://doi.org/10.1016%2Fj.scitotenv.2019.01.416, doi:10.1016/j.scitotenv.2019.01.416.

Chen, J., Theller, L., Gitau, M.W., Engel, B.A., Harbor, J.M., 2017. Urbanization impacts on surface runoff of the contiguous united states. Journal of Environmental Management 187, 470–481. URL: https://doi.org/10.1016%2Fj.jenvman.2016.11.017, doi:10.1016/j.jenvman.2016.11.017.

Cheng, L., AghaKouchak, A., 2014. Nonstationary precipitation intensity-duration-frequency curves for infrastructure design in a changing climate. Scientific Reports 4. URL: https://doi.org/10.1038%2Fsrep07093, doi:10.1038/srep07093.

Cheng, L., AghaKouchak, A., Gilleland, E., Katz, R.W., 2014. Non-stationary extreme value analysis in a changing climate. Climatic Change 127, 353–369. URL: https://doi.org/10.1007%2Fs10584-014-1254-5, doi:10.1007/s10584-014-1254-5.

Cheng, Y., Wang, R., 2018. A novel stormwater management system for urban roads in china based on local conditions. Sustainable Cities and Society 39, 163–171. URL: https://doi.org/10.1016%2Fj.scs.2017.09.001, doi:10.1016/j.scs.2017.09.001.

Cho, S., Kang, M., Kwon, H., Lee, J., Kim, S., 2013. Evaluation of the effectiveness of low impact development practices in an urban area: non-point pollutant removal measures using epa-swmm. Journal of Korean Society on water environment 29, 466–475.

Choto, M., Fetene, A., 2019. Impacts of land use/land cover change on stream flow and sediment yield of gojeb watershed, omo-gibe basin, ethiopia. Remote Sensing Applications: Society and Environment 14, 84–99. URL: https://doi.org/10.1016%2Fj.rsase.2019.01.003, doi:10.1016/j.rsase.2019.01.003.

Chughtai, A.H., Abbasi, H., Karas, I.R., 2021. A review on change detection method and accuracy assessment for land use land cover. Remote Sensing Applications: Society and Environment 22, 100482. URL: https://doi.org/10.1016%2Fj.rsase.2021.100482, doi:10.1016/j.rsase.2021.100482.

Cook, L.M., McGinnis, S., Samaras, C., 2020. The effect of modeling choices on updating intensity-duration-frequency curves and stormwater infrastructure designs for climate change. Climatic Change 159, 289–308. URL: https://doi.org/10.1007%2Fs10584-019-02649-6, doi:10.1007/s10584-019-02649-6.

CPHEEO, 2019. Manual on storm water drainage system (vol. i, part-a engineering design).

Dadashpoor, H., Azizi, P., Moghadasi, M., 2019. Land use change, urbanization, and change in landscape pattern in a metropolitan area. Science of The Total Environment 655, 707–719. URL: https://doi.org/10.1016%2Fj.scitotenv.2018.11.267, doi:10.1016/j.scitotenv.2018.11.267.

Dankers, R., Christensen, O.B., Feyen, L., Kalas, M., de Roo, A., 2007. Evaluation of very high-resolution climate model data for simulating flood hazards in the upper danube basin. Journal of Hydrology 347, 319–331. URL: https://doi.org/10.1016%2Fj.jhydrol.2007.09.055, doi:10.1016/j.jhydrol.2007.09.055.

Darnthamrongkul, W., Mozingo, L.A., 2021. Toward sustainable stormwater management: Understanding public appreciation and recognition of urban low impact development (LID) in the san francisco bay area. Journal of Environmental Management 300, 113716. URL: https://doi.org/10.1016%2Fj.jenvman.2021.113716, doi:10.1016/j.jenvman.2021.113716.

Denault, C., Millar, R.G., Lence, B.J., 2006. Assessment of possible impacts of climate change in an urban catchment. Journal of the American Water Resources Association 42, 685–697. URL: https://doi.org/10.1111%2Fj.1752-1688.2006.tb04485.x, doi:10.1111/j.1752-1688.2006.tb04485.x.

Deng, Z., Qiu, X., Liu, J., Madras, N., Wang, X., Zhu, H., 2015. Trend in frequency of extreme precipitation events over ontario from ensembles of multiple GCMs. Climate Dynamics 46, 2909–2921. URL: https://doi.org/10.1007%2Fs00382-015-2740-9, doi:10.1007/s00382-015-2740-9.

Dobler, A., Yaoming, M., Sharma, N., Kienberger, S., Ahrens, B., 2011. Regional climate projections in two alpine river basins: Upper danube and upper brahmaputra. Advances in Science and Research 7, 11–20. URL: https://doi.org/10.5194%2Fasr-7-11-2011, doi:10.5194/asr-7-11-2011.

Douglas, E.M., Fairbank, C.A., 2011. Is precipitation in northern new england becoming more extreme? statistical analysis of extreme rainfall in massachusetts, new hampshire, and maine and updated estimates of the 100-year storm. Journal of Hydrologic Engineering 16, 203–217. URL: https://doi.org/10.1061%2F%28asce%29he.1943-5584.0000303, doi:10.1061/(asce)he.1943-5584.0000303.

Dourte, D., Shukla, S., Singh, P., Haman, D., 2013. Rainfall intensity-duration-frequency relationships for andhra pradesh, india: Changing rainfall patterns and implications for runoff and groundwater recharge. Journal of Hydrologic Engineering 18, 324–330. URL: https://doi.org/10.1061%2F%28asce%29he.1943-5584.0000625, doi:10.1061/(asce)he.1943-5584.0000625.

Du, J., Qian, L., Rui, H., Zuo, T., Zheng, D., Xu, Y., Xu, C.Y., 2012. Assessing the effects of urbanization on annual runoff and flood events using an integrated hydrological modeling system for qinhuai river basin, china. Journal of Hydrology 464-465, 127–139. URL: https://doi.org/10.1016%2Fj.jhydrol.2012.06.057, doi:10.1016/j.jhydrol.2012.06.057.

Ebrahimian, A., Wilson, B.N., Gulliver, J.S., 2016. Improved methods to estimate the effective impervious area in urban catchments using rainfall-runoff data. Journal of Hydrology 536, 109–118. URL: https://doi.org/10.1016%2Fj.jhydrol.2016.02.023, doi:10.1016/j.jhydrol.2016.02.023.

Eckart, K., McPhee, Z., Bolisetti, T., 2018. Multiobjective optimization of low impact development stormwater controls. Journal of Hydrology 562, 564–576. URL: https://doi.org/10.1016%2Fj.jhydrol.2018.04.068, doi:10.1016/j.jhydrol.2018.04.068.

Ömer Ekmekcioğlu, Yılmaz, M., Özger, M., Tosunoğlu, F., 2021. Investigation of the low impact development strategies for highly urbanized area via auto-calibrated storm water management model (SWMM). Water Science and Technology 84, 2194–2213. URL: https://doi.org/10.2166%2Fwst.2021.432, doi:10.2166/wst.2021.432.

Ekström, M., Grose, M.R., Whetton, P.H., 2015. An appraisal of downscaling methods used in climate change research. WIREs Climate Change 6, 301–319. URL: https://doi.org/10.1002%2Fwcc.339, doi:10.1002/wcc.339.

Fan, G., Lin, R., Wei, Z., Xiao, Y., Shangguan, H., Song, Y., 2022. Effects of low impact development on the stormwater runoff and pollution control. Science of The Total Environment 805, 150404. URL: https://doi.org/10.1016%2Fj.scitotenv.2021.150404, doi:10.1016/j.scitotenv.2021.150404.

Faramarzi, M., Abbaspour, K.C., Vaghefi, S.A., Farzaneh, M.R., Zehnder, A.J., Srinivasan, R., Yang, H., 2013. Modeling impacts of climate change on freshwater availability in africa. Journal of Hydrology 480, 85–101. URL: https://doi.org/10.1016%2Fj.jhydrol.2012.12.016, doi:10.1016/j.jhydrol.2012.12.016.

Ficklin, D.L., Stewart, I.T., Maurer, E.P., 2012. Effects of projected climate change on the hydrology in the mono lake basin, california. Climatic Change 116, 111–131. URL: https://doi.org/10.1007%2Fs10584-012-0566-6, doi:10.1007/s10584-012-0566-6.

Fletcher, T., Andrieu, H., Hamel, P., 2013. Understanding, management and modelling of urban hydrology and its consequences for receiving waters: A state of the art. Advances in Water Resources 51, 261–279. URL: https://doi.org/10.1016%2Fj.advwatres.2012.09.001, doi:10.1016/j.advwatres.2012.09.001.

Fletcher, T.D., Shuster, W., Hunt, W.F., Ashley, R., Butler, D., Arthur, S., Trowsdale, S., Barraud, S., Semadeni-Davies, A., Bertrand-Krajewski, J.L., Mikkelsen, P.S., Rivard, G., Uhl, M., Dagenais, D., Viklander, M., 2014. SUDS, LID, BMPs, WSUD and more – the evolution and application of terminology surrounding urban drainage. Urban Water Journal 12, 525–542. URL: https://doi.org/10.1080%2F1573062x.2014.916314, doi:10.1080/1573062x.2014.916314.

Fu, G., Butler, D., Khu, S.T., Sun, S., 2011. Imprecise probabilistic evaluation of sewer flooding in urban drainage systems using random set theory. Water Resources Research 47. URL: https://doi.org/10.1029%2F2009wr008944, doi:10.1029/2009wr008944.

Galavi, H., Mirzaei, M., Yu, B., Lee, J., 2022. Bootstrapped ensemble and reliability ensemble averaging approaches for integrated uncertainty analysis of streamflow projections. Stochastic Environmental Research and Risk Assessment 37, 1213–1227. URL: https://doi.org/10.1007%2Fs00477-022-02337-5, doi:10.1007/s00477-022-02337-5.

Ganguli, P., Coulibaly, P., 2019. Assessment of future changes in intensity-duration-frequency curves for southern ontario using north american (NA)-CORDEX models with nonstationary methods. Journal of Hydrology: Regional Studies 22, 100587. URL: https://doi.org/10.1016%2Fj.ejrh.2018.12.007, doi:10.1016/j.ejrh.2018.12.007.

Gebru, T.A., 2020. Rainfall intensity-duration-frequency relations under changing climate for selected stations in the tigray region, ethiopia. Journal of Hydrologic Engineering 25, 05020041. URL: https://doi.org/10.1061%2F%28asce%29he.1943-5584.0001999, doi:10.1061/(asce)he.1943-5584.0001999.

Genest, C., MacKay, J., 1986. The joy of copulas: Bivariate distributions with uniform marginals. The American Statistician 40, 280. URL: https://doi.org/10.2307%2F2684602, doi:10.2307/2684602.

Genest, C., Rivest, L.P., 1993. Statistical inference procedures for bivariate archimedean copulas. Journal of the American Statistical Association 88, 1034–1043. URL: https://doi.org/10.1080%2F01621459.1993.10476372, doi:10.1080/01621459.1993.10476372.

Getachew, B., Manjunatha, B., Bhat, H.G., 2021. Modeling projected impacts of climate and land use/land cover changes on hydrological responses in the lake tana basin, upper blue nile river basin, ethiopia. Journal of Hydrology 595, 125974. URL: https://doi.org/10.1016%2Fj.jhydrol.2021.125974, doi:10.1016/j.jhydrol.2021.125974.

Ghodsi, S.H., Zahmatkesh, Z., Goharian, E., Kerachian, R., Zhu, Z., 2020. Optimal design of low impact development practices in response to climate change. Journal of Hydrology 580, 124266. URL: https://doi.org/10.1016%2Fj.jhydrol.2019.124266, doi:10.1016/j.jhydrol.2019.124266.

Ghosh, S., Mujumdar, P., 2006. Future rainfall scenario over orissa with gcm projections by statistical downscaling. Current Science , 396–404.

Giorgi, F., Mearns, L.O., 2002. Calculation of average, uncertainty range, and reliability of regional climate changes from AOGCM simulations via the "reliability ensemble averaging" (REA) method. Journal of Climate 15, 1141–1158. URL: https://doi.org/10.1175%2F1520-0442%282002%29015%3C1141%3Acoaura%3E2.0.co%3B2, doi:10.1175/1520-0442(2002)015<1141:coaura>2.0.co;2.

Giorgi, F., Mearns, L.O., 2003. Probability of regional climate change based on the reliability ensemble averaging (REA) method. Geophysical Research Letters 30. URL: https://doi.org/10.1029%2F2003gl017130, doi:10.1029/2003gl017130.

Golroudbary, V.R., Zeng, Y., Mannaerts, C.M., Su, Z.B., 2017. Detecting the effect of urban land use on extreme precipitation in the netherlands. Weather and Climate Extremes 17, 36–46.

Goncalves, M., Zischg, J., Rau, S., Sitzmann, M., Rauch, W., Kleidorfer, M., 2018. Modeling the effects of introducing low impact development in a tropical city: A case study from joinville, brazil. Sustainability 10, 728. URL: https://doi.org/10.3390%2Fsu10030728, doi:10.3390/su10030728.

Guan, M., Sillanpää, N., Koivusalo, H., 2015. Storm runoff response to rainfall pattern, magnitude and urbanization in a developing urban catchment. Hydrological Processes , n/a–n/aURL: https://doi.org/10.1002%2Fhyp.10624, doi:10.1002/hyp.10624.

Guan, X., Wang, J., Xiao, F., 2021. Sponge city strategy and application of pavement materials in sponge city. Journal of Cleaner Production 303, 127022. URL: https://doi.org/10.1016%2Fj.jclepro.2021.127022, doi:10.1016/j.jclepro.2021.127022.

Guinot, V., Sanders, B.F., Schubert, J.E., 2017. Dual integral porosity shallow water model for urban flood modelling. Advances in Water Resources 103, 16–31. URL: https://doi.org/10.1016%2Fj.advwatres.2017.02.009, doi:10.1016/j.advwatres.2017.02.009.

Guo, T., Srivastava, A., Flanagan, D.C., Liu, Y., Engel, B.A., McIntosh, M.M., 2021. Evaluation of costs and efficiencies of urban low impact development (LID) practices on stormwater runoff and soil erosion in an urban watershed using the water erosion prediction project (WEPP) model. Water 13, 2076. URL: https://doi.org/10.3390%2Fw13152076, doi:10.3390/w13152076.

Gupta, A.K., Anderson, D.M., Overpeck, J.T., 2003. Abrupt changes in the asian southwest monsoon during the holocene and their links to the north atlantic ocean. Nature 421, 354–357. URL: http://dx.doi.org/10.1038/nature01340, doi:10.1038/nature01340.

Gupta, A.K., Nair, S.S., 2011. Urban floods in bangalore and chennai: risk management challenges and lessons for sustainable urban ecology. Current Science , 1638–1645.

Hamzah, F.B., Hamzah, F.M., Razali, S.F.M., Samad, H., 2021. A comparison of multiple imputation methods for recovering missing data in hydrological studies. Civil Engineering Journal 7, 1608–1619. URL: https://doi.org/10.28991%2Fcej-2021-03091747, doi:10.28991/cej-2021-03091747.

Han, D., Currell, M.J., Cao, G., Hall, B., 2017. Alterations to groundwater recharge due to anthropogenic landscape change. Journal of Hydrology 554, 545–557. URL: https://doi.org/10.1016%2Fj.jhydrol.2017.09.018, doi:10.1016/j.jhydrol.2017.09.018.

Han, W.S., Burian, S.J., 2009. Determining effective impervious area for urban hydrologic modeling. Journal of Hydrologic Engineering 14, 111–120. URL: https://doi.org/10.1061%2F%28asce%291084-0699%282009%2914%3A2%28111%29, doi:10.1061/(asce)1084-0699(2009)14:2(111).

Hao, Y., Sun, F., Wang, H., Liu, W., Shen, Y.J., Li, Z., Hu, S., 2022. Understanding climate-induced changes of snow hydrological processes in the kaidu river basin through the CemaNeige-GR6j model. CATENA 212, 106082. URL: https://doi.org/10.1016%2Fj.catena.2022.106082, doi:10.1016/j.catena.2022.106082.

Hassanzadeh, E., Nazemi, A., Elshorbagy, A., 2014. Quantile-based downscaling of precipitation using genetic programming: Application to IDF curves in saskatoon. Journal of Hydrologic Engineering 19, 943–955. URL: https://doi.org/10.1061%2F%28asce%29he.1943-5584.0000854, doi:10.1061/(asce)he.1943-5584.0000854.

Hathaway, J., Brown, R., Fu, J., Hunt, W., 2014. Bioretention function under climate change scenarios in north carolina, USA. Journal of Hydrology 519, 503–511. URL: https://doi.org/10.1016%2Fj.jhydrol.2014.07.037, doi:10.1016/j.jhydrol.2014.07.037.

Hawken, S., Sepasgozar, S., Prodanovic, V., Jing, J., Bakelmun, A., Avazpour, B., Che, S., Zhang, K., 2021. What makes a successful sponge city project? expert perceptions of critical factors in integrated urban water management in the asia-pacific. Sustainable Cities and Society 75, 103317. URL: https://doi.org/10.1016%2Fj.scs.2021.103317, doi:10.1016/j.scs.2021.103317.

Hénonin, J., Hongtao, M., Zheng-Yu, Y., Hartnack, J., Havnø, K., Gourbesville, P., Mark, O., 2013. Citywide multi-grid urban flood modelling: the july 2012 flood in beijing. Urban Water Journal 12, 52–66. URL: https://doi.org/10.1080%2F1573062x.2013.851710, doi:10.1080/1573062x.2013.851710.

Herath, S.M., Sarukkalige, P.R., Nguyen, V.T.V., 2016. A spatial temporal downscaling approach to development of IDF relations for perth airport region in the context of climate change. Hydrological Sciences Journal 61, 2061–2070. URL: https://doi.org/10.1080%2F02626667.2015.1083103, doi:10.1080/02626667.2015.1083103.

Hewitson, B., Crane, R., 1996. Climate downscaling: techniques and application. Climate Research 7, 85–95. URL: https://doi.org/10.3354%2Fcr007085, doi:10.3354/cr007085.

Horritt, M., Bates, P., 2001. Effects of spatial resolution on a raster based model of flood flow. Journal of Hydrology 253, 239–249. URL: https://doi.org/10.1016%2Fs0022-1694%2801%2900490-5, doi:10.1016/s0022-1694(01)00490-5.

Hosseinzadehtalaei, P., Tabari, H., Willems, P., 2020. Climate change impact on short-duration extreme precipitation and intensity–duration–frequency curves over europe. Journal of Hydrology 590, 125249. URL: https://doi.org/10.1016%2Fj.jhydrol.2020.125249, doi:10.1016/j.jhydrol.2020.125249.

Hu, M., Sayama, T., Zhang, X., Tanaka, K., Takara, K., Yang, H., 2017. Evaluation of low impact development approach for mitigating flood inundation at a watershed scale in china. Journal of Environmental Management 193, 430–438. URL: http://dx.doi.org/10.1016/j.jenvman.2017.02.020, doi:10.1016/j.jenvman.2017.02.020.

Hurkmans, R.T.W.L., Terink, W., Uijlenhoet, R., Moors, E.J., Troch, P.A., Verburg, P.H., 2009. Effects of land use changes on streamflow generation in the rhine basin. Water Resources Research 45. URL: https://doi.org/10.1029%2F2008wr007574, doi:10.1029/2008wr007574.

Hussain, S.N., Zwain, H.M., Nile, B.K., 2021. Modeling the effects of land-use and climate change on the performance of stormwater sewer system using SWMM simulation: case study. Journal of Water and Climate Change 13, 125–138. URL: https://doi.org/10.2166%2Fwcc.2021.180, doi:10.2166/wcc.2021.180.

IPCC, 2007. 2007: Climate Change 2007: Synthesis Report. Contribution of Working Groups I, II and III to the Fourth Assessment Report of the Intergovernmental Panel on Climate Change [Core Writing Team, Pachauri, R.K and Reisinger, A. (eds.)]. IPCC, Geneva, Switzerland, 104pp.

IPCC, 2014. 2014: Climate Change 2014: Synthesis Report. Contribution of Working Groups I, II and III to the Fifth Assessment Report of the Intergovernmental Panel on Climate Change [Core Writing Team, R.K. Pachauri and L.A. Meyer (eds.)]. IPCC, Geneva, Switzerland, 151pp.

IPCC, 2021. 2021: Climate Change 2021: The Physical Science Basis. Contribution of Working Group I to the Sixth Assessment Report of the Intergovernmental Panel on Change[Masson-Delmotte, V., P. Zhai, A. Pirani, S.L. Connors, C. Péan, S. Berger, N. Caud, Y. Chen, L. Goldfarb, M.I. Gomis, M. Huang, K. Leitzell, E. Lonnoy, J.B.R. Matthews, T.K. Maycock, T. Waterfield, O. Yelekçi, R. Yu, and B. Zhou (eds.)]. , In press,. Cambridge University Press, Cambridge, United Kingdom and New York, NY, USA. doi:10.1017/9781009157896.

Islam, Z., Gan, T.Y., 2014. Effects of climate change on the surface-water management of the south saskatchewan river basin. Journal of Water Resources Planning and Management 140, 332–342. URL: https://doi.org/10.1061%2F%28asce%29wr.1943-5452.0000326, doi:10.1061/(asce)wr.1943-5452.0000326.

Islami, F.A., Tarigan, S.D., Wahjunie, E.D., Dasanto, B.D., 2022. Accuracy assessment of land use change analysis using google earth in sadar watershed mojokerto regency. IOP Conference Series: Earth and Environmental Science 950, 012091. URL: https://doi.org/10.1088%2F1755-1315%2F950%2F1%2F012091, doi:10.1088/1755-1315/950/1/012091.

Jamei, Y., Rajagopalan, P., Sun, Q.C., 2019. Spatial structure of surface urban heat island and its relationship with vegetation and built-up areas in melbourne, australia. Science of The Total Environment 659, 1335–1351. URL: https://doi.org/10.1016%2Fj.scitotenv.2018.12.308, doi:10.1016/j.scitotenv.2018.12.308.

Jane, R., Cadavid, L., Obeysekera, J., Wahl, T., 2020. Multivariate statistical modelling of the drivers of compound flood events in south florida. Natural Hazards and Earth System Sciences 20, 2681–2699. URL: https://doi.org/10.5194%2Fnhess-20-2681-2020, doi:10.5194/nhess-20-2681-2020.

Joe, H., 2014. Dependence modeling with copulas. CRC press.

Joseph, G., 2005. Fundamentals of remote sensing. Universities Press.

Kandakji, T., Gill, T.E., Lee, J.A., 2021. Drought and land use/land cover impact on dust sources in southern great plains and chihuahuan desert of the u.s.: Inferring anthropogenic effect. Science of The Total Environment 755, 142461. URL: https://doi.org/10.1016%2Fj.scitotenv.2020.142461, doi:10.1016/j.scitotenv.2020.142461.

Kao, S.C., Govindaraju, R.S., 2007. A bivariate frequency analysis of extreme rainfall with implications for design. Journal of Geophysical Research: Atmospheres 112. URL: https://doi.org/10.1029%2F2007jd008522, doi:10.1029/2007jd008522.

Kao, S.C., Govindaraju, R.S., 2008. Trivariate statistical analysis of extreme rainfall events via the plackett family of copulas. Water Resources Research 44. URL: https://doi.org/10.1029%2F2007wr006261, doi:10.1029/2007wr006261.

Kauffman, G.J., Corrozi, M.B., Vonck, K.J., 2006. Imperviousness: A performance measure of a delaware water resource protection area ordinance. Journal of the American Water Resources Association 42, 603–615. URL: https://doi.org/10.1111%2Fj.1752-1688.2006.tb04479.x, doi:10.1111/j.1752-1688.2006.tb04479.x.

Kaufmann, R.K., Seto, K.C., Schneider, A., Liu, Z., Zhou, L., Wang, W., 2007. Climate response to rapid urban growth: Evidence of a human-induced precipitation deficit. Journal of Climate 20, 2299–2306. URL: http://dx.doi.org/10.1175/jcli4109.1, doi:10.1175/jcli4109.1.

Kayitesi, N.M., Guzha, A.C., Mariethoz, G., 2022. Impacts of land use land cover change and climate change on river hydro-morphology- a review of research studies in tropical regions. Journal of Hydrology 615, 128702. URL: https://doi.org/10.1016%2Fj.jhydrol.2022.128702, doi:10.1016/j.jhydrol.2022.128702.

Kendall, M.G., 1957. Rank correlation methods. Biometrika 44, 298. URL: https://doi.org/10.2307%2F2333282, doi:10.2307/2333282.

Khare, D., Mondal, A., Kundu, S., Mishra, P.K., 2016. Climate change impact on soil erosion in the mandakini river basin, north india. Applied Water Science 7, 2373–2383. URL: https://doi.org/10.1007%2Fs13201-016-0419-y, doi:10.1007/s13201-016-0419-y.

Khazaei, M.R., 2021. A robust method to develop future rainfall IDF curves under climate change condition in two major basins of iran. Theoretical and Applied Climatology 144, 179–190. URL: https://doi.org/10.1007%2Fs00704-021-03540-0, doi:10.1007/s00704-021-03540-0.

Kiptala, J.K., Mohamed, Y., Mul, M.L., der Zaag, P.V., 2013. Mapping evapotranspiration trends using MODIS and SEBAL model in a data scarce and heterogeneous landscape in eastern africa. Water Resources Research 49, 8495–8510. URL: https://doi.org/10.1002%2F2013wr014240, doi:10.1002/2013wr014240.

Kothyari, U.C., Garde, R.J., 1992. Rainfall intensity-duration-frequency formula for india. Journal of Hydraulic Engineering 118, 323–336. URL: https://doi.org/10.1061%2F%28asce%290733-9429%281992%29118%3A2%28323%29, doi:10.1061/(asce)0733-9429(1992)118:2(323).

Kourtis, I.M., Nalbantis, I., Tsakiris, G., Psiloglou, B.E., Tsihrintzis, V.A., 2022. Updating idf curves under climate change: Impact on rainfall-induced runoff in urban basins. Water Resources Management , 1–26doi:10.1007/s11269-022-03252-8.

Koutsoyiannis, D., Kozonis, D., Manetas, A., 1998. A mathematical framework for studying rainfall intensity-duration-frequency relationships. Journal of Hydrology 206, 118–135. URL: https://doi.org/10.1016%2Fs0022-1694%2898%2900097-3, doi:10.1016/s0022-1694(98)00097-3.

Kuller, M., Bach, P.M., Roberts, S., Browne, D., Deletic, A., 2019. A planning-support tool for spatial suitability assessment of green urban stormwater infrastructure. Science of The Total Environment 686, 856–868. URL: https://doi.org/10.1016%2Fj.scitotenv.2019.06.051, doi:10.1016/j.scitotenv.2019.06.051.

Kumar, M., Denis, D.M., Kundu, A., Joshi, N., Suryavanshi, S., 2022a. Understanding land use/land cover and climate change impacts on hydrological components of usri watershed, india. Applied Water Science 12. URL: https://doi.org/10.1007%2Fs13201-021-01547-6, doi:10.1007/s13201-021-01547-6.

Kumar, S., Agarwal, A., Ganapathy, A., Villuri, V.G.K., Pasupuleti, S., Kumar, D., Kaushal, D.R., Gosain, A.K., Sivakumar, B., 2021. Impact of climate change on stormwater drainage in urban areas. Stochastic Environmental Research and Risk Assessment 36, 77–96. URL: https://doi.org/10.1007%2Fs00477-021-02105-x, doi:10.1007/s00477-021-02105-x.

Kumar, S., Guntu, R.K., Agarwal, A., Villuri, V.G.K., Pasupuleti, S., Kaushal, D., Gosian, A.K., Bronstert, A., 2022b. Multi-objective optimization for stormwater management by green-roofs and infiltration trenches to reduce urban flooding in central delhi. Journal of Hydrology 606, 127455. URL: https://doi.org/10.1016%2Fj.jhydrol.2022.127455, doi:10.1016/j.jhydrol.2022.127455.

Kuo, C.C., Gan, T.Y., Gizaw, M., 2015. Potential impact of climate change on intensity duration frequency curves of central alberta. Climatic Change 130, 115–129. URL: https://doi.org/10.1007%2Fs10584-015-1347-9, doi:10.1007/s10584-015-1347-9.

Kurowicka, D., van Horssen, W.T., 2015. On an interaction function for copulas. Journal of Multivariate Analysis 138, 127–142. URL: https://doi.org/10.1016%2Fj.jmva.2014.12.012, doi:10.1016/j.jmva.2014.12.012.

Lee, J., hak Hyun, K., soo Choi, J., 2013. Analysis of the impact of low impact development on runoff from a new district in korea. Water Science and Technology 68, 1315–1321. URL: https://doi.org/10.2166%2Fwst.2013.346, doi:10.2166/wst.2013.346.

Lee, T., Jeong, C., 2014. Nonparametric statistical temporal downscaling of daily precipitation to hourly precipitation and implications for climate change scenarios. Journal of Hydrology 510, 182–196. URL: https://doi.org/10.1016%2Fj.jhydrol.2013.12.027, doi:10.1016/j.jhydrol.2013.12.027.

Lee, T., Son, C., Kim, M., Lee, S., Yoon, S., 2020. Climate change adaptation to extreme rainfall events on a local scale in namyangju, south korea. Journal of Hydrologic Engineering 25, 05020005. URL: https://doi.org/10.1061%2F%28asce%29he.1943-5584.0001906, doi:10.1061/(asce)he.1943-5584.0001906.

Lenka, S., Devi, R., Joseph, C.M., Gouda, K.C., 2022. Effect of large-scale oceanic and atmospheric processes on the indian summer monsoon. Theoretical and Applied Climatology 147, 1561–1576. URL: http://dx.doi.org/10.1007/s00704-021-03896-3, doi:10.1007/s00704-021-03896-3.

Li, K., Tong, Z., Liu, X., Zhang, J., Tong, S., 2020a. Quantitative assessment and driving force analysis of vegetation drought risk to climate change:methodology and application in northeast china. Agricultural and Forest Meteorology 282-283, 107865. URL: https://doi.org/10.1016%2Fj.agrformet.2019.107865, doi:10.1016/j.agrformet.2019.107865.

Li, M., Zang, S., Zhang, B., Li, S., Wu, C., 2014. A review of remote sensing image classification techniques: the role of spatio-contextual information. European Journal of Remote Sensing 47, 389–411. URL: https://doi.org/10.5721%2Feujrs20144723, doi:10.5721/eujrs20144723.

Li, X., Stringer, L.C., Dallimer, M., 2022. The role of blue green infrastructure in the urban thermal environment across seasons and local climate zones in east africa. Sustainable Cities and Society 80, 103798. URL: https://doi.org/10.1016%2Fj.scs.2022.103798, doi:10.1016/j.scs.2022.103798.

Li, Y., Li, H.X., Huang, J., Liu, C., 2020b. An approximation method for evaluating flash flooding mitigation of sponge city strategies – a case study of central geelong. Journal of Cleaner Production 257, 120525. URL: https://doi.org/10.1016%2Fj.jclepro.2020.120525, doi:10.1016/j.jclepro.2020.120525.

Lillesand, T., Kiefer, R.W., Chipman, J., 2015. Remote sensing and image interpretation. John Wiley & Sons.

Liu, O.Y., Russo, A., 2021. Assessing the contribution of urban green spaces in green infrastructure strategy planning for urban ecosystem conditions and services. Sustainable Cities and Society 68, 102772. URL: https://doi.org/10.1016%2Fj.scs.2021.102772, doi:10.1016/j.scs.2021.102772.

Ma, Y., He, W., Zhao, H., Zhao, J., Wu, X., Wu, W., Li, X., Yin, C., 2019. Influence of low impact development practices on urban diffuse pollutant transport process at catchment scale. Journal of Cleaner Production 213, 357–364. URL: https://doi.org/10.1016%2Fj.jclepro.2018.12.198, doi:10.1016/j.jclepro.2018.12.198.

de Macedo, M.B., Júnior, M.N.G., de Oliveira, T.R.P., Giacomoni, M.H., Imani, M., Zhang, K., do Lago, C.A.F., Mendiondo, E.M., 2022. Low impact development practices in the context of united nations sustainable development goals: A new concept, lessons learned and challenges. Critical Reviews in Environmental Science and Technology 52, 2538–2581. URL: https://doi.org/10.1080/10643389.2021.1886889, doi:10.1080/10643389.2021.1886889.

de Macedo, M.B., do Lago, C.A.F., Mendiondo, E.M., Giacomoni, M.H., 2019. Bioretention performance under different rainfall regimes in subtropical conditions: A case study in são carlos, brazil. Journal of Environmental Management 248, 109266. URL: https://doi.org/10.1016%2Fj.jenvman.2019.109266, doi:10.1016/j.jenvman.2019.109266.

Mailhot, A., Beauregard, I., Talbot, G., Caya, D., Biner, S., 2011. Future changes in intense precipitation over canada assessed from multi-model NARCCAP ensemble simulations. International Journal of Climatology 32, 1151–1163. URL: https://doi.org/10.1002%2Fjoc.2343, doi:10.1002/joc.2343.

Mailhot, A., Duchesne, S., Caya, D., Talbot, G., 2007. Assessment of future change in intensity–duration–frequency (IDF) curves for southern quebec using the canadian regional climate model (CRCM). Journal of Hydrology 347, 197–210. URL: https://doi.org/10.1016%2Fj.jhydrol.2007.09.019, doi:10.1016/j.jhydrol.2007.09.019.

Mamo, T.G., 2015. Evaluation of the potential impact of rainfall intensity variation due to climate change on existing drainage infrastructure. Journal of Irrigation and Drainage Engineering 141, 05015002. URL: https://doi.org/10.1061%2F%28asce%29ir.1943-4774.0000887, doi:10.1061/(asce)ir.1943-4774.0000887.

Mann, H.B., 1945. Nonparametric tests against trend. Econometrica 13, 245. URL: https://doi.org/10.2307%2F1907187, doi:10.2307/1907187.

Marando, F., Heris, M.P., Zulian, G., Udías, A., Mentaschi, L., Chrysoulakis, N., Parastatidis, D., Maes, J., 2022. Urban heat island mitigation by green infrastructure in european functional urban areas. Sustainable Cities and Society 77, 103564. URL: https://doi.org/10.1016%2Fj.scs.2021.103564, doi:10.1016/j.scs.2021.103564.

Maraun, D., 2013. Bias correction, quantile mapping, and downscaling: Revisiting the inflation issue. Journal of Climate 26, 2137–2143. URL: https://doi.org/10.1175%2Fjcli-d-12-00821.1, doi:10.1175/jcli-d-12-00821.1.

Martin-Mikle, C.J., de Beurs, K.M., Julian, J.P., Mayer, P.M., 2015. Identifying priority sites for low impact development (lid) in a mixed-use watershed. Landscape and Urban Planning 140, 29–41. URL: http://dx.doi.org/10.1016/j.landurbplan.2015.04.002, doi:10.1016/j.landurbplan.2015.04.002.

Miller, J.D., Hess, T., 2017. Urbanisation impacts on storm runoff along a rural-urban gradient. Journal of Hydrology 552, 474–489. URL: https://doi.org/10.1016%2Fj.jhydrol.2017.06.025, doi:10.1016/j.jhydrol.2017.06.025.

Mirhosseini, G., Srivastava, P., Fang, X., 2014. Developing rainfall intensity-duration-frequency curves for alabama under future climate scenarios using artificial neural networks. Journal of Hydrologic Engineering 19, 04014022. URL: https://doi.org/10.1061%2F%28asce%29he.1943-5584.0000962, doi:10.1061/(asce)he.1943-5584.0000962.

Moftakhari, H., Schubert, J.E., AghaKouchak, A., Matthew, R.A., Sanders, B.F., 2019. Linking statistical and hydrodynamic modeling for compound flood hazard assessment in tidal channels and estuaries. Advances in Water Resources 128, 28–38. URL: https://doi.org/10.1016%2Fj.advwatres.2019.04.009, doi:10.1016/j.advwatres.2019.04.009.

Mohebbi, A., Akbariyeh, S., Maruf, M., Wu, Z., Acuna, J.C., Adams, K.R., 2021. Development of rainfall intensity-duration-frequency curves based on dynamically downscaled climate data: Arizona case study. Journal of Hydrologic Engineering 26, 05021005. URL: https://doi.org/10.1061%2F%28asce%29he.1943-5584.0002068, doi:10.1061/(asce)he.1943-5584.0002068.

Morsy, M.M., Goodall, J.L., Shatnawi, F.M., Meadows, M.E., 2016. Distributed stormwater controls for flood mitigation within urbanized watersheds: Case study of rocky branch watershed in columbia, south carolina. Journal of Hydrologic Engineering 21, 05016025. URL: https://doi.org/10.1061%2F%28asce%29he.1943-5584.0001430, doi:10.1061/(asce)he.1943-5584.0001430.

Naulin, J.P., Payrastre, O., Gaume, E., 2013. Spatially distributed flood forecasting in flash flood prone areas: Application to road network supervision in southern france. Journal of Hydrology 486, 88–99. URL: https://doi.org/10.1016%2Fj.jhydrol.2013.01.044, doi:10.1016/j.jhydrol.2013.01.044.

Nelsen, R.B., 1999. Archimedean copulas, in: An Introduction to Copulas. Springer New York, pp. 89–124. URL: https://doi.org/10.1007%2F978-1-4757-3076-0_4, doi:10.1007/978-1-4757-3076-0_4.

Nelsen, R.B., 2007. An introduction to copulas. Springer science & business media.

Neupane, B., Vu, T.M., Mishra, A.K., 2021. Evaluation of land-use, climate change, and low-impact development practices on urban flooding. Hydrological Sciences Journal 66, 1729–1742. URL: https://doi.org/10.1080%2F02626667.2021.1954650, doi:10.1080/02626667.2021.1954650.

Nguyen, T.H., Nguyen, V.T.V., 2020. Linking climate change to urban storm drainage system design: An innovative approach to modeling of extreme rainfall processes over different spatial and temporal scales. Journal of Hydro-environment Research 29, 80–95. URL: https://doi.org/10.1016%2Fj.jher.2020.01.006, doi:10.1016/j.jher.2020.01.006.

Nguyen, V.T.V., Nguyen, T.D., Cung, A., 2007. A statistical approach to downscaling of sub-daily extreme rainfall processes for climate-related impact studies in urban areas. Water Science and Technology: Water Supply 7, 183–192. URL: https://doi.org/10.2166%2Fws.2007.053, doi:10.2166/ws.2007.053.

Nicholls, R., HOOZEMANS, F., MARCHAND, M., 1999. Increasing flood risk and wetland losses due to global sea-level rise: regional and global analyses. Global Environmental Change 9, S69–S87. URL: https://doi.org/10.1016%2Fs0959-3780%2899%2900019-9, doi:10.1016/s0959-3780(99)00019-9.

Nilawar, A.P., Waikar, M.L., 2019. Impacts of climate change on streamflow and sediment concentration under RCP 4.5 and 8.5: A case study in purna river basin, india. Science of The Total Environment 650, 2685–2696. URL: https://doi.org/10.1016%2Fj.scitotenv.2018.09.334, doi:10.1016/j.scitotenv.2018.09.334.

Noor, M., Ismail, T., Chung, E.S., Shahid, S., Sung, J., 2018. Uncertainty in rainfall intensity duration frequency curves of peninsular malaysia under changing climate scenarios. Water 10, 1750. URL: https://doi.org/10.3390%2Fw10121750, doi:10.3390/w10121750.

Odongo, V.O., van Oel, P.R., van der Tol, C., Su, Z., 2019. Impact of land use and land cover transitions and climate on evapotranspiration in the lake naivasha basin, kenya. Science of The Total Environment 682, 19–30. URL: https://doi.org/10.1016%2Fj.scitotenv.2019.04.062, doi:10.1016/j.scitotenv.2019.04.062.

Olsson, J., Berggren, K., Olofsson, M., Viklander, M., 2009. Applying climate model precipitation scenarios for urban hydrological assessment: A case study in kalmar city, sweden. Atmospheric Research 92, 364–375. URL: https://doi.org/10.1016%2Fj.atmosres.2009.01.015, doi:10.1016/j.atmosres.2009.01.015.

Palermo, S.A., Talarico, V.C., Turco, M., 2020. On the LID systems effectiveness for urban stormwater management: case study in southern italy. IOP Conference Series: Earth and Environmental Science 410, 012012. URL: https://doi.org/10.1088%2F1755-1315%2F410%2F1%2F012012, doi:10.1088/1755-1315/410/1/012012.

Palla, A., Gnecco, I., 2015. Hydrologic modeling of low impact development systems at the urban catchment scale. Journal of Hydrology 528, 361–368. URL: https://doi.org/10.1016%2Fj.jhydrol.2015.06.050, doi:10.1016/j.jhydrol.2015.06.050.

Pandey, B.K., Gosain, A.K., Paul, G., Khare, D., 2016. Climate change impact assessment on hydrology of a small watershed using semi-distributed model. Applied Water Science 7, 2029–2041. URL: https://doi.org/10.1007%2Fs13201-016-0383-6, doi:10.1007/s13201-016-0383-6.

Paola, F.D., Giugni, M., Topa, M., Bucchignani, E., 2014. Intensity-duration-frequency (IDF) rainfall curves, for data series and climate projection in african cities. SpringerPlus 3, 133. URL: https://doi.org/10.1186%2F2193-1801-3-133, doi:10.1186/2193-1801-3-133.

Paul, S., Ghosh, S., Oglesby, R., Pathak, A., Chandrasekharan, A., Ramsankaran, R., 2016. Weakening of indian summer monsoon rainfall due to changes in land use land cover. Scientific Reports 6. URL: https://doi.org/10.1038%2Fsrep32177, doi:10.1038/srep32177.

Pereira, M.J.M.G., Fernandes, L.F.S., Macário, E.M.B., Gaspar, S.M., Pinto, J.G., 2015. Climate change impacts in the design of drainage systems: Case study of portugal. Journal of Irrigation and Drainage Engineering 141, 05014009. URL: https://doi.org/10.1061%2F%28asce%29ir.1943-4774.0000788, doi:10.1061/(asce)ir.1943-4774.0000788.

Perumal, M., Sahoo, B., 2010. Real-time flood forecasting by a hydrometric data-based technique, in: Natural and Anthropogenic Disasters. Springer Netherlands, pp. 169–196. URL: https://doi.org/10.1007%2F978-90-481-2498-5_9, doi:10.1007/978-90-481-2498-5_9.

Pour, S.H., Wahab, A.K.A., Shahid, S., Asaduzzaman, M., Dewan, A., 2020. Low impact development techniques to mitigate the impacts of climate-change-induced urban floods: Current trends, issues and challenges. Sustainable Cities and Society 62, 102373. URL: https://doi.org/10.1016%2Fj.scs.2020.102373, doi:10.1016/j.scs.2020.102373.

Qiao, X.J., Liao, K.H., Randrup, T.B., 2020. Sustainable stormwater management: A qualitative case study of the sponge cities initiative in china. Sustainable Cities and Society 53, 101963. URL: https://doi.org/10.1016%2Fj.scs.2019.101963, doi:10.1016/j.scs.2019.101963.

Quichimbo-Miguitama, F., Matamoros, D., Jiménez, L., Quichimbo-Miguitama, P., 2022. Influence of low-impact development in flood control: A case study of the febres cordero stormwater system of guayaquil (ecuador). Sustainability 14, 7109. URL: https://doi.org/10.3390%2Fsu14127109, doi:10.3390/su14127109.

Rafieeinasab, A., Norouzi, A., Kim, S., Habibi, H., Nazari, B., Seo, D.J., Lee, H., Cosgrove, B., Cui, Z., 2015. Toward high-resolution flash flood prediction in large urban areas – analysis of sensitivity to spatiotemporal resolution of rainfall input and hydrologic modeling. Journal of Hydrology 531, 370–388. URL: https://doi.org/10.1016%2Fj.jhydrol.2015.08.045, doi:10.1016/j.jhydrol.2015.08.045.

Rahmani, M.A., Zarghami, M., 2013. A new approach to combine climate change projections by ordered weighting averaging operator; applications to northwestern provinces of iran. Global and Planetary Change 102, 41–50. URL: https://doi.org/10.1016%2Fj.gloplacha.2013.01.007, doi:10.1016/j.gloplacha.2013.01.007.

Rajeevan, M., Bhate, J., Jaswal, A.K., 2008. Analysis of variability and trends of extreme rainfall events over india using 104 years of gridded daily rainfall data. Geophysical Research Letters 35. URL: https://doi.org/10.1029%2F2008gl035143, doi:10.1029/2008gl035143.

Ramezani, M.R., Helfer, F., Yu, B., 2023. Individual and combined impacts of urbanization and climate change on catchment runoff in southeast queensland, australia. Science of The Total Environment 861, 160528. URL: https://doi.org/10.1016%2Fj.scitotenv.2022.160528, doi:10.1016/j.scitotenv.2022.160528.

Rangari, V.A., Umamahesh, N., Patel, A.K., 2021. Flood-hazard risk classification and mapping for urban catchment under different climate change scenarios: A case study of hyderabad city. Urban Climate 36, 100793. URL: https://doi.org/10.1016%2Fj.uclim.2021.100793, doi:10.1016/j.uclim.2021.100793.

Rashetnia, S., Sharma, A.K., Ladson, A.R., Browne, D., Yaghoubi, E., 2022. A scoping review on water sensitive urban design aims and achievements. Urban Water Journal 19, 453–467. URL: https://doi.org/10.1080%2F1573062x.2022.2044494, doi:10.1080/1573062x.2022.2044494.

Requena, A.I., Burn, D.H., Coulibaly, P., 2019. Pooled frequency analysis for intensity–duration–frequency curve estimation. Hydrological Processes 33, 2080–2094. URL: https://doi.org/10.1002%2Fhyp.13456, doi:10.1002/hyp.13456.

Reshmidevi, T., Kumar, D.N., Mehrotra, R., Sharma, A., 2018. Estimation of the climate change impact on a catchment water balance using an ensemble of GCMs. Journal of Hydrology 556, 1192–1204. URL: https://doi.org/10.1016%2Fj.jhydrol.2017.02.016, doi:10.1016/j.jhydrol.2017.02.016.

Rossman, L.A., Huber, W.C., 2016a. Storm water management model reference manual. Volume III—Water Quality .

Rossman, L.A., Huber, W.C., 2016b. Storm water management model reference manual volume i–hydrology. US Environmental Protection Agency 3.

Roy, P.S., Ramachandran, R.M., Paul, O., Thakur, P.K., Ravan, S., Behera, M.D., Sarangi, C., Kanawade, V.P., 2022. Anthropogenic land use and land cover changes—a review on its environmental consequences and climate change. Journal of the Indian Society of Remote Sensing 50, 1615–1640. URL: https://doi.org/10.1007%2Fs12524-022-01569-w, doi:10.1007/s12524-022-01569-w.

Ruelland, D., Ardoin-Bardin, S., Collet, L., Roucou, P., 2012. Simulating future trends in hydrological regime of a large sudano-sahelian catchment under climate change. Journal of Hydrology 424-425, 207–216. URL: https://doi.org/10.1016%2Fj.jhydrol.2012.01.002, doi:10.1016/j.jhydrol.2012.01.002.

Saadatpour, M., Delkhosh, F., Afshar, A., Solis, S.S., 2020. Developing a simulation-optimization approach to allocate low impact development practices for managing hydrological alterations in urban watershed. Sustainable Cities and Society 61, 102334. URL: https://doi.org/10.1016%2Fj.scs.2020.102334, doi:10.1016/j.scs.2020.102334.

Sadegh, M., Ragno, E., AghaKouchak, A., 2017. Multivariate copula analysis toolbox (MvCAT): Describing dependence and underlying uncertainty using a bayesian framework. Water Resources Research 53, 5166–5183. URL: https://doi.org/10.1002%2F2016wr020242, doi:10.1002/2016wr020242.

Sahoo, S.N., 2014. Determination of imperviousness and its impact on risk based urban flood modeling. Ph.D. thesis. Indian Institute of Technology Guwahati.

Sahoo, S.N., Pekkat, S., 2014. Determination of urbanisation based on imperviousness. Proceedings of the Institution of Civil Engineers - Urban Design and Planning 167, 49–57. URL: https://doi.org/10.1680%2Fudap.13.00027, doi:10.1680/udap.13.00027.

Sahoo, S.N., Sreeja, P., 2013. A methodology for determining runoff based on imperviousness in an ungauged peri-urban catchment. Urban Water Journal 11, 42–54. URL: https://doi.org/10.1080%2F1573062x.2013.765491, doi:10.1080/1573062x.2013.765491.

Sahoo, S.N., Sreeja, P., 2016. Determination of effective impervious area for an urban indian catchment. Journal of Hydrologic Engineering 21. URL: https://doi.org/10.1061%2F%28asce%29he.1943-5584.0001346, doi:10.1061/(asce)he.1943-5584.0001346.

Sahoo, S.N., Sreeja, P., 2017. Sensitivity of imperviousness determination methodology on runoff prediction. ISH Journal of Hydraulic Engineering 23, 276–282. URL: https://doi.org/10.1080%2F09715010.2017.1301832, doi:10.1080/09715010.2017.1301832.

Sajikumar, N., Remya, R., 2015. Impact of land cover and land use change on runoff characteristics. Journal of Environmental Management 161, 460–468. URL: https://doi.org/10.1016%2Fj.jenvman.2014.12.041, doi:10.1016/j.jenvman.2014.12.041.

Salas, J.D., Obeysekera, J., 2014. Revisiting the concepts of return period and risk for nonstationary hydrologic extreme events. Journal of Hydrologic Engineering 19, 554–568. URL: https://doi.org/10.1061%2F%28asce%29he.1943-5584.0000820, doi:10.1061/(asce)he.1943-5584.0000820.

Salem, A., Abduljaleel, Y., Dezső, J., Lóczy, D., 2023. Integrated assessment of the impact of land use changes on groundwater recharge and groundwater level in the drava floodplain, hungary. Scientific Reports 13. URL: https://doi.org/10.1038%2Fs41598-022-21259-4, doi:10.1038/s41598-022-21259-4.

Salvadori, G., Michele, C.D., 2004. Frequency analysis via copulas: Theoretical aspects and applications to hydrological events. Water Resources Research 40. URL: https://doi.org/10.1029%2F2004wr003133, doi:10.1029/2004wr003133.

Samantaray, P., Gouda, K.C., 2023. A review on the extreme rainfall studies in india. Natural Hazards Research URL: http://dx.doi.org/10.1016/j.nhres.2023.08.005, doi:10.1016/j.nhres.2023.08.005.

Saniei, K., Yazdi, J., MajdzadehTabatabei, M.R., 2021. Optimal size, type and location of low impact developments (lids) for urban stormwater control. Urban Water Journal 18, 585–597.

Santy, S., Mujumdar, P., Bala, G., 2020. Potential impacts of climate and land use change on the water quality of ganga river around the industrialized kanpur region. Scientific Reports 10. URL: https://doi.org/10.1038%2Fs41598-020-66171-x, doi:10.1038/s41598-020-66171-x.

Sanyal, J., Densmore, A.L., Carbonneau, P., 2014. Analysing the effect of land-use/cover changes at sub-catchment levels on downstream flood peaks: A semi-distributed modelling approach with sparse data. CATENA 118, 28–40. URL: https://doi.org/10.1016%2Fj.catena.2014.01.015, doi:10.1016/j.catena.2014.01.015.

Sarhadi, A., Burn, D.H., Ausín, M.C., Wiper, M.P., 2016. Time-varying nonstationary multivariate risk analysis using a dynamic bayesian copula. Water Resources Research 52, 2327–2349. URL: https://doi.org/10.1002%2F2015wr018525, doi:10.1002/2015wr018525.

Schwarz, G., 1978. Estimating the dimension of a model. The Annals of Statistics 6, 461–464. URL: https://doi.org/10.1214%2Faos%2F1176344136, doi:10.1214/aos/1176344136.

Schweizer, B., 2007. Introduction to copulas. Journal of Hydrologic Engineering 12, 346–346.

Sen, P.K., 1968. Estimates of the regression coefficient based on kendall's tau. Journal of the American statistical association 63, 1379–1389.

Sharma, D., Gupta, A.D., Babel, M.S., 2007. Spatial disaggregation of bias-corrected GCM precipitation for improved hydrologic simulation: Ping river basin, thailand. Hydrology and Earth System Sciences

11, 1373–1390. URL: https://doi.org/10.5194%2Fhess-11-1373-2007, doi:10.5194/hess-11-1373-2007.

Sherman, C.W., 1931. Frequency and intensity of excessive rainfalls at boston, massachusetts. Transactions of the American Society of Civil Engineers 95, 951–960.

Shi, P.J., Yuan, Y., Zheng, J., Wang, J.A., Ge, Y., Qiu, G.Y., 2007. The effect of land use/cover change on surface runoff in shenzhen region, china. CATENA 69, 31–35. URL: https://doi.org/10.1016%2Fj.catena.2006.04.015, doi:10.1016/j.catena.2006.04.015.

Shi, Y., Song, J., Zhang, J., Huang, P., Sun, H., Wu, Q., Cheng, L., Zhang, J., Xing, L., Lyu, S., Zhai, Y., 2023. Hydrological response to climate change and human activities in the bahe river, china. Journal of Hydrology 617, 128762. URL: https://doi.org/10.1016%2Fj.jhydrol.2022.128762, doi:10.1016/j.jhydrol.2022.128762.

Shkaruba, A., Skryhan, H., Likhacheva, O., Katona, A., Maryskevych, O., Kireyeu, V., Sepp, K., Shpakivska, I., 2021. Development of sustainable urban drainage systems in eastern europe: an analytical overview of the constraints and enabling conditions. Journal of Environmental Planning and Management 64, 2435–2458. URL: https://doi.org/10.1080%2F09640568.2021.1874893, doi:10.1080/09640568.2021.1874893.

Shrestha, A., Babel, M., Weesakul, S., Vojinovic, Z., 2017. Developing intensity–duration–frequency (IDF) curves under climate change uncertainty: The case of bangkok, thailand. Water 9, 145. URL: https://doi.org/10.3390%2Fw9020145, doi:10.3390/w9020145.

Shrestha, A., Mascaro, G., Garcia, M., 2022. Effects of stormwater infrastructure data completeness and model resolution on urban flood modeling. Journal of Hydrology 607, 127498. URL: https://doi.org/10.1016%2Fj.jhydrol.2022.127498, doi:10.1016/j.jhydrol.2022.127498.

Siddik, M.S., Tulip, S.S., Rahman, A., Islam, M.N., Haghighi, A.T., Mustafa, S.M.T., 2022. The impact of land use and land cover change on groundwater recharge in northwestern bangladesh. Journal of Environmental Management 315, 115130. URL: https://doi.org/10.1016%2Fj.jenvman.2022.115130, doi:10.1016/j.jenvman.2022.115130.

Simonovic, S.P., Schardong, A., Sandink, D., 2017. Mapping extreme rainfall statistics for canada under climate change using updated intensity-duration-frequency curves. Journal of Water Resources Planning and Management 143, 04016078. URL: https://doi.org/10.1061%2F%28asce%29wr.1943-5452.0000725, doi:10.1061/(asce)wr.1943-5452.0000725.

Singh, G., Pandey, A., 2021. Evaluation of classification algorithms for land use land cover mapping in the snow-fed alaknanda river basin of the northwest himalayan region. Applied Geomatics 13, 863–875. URL: https://doi.org/10.1007%2Fs12518-021-00401-3, doi:10.1007/s12518-021-00401-3.

Singh, R., Arya, D.S., Taxak, A.K., Vojinovic, Z., 2016. Potential impact of climate change on rainfall intensity-duration-frequency curves in roorkee, india. Water Resources Management 30, 4603–4616. URL: https://doi.org/10.1007%2Fs11269-016-1441-4, doi:10.1007/s11269-016-1441-4.

Singh, V.P., Zhang, L., 2007. IDF curves using the frank archimedean copula. Journal of Hydrologic Engineering 12, 651–662. URL: https://doi.org/10.1061%2F%28asce%291084-0699%282007%2912%3A6%28651%29, doi:10.1061/(asce)1084-0699(2007)12:6(651).

Sohn, W., Brody, S.D., Kim, J.H., Li, M.H., 2020. How effective are drainage systems in mitigating flood losses? Cities 107, 102917. URL: https://doi.org/10.1016%2Fj.cities.2020.102917, doi:10.1016/j.cities.2020.102917.

Sohn, W., Kim, J.H., Li, M.H., Brown, R., 2019. The influence of climate on the effectiveness of low impact development: A systematic review. Journal of Environmental Management 236, 365–379. URL: https://doi.org/10.1016%2Fj.jenvman.2018.11.041, doi:10.1016/j.jenvman.2018.11.041.

Soltani, S., Almasi, P., Helfi, R., Modarres, R., Esfahani, P.M., Dehno, M.G., 2020. A new approach to explore climate change impact on rainfall intensity–duration–frequency curves. Theoretical and Applied Climatology URL: https://doi.org/10.1007%2Fs00704-020-03309-x, doi:10.1007/s00704-020-03309-x.

de Souza Costa, C.E.A., Blanco, C.J.C., de Oliveira-Júnior, J.F., 2019. IDF curves for future climate scenarios in a locality of the tapajós basin, amazon, brazil. Journal of Water and Climate Change 11, 760–770. URL: https://doi.org/10.2166%2Fwcc.2019.202, doi:10.2166/wcc.2019.202.

Sreeja, P., Gupta, K., 2006. An alternate approach for transient flow modeling in urban drainage systems. Water Resources Management 21, 1225–1244. URL: https://doi.org/10.1007%2Fs11269-006-9078-3, doi:10.1007/s11269-006-9078-3.

Srivastav, R.K., Schardong, A., Simonovic, S.P., 2014. Equidistance quantile matching method for updating IDFCurves under climate change. Water Resources Management 28, 2539–2562. URL: https://doi.org/10.1007%2Fs11269-014-0626-y, doi:10.1007/s11269-014-0626-y.

Sudharsan, N., Karmakar, S., Fowler, H.J., Hari, V., 2020. Large-scale dynamics have greater role than thermodynamics in driving precipitation extremes over india. Climate Dynamics 55, 2603–2614. URL: http://dx.doi.org/10.1007/s00382-020-05410-3, doi:10.1007/s00382-020-05410-3.

Suriya, S., Mudgal, B., 2012. Impact of urbanization on flooding: The thirusoolam sub watershed – a case study. Journal of Hydrology 412-413, 210–219. URL: https://doi.org/10.1016%2Fj.jhydrol.2011.05.008, doi:10.1016/j.jhydrol.2011.05.008.

Sutherland, R.C., 1995. Methodology for estimating the effective impervious area of urban watersheds. Watershed Protection Techniques 2, 282–284.

Switzman, H., Razavi, T., Traore, S., Coulibaly, P., Burn, D.H., Henderson, J., Fausto, E., Ness, R., 2017. Variability of future extreme rainfall statistics: Comparison of multiple IDF projections. Journal of Hydrologic Engineering 22, 04017046. URL: https://doi.org/10.1061%2F%28asce%29he.1943-5584.0001561, doi:10.1061/(asce)he.1943-5584.0001561.

Taji, S.G., Regulwar, D.G., 2019. LID coupled design of drainage model using GIS and SWMM. ISH Journal of Hydraulic Engineering 27, 376–389. URL: https://doi.org/10.1080%2F09715010.2019.1660919, doi:10.1080/09715010.2019.1660919.

Tavakol-Davani, H., Goharian, E., Hansen, C.H., Tavakol-Davani, H., Apul, D., Burian, S.J., 2016. How does climate change affect combined sewer overflow in a system benefiting from rainwater harvesting systems? Sustainable Cities and Society 27, 430–438. URL: https://doi.org/10.1016%2Fj.scs.2016.07.003, doi:10.1016/j.scs.2016.07.003.

Teklesadik, A.D., Alemayehu, T., van Griensven, A., Kumar, R., Liersch, S., Eisner, S., Tecklenburg, J., Ewunte, S., Wang, X., 2017. Inter-model comparison of hydrological impacts of climate change on the upper blue nile basin using ensemble of hydrological models and global climate models. Climatic Change 141, 517–532. URL: https://doi.org/10.1007%2Fs10584-017-1913-4, doi:10.1007/s10584-017-1913-4.

Trenberth, K., 2011. Changes in precipitation with climate change. Climate Research 47, 123–138. URL: http://dx.doi.org/10.3354/cr00953, doi:10.3354/cr00953.

UN, 2019. World urbanization prospects the 2018 revision. 2018. New York: Population Division, Department of Economic and Social Affairs, United Nations .

Uraba, M.B., Gunawardhana, L.N., Al-Rawas, G.A., Baawain, M.S., 2019. A downscaling-disaggregation approach for developing IDF curves in arid regions. Environmental Monitoring and Assessment 191. URL: https://doi.org/10.1007%2Fs10661-019-7385-4, doi:10.1007/s10661-019-7385-4.

Ureta, J., Motallebi, M., Scaroni, A.E., Lovelace, S., Ureta, J.C., 2021. Understanding the public's behavior in adopting green stormwater infrastructure. Sustainable Cities and Society 69, 102815.

Uttarwar, S.B., Barma, S.D., Mahesha, A., 2020. Bivariate modeling of hydroclimatic variables in humid tropical coastal region using archimedean copulas. Journal of Hydrologic Engineering 25, 05020026. URL: https://doi.org/10.1061%2F%28asce%29he.1943-5584.0001981, doi:10.1061/(asce)he.1943-5584.0001981.

Vinnarasi, R., Dhanya, C., 2019. Bringing realism into a dynamic copula-based non-stationary intensity-duration model. Advances in Water Resources 130, 325–338. URL: https://doi.org/10.1016%2Fj.advwatres.2019.06.009, doi:10.1016/j.advwatres.2019.06.009.

Vinnarasi, R., Dhanya, C.T., 2016. Changing characteristics of extreme wet and dry spells of indian monsoon rainfall. Journal of Geophysical Research: Atmospheres 121, 2146–2160. URL: https://doi.org/10.1002%2F2015jd024310, doi:10.1002/2015jd024310.

Vittal, H., Ghosh, S., Karmakar, S., Pathak, A., Murtugudde, R., 2016. Lack of dependence of indian summer monsoon rainfall extremes on temperature: An observational evidence. Scientific Reports 6. URL: http://dx.doi.org/10.1038/srep31039, doi:10.1038/srep31039.

Vittal, H., Karmakar, S., Ghosh, S., 2013. Diametric changes in trends and patterns of extreme rainfall over india from pre-1950 to post-1950. Geophysical Research Letters 40, 3253–3258. URL: https://doi.org/10.1002%2Fgrl.50631, doi:10.1002/grl.50631.

Vu, M.T., Raghavan, S.V., Liu, J., Liong, S.Y., 2018. Constructing short-duration IDF curves using coupled dynamical-statistical approach to assess climate change impacts. International Journal of Climatology 38, 2662–2671. URL: https://doi.org/10.1002%2Fjoc.5451, doi:10.1002/joc.5451.

Wang, C., Wang, Y., Wang, R., Zheng, P., 2018a. Modeling and evaluating land-use/land-cover change for urban planning and sustainability: A case study of dongying city, china. Journal of Cleaner Production 172, 1529–1534. URL: https://doi.org/10.1016%2Fj.jclepro.2017.10.294, doi:10.1016/j.jclepro.2017.10.294.

Wang, H., Hu, Y., Guo, Y., Wu, Z., Yan, D., 2022. Urban flood forecasting based on the coupling of numerical weather model and stormwater model: A case study of zhengzhou city. Journal of Hydrology: Regional Studies 39, 100985. URL: https://doi.org/10.1016%2Fj.ejrh.2021.100985, doi:10.1016/j.ejrh.2021.100985.

Wang, N., Liu, X., Yin, J., 2011a. Improved gath–geva clustering for fuzzy segmentation of hydrometeorological time series. Stochastic Environmental Research and Risk Assessment 26, 139–155. URL: https://doi.org/10.1007%2Fs00477-011-0542-0, doi:10.1007/s00477-011-0542-0.

Wang, X., Gebremichael, M., Yan, J., 2010. Weighted likelihood copula modeling of extreme rainfall events in connecticut. Journal of Hydrology 390, 108–115. URL: https://doi.org/10.1016%2Fj.jhydrol.2010.06.039, doi:10.1016/j.jhydrol.2010.06.039.

Wang, Y., Chen, A.S., Fu, G., Djordjević, S., Zhang, C., Savić, D.A., 2018b. An integrated framework for high-resolution urban flood modelling considering multiple information sources and urban features. Environmental Modelling and Software 107, 85–95. URL: https://doi.org/10.1016%2Fj.envsoft.2018.06.010, doi:10.1016/j.envsoft.2018.06.010.

Wang, Z., Ficklin, D.L., Zhang, Y., Zhang, M., 2011b. Impact of climate change on streamflow in the arid shiyang river basin of northwest china. Hydrological Processes 26, 2733–2744. URL: https://doi.org/10.1002%2Fhyp.8378, doi:10.1002/hyp.8378.

Westra, S., Fowler, H.J., Evans, J.P., Alexander, L.V., Berg, P., Johnson, F., Kendon, E.J., Lenderink, G., Roberts, N.M., 2014. Future changes to the intensity and frequency of short-duration extreme rainfall. Reviews of Geophysics 52, 522–555. URL: https://doi.org/10.1002%2F2014rg000464, doi:10.1002/2014rg000464.

Willems, P., 2013. Multidecadal oscillatory behaviour of rainfall extremes in europe. Climatic Change 120, 931–944. URL: http://dx.doi.org/10.1007/s10584-013-0837-x, doi:10.1007/s10584-013-0837-x.

Willems, P., Arnbjerg-Nielsen, K., Olsson, J., Nguyen, V., 2012. Climate change impact assessment on urban rainfall extremes and urban drainage: Methods and shortcomings. Atmospheric Research 103, 106–118. URL: https://doi.org/10.1016%2Fj.atmosres.2011.04.003, doi:10.1016/j.atmosres.2011.04.003.

Winkler, K., Fuchs, R., Rounsevell, M., Herold, M., 2021. Global land use changes are four times greater than previously estimated. Nature Communications 12. URL: https://doi.org/10.1038%2Fs41467-021-22702-2, doi:10.1038/s41467-021-22702-2.

Woltemade, C.J., Hawkins, T.W., Jantz, C., Drzyzga, S., 2020. Impact of changing climate and land cover on flood magnitudes in the delaware river basin, USA. Journal of the American Water Resources Association 56, 507–527. URL: https://doi.org/10.1111%2F1752-1688.12835, doi:10.1111/1752-1688.12835.

Xu, K., Ma, C., Lian, J., Bin, L., 2014. Joint probability analysis of extreme precipitation and storm tide in a coastal city under changing environment. PLoS ONE 9, e109341. URL: https://doi.org/10.1371%2Fjournal.pone.0109341, doi:10.1371/journal.pone.0109341.

Yamamoto, K., Sayama, T., Apip, 2021. Impact of climate change on flood inundation in a tropical river basin in indonesia. Progress in Earth and Planetary Science 8. URL: https://doi.org/10.1186%2Fs40645-020-00386-4, doi:10.1186/s40645-020-00386-4.

Yan, D., Werners, S.E., Ludwig, F., Huang, H.Q., 2015. Hydrological response to climate change: The pearl river, china under different RCP scenarios. Journal of Hydrology: Regional Studies 4, 228–245. URL: https://doi.org/10.1016%2Fj.ejrh.2015.06.006, doi:10.1016/j.ejrh.2015.06.006.

Yang, B., Zhang, T., Li, J., Feng, P., Miao, Y., 2023. Optimal designs of LID based on LID experiments and SWMM for a small-scale community in tianjin, north china. Journal of Environmental Management 334, 117442. URL: https://doi.org/10.1016%2Fj.jenvman.2023.117442, doi:10.1016/j.jenvman.2023.117442.

Yang, K., Pan, M., Luo, Y., Chen, K., Zhao, Y., Zhou, X., 2018. A time-series analysis of urbanization-induced impervious surface area extent in the dianchi lake watershed from 1988–2017. International Journal of Remote Sensing 40, 573–592. URL: https://doi.org/10.1080%2F01431161.2018.1516312, doi:10.1080/01431161.2018.1516312.

Yang, W., Zhang, J., Krebs, P., 2022. Low impact development practices mitigate urban flooding and non-point pollution under climate change. Journal of Cleaner Production 347, 131320. URL: https://doi.org/10.1016%2Fj.jclepro.2022.131320, doi:10.1016/j.jclepro.2022.131320.

Yeo, M.H., Nguyen, V.T.V., Kpodonu, T.A., 2020. Characterizing extreme rainfalls and constructing confidence intervals for IDF curves using scaling-GEV distribution model. International Journal of Climatology 41, 456–468. URL: https://doi.org/10.1002%2Fjoc.6631, doi:10.1002/joc.6631.

Yılmaz, M., Alp, H., Tosunoğlu, F., Ömer Levend Aşıkoğlu, Eriş, E., 2022. Impact of climate change on meteorological and hydrological droughts for upper coruh basin, turkey. Natural Hazards 112, 1039–1063. URL: https://doi.org/10.1007%2Fs11069-022-05217-x, doi:10.1007/s11069-022-05217-x.

Yue, S., Ouarda, T., Bobée, B., 2001. A review of bivariate gamma distributions for hydrological application. Journal of Hydrology 246, 1–18. URL: https://doi.org/10.1016%2Fs0022-1694%2801%2900374-2, doi:10.1016/s0022-1694(01)00374-2.

Zahmatkesh, Z., Burian, S.J., Karamouz, M., Tavakol-Davani, H., Goharian, E., 2015a. Low-impact development practices to mitigate climate change effects on urban stormwater runoff: Case study of new york city. Journal of Irrigation and Drainage Engineering 141, 04014043. URL: https://doi.org/10.1061%2F%28asce%29ir.1943-4774.0000770, doi:10.1061/(asce)ir.1943-4774.0000770.

Zahmatkesh, Z., Karamouz, M., Goharian, E., Burian, S.J., 2015b. Analysis of the effects of climate change on urban storm water runoff using statistically downscaled precipitation data and a change factor approach. Journal of Hydrologic Engineering 20, 05014022. URL: https://doi.org/10.1061%2F%28asce%29he.1943-5584.0001064, doi:10.1061/(asce)he.1943-5584.0001064.

Zhang, J.Y., Wang, G.Q., Pagano, T.C., Jin, J.L., Liu, C.S., He, R.M., Liu, Y.L., 2013. Using hydrologic simulation to explore the impacts of climate change on runoff in the huaihe river basin of china. Journal of Hydrologic Engineering 18, 1393–1399. URL: https://doi.org/10.1061%2F%28asce%29he.1943-5584.0000581, doi:10.1061/(asce)he.1943-5584.0000581.

Zhang, L., Singh, V.P., 2006. Bivariate flood frequency analysis using the copula method. Journal of Hydrologic Engineering 11, 150–164. URL: https://doi.org/10.1061%2F%28asce%291084-0699%282006%2911%3A2%28150%29, doi:10.1061/(asce)1084-0699(2006)11:2(150).

Zhang, Y., Pang, X., Xia, J., Shao, Q., Yu, E., Zhao, T., She, D., Sun, J., Yu, J., Pan, X., Zhai, X., 2019. Regional patterns of extreme precipitation and urban signatures in metropolitan areas. Journal of Geophysical Research: Atmospheres 124, 641–663. URL: http://dx.doi.org/10.1029/2018jd029718, doi:10.1029/2018jd029718.

Zhang, Z., Hu, W., Wang, W., Zhou, J., Liu, D., Qi, X., Zhao, X., 2022. The hydrological effect and uncertainty assessment by runoff indicators based on SWMM for various LID facilities. Journal of Hydrology 613, 128418. URL: https://doi.org/10.1016%2Fj.jhydrol.2022.128418, doi:10.1016/j.jhydrol.2022.128418.

Zhao, L., Cui, N., Guan, J., Du, P., Zhang, Y., Jiang, S., 2021. Copula-based risk analysis of agricultural water shortage under natural precipitation conditions in the guanzhong plain, a drought-prone region of china. Journal of Hydrologic Engineering 26, 04021016. URL: https://doi.org/10.1061%2F%28asce%29he.1943-5584.0002084, doi:10.1061/(asce)he.1943-5584.0002084.

Zhou, Q., Leng, G., Huang, M., 2018. Impacts of future climate change on urban flood volumes in hohhot in northern china: benefits of climate change mitigation and adaptations. Hydrology and Earth System Sciences 22, 305–316. URL: https://doi.org/10.5194%2Fhess-22-305-2018, doi:10.5194/hess-22-305-2018.

Zhu, H., Yu, M., Zhu, J., Lu, H., Cao, R., 2019. Simulation study on effect of permeable pavement on reducing flood risk of urban runoff. International Journal of Transportation Science and Technology 8, 373–382. URL: https://doi.org/10.1016%2Fj.ijtst.2018.12.001, doi:10.1016/j.ijtst.2018.12.001.

Zope, P., Eldho, T., Jothiprakash, V., 2016. Impacts of land use–land cover change and urbanization on flooding: A case study of oshiwara river basin in mumbai, india. CATENA 145, 142–154. URL: https://doi.org/10.1016%2Fj.catena.2016.06.009, doi:10.1016/j.catena.2016.06.009.

List of Publications

Journal Articles:

1. Suresh, A., Pekkat, S. and Subbiah, S., 2023. Quantifying the Efficacy of Low Impact Developments (LIDs) for Flood Reduction in Micro-urban Watersheds Incorporating Climate Change. Sustainable Cities and Society, 95, p.104601. DOI: 10.1016/j.scs.2023.104601.

2. Suresh, A. and Pekkat, S., 2023. Importance of Copula-Based Bivariate Rainfall Intensity-Duration-Frequency Curves for an Urbanized Catchment Incorporating Climate Change. Journal of Hydrologic Engineering, 28(7), p.05023012. DOI: 10.1016/j.trc.2020.102847.

To be Submitted:

1. Suresh, A. and Pekkat, S. Impact of Land Use and Climate Change on Urban Flood Characteristics.

2. Suresh, A. and Pekkat, S. Characterization of Short-duration Rainfall and its Impact on Urban Flood.

3. Suresh, A. and Pekkat, S. A Comparative Analysis of Best Management Practices for Flood Mitigation in Micro-urban Watersheds and Macro-urban Watersheds.

Book Chapters:

1. Suresh, A. and Pekkat, S., 2022. Climate Change and Its Impact on Surface Runoff Characteristics of an Urban Catchment. In Sustainable Water Resources Management: Proceedings of SWARM 2020 (pp. 3-11). Singapore: Springer Nature Singapore. DOI: 10.1007/978-981-16-7535-5.

2. Suresh, A. and Sreeja, P., 2021. Identification of Historical Shift, Dispersion, and Trend of the Monsoon Season for Guwahati City Using Fuzzy Segmentation and Trend Analyses. In Climate Change Impacts on Water Resources: Hydraulics, Water Resources and Coastal Engineering (pp. 393-405). Cham: Springer International Publishing. DOI: 10.1007/978-3-030-64202-0.

Conference Proceedings:

1. Suresh, A., Pekkat, S. and Subbiah, S., 2023. Impact of Climate Change on the Implementation of Green Roof on a Micro-urban Watershed. 20th Annual Meeting of the Asia Oceania Geosciences Society (AOGS), SUNTEC, Singapore.

2. Suresh, A. and Pekkat, S., 2021. Assessment of Uncertainty in the Intensity Duration Frequency Curves Due to Different GCMs, Probability Distribution, and Climate periods. AGU Fall Meeting, New Orleans, LA, USA.

3. Suresh, A. and Pekkat, S., 2021. Analysis of the Effects of Various Covariates on Extreme Rainfall of Short Duration. 15th International Conference on Urban Drainage (ICUD), Melbourne, Australia.

4. Suresh, A. and Pekkat, S., 2021. Climate Change Assessment for an Urban Catchment of Northeast India. 4th International Conference on System, Energy and Environment (ICSEE), Kannur, Kerala, India.

5. Suresh, A. and Pekkat, S., 2020. Appraisal of Low Impact Developments (LIDs) for Effective Storm Water Management of Urbanized Catchments. 2nd ASCE India Conference on "Challenges of Resilient and Sustainable Infrastructure Development in Emerging Economies" (CRSIDE), Kolkata, West Bengal, India.

6. Suresh, A. and Pekkat, S., 2019. Identification of Historical Shift, Dispersion, and Trend of the Monsoon Season for Guwahati City Using Fuzzy Segmentation and Trend Analyses. HYDRO-2019 International (Hydraulics, Water Resources and Coastal Engineering), NIT Patna, Bihar, India.

7. Suresh, A. and Pekkat, S., 2019. Impact of Climatic Shift and Dispersion on Analyzing the Climate Change with Crisp Seasonal Boundaries. 16th Annual Meeting of the Asia Oceania Geosciences Society (AOGS), SUNTEC Singapore.

8. Suresh, A. and Pekkat, S., 2019. Time Series Analysis of Shift, Dispersion, and Trend of Monsoon Season for Guwahati City Using Fuzzy Segmentation. Research Conclave, IIT Guwahati, Assam, India.

9. Suresh, A. and Pekkat, S., 2016. Statistical Analysis and Comparison of Point Gauge Rainfall and Downscaled Rainfall For Guwahati City. HYDRO-2016 International (Hydraulics, Water Resources and Coastal Engineering), Pune, Maharashtra, India.